

**FATIGUE DAMAGE ASSESSMENT OF STEEL  
CATENARY RISERS IN THE TOUCHDOWN ZONE  
WITH INCORPORATION OF TIME-DEPENDANT  
SEABED INTERACTION EFFECTS**

by

©Hossein Janbazi

A Thesis Submitted to the

School of Graduate Studies

in partial fulfillment of the requirements for the degree of

**Doctor of Philosophy**

**Faculty of Engineering and Applied Science**

Memorial University of Newfoundland

**October 2023**

St. John's

Newfoundland

Canada



## **ABSTRACT**

Steel catenary riser (SCR) design is heavily affected by fatigue performance in the touchdown zone (TDZ). Within the TDZ, the riser cyclically interacts with the seabed, resulting in the progressive generation of excess pore water pressure, leading to soil softening and remoulding. However, the soil may undergo a consolidation process during the intervening pause period, i.e., the calm weather or the inactive periods of SCR's oscillation, allowing the pore water pressure to dissipate. This process results in the regaining of effective stress and consequently achieving a higher soil strength, which is detrimental to the fatigue damage accumulation in the TDZ. The existing advanced hysteretic non-linear riser-seabed interaction models do not account for the consolidation effects. Besides, a secondary mechanism, i.e., the seabed erosion due to combined vortices generated by subsea currents and seawater entrapped between the oscillating riser and the trench may contribute to the cyclic riser embedment. The existing riser-seabed interaction models do not capture this secondary mechanism as well. In this research project, first, these key knowledge gaps were addressed by developing global and local riser-seabed-seawater interaction models and incorporation of the consolidation and erosion effects. Later, the developed models were used to propose novel methodologies for incorporation of the trench effects into the riser fatigue analysis. The consolidation effects were added by coding an effective stress framework into a user-defined subroutine (UEL) in ABAQUS. This was integrated with the global riser model to determine the long-term soil stiffness associated with damage accumulation during SCR cyclic motions and soil strength recovery during the intervening pause period. The seabed soil erosion effect on trench formation was investigated by developing a three-domain model of riser-soil-fluid interaction. The

model was used to study the combined effect of soil erosion, soil fluidization, and cyclic riser oscillations on the plastic soil deformation and riser embedment. A Coupled Eulerian-Lagrangian (CEL) technique was employed and the strain rate and soil softening effects in an Eulerian domain were coded into the VUSDFLD subroutine of ABAQUS. The developed models were successfully verified against the experimental studies from the literature. As proven by subsea surveys, all of these riser-seabed-seawater interaction mechanisms result in a trench formation several riser diameter deep (3D to 7D) that can significantly affect the fatigue life in the TDZ. Although most of the studies in the literature show a beneficial effect of the trench on fatigue, there is still no coherent agreement amongst researchers on the beneficial or detrimental trench effects. To further investigate the trench effect on fatigue, first, two new methodologies were proposed, i.e., i) an alternative vessel excitation algorithm called the equivalent motion method (EMM) and ii) an equivalent soil stiffness approach called the hybrid trench model (HTM). The first method was investigated to predict the fatigue damage of the riser in the linear elastic seabed using the same riser on the rigid seabed but with a virtual vessel motion algorithm. An equation was extracted from a comprehensive set of analyses for a given riser resting on an elastic seabed to obtain an equivalent vessel motion amplitude on a rigid seabed with the same cyclic damage. As an alternative solution, the proposed EMM was found to be a promising basis for further extension into the non-linear riser-seabed interaction. The second methodology provides equivalent soil stiffness to simulate the target riser embedment, which is usually obtained from non-linear hysteretic riser-seabed interaction models. The capability of HTM in developing deep trenches, e.g., 5D, was examined along with perfect compatibility with the natural catenary shape of the riser to resolve any pressure hot



spots and premature stabilization problems frequently reported in the literature. This novel methodology was integrated with the effective stress analysis developed earlier in this study to deeply investigate the trench effect on the fatigue performance of SCR in the TDZ, while considering the consolidation. Besides developing several advanced tools for enhanced analysis of SCR-seabed interaction, the study extended the insight into the fatigue performance of steel catenary risers in the touchdown zone that can be used by field operators and riser life extension authorities.

## STATEMENT OF AUTHORSHIP

I, Hossein Janbazi, hereby declare that I have been the first author and the main contributor to the conducted work presented in this doctoral dissertation. I undertook various tasks throughout this research process, including numerical modelling, data analysis, post-processing, visualization, and manuscript preparation. Dr. Hodjat Shiri, my supervisor, played a significant role in shaping the research topics, outlining the overall approach, offering valuable advice, checking the results, reviewing and editing the paper drafts. The list of published papers and submitted manuscripts is shown below:

- Janbazi, H., Shiri, H., 2023. Incorporation of seabed soil effective stress analysis into the numerical modeling of the steel catenary riser accounting for soil remoulding and reconsolidation effect, *Géotechnique* (Under review).
- Janbazi, H., Shiri, H., 2023. Incorporation of the riser-seabed-seawater interaction effect into the trench formation beneath the steel catenary riser in the touchdown zone, *Ocean Engineering* (Under review).
- Janbazi, H., Shiri, H., 2022. An alternative vessel excitation algorithm to incorporate the trench effect into the fatigue analysis of steel catenary risers in the touchdown zone, *Applied Ocean Research*, 126-103292.
- Janbazi, H., Shiri, H., 2022. A hybrid model to simulate the trench effect on the fatigue analysis of steel catenary risers in the touchdown zone, *Canadian Geotechnical Journal*, <https://doi.org/10.1139/cgj-2022-0103>.
- Janbazi, H., Shiri, H., 2023. Investigation of trench effect on fatigue response of steel catenary risers using an effective stress analysis, *Computers & Geotechnics Journal*, 160-105506.

- Janbazi, H., Shiri, H., 2023. Incorporation of the consistent trench into the SCR fatigue performance by using an equivalent soil stiffness methodology, 33<sup>rd</sup> International Ocean and Polar Engineering Conference (ISOPE), Ottawa, Canada, June 19–23, 2023.

## **ACKNOWLEDGMENT**

Firstly, I would like to express my gratitude to my supervisor, Dr. Hodjat Shiri, for offering me valuable opportunities to become a member of his esteemed research team and contribute to this challenging research topic. His kind support are not limited to my academic life, introducing me to a well-known oil and gas company for a part-time job, where I could feel hands-on real challenges directly in my PhD area of research. Under His guidance, my technical skillset and capacity for critical thinking have flourished, proving invaluable in both industry and academia. His dedicated investment of time and focused attention in numerous hours of teaching, discussions, comprehensive reviews, and constructive critiques has played an immeasurable role in shaping my professional development. I extend my sincere appreciation.

I would like to extend my appreciation to Dr. Sohrab Zendehboudi and Dr. Stephen Bruneau, the members of my supervisory committee, for their supportive advice, and professional suggestions aimed at enhancing the quality of my research.

I gratefully acknowledge the financial support of this research by the “Natural Science and Engineering Research Council of Canada (NSERC)” through the Discovery program and the Memorial University of Newfoundland through the school of graduate studies (SGS) funding support. These financial supports allowed me to sustain a comfortable lifestyle, enabling me to concentrate on my work with heightened focus. Additionally, these funds facilitated my attendance at a recent conference, affording me the opportunity to showcase my research. This experience not only enriched my overall learning journey but also broadened my professional connections.

I would like to express my appreciation to the Engineering Graduate Studies Office staff for their patience and cooperation during my stay at MUN; and all my friends and colleagues in the office for their companionship and scientific discussions throughout this journey, with a special acknowledgment to Rahim Shoghi for his willingness help.

I am sincerely grateful to my wife, Hajar Janbazi, for her unconditional love, invaluable support, and profound understanding throughout the demanding four years of my research work. Her dedication and sacrifices, particularly during my busy times and prolonged absences, have been truly remarkable and deeply appreciated. Last but not least, I would like to express my heartfelt gratitude to my amazing parents, for their continuing caring, prayers and sacrifices that have consistently motivated me to strive for excellence in my professional endeavours; to my wife's parents for their spiritual support and encouragement, as their role has been pivotal in enhancing the quality of our lives.

**Hossein Janbazi**

**October 2023**

# Contents

<b>ABSTRACT</b> .....	<b>3</b>
<b>STATEMENT OF AUTHORSHIP</b> .....	<b>6</b>
<b>ACKNOWLEDGMENT</b> .....	<b>8</b>
<b>List of Figures</b> .....	<b>14</b>
<b>List of Tables</b> .....	<b>20</b>
<b>List of Abbreviations and Symbols</b> .....	<b>22</b>
<b>CHAPTER 1</b> .....	<b>35</b>
<b>Introduction</b> .....	<b>35</b>
1.1. Overview .....	35
1.2. Problem Definition.....	38
1.2.1. Consolidation Effect .....	38
1.2.2. Riser-Seabed-Seawater Interaction .....	39
1.2.3. Incorporation of Trench Effect .....	39
1.3. UEL Subroutines.....	40
1.4. Research Objectives .....	41
1.5. Organization of the Thesis .....	41
1.6. Thesis outcomes.....	43
<b>CHAPTER 2</b> .....	<b>46</b>
<b>Literature Review</b> .....	<b>46</b>
2.1. Overview .....	46
2.2. Literature Review.....	46
2.2.1. Steel Catenary Riser Mechanism .....	46
2.2.2. Riser-Seabed Interaction .....	48
2.2.3. Consolidation Effect .....	52
2.2.4. Pipe-Seabed-Seawater Interaction .....	54
2.2.5. Incorporation of Trench Effect .....	58
<b>CHAPTER 3</b> .....	<b>72</b>

<b>Incorporation of Effective Stress Analysis into the Numerical Model of the Steel Catenary Riser; Accounting for Soil Remoulding and Reconsolidation Effect .....</b>	<b>72</b>
3.1. Introduction.....	74
3.2. Effective Stress Methodology .....	77
3.3. Global Analysis of SCR based on Effective Stress Analysis.....	79
3.3.1. Generation of Excess Pore Water Pressure .....	81
3.3.2. Dissipation of Excess Pore Water Pressure .....	84
3.4. SCR - Case Study.....	87
3.4.1. SCR-Soil Stiffness in the TDZ .....	93
3.4.2. Validation of UEL subroutine developed for SCR-soil interaction model.....	95
3.4.3. Axial stress range along TDZ .....	98
3.5. Stochastic fatigue analysis with incorporation of consolidation effect.....	100
3.6. Conclusion .....	103
3.7. Acknowledgments.....	104
<b>CHAPTER 4.....</b>	<b>110</b>
<b>Incorporation of the Riser-Seabed-Seawater Interaction Effect into the Trench Formation beneath the Steel Catenary Riser in the Touchdown Zone .....</b>	<b>110</b>
4.1. Introduction.....	112
4.2. Large Deformation Finite Element Technique .....	116
4.2.1. Numerical Model .....	117
4.3. Seabed soil strain rate and softening effects .....	119
4.3.1. Parametric study to validate the FE model .....	120
4.4. FE Analysis for a Case Study .....	124
4.5. Contribution of water entrainment and lateral movements in trench formation ....	134
4.6. Conclusion .....	144
<b>CHAPTER 5.....</b>	<b>154</b>
<b>An Alternative Vessel Excitation Algorithm to Incorporate the Trench Effect into the Fatigue Analysis of Steel Catenary Risers in the Touchdown Zone.....</b>	<b>154</b>

5.1.	Introduction.....	156
5.2.	Numerical Model .....	159
5.2.1.	Model configuration.....	159
5.2.2.	Fatigue damage assessment .....	163
5.3.	Concept of the proposed methodology .....	164
5.4.	Analysis procedure and the trends observed.....	168
5.5.	Obtaining a curve fit for equivalent vessel motions.....	173
5.5.1.	Verification of the proposed curve fit.....	180
5.5.1.1.	Peak stress range in critical nodes.....	180
5.5.1.2.	Stress range in the entire length of SCR .....	182
5.5.2.	EMM performance in fatigue analysis.....	183
5.6.	Conclusion .....	185
<b>CHAPTER 6.....</b>		<b>197</b>
<b>A hybrid model to simulate the trench effect on the fatigue analysis of steel catenary risers in the touchdown zone .....</b>		<b>197</b>
6.1.	Introduction.....	199
6.2.	Hybrid Trench Model (HTM).....	202
6.2.1.	Numerical model of riser .....	207
6.2.2.	Sensitivity analysis of the dimensionless parameters .....	208
6.3.	Verification of the Hybrid Trench Model (HTM).....	210
6.3.1.	Verification of trench profile .....	210
6.3.2.	Verification of cyclic axial stress range.....	214
6.4.	Creation of deep trenches by the hybrid model .....	219
6.5.	Incorporation of the trench into the fatigue analysis.....	228
6.6.	Conclusion .....	232
<b>CHAPTER 7.....</b>		<b>240</b>
<b>Investigation of trench effect on fatigue response of steel catenary risers using an effective stress analysis .....</b>		<b>240</b>
7.1.	Introduction.....	242



7.2.	Effective stress framework.....	245
7.2.1.	Soil strength .....	252
7.3.	Validation of framework through an example T-bar model test.....	254
7.4.	Numerical analysis of SCR.....	259
7.5.	A SCR case study analysis.....	262
7.5.1.	SCR-Soil Stiffness based on remoulding and consolidation .....	264
7.6.	Incorporation of trench effect into fatigue analysis with the presence of consolidation.. .....	271
7.6.1.	Hybrid Trench Model for trench generation .....	271
7.6.2.	Stochastic analysis of fatigue damage .....	278
7.7.	Conclusion .....	287
<b>CHAPTER 8</b>	<b>.....</b>	<b>297</b>
<b>Conclusions, Limitations and Recommendations</b>	<b>.....</b>	<b>297</b>
8.1.	Conclusion .....	297
8.2.	Limitations .....	302
8.3.	Recommendations for Future Study.....	303
<b>Bibliography</b>	<b>.....</b>	<b>305</b>
<b>APPENDIX</b>	<b>.....</b>	<b>323</b>
<b>Appendix A</b>	<b>.....</b>	<b>324</b>
<b>Incorporation of the Compatible Trench into the SCR Fatigue Performance by Using an Equivalent Soil Stiffness Methodology</b>	<b>.....</b>	<b>324</b>
<b>Abstract</b>	<b>.....</b>	<b>325</b>
A.1.	Introduction.....	326
A.2.	Concept of the Proposed Methodology.....	328
A.3.	Case Study : A Sample SCR.....	332
A.4.	Creation of Trench .....	333
A.5.	Fatigue Analysis of SCR with Incorporation of Trench Effect.....	338
A.6.	Conclusion .....	343

## List of Figures

Figure 1-1. Different types of subsea risers categorized with water depth and year of installation (Offshore Magazine, May 2013).....	36
Figure 1-2. Schematic view of SCR connected to a floating system .....	37
Figure 1-3. Demonstrating the knowledge gaps conducted in the current study .....	38
Figure 2-1. SCR general arrangement (Bridge, 2005) .....	47
Figure 2-2. Non-linear soil model characteristics developed by Randolph and Quiggin (2009) .....	51
Figure 2-3. SCR-seabed-seawater interaction observed in SCR full scale test, Watchet Harbor, UK (Bridge & Willis, 2002) .....	58
Figure 3-1. Time-dependent SCR-seabed stiffness, accounting for remoulding and consolidation .....	77
Figure 3-2. Definition of the effective stress framework with the schematic variation of effective stress and excess pore pressure during remoulding and consolidation process .....	78
Figure 3-3. Schematic illustration of user-defined elements implemented into the UEL subroutine of Abaqus .....	80
Figure 3-4. Remoulding process for a sample node in TDZ based on the effective stress analysis .....	82
Figure 3-5. Damage accumulation of the surrounding soil with each Node; cyclic movement	84
Figure 3-6. Schematic illustration of excess pore pressure dissipation during the consolidation process.....	85
Figure 3-7. Soil strength definition for a sample SCR-seabed user-defined element in the TDZ (a) Contribution of the surrounded soil for average strength (b) soil mobilization after the change in pipe direction .....	86
Figure 3-8. ABAQUS main procedure flowchart conducted for the numerical model of SCR	89
Figure 3-9: Numerical analysis of SCR over 600 cycles based on effective stress analysis: (a) normalized penetration; (b) total resistance-penetration for sample nodes 356, 366.....	92
Figure 3-10. Normalized uplift secant stiffness for some nodes in TDZ, with more focus on Node 366.....	94
Figure 3-11. Variations in normalized secant stiffness for Node 366 based on the current model and an existing non-linear spring model (R-Q model) .....	95
Figure 3-12. Results of degradation factor based on the UEL subroutine developed for SCR-soil interaction model and centrifuge model tests.....	96

Figure 3-13. Degradation factor at stabilized condition for specific nodes in TDZ, based on the effects stress and total stress approaches .....	97
Figure 3-14. Axial stress range and trench formation along the TDZ based on effective stress analysis.....	99
Figure 3-15. Consolidation effect on fatigue performance of SCR with degree of dissipation: U=90% (a) SS3, (b) SS4 .....	101
Figure 3-16. Peak fatigue damage variation due to the different dissipation rate.....	103
Figure 4-1. Steel Catenary Riser system: (a) typical SCR-soil interaction model during vertical cyclic motions; (b) SCR-seabed-seawater interaction defined in the current study.....	115
Figure 4-2. Schematic illustration of CEL model: Three-domain model with boundary conditions .....	118
Figure 4-3. Penetration resistance for the first one-half cycle: (a) without water entrainment, (b) with water entrainment.....	122
Figure 4-4. Vertical resistance obtained from CEL and centrifuge model test without water entrainment .....	123
Figure 4-5. Vertical resistance obtained from CEL and centrifuge model test with water entrainment .....	124
Figure 4-6. Normalized geotechnical resistance for pipe-soil and fluid-pipe-soil interaction	127
Figure 4-7. (a) Schematic illustration of soil heave during $z/D = -0.4$ with and without water entrainment; (b) the selected values for $f_b$ .....	130
Figure 4-8. Fitting vertical resistance in the CEL method with the theoretical method .....	133
Figure 4-9. Derived values for bearing capacity factors, with and without water entrainment .....	134
Figure 4-10. Existing methods commonly used for global analysis of SCRs.....	135
Figure 4-11. (a) SCR profile in the TDZ; (b) The range of riser oscillations and soil resistance for sample nodes in the TDZ.....	137
Figure 4-12. Time history of vertical displacement defined with load control analysis .....	138
Figure 4-13. Evolution of vertical trench depth in response to the effects of lateral movement and water entrainment.....	140
Figure 4-14. Evolution of seabed profile and berm formation surrounding pipeline.....	142
Figure 4-15. Fluid velocity vectors in the scale of $0.25 \text{ m/s}$ within the largest arrow for (a) without lateral movements; (b) lateral oscillation= $0.2D$ ; (c) lateral oscillation= $0.4D$ .....	143
Figure 5-1. Schematic representation of the concept behind the EMM proposed in the current study.....	158
Figure 5-2. 2D view of SCR configuration.....	160

Figure 5-3. Comparison of the normalized SCR shape of the current base cases with the published work (Quéau et al., 2014a): (a) zoom around the HOP; and (b) zoom around the TDP .....	161
Figure 5-4. Comparison of the normalized stress of the current base cases with the published work (Quéau et al., 2014a), zoom around the TDP .....	162
Figure 5-5. S–N curve for fatigue analysis .....	163
Figure 5-6. Relation between linear soil and rigid seabed to find equivalent motion amplitudes .....	165
Figure 5-7. Same peak damage results for linear soil models and rigid seabed by defining EMM .....	167
Figure 5-8. Maximum stress range of BC1 in rigid seabed through different vessel motions and periods.....	169
Figure 5-9. Maximum stress range of BC2 in rigid seabed through different vessel motions and periods.....	169
Figure 5-10. Variations of equivalent motions ( $H_{eq}$ ) against vessel amplitudes ( $H$ ) through different soil stiffness and periods .....	174
Figure 5-11. Summary of the procedure to find max stress range based on the EMM and LM .....	176
Figure 5-12. Results of maximum stress range based on the elastic seabed and EMM (for BC3) .....	181
Figure 5-13. Stress range for the entire length of BC3 based on the EMM and LM: (a) $k=10$ kPa; (b) $k=50$ kPa; (c) $k=100$ kPa; (d) $k=500$ kPa.....	183
Figure 5-14. Fatigue damage for sample riser (BC3) based on the EMM and LM: (a) $k=10$ kPa; (b) $k=50$ kPa; (c) $k=100$ kPa; (d) $k=500$ kPa.....	185
Figure 6-1. Schematic concept of the HTM proposed in the current study .....	202
Figure 6-2. Configuration of the trenched seabed: (a) trench profile with some key points; (b) incremental embedment of riser (R-Q model) .....	203
Figure 6-3. Schematic soil stiffness changing from linear to the equivalent stiffness: (a) linear stiffness; (b) equivalent stiffness.....	205
Figure 6-4. The global geometry of SCR modelled by ABAQUS.....	207
Figure 6-5. Sensitivity analysis of $\alpha$ with the constant $\eta$ .....	209
Figure 6-6. Sensitivity analysis of $\eta$ with the constant $\alpha$ .....	209
Figure 6-7. Cyclic embedment of the R-Q model and gradual penetration of the HTM ( $s_{u0} = 0$ kPa) .....	212

Figure 6-8. Cyclic embedment of the R-Q model and gradual penetration of the HTM ( $s_{u0} = 0.5$ kPa) .....	212
Figure 6-9. Cyclic embedment of the R-Q model and gradual penetration of the HTM ( $s_{u0} = 1$ kPa) .....	213
Figure 6-10. Maximum depth of penetration and variations of $\alpha$ through a number of cycles .....	214
Figure 6-11. The flowchart of ABAQUS main procedure conducted for HTM and R-Q model .....	216
Figure 6-12. Total stress range in TDZ based on the R-Q ( $s_{u0} = 0$ kPa) and HTM ( $\alpha = 0.292, \eta = 340$ ) .....	217
Figure 6-13. Total stress range in TDZ based on the R-Q ( $s_{u0} = 0.5$ kPa) and HTM ( $\alpha = 0.099, \eta = 310$ ) .....	217
Figure 6-14. Total stress range in TDZ based on the R-Q ( $s_{u0} = 1$ kPa) and HTM ( $\alpha = 0.112, \eta = 305$ ) .....	218
Figure 6-15. Comparison of different trench types .....	220
Figure 6-16. Contact force of riser in equilibrium condition, 5D trenched seabed with $k = 300$ kPa: (a) HTM; (b) Langner's trench; (c) Shiri's trench; (d) Shiri and Randolph's trench....	222
Figure 6-17. Cyclic contact force in TDZ under $H = 2$ m and $T = 15$ s: (a) maximum values; (b) cyclic .....	223
Figure 6-18. Cyclic fluctuations of SCR in TDZ under $H = 2$ m and $T = 15$ s by: (a) HTM; (b) Shiri and Randolph's trench.....	225
Figure 6-19. Cyclic bending moment in TDZ under $H = 2$ m and $T = 15$ s: (a) maximum values; (b) cyclic variations.....	227
Figure 6-20. Cyclic total axial stress in TDZ under $H = 2$ m and $T = 15$ s: (a) maximum values; (b) cyclic variations.....	227
Figure 6-21. Cyclic contact force and axial stress range in TDZ under ( $H = 0.1, 0.3, 0.6$ m & $T = 10$ s) .....	231
Figure 6-22. Cyclic contact force and axial stress range in TDZ under ( $H = 0.9, 1.2, 1.6$ m & $T = 15$ s) .....	232
Figure 7-1. Definition of the effective stress framework associated with the remoulding and reconsolidation.....	246
Figure 7-2: Cycle number definition with schematic variations of effective stress and excess pore pressure during (a) remoulding and (b) consolidation process .....	248
Figure 7-3. Schematic concept of excess pore pressure dissipation with the given degree of consolidation.....	252

Figure 7-4. Definition of shear strength (a) Contribution of the surrounded soil for average shear strength (b) soil mobilization after the change in pipe direction.....	253
Figure 7-5. Operative shear strength for ranges of soil depth: (a) cyclic episode 1, (b) cyclic episode 2, (c) cyclic episode 3 .....	257
Figure 7-6. Results of degradation factor based on the (a) effective stress framework (current study) and (b) experimental model tests (Hodder et al., 2009).....	257
Figure 7-7. Degradation factor due to the remoulding and consolidation effects obtained from effective stress framework (current study) and experimental model tests (Al-Janabi et al., 2019) .....	258
Figure 7-8. 2D configuration of SCR within user-defined elements implemented into the UEL subroutine.....	261
Figure 7-9. Definition of unloading secant stiffness.....	262
Figure 7-10. Numerical penetration of SCR at the remoulding states of each episode .....	264
Figure 7-11. (a) Non-dimensional secant stiffness against cycle number at $\Delta z/D = 0.0025$ for Node 356, (b) SCR profiles in the TDZ.....	265
Figure 7-12. Numerical analysis of SCR over 600 cycles based on the effective stress framework: SCR penetration-resistance for Node 356 .....	266
Figure 7-13. Numerical analysis of SCR over 600 cycles based on the non-linear soil model (R-Q), $s_{u0}=0$ kPa, $\rho=1$ kPa/m: (a) SCR profile, (b) SCR penetration resistance for node 356....	268
Figure 7-14. Numerical analysis of SCR over 600 cycles based on the non-linear soil model (R-Q), $s_{u0}=1$ kPa, $\rho=1.2$ kPa/m: (a) SCR profile, (b) SCR penetration resistance for node 350.	269
Figure 7-15. Normalized uplift secant stiffness based on the effective stress framework and non-linear soil model.....	271
Figure 7-16. Schematic concept of the HTM proposed in the current study .....	272
Figure 7-17. A general configuration of trench formation in profile view (a) Observations of Allegheny Trench Survey (Bridge and Howells, 2007) (b) comparison of different approaches for trench profile .....	274
Figure 7-18. Overview of trench formation (a) profile view of the trench (b) transverse view of the trench.....	275
Figure 7-19. Configuration of the trenched seabed (a) trench profile with some key points, (b) incremental embedment of SCR by using effective stress framework and HTM.....	276
Figure 7-20. Contact force of riser in equilibrium condition, 5D trenched seabed with $k = 300$ kPa .....	277
Figure 7-21: The procedure of wave analysis implemented in the UWAVE subroutine of ABAQUS .....	281

Figure 7-22. Combination of HTM and effective stress framework for stochastic fatigue analysis: (a) schematic view of deep trench generation, (b) 3-hour simulation time with considering remoulding and reconsolidation processes .....	282
Figure 7-23: Consolidation effect on fatigue performance under 3-hour simulation of SS3 based on the effective stress framework in different trench depths: (a) 1D, (b) 3.8D, (c) 5D .....	284
Figure 7-24: Consolidation effect on fatigue performance under 3-hour simulation of SS4 based on the effective stress framework in different trench depths: (a) 1D, (b) 3.8D, (c) 5D .....	285
Figure 7-25: Normalized peak fatigue damage for different trench depths with and without consolidation effect under two sea states SS3 & SS4 .....	286
Figure A-1. Schematic concept of the non-linear, linear and equivalent stiffness along the SCR .....	327
Figure A-2. Definition of trench formation created by (a) non-linear soil model (R-Q), (b) equivalent soil stiffness.....	330
Figure A-3. Patterns of equivalent stiffness used in the current study.....	331
Figure A-4. The global geometry of case study modelled by ABAQUS.....	333
Figure A-5. Comparison of the trench profiles (a) gradual penetration based on the R-Q model and equivalent stiffness, (b) creation of deep trench.....	335
Figure A-6. Contact forces in SCR equilibrium condition based on: (a) Langner’s trench, (b) Shiri’s trench, (c) Equivalent stiffness method.....	337
Figure A-7. Normalized fatigue damage and SCR oscillations based on the trenched and flat seabed, $H_{tan} = 0.3$ m and $T = 10$ s .....	339
Figure A-8. Normalized fatigue damage and SCR oscillations based on the trenched and flat seabed, $H_{tan} = 1$ m and $T = 15$ s .....	340
Figure A-9. Normalized fatigue damage and SCR oscillations based on the trenched and flat seabed, $H_{tan} = 2$ m and $T = 15$ s .....	340
Figure A-10. Normalized fatigue damage and SCR oscillations based on the trenched and flat seabed, $H_{tan} = 3.3$ m and $T = 15$ s.....	341
Figure A-11. Elimination of the sharp edge at the trench mouth.....	342
Figure A-12. Normalized fatigue damage and SCR oscillations based on the modified trench, old trench and flat seabed, $H_{tan} = 3.3$ m and $T = 15$ s .....	343

## List of Tables

Table 3-1. List of studies worked on an effective stress framework for pipe-seabed interaction .....	75
Table 3-2. Main parameters of SCR .....	87
Table 3-3. Main parameters for the effective stress analysis .....	90
Table 4-1. Summary of pipe motion scenarios used for displacement control analysis .....	125
Table 4-2. Naming of FE simulations within different shear strength properties .....	125
Table 4-3. Main Features of the current study compared to the previous works on power law coefficients .....	131
Table 4-4. Main parameters of the soil properties and SCR used for global analysis .....	136
Table 4-5. Summary of pipe motion scenarios used for load control analysis .....	139
Table 5-1. SCR model parameters (BC1 and BC2) .....	160
Table 5-2. Equivalent motion amplitudes for one scenario of motion in different linear stiffness .....	167
Table 5-3. Results of LM analysis and EMM (model case: BC1) .....	170
Table 5-4. Results of LM analysis and EMM (model case: BC2) .....	171
Table 5-5. Ranges of input parameters considered for predicting simplified equation .....	173
Table 5-6. Results obtained directly from linear soil models and proposed curve fit within the relative difference in $\Delta\sigma_{\max}$ (in BC1) .....	177
Table 5-7. Results obtained directly from linear soil models and proposed curve fit within the relative difference in $\Delta\sigma_{\max}$ (in BC2) .....	178
Table 5-8. Main parameters of BC3.....	180
Table 5-9. Results obtained directly from linear soil models and proposed equation within the relative difference in $\Delta\sigma_{\max}$ (in BC3) .....	182
Table 5-10. Manipulated wave scatter diagram for a 30 year service life in Gulf of Mexico (Shiri and Randolph, 2010).....	184
Table 5-11. Results of maximum stress range and corresponding equivalent motions through different groups of soil stiffness.....	188
Table 6-1. Main parameters of SCR .....	208
Table 6-2. Input parameters for the R-Q nonlinear soil model .....	210
Table 6-3. Comparison between HTM and the R-Q soil model in the critical point .....	218
Table 6-4. Ranges of motions amplitude for fatigue analysis.....	228
Table 7-1. Main parameters for effective stress framework used in this study.....	254
Table 7-2. Main parameters of the SCR model developed in this study.....	259
Table 7-3. Input parameters for the R-Q model.....	267



Table A-1. Input parameters for R-Q soil model ..... 334

# List of Abbreviations and Symbols

## Abbreviations

AB model	Aubeny and Biscontin soil model
ALE	arbitrary lagrangian–eulerian
API	American petroleum institute
BLM	boundary layer method
CEL	coupled eulerian lagrangian
CFD	computational fluid dynamics
CoG	center of gravity
CSM	critical state model
CSSM	critical state soil mechanics
DF	degradation Factor
DISP	user-defined boundary condition subroutine in ABAQUS
DOF	degree of freedom
DNV	Det Norske Veritas
EMM	Equivalent Motion Method
EoS	equation of state
EVF	Eulerian Volume Fraction
FEA	Finite element analysis
FE	Finite element
FOZ	far offset zone of trench
GoM	Gulf of Mexico
HTM	hybrid trench model
JIPs	Joint Industry Projects

LDFE	large deformation finite element
LM	Linear Model
MC	Mohr-Coulomb
MMC	modified Mohr-Coulomb
NCL	normal compression line
NOZ	near offset zone of trench
OCR	Over-Consolidation Ratio
PIP	Pushed-in-place
RANS	Reynolds-averaged Navier-Stokes
RAO	response amplitude operator
RITTS	re-meshing and interpolation technique with small strain
RMS	root mean square
ROV	remote operation vehicle
R-Q model	Randolph and Quiggin model
RSL	remoulded state line
SCR	steel catenary riser
SLWR	steel lazy wave riser
SS	sea state
STRIDE	steel catenary risers in deepwater environments
TBP	trench bottom point
TDP	touchdown point
TDZ	touchdown zone
TLP	tension leg platform
TSP	trench surface point
TTR	top tensioned riser

UEL	user-defined element subroutine in ABAQUS
UWAVE	user subroutine to define wave kinematics in ABAQUS
VUAMP	user-defined current amplitude subroutine in ABAQUS
VUSDFLD	user-defined field variables subroutine in ABAQUS
WA	Western Australia
WF	wave-frequency
WIP	wished-in-place

## Symbols

### Chapter 3

$q_b$	soil buoyancy forces per unit length
$q_s$	soil resistance per unit length
$q_t$	vertical resistance per unit length
$f_b$	soil buoyancy factor
$A_s$	nominal area of the pipe embedded below the seabed mudline
$D$	SCR pipe diameter
$\rho_{soil}$	saturated density of the soil
$\rho_{water}$	density of water
$s_u$	undrained shear strength of soil
$N_c$	soil bearing factor
$a$	power law coefficient
$b$	power law coefficient
$g$	gravitational acceleration
$i$	a series of user-defined elements were used along the TDZ
$z$	depth below soil surface
$\hat{z}$	normalized depth, $z/D$
$z_m$	depth of mid-height of pipe below soil surface
$\hat{z}_{i,m}$	the current vertical displacement of each user-defined element, Node <sub><i>i</i></sub> , normalized by the SCR diameter
$\lambda$	Slope of normal compression line
$\kappa$	Slope of swelling/reconsolidation line
$\hat{\eta}_i$	The current vertical location of the given soil horizon relative to each node, normalized by the diameter
$\gamma'$	Effective unit weight
$N(\hat{z}_i)$	damage accumulation of the surrounding soil
$\mu(\hat{z}_i)$	influence damage zone
$\beta$	Cycle number influence zone extent
$u(\hat{z}_i)$	excess pore pressure
$u_{max}(\hat{z}_i)$	maximum excess pore pressure

$a_u$	pore pressure component parameter
$N_{95,u1}, N_{95,u2}$	pore pressure decay rate parameters
$\sigma'_{v0}(\hat{z}_i)$	in-situ vertical effective stress
$\sigma'_{v,RSL}(\hat{z}_i)$	effective stress in the fully remoulded condition
$\left[ \frac{s_u}{\sigma'_{v0}} \right]_{NC}$	normally consolidated undrained strength ratio
$\phi(\hat{z}_i)$	lumped strength parameter
$S_{t,cycle}$	cyclic sensitivity of the soil
$\Lambda$	plastic volumetric strain ratio
$\Gamma_{NCL}$	Specific volume at $\sigma'_v = 1 \text{ kPa}$
$v$	specific volume
$v_{initial}(\hat{z}_i)$	initial specific volume
$k_\phi$	strength parameter multiplier = $OCR(\hat{z})^b$ ( $b$ is a peak strength parameter)
$\phi_{steady}$	Steady strength parameter
$N_{95,\phi}$	Peak strength ductility
$u_c(\hat{z}_i)$	current excess pore pressure
$U$	degree of dissipation
$u_0(\hat{z}_i)$	initial value of excess pore pressure
$\sigma'_v(\hat{z}_i)$	current vertical effective stress
$v(\hat{z}_i)$	strength influence zone
$s_{u,op}(\hat{z}_{i,m})$	operative undrained shear strength
$s_{u,avg}(\hat{z}_{i,m})$	average undrained shear strength
$\Delta\hat{z}_{i,m}$	change in vertical displacement from a reversal point while Node <sub>i</sub> changes its direction to uplift mode.
$\hat{z}_{mob}$	Strength mobilized distance
$t$	total elapsed time of the intervening pause period
$\Delta Z$	water depth
$A$	Cross sectional area of SCR
$I$	moment inertia
$m_s g$	submerged weight

$E$	young modulus of steel
$\theta_{HO}$	hang off angle
$EI$	bending stiffness
$E'$	Young's modulus of soil
$k$	permeability
$\nu'$	drained Poisson's ratio
$c_v$	coefficient of consolidation
$\gamma_w$	water unit weight
$\alpha$	Strength influence zone extent
$H_{tan}$	heave amplitude in the tangential direction of the local coordinate system at the SCR hang-off point
$T$	Period
$K_{sec}$	normalized unloading secant stiffness
$z_{trench}$	trench depth
$s_{u0}$	Mudline shear strength
$\rho$	Shear strength gradient
$f_{suc}$	Suction ratio (in R-Q model)
$\lambda_{suc}$	Suction decay parameter (in R-Q model)
$\lambda_{rep}$	Re-penetration parameter (in R-Q model)
$H_s$	Significant wave height
$T_p$	spectral peak period
$T$	dimensionless time factor
$d$	pipe embedment depth

#### Chapter 4

$D$	pipe diameter
$L$	pipe length
$s_{u0}$	n-situ undrained shear strength at the invert of the pipe
$s_{um}$	undrained shear strength at the mudline
$k$	strength gradient
$z$	depth of the soil horizon

$\alpha$	friction coefficient
$\tau_{max}$	maximum shear resistance
$S_t$	soil sensitivity
$\rho_w$	density of water
$\mu$	viscosity
$\dot{\gamma}_{max}$	maximum shear strain
$\xi$	accumulated absolute maximum plastic shear strain
$s_u$	undrained shear strength with incorporation of shear strain and soil softening
$\dot{\gamma}_{ref}$	reference shear strain rate
$\delta_{rem}$	the ratio of fully remoulded and initial shear strength
$\xi_{95}$	value of $\xi$ for 95% shear strength degradation
$\mu$	rate of strength increase per log cycle
$\Delta\varepsilon_1, \Delta\varepsilon_3$	major and minor principal plastic strain components
$\Delta t$	time increment
$E$	Young's modulus
$\gamma'$	effective submerged weight
$F_g$	geotechnical resistance
$F_s$	soil resistance
$F_b$	soil buoyancy force
$q_g$	geotechnical resistance per unit length
$A_s$	nominal area of the pipe embedded below the seabed mudline
$\rho_{soil}$	saturated density of the soil
$\rho_{water}$	density of water
$N_c$	soil bearing factor
$a$	power law coefficient
$b$	power law coefficient
$g$	gravitational acceleration
$i$	a series of user-defined elements were used along the TDZ
$z$	depth below soil surface



$H_{tan}$	heave amplitude in the tangential direction of the local coordinate system at the SCR hang-off point
$T$	Period

## Chapter 5

$D_o$	SCR pipe diameter
$t$	pipe thickness
$\Delta Z$	water depth
$A$	Cross sectional area of SCR
$I$	moment inertia
$m_s g$	submerged weight
$E$	young modulus of steel
$\theta_{HO}$	hang off angle
$EI$	bending stiffness
$x$	horizontal coordinates of the nodes measured from the TDP
$X_t$	horizontal offset from TDP to the hang-off point
$X_n$	normalized horizontal coordinate
$z$	vertical coordinates of the nodes measured from the TDP
$Z_n$	normalized vertical coordinate ( $z / \Delta z$ )
$L$	length of riser
$s$	arc length
$S_t$	suspended length of the riser in equilibrium condition (arc length from hang-off point to TDP)
$S_n$	normalized arc length
$k$	soil stiffness
$H$	heave amplitude in the tangential direction of the local coordinate system at the SCR hang-off point
$\Delta\sigma_{max}$	peak stress range
$H_{eq}$	Equivalent motion amplitude
$\sigma_t$	total stress
$\sigma$	axial stress

$\sigma_a$	tensile stress
$\sigma_m$	bending stress
$T_w$	wall tension of riser
$\sigma_{min}, \sigma_{max}$	minimum and maximum stress
$M$	bending moment
$N$	number of stress cycles to failure
$\bar{a}$	empirical factors for fatigue analysis
$m$	empirical factors for fatigue analysis
$\Delta\sigma$	total axial stress range
$n$	number of stress cycles
$D$	damage accumulation based on Palmgren–Miner’s rule
$arcL_{crit}$	location of peak damage
$a_1, a_2$	non-dimensional coefficients
$A_1$	coefficient
$H_N, T_N$	normalized heave amplitude and normalized period in the linear soil models
$\lambda_1, \lambda_2$	non-dimensional coefficients
$T_0$	tension of riser
$P$	unit submerged weight

### Chapter 6, Chapter 7 and Appendix

$D_o$	SCR pipe diameter
$t$	pipe thickness
$\Delta Z$	water depth
$A$	cross sectional area of SCR
$I$	moment inertia
$m_s g$	submerged weight
$E$	young modulus of steel
$\theta_{HO}$	hang off angle
$EI$	bending stiffness
$k_0$	reference stiffness

$\alpha$	depth correlation factor
$\eta$	longitudinal adjustment factor
$\hat{x}$	absolute value of the horizontal coordinate of each node from the anchored end normalized by 1 m
$z_0$	initial riser embedment under its submerged weight
$k$	linear soil stiffness
$k_{eq}$	equivalent soil stiffness
$P_u$	ultimate soil penetration resistance
$S_u$	undrained shear strength
$f_b$	soil buoyancy factor
$A_{disp}$	nominal area of the pipe embedded below the seabed mudline
$\rho_{soil}$	saturated density of the soil
$\rho_{water}$	density of water
$N_c$	soil bearing factor
$g$	gravitational acceleration
$s_{u0}$	Mud-line shear strength
$\rho$	Shear strength gradient
$a$	Power law parameter
$b$	Power law parameter
$K$	Normalized maximum stiffness
$f_{suc}$	Suction ratio
$\lambda_{suc}$	Suction decay parameter
$\lambda_{rep}$	Re-penetration parameter
$H$	heave amplitude in the tangential direction of the local coordinate system at the SCR hang-off point
$T$	Period
$\alpha_{min}$	minimum depth correlation factor
$\sigma$	axial stress
$\sigma_a$	tensile stress
$\sigma_m$	bending stress
$T_w$	wall tension of riser

$\sigma_{min}, \sigma_{max}$	minimum and maximum stress
$M$	bending moment
$N$	number of stress cycles to failure
$\bar{a}$	empirical factors for fatigue analysis
$m$	empirical factors for fatigue analysis
$\Delta\sigma$	total axial stress range
$x_{critical}$	horizontal coordinate from the critical node to the anchor point
$\Delta\sigma_{max}$	peak stress range
$z$	depth below soil surface
$\hat{z}$	normalized depth, $z/D$
$z_m$	depth of mid-height of pipe below soil surface
$\lambda$	Slope of normal compression line
$\kappa$	Slope of swelling/reconsolidation line
$\hat{\eta}$	The current vertical location of the given soil horizon relative to each node, normalized by the diameter
$\delta N(\hat{z})$	incremental cumulative damage
$\delta \hat{z}_m$	incremental embedment of the pipe
$u_1, u_2$	components of excess pore pressure ( $\Delta \hat{u}_1(\hat{z}), \Delta \hat{u}_2(\hat{z})$ ): increments)
$\gamma'$	Effective unit weight
$N(\hat{z})$	damage accumulation of the surrounding soil
$\mu(\hat{z})$	influence damage zone
$\beta$	Cycle number influence zone extent
$u(\hat{z})$	excess pore pressure
$u_{max}(\hat{z})$	maximum excess pore pressure
$a_u$	pore pressure component parameter
$N_{95,u1}, N_{95,u2}$	pore pressure decay rate parameters
$\sigma'_{v0}(\hat{z})$	in-situ vertical effective stress

$\sigma'_{v,RSL}(\hat{z})$	effective stress in the fully remoulded condition
$\left[ \frac{s_u}{\sigma'_{v0}} \right]_{NC}$	normally consolidated undrained strength ratio
$\phi(\hat{z})$	lumped strength parameter
$S_t$	soil sensitivity
$S_{t,cycle}$	cyclic sensitivity of the soil
$\Lambda$	plastic volumetric strain ratio
$\Gamma_{NCL}$	Specific volume at $\sigma'_v = 1 \text{ kPa}$
$v$	specific volume
$v_{initial}(\hat{z})$	initial specific volume
$k_\phi$	strength parameter multiplier = $OCR(\hat{z})^b$ ( $b$ is a peak strength parameter)
$\phi_{steady}$	Steady strength parameter
$N_{95,\phi}$	Peak strength ductility
$u_c$	current excess pore pressure
$U$	degree of dissipation
$u_0$	initial value of excess pore pressure
$v(\hat{z})$	strength influence zone
$\Delta v(\hat{z})$	specific volume variation
$\Delta \sigma'_v(\hat{z})$	variation in vertical effective stress
$\sigma'_v(\hat{z})$	current vertical effective stress
$\Delta u_e(\hat{z})$	pore pressure dissipation
$s_{u,avg}$	average undrained shear strength
$s_{u,op}$	operative undrained shear strength
$s_{u,initial}$	initial soil strength

$s_{u,cycle}$	soil strength during cyclic penetration and extraction
$\chi$	Lateral extent of excess pore pressure column
$\Delta\hat{z}_m$	change in pipe displacement due to a change of direction
$\hat{z}_{mob}$	Strength mobilized distance
$t$	total elapsed time of the intervening pause period
$c_v$	coefficient of consolidation
$\gamma_w$	water unit weight
$\alpha$	Strength influence zone extent
$K_{sec}$	normalized unloading secant stiffness
$s_{u0}$	Mudline shear strength
$\rho$	strength gradient
$q_g$	geotechnical resistance per unit length
$q_0$	resistance at the last point of reversal load
$z_0$	vertical coordinate of the last point of reversal load
$H_s$	Significant wave height
$T_p$	spectral peak period
$T$	dimensionless time factor

# CHAPTER 1

## Introduction

### 1.1. Overview

Deep offshore oil and gas production has experienced significant growth in the past two decades due to the depletion of onshore and nearshore hydrocarbon resources. The development of advanced technologies in the oil and gas industry has made it possible to explore and extract hydrocarbons from deep offshore fields, which are considerably larger in size compared to onshore and shallow water reservoirs. The production and transmission of hydrocarbons in deep offshore developments require sophisticated technology and careful attention to engineering capabilities and environmental impacts. Subsea risers play a crucial role in the development of deep offshore fields, facilitating the production, export, and service phases. They are typically composed of a series of interconnected pipes that extend from the seabed to the production vessel. Figure 1-1 illustrates commonly used types of risers in deep offshore fields, categorized according to the water depth and corresponding year of installation.

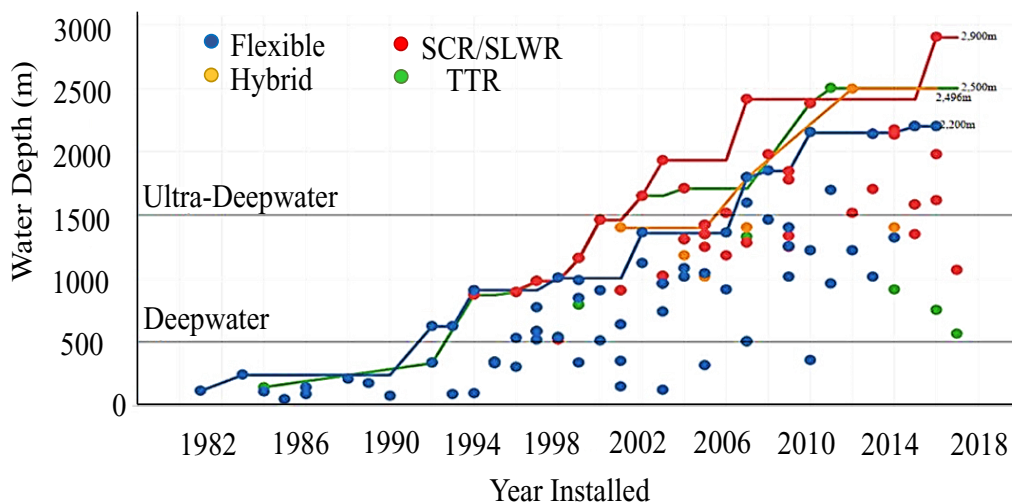


Figure 1-1. Different types of subsea risers categorized with water depth and year of installation (Offshore Magazine, May 2013)

It is worth noting that the choice of riser type depends on various factors, including water depth, environmental conditions, field characteristics, and project economics. Each type has its advantages and limitations, and the selection is typically based on a comprehensive engineering evaluation and analysis specific to the project requirements. Steel catenary risers (SCRs) are considered one of the most favourable riser options, as they consist of a connected series of welded steel pipes suspended from the platform to the seafloor. The catenary shape allows the riser to accommodate the vertical movement of the floating platform while maintaining a continuous connection to the subsea equipment. The initial SCR installation took place in the Auger field in 1994, where a 12-inch pipe was connected to a Seastar mini TLP production vessel in a water depth of 992 meters (Howells, 1995). Despite the sophisticated design procedure, SCRs often offer a more cost-effective solution for deep-water developments, requiring less material and offering simpler installation and maintenance processes compared to other types of risers, such as Top Tensioned Riser (TTR) or flexible risers. However, SCRs are susceptible to fatigue due to the dynamic and cyclic nature of the environmental and operational loads they experience. Fatigue damage accumulation in SCRs is significant in two key areas: the hang-off point where the riser is connected to the vessel, and the touchdown zone (TDZ) where the SCR interacts cyclically with the seabed soil. The latter aspect is probably the most challenging issue in SCR engineering design because of the complex riser-seabed-seawater interaction that results in a trench formation underneath the SCR and affects the fatigue life in the TDZ. Figure 1-2 depicts a schematic view of a SCR along with its key components.



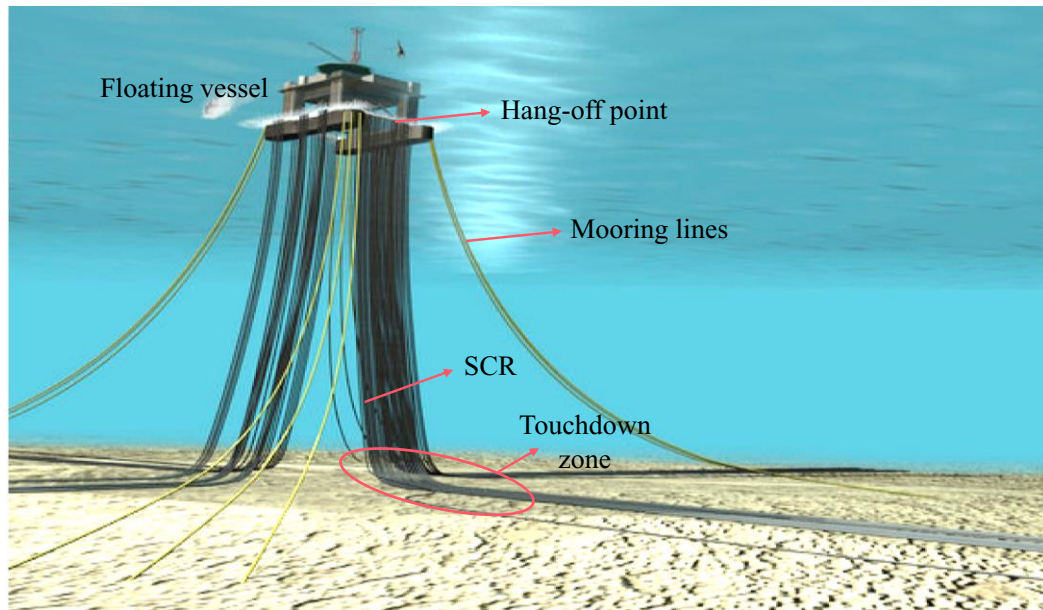


Figure 1-2. Schematic view of SCR connected to a floating system

Fatigue studies for SCRs have been traditionally carried out using linear elastic soil models, which treat the seabed as a linear spring. This approach tends to be conservative in fatigue design, potentially overestimating the fatigue damage in SCRs (Pesce, 1998). However, the initial application of SCRs in the Auger field of the Gulf of Mexico prompted the STRIDE and CARISIMA Joint Industry Projects (JIPs) (1999) to explore more advanced models that consider the complex interaction between the riser and the seabed (Campbell, 1999; Thethi and Moros, 2001). Over the past two decades, significant progress has been made in the development of non-linear soil models. These models were specifically designed to provide more accurate predictions of SCR-soil interaction, with a particular focus on fatigue assessment within the TDZ.

Despite these advancements, there are limitations and shortcomings in the existing SCR-soil interaction models, leading to challenges in accurately determining fatigue damage in the TDZ. Therefore, developing reliable methodologies for SCR-seabed interactions while addressing previous shortcomings remains a knowledge gap that necessitates further investigation. The present research project aims to fill these gaps by

establishing several problem definitions, followed by a set of research objectives that are designed to accomplish the primary goals of the study.

## 1.2. Problem Definition

Figure 1-3 illustrates an overview of the knowledge gaps associated with the SCR-seabed interaction model that have been explored in the present research. Each item has been thoroughly discussed to provide detailed insights.

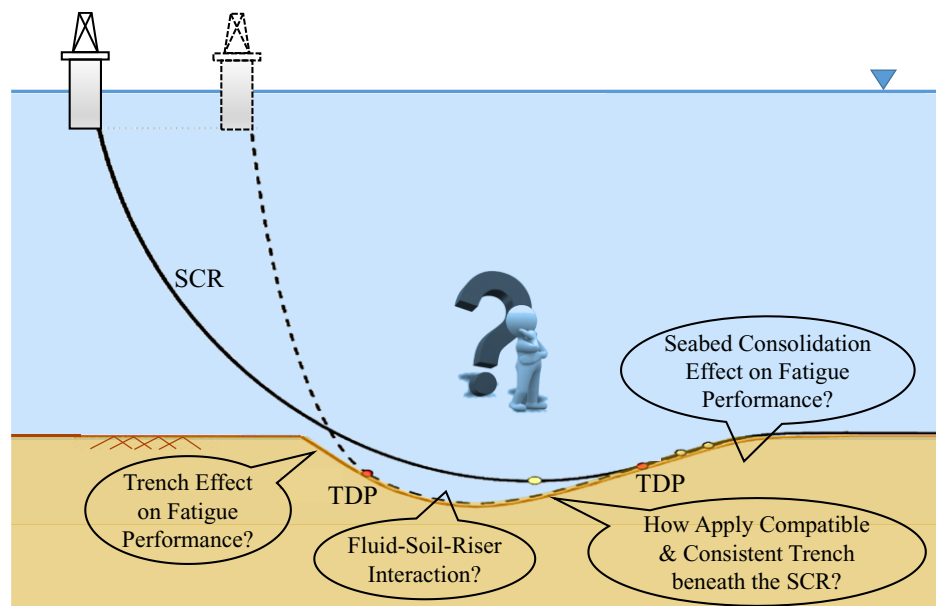


Figure 1-3. Demonstrating the knowledge gaps conducted in the current study

### 1.2.1. Consolidation Effect

Cyclic motions of a catenary riser commonly occur at a rate that induces an undrained shearing of the surrounding soil, resulting in the progressive generation of excess pore water pressure. This causes a reduction in effective stress and consequently results in progressive seabed soil degradation. Over a long time of riser operations, the surrounding soil undergoes a drainage condition. This is primarily attributed to the minimal movements within the TDZ, such as small motion amplitudes of steel catenary risers during calm weather conditions or limited TDZ movements in steel lazy wave

risers (SLWRs) as a result of their lazy wave configuration. During the inactivity period, the gradual dissipation of excess pore water pressure through the seabed soil leads to a consolidation process. This process results in the regain of soil stiffness or strength, which is not captured by the existing advanced non-linear soil models with hysteretic load-displacement behaviour that have been used for global riser analysis. This overlooked consolidation effect on soil strength in existing design practices may lead to underestimating fatigue damage, emphasizing the need to address knowledge gaps in this study area.

### **1.2.2. Riser-Seabed-Seawater Interaction**

In reality, cyclic soil remoulding and consolidation are not the sole mechanisms responsible for riser embedment in the TDZ. Additional mechanisms, such as seabed erosion caused by combined vortices generated by subsea currents and the entrapment of water fluid between the oscillating riser and the trench, can also contribute to increased riser embedment by scraping the seabed soil. Recent advancements have led to the development of advanced non-linear hysteretic riser-soil interaction models, which enable the simulation of soil remoulding influenced by cyclic riser oscillations. However, these models typically focus on two domains of interaction – the soil and the riser – while neglecting the contribution of seawater surrounding the riser as a third influential factor. To enhance the understanding of SCR's fatigue, it is crucial to develop more accurate models that incorporate these three domains and simulate the riser-seabed-seawater interaction comprehensively.

### **1.2.3. Incorporation of Trench Effect**

As observed by remote operating vehicles (ROV), the trench formation under the SCR is mostly developed during the early stages of the riser operation life, first 2-3 years,

and ultimately reaches several diameters deep, e.g.,  $3.5D$  to  $7D$  where  $D$  is the pipe diameter (Bridge and Howells, 2007). Over the past two decades, extensive research has established the significance of trench formation in influencing the fatigue response of SCRs in the TDZ, utilizing various methodologies. However, a challenging question has arisen regarding whether the trench formation ultimately benefits or detrimentally affects the fatigue life of SCRs. While certain studies have reported results indicating improved or reduced fatigue life due to trench formation, there is still no coherent agreement between them. The current research aims to identify the reasons behind the contradictory results regarding the effect of the trench on SCR fatigue life and propose robust and novel methodologies to address these issues, ensuring reliable incorporation of trench formation beneath the SCR.

### **1.3. UEL Subroutines**

The UEL subroutines developed in the current research work can be summarized as follows:

In Chapter 3, an UEL subroutine was developed to implement effective stress analysis based on critical state soil mechanics. This subroutine was utilized to account for both remoulding and consolidation effects in a global analysis of the SCR.

In Chapter 4, another UEL subroutine was developed to model advanced non-linear soil behavior, the model developed by Randolph and Quiggin in 2009. This subroutine was employed to determine the maximum load limit, which served as input for the subsequent local CEL analysis of SCR-soil-seawater interaction.

In Chapter 6, the trench hybrid model (HTM) was proposed using an equivalent soil stiffness parameter that was integrated into the UEL subroutine. This innovative

technique was applied to reliably simulate trench formation underneath the SCR, addressing challenges previously reported in the literature.

In Chapter 7, the subroutines developed in earlier chapters were combined to consider both consolidation and trench effects, providing a comprehensive analysis of SCR behavior.

#### **1.4. Research Objectives**

The short-term objectives of this research project were as follows:

- (i) Incorporate the seabed soil consolidation effects into the global SCR analysis using an effective stress framework to investigate the influence of consolidation on riser fatigue life in the touchdown zone.
- (ii) Incorporate the riser-seabed-seawater interaction effects into the trench formation and plastic soil deformations under an oscillating riser.
- (iii) Develop new methodologies to incorporate the trench effect into the fatigue analysis of the SCR and resolve the drawback of existing models.
- (iv) Investigate the effect of different trenched seabed on the fatigue life of SCR in TDZ in presence of the consolidation.

The long-term objective of the current research is to improve the safety, integrity, and cost-effective practice for fatigue life extension of SCRs.

#### **1.5. Organization of the Thesis**

The present doctoral thesis comprises eight chapters, consisting of five journal papers (three of which have been published, and two are currently under-review by two journals) and one Appendix, which includes a peer-reviewed conference paper. Chapter 1 presents an introduction to the topic, along with a discussion on the significance, novelty, and motivation behind the conducted research work. Chapter 2 summarizes the

literature review focusing on the SCR-seabed interaction models, recent advancements, and fatigue performance of SCR in the TDZ. Moreover, a more targeted literature review was included in each chapter to facilitate conveying the message of each paper. Chapter 3, which is an under-review journal paper, presents a time-dependent riser-seabed interaction model that incorporates the effective stress framework and consolidation effects into the fatigue analysis of SCR. Chapter 4, which is another under-review journal paper, has focused on modeling the riser-seabed-seawater interaction effects using a large deformation Coupled Eulerian-Lagrangian (CEL) approach. This chapter investigates the seawater flow infiltrating underneath the SCR and causing excess pressure build-up that leads to erosion and is further exacerbated by lateral pipe oscillations. Chapter 5, which is a journal paper published in Applied Ocean Research, presents a new methodology called the Equivalent Motion Method (EMM) to introduce an alternative vessel excitation algorithm facilitating the incorporation of the trench effect in SCR fatigue analysis. The proposed methodology uses a rigid seabed to achieve a target peak damage, which is derived from the same riser on a linear elastic seabed. Chapter 6 presents a journal paper published in Canadian Geotechnical Journal, where a methodology called the Hybrid Trench Model (HTM) was developed to incorporate the trench effect into the fatigue analysis of SCR. By providing an equivalent stiffness distribution in the TDZ, the HTM ensures compatibility between the trench profile and the catenary shape of the SCR. This simplified alternative solution aimed to incorporate the trench effect into the SCR fatigue analysis in the TDZ and resolve the issue of pressure hot spots and premature stabilizations repeatedly reported in the literature. Chapter 7, which is a journal paper published in Computers and Geotechnics, investigates the trench effect on SCR fatigue life in the presence of

consolidation effects. This chapter combines the findings of Chapter 3 and Chapter 6 to perform the investigation. Chapter 8 summarizes the key findings of the study and the recommendations for future studies. Appendix A includes a conference paper, presented in the 33<sup>rd</sup> International Ocean and Polar Engineering Conference, Ottawa, Canada, June 19–23, 2023. The paper further discusses the findings of Chapter 6.

## **1.6. Thesis outcomes**

The research work conducted in this study resulted in some new developments and novel methodologies that can be used for enhanced assessment of the SCR-seabed-seawater interaction on riser fatigue performance in the TDZ. The findings of the study offers valuable insight for engineers who are designing the SCRs and working on riser life extension. The results obtained from the study can effectively contribute to the optimization of SCR design, accurate fatigue life assessment, and the development of effective damage mitigation strategies resulting in enhanced safety and integrity of SCRs. The outcomes of the current research work were published by or are under review by high-impact top-notch ISI journals and peer-reviewed conference as outline below:

- Janbazi, H., Shiri, H., 2023. Incorporation of seabed soil effective stress analysis into the numerical modeling of the steel catenary riser accounting for soil remoulding and reconsolidation effect, *Géotechnique* (Under review).
- Janbazi, H., Shiri, H., 2023. Incorporation of the riser-seabed-seawater interaction effect into the trench formation beneath the steel catenary riser in the touchdown zone, *Ocean Engineering* (Under review).
- Janbazi, H., Shiri, H., 2022. An alternative vessel excitation algorithm to incorporate the trench effect into the fatigue analysis of steel catenary risers in the touchdown zone, *Applied Ocean Research*, 126-103292.

- Janbazi, H., Shiri, H., 2022. A hybrid model to simulate the trench effect on the fatigue analysis of steel catenary risers in the touchdown zone, *Canadian Geotechnical Journal*, <https://doi.org/10.1139/cgj-2022-0103>.
- Janbazi, H., Shiri, H., 2023. Investigation of trench effect on fatigue response of steel catenary risers using an effective stress analysis, *Computers & Geotechnics Journal*, 160-105506.
- Janbazi, H., Shiri, H., 2023. Incorporation of the consistent trench into the SCR fatigue performance by using an equivalent soil stiffness methodology, 33<sup>rd</sup> International Ocean and Polar Engineering Conference (ISOPE), Ottawa, Canada, June 19–23, 2023.

## References

Bridge, C., Howells, H. (2007). “Observations and modeling of steel catenary riser trenches.” In: The seventeenth international offshore and polar engineering conference, ISOPE 2007, Lisbon, Portugal, 803–13.

Campbell, M. (1999). “The Complexities of Fatigue Analysis for Deepwater Risers.” Deepwater Pipeline Conference, New Orleans, USA.

Howells H. (1995). “Advances in Steel Catenary Riser Design.” 2H OffShore Engineering Ltd, Surrey.

“Deepwater field developments”, *Offshore Magazine*, May 2013.

Pesce, C. P., Aranha, J. A. P., and Martins, C. A. (1998). “The Soil Rigidity Effect in the Touchdown Boundary-Layer of a Catenary Riser: Static Problem.” Eighth International Offshore and Polar Engineering Conference, Montreal, Canada, 207-213.



Thethi, R., Moros, T. (2001). "Soil interaction effects on simple catenary riser response." Deepwater Pipeline and Riser Technology Conference, Houston, Texas, USA.

## **CHAPTER 2**

### **Literature Review**

#### **2.1. Overview**

Since the thesis is manuscript-based, each chapter has its independent literature review. However, a summary of the literature review has been included within this chapter to facilitate reading the thesis.

#### **2.2. Literature Review**

##### **2.2.1. Steel Catenary Riser Mechanism**

Steel Catenary Risers (SCRs) are extensively employed in offshore field development for the transportation of hydrocarbons from the seabed to floating facilities. These commonly utilized risers are constructed using thick-walled steel pipes and are connected to the floating facilities through a specialized flexible joint known as a "flexjoint", as specified in API-RP-2RD (2013). SCRs are hanging in a catenary shape from the floating vessel to the seabed, providing a technically feasible and commercially efficient solution, especially when high pressure and temperature are involved (Phifer et al., 1994; Quintin et al., 2007). The initial implementation of a steel catenary riser can be observed in the Gulf of Mexico with the installation of the Auger export pipeline, which was supported by Shell's tension leg platform (TLP) (Phifer et al., 1994; Howells, 1995). SCRs offer numerous advantages, including their compatibility with various floating systems across different water depths and geographical zones, their ability to withstand harsh operating environments, their elimination of the need for heave motion compensation, and their avoidance of special subsea connections. These inherent benefits have contributed to the widespread adoption of SCRs as a preferred solution in

the development of deepwater offshore fields. Ensuring the safe operation of SCRs throughout their intended service life is of paramount importance. The integrity and design conditions of the SCRs are significantly influenced by the assessment of riser-seabed interaction in the touchdown zone (TDZ).

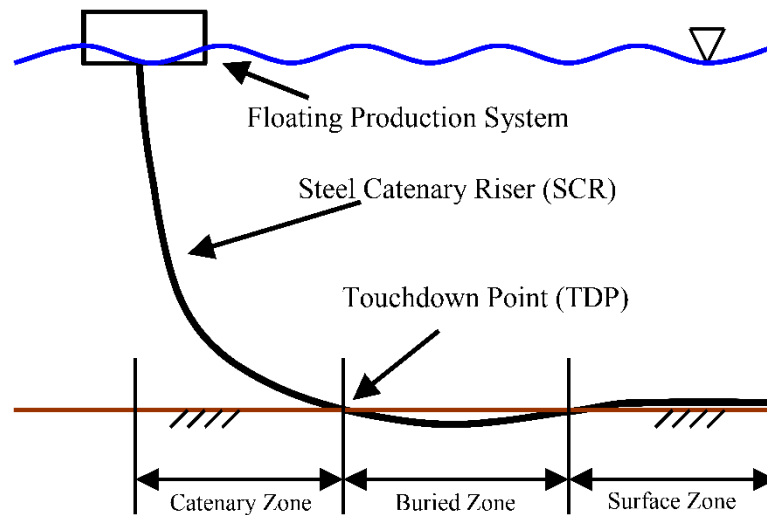


Figure 2-1. SCR general arrangement (Bridge, 2005)

This complex assessment directly impacts the SCR's overall design, encompassing both ultimate and fatigue limit states. The ultimate limit state of SCRs involves evaluating their response to extreme environmental loads, potential mooring system failure, and out-of-plane motions. In this scenario, the lateral soil resistance exerted on the riser can lead to excessive bending and tensile stresses. These stresses are attributed to both the partial embedment of the riser and the formation of a trench caused by riser oscillations. The fatigue limit state of steel catenary risers pertains to the cyclic bending stress experienced by the riser, particularly in the TDZ where the riser repeatedly makes contact with the seabed. The magnitude of stress variations induced by bending is closely influenced by the distribution of shear forces across the TDZ. The current study specifically investigates this area to gain insights into its behavior and characteristics.

### **2.2.2. Riser-Seabed Interaction**

The design of SCRs is significantly influenced by their fatigue performance in the TDZ, which is the region where the risers undergo repeated contact with the seabed due to cyclic environmental loading, including wind and waves (Campbell M. 1999, Larsen and Halse 1997). Riser-seabed interaction holds significant importance from various perspectives, encompassing aspects such as static embedment, mobilization of lateral and axial friction, on-bottom stability, self-burial, liquefaction surrounding the pipeline, sediment transport, heat transfer, response to submarine slides, ploughing, and trenching. These diverse factors collectively contribute to the understanding and analysis of the interaction between the riser and the seabed, ensuring the integrity and operational effectiveness of the system in offshore environments. However, the vertical interaction between the riser and the seabed, leading to cyclic degradation of seabed soil stiffness and the gradual formation of a trench, is the most critical factor in terms of the ultimate fatigue life (Cathie et al. 2005, Randolph and White 2008). There are two primary strategies for modeling riser-seabed interaction: simplified beam-spring models and constitutive soil models combined with various numerical approaches. The latter approach offers higher accuracy but also entails a higher computational cost. As a result, this approach may be less appealing for industrial applications due to the increased computational effort required, especially in coupled analyses. However, using the constitutive soil models with appropriate numerical approaches can serve as a strong tool for investigating various aspects of riser-seabed interaction mechanisms through research projects. The beam-spring strategy represents the soil response using simple springs. From a geotechnical perspective, this approach can be seen as an oversimplification since certain soil characteristics like dilatation and creep are not

adequately captured during the soil discretization process. However, despite these limitations, the beam-spring approach offers a substantial reduction in computational cost without significant loss of accuracy, especially when the soil stiffness parameters are appropriately adjusted. The simplicity and reasonably acceptable accuracy of the beam-spring method have led to its widespread application across various design challenges in the industry.

Fatigue studies for SCRs have been traditionally carried out using linear elastic soil (API-ST-2RD 2013; DNV-RP-F204; Pesce, 1998). In this approach, the seabed is simplified as a linear spring, which can lead to a conservative perspective on fatigue design. The introduction of SCR technology in the Auger field of the Gulf of Mexico triggered further investigation into the riser-seabed interaction. This led to the initiation of the STRIDE and CARISIMA Joint Industry Projects (JIPs) by 2H Offshore Engineering Ltd from 1999 to 2004. The primary objective of these JIPs was to explore the need for advanced models that accurately capture the complex interaction between the riser and the seabed, highlighting the importance of improving the understanding and analysis of this critical aspect. Bridge and Willis (2002) conducted a study on a specific steel catenary riser, which was 110 meters long and had a diameter of 168.3 mm. To replicate vessel motions, they employed an actuator within a harbor area. The purpose of their research was to investigate the behavior of riser-soil interaction, utilizing soil parameters similar to those found in the Gulf of Mexico. Additionally, Bridge et al. (2004) presented state-of-the-art models in their work, incorporating published data and experimental findings from the STRIDE and CARISIMA Joint Industry Projects (JIPs). Their contributions advanced the understanding and modeling of vertical riser-seabed interaction, further enhancing the knowledge base in this area.

Aubeny et al., (2005) conducted a study focusing on the collapse load of a cylinder embedded in cohesive soil. Their research aimed to propose simplified equations that could effectively model the trench effect in fatigue analysis. Aubeny and Biscontin (2008) (AB model) developed a closed hysteretic loop model that effectively simulated the non-linear behaviour of soil, addressing the limitations of previous models by incorporating cyclic softening through unloading and re-loading paths. Aubeny and Biscontin (2009) introduced a simplified model that comprises four equations to represent the characteristics of the soil springs during each load cycle. The first equation represents the intact soil response as a backbone curve. The second equation accounts for elastic rebound, simulating the soil's response during the uplift process of the SCR. The third equation captures the partial separation between the riser and soil during the uplift episode until complete detachment. Finally, a reloading curve models the re-penetration of the riser into the disturbed soil. Additional intermediate equations are employed to model the local load cycles. The proposed model was further improved by Nakhaee and Zhang to represent the trench formation (Nakhaei and Zhang, 2008). They conducted a numerical study that focused on incorporating the gradual degradation of seabed soil stiffness and cyclic riser embedment through two different riser configurations. They enhanced a numerical code to accurately capture stiffness degradation resulting from cyclic loading. The study specifically considered wave-frequency vessel motions and obtained maximum penetration depths of approximately  $0.4D$  and  $0.8D$ , where  $D$  represents the riser diameter. The authors observed a cyclic reduction in the maximum variation of the bending moment and concluded that trench formation enhances the fatigue life in the vicinity of the TDZ. Randolph and Quiggin (2009) used a combination of hyperbolic and exponential functions within four main

episodes of riser-seabed cyclic contact: initial penetration, uplift, separation, and re-penetration, to simulate hysteretic soil behaviour under a vertical oscillating riser (see Figure 2-2).

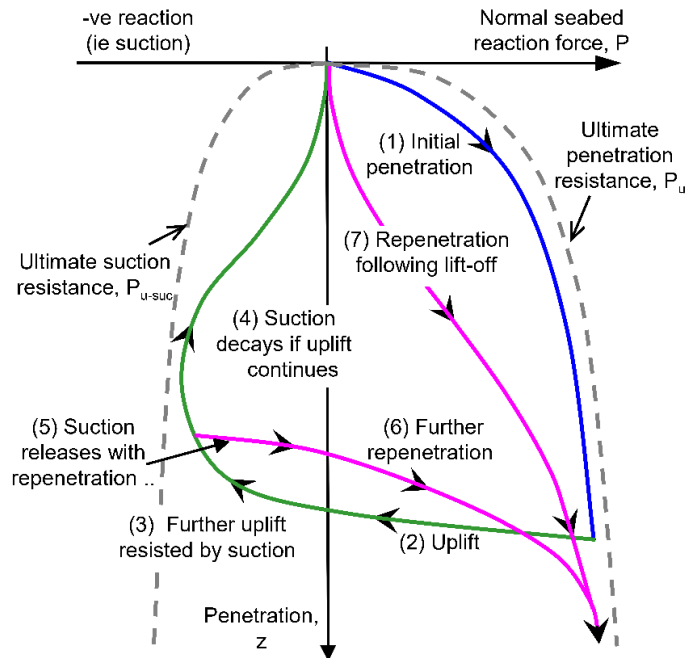


Figure 2-2. Non-linear soil model characteristics developed by Randolph and Quiggin (2009)

This model was implemented in a commercial riser analysis program, OrcaFlex (Orcina 2010), and also coded through user-defined element subroutine (UEL) within the ABAQUS software to explore the pros and cons for future developments (Shiri, 2010). Elliot et al., (2013a) designed and developed an apparatus specifically for modeling the interaction between the riser and the soil in centrifuge tests. The objective was to create a realistic experimental setup that could accurately replicate the riser-soil interaction. The performance and functionality of the apparatus were thoroughly validated through a series of tests conducted on an elastic seabed. Additionally, numerical analysis was employed to further validate the results obtained from the experimental setup. This comprehensive validation process ensures the reliability and accuracy of the apparatus for studying and understanding the riser-soil interaction phenomenon.

Clukey et al., (2017) assessed the state-of-the-art review of the riser-seabed interaction. Their analysis indicated that improved modeling techniques and understanding of riser-seabed interaction, particularly in the TDZ, have the potential to significantly enhance the fatigue life of risers in the TDZ. Zargar et al., (2019) made significant advancements by developing an improved version of the R-Q model. The enhanced model incorporates a secondary non-linear mechanism and utilizes a unified mathematical approach to capture various modes of soil-riser interaction. Notably, the model introduces an explicit degradation model to accurately represent the behavior of the soil. It also allows for the incorporation of variable parameters based on riser penetration rates and depth. Dong and Shiri (2018, 2019) evaluated the nodal and global performance of the R-Q model, which aims to simulate the behavior of riser-seabed interaction. They found that while the model did not explicitly replicate realistic trench formation, it still served as a robust tool for non-linear seabed simulation.

### **2.2.3. Consolidation Effect**

Advanced non-linear hysteretic soil models used for representing the riser-seabed interaction are mainly based on the total stress approach, accounting for soil strength degradation in an undrained condition (Aubeny and Biscontin, 2008; Randolph and Quiggin, 2009; Clukey and Zakeri, 2017b; Zargar et al., 2019). However, over a long time, soil might be undergoing a drainage condition over a long-term operation of a SCR, which comes from several factors: e.g., small motion amplitudes due to calm weather or changes in wave directions (Clukey et al., 2017; Al-Janabi et al., 2019), as well as limited contact with the seabed resulting from vessel repositioning according to the vessel relocation plan (Zhao et al., 2015; Ogbeifun et al., 2021 and 2022). This minimal disturbance in the soil allows a gradual dissipation of the excess pore water



pressure through the seabed (Hodder et al., 2009; Chatterjee et al., 2013; Clukey and Zakeri, 2017b; Yuan et al., 2017; Hou et al., 2018; Zhou et al., 2020). The significance of reconsolidation on soil strength has been accepted in the literature by conducting different numerical modelling and centrifuge model tests. These studies have shown that the long-term pipe-seabed stiffness gradually increases (Hodder et al., 2009; Elliot et al., 2013b; Yuan et al., 2017; Zhou et al., 2019). It is noted that some works showed low values for normalized stiffness even after wait periods (Clukey et al., 2005; Clukey et al., 2008). It is worth noting that the existing advanced hysteretic non-linear riser-seabed interaction models do not account for the consolidation effects. To address this limitation, certain studies employed an effective stress framework to capture both remoulding and reconsolidation effects within shortened segment of the pipe. This framework is based on the critical state soil mechanics (CSSM) in which the undrained shear strength is linked to the current specific volume of the one-dimensional column of the soil elements (Palmer, 1997). The applicability of this framework was highlighted by White and Hodder, 2010, including three episodes of cyclic undrained loading of a penetrometer within intervening pause periods between the episodes to consider the reconsolidation effects. Accordingly, a series of T-bar model tests were used to examine the validation of the proposed framework, which was found in good functionality both in terms of soil degradation and reconsolidation (White and Hodder et al., 2010; Hodder et al., 2009 and 2013). Due to the continuous nature of actual loading rather than episodic, more investigations were conducted later (Zhou et al., 2020), and results showed that the framework was able to predict long-term pipe-seabed stiffness with reasonable accuracy relative to the centrifuge tests (Yuan et al., 2017). While the proposed framework represents a significant advancement in incorporating the

consolidation effect into pipe-soil interaction, its applicability for the global analysis of risers along the entire length in the TDZ remains a knowledge gap that has been addressed in the present research work.

#### **2.2.4. Pipe-Seabed-Seawater Interaction**

The significance of three-domain fluid-pipe-soil interaction has been examined in the literature, particularly emphasizing the occurrence of scour beneath the subsea structures. Lucassen (1984) conducted a series of experiments focusing on a limited range of wave and current conditions to study scour depth. Leeuwestein et al. (1985) conducted research on the natural self-burial of pipelines, focusing on identifying key mechanisms that contribute to the lowering of the pipeline. They highlighted two significant mechanisms: midspan sagging and span shoulder collapse, which become more pronounced as the span length increases. Mao (1986) conducted experiments to investigate the formation of scour caused by current in two different flow regimes: clear-water and live-bed conditions. These experiments serve as a valuable benchmark due to the availability of scour profiles at various stages of development, allowing for a comprehensive comparison between the simulated and observed scour processes and progression. Mao (1986) presents results for current-induced scour with a pipeline diameter of 0.1 m and a sediment grain size of 0.36 mm. Staub and Bijker (1990) conducted extensive observations of pipeline burial in the Dutch sector of the North Sea. They made extensive observations and proposed models for predicting pipeline burial. Their research included a significant focus on natural backfilling, which refers to the process where the eroded hole upstream of the pipeline gradually captures sediment as the pipeline sinks deeper. This phenomenon highlights the importance of understanding the dynamics of sediment capture and backfilling in predicting pipeline

burial. The subject of natural backfilling of pipelines has also been experimentally investigated by Sumer and Fredsoe (1993). Their study confirmed the significance of pipe sinking at the span shoulders in the backfilling process. However, the study did not provide quantified models for the rate of backfilling. Moreover, Sumer and Fredsøe (1996) extended the scope of investigation by conducting comprehensive research on scour depth, considering a wider range of combined wave and current conditions. Myrhaug et al. (2009) specifically examined the scour depth below pipelines caused by the combined effect of second-order random waves and currents. Their study aimed to understand the influence of these combined forces on scour development.

On the other hand, Cheng et al. (2014) conducted research on the propagation speed of scour along the length of pipelines. Their investigation focused on determining how scour develops and progresses over time, providing insights into the dynamics and characteristics of scour propagation in pipeline systems. Recent advancements in numerical approaches have focused on investigating the backfilling of scour holes around subsea pipelines. Notable studies in this area include the work conducted by Fuhrman et al., (2014) and Sumer et al., (2014). These studies utilize RANS (Reynolds-averaged Navier-Stokes) CFD (Computational Fluid Dynamics)-based models that incorporate morphodynamic models to account for the evolution of soil profiles through sediment transport. By integrating these models, these numerical approaches have the capability to capture both the scouring process and the subsequent sedimentation, enabling a more comprehensive understanding of the backfilling phenomenon around subsea pipelines. Fuyu et al., (2015) conducted the concept of a shear-stress shadow, which refers to a region of reduced shear stress, has been utilized to analyze the likelihood of sediment accumulation within an arbitrary “control volume” surrounding

a pipeline located near the bed. This approach allows for the assessment of the potential for sediment deposition in the vicinity of the pipeline based on the variations in shear stress caused by the pipeline's presence. Draper et al., (2015) utilized a recirculating O-Tube flume at a scale of approximately 1:1 to conduct experimental investigations on pipeline stability during the development stage of a storm. The stability of a 196 mm pipeline was directly assessed in the case of a sinking pipeline, while hydrodynamic forces were measured to interpret stability for a sagging pipeline. The experimental focus was on examining the rate at which storm velocities increase (specifically for sinking pipelines) and the rate at which the pipeline lowers (specifically for sagging pipelines). The objective was to understand the impact of these rates on the stability of the pipeline when situated on a mobile seabed.

However, the majority of these studies have primarily focused on considering seabed soil as either an impermeable wall (Li and Cheng, 2000, 2001; Liang and Cheng, 2005a; Smith and Foster, 2005; Brørs, 1999; Fuhrman et al., 2014; Larsen et al., 2016) or a medium porous material (Liang et al., 2005b; Lu and Chiew, 2007; Lu et al., 2008; Li et al., 2013; Tom et al., 2018; Li et al., 2020), while only a limited number of studies have specifically investigated the influence of water fluid on low porosity soils, such as clay. In order to address this gap, several studies have numerically investigated the three-domain pipe-soil-fluid interaction using cohesive soil models. These investigations revealed notable variations in soil resistance, especially during the suction mode, and a reduction in soil stiffness when water was considered (Clukey et al., 2008; Fouzder et al., 2012). The significance of water fluid entrainment was investigated through physical modelling experiments conducted at the University of Western Australia, utilizing various scenarios of vertical pipe motions within centrifuge

model tests using Kaolin clay. The results obtained from these tests revealed that water entrainment could lead to an additional reduction in soil strength, accelerating soil degradation by a factor of approximately 1.6 (Yuan et al., 2017). Subsequent research studies have drawn inspiration from these experiments and have made adjustments to soil properties by considering higher soil sensitivity to incorporate the effects of fluid in the degradation of clay soils (Zhou et al., 2020). Although some studies have examined the impact of water fluid on cohesive soil, there is a need for further investigations to address the gaps in knowledge related to sediment transport during riser oscillations and the evolution of trench morphology within a comprehensive three-domain analysis.



Figure 2-3. SCR-seabed-seawater interaction observed in SCR full scale test, Watchet Harbor, UK (Bridge & Willis, 2002)

### **2.2.5. Incorporation of Trench Effect**

Shiri and Randolph (2010) incorporated the non-linear hysteretic riser-seabed interaction model proposed by Randolph and Quiggin into a comprehensive fatigue analysis. The authors developed a methodology to automatically account for the trenching effect in fatigue analysis. The study concluded that deeper trenches result in increased fatigue damage, and as trench formation gradually occurs, the location of peak fatigue damage shifts closer to the vessel. Elliot et al. (2013b) utilized the previously developed apparatus to investigate the influence of gradual trench formation caused by cyclic riser motions on the fatigue life in the touchdown zone (TDZ). The researchers

focused on obtaining the time-domain variation of the bending moment at various locations along a truncated riser. By analyzing these variations, they were able to draw conclusions regarding the impact of trench formation on the fatigue life of steel catenary risers (SCRs). The study ultimately indicated that trench formation has the potential to improve the fatigue life of SCR systems. In the analysis conducted by Shiri (2014a), the R-Q model was implemented into the ABAQUS software to investigate riser-seabed interaction. The study focused on capturing the gradual development of a trench in the TDZ by simulating the cyclic degradation of seabed stiffness. The author examined the possibility of artificially inserting a trench into the TDZ and highlighted the associated risks. The findings revealed incompatibilities between the natural catenary profile of the SCR and the inserted trench profile, particularly at the trench mouth. This suggests that artificially inserting a trench in the TDZ can introduce significant challenges and risks to the integrity and performance of the SCR system. The author expanded the work by proposing two linear and quadratic-exponential equations to simulate the trench profile in the TDZ (Shiri, 2014b).

In summary, the incorporation of a trench effect into fatigue analysis of SCR within the TDZ has been investigated through two primary approaches: a) insertion of a mathematically expressed trench profile in the TDZ (e.g., Langner, 2003; Li and Low, 2012; Randolph et al., 2013; Shiri, 2014b; Wang et al., 2016), b) automatic trench formation using non-linear hysteretic riser-seabed interaction models (e.g., Nakhaei and Zhang, 2008; Shiri and Randolph, 2010, Shiri 2014a).

In the first approach, the predefined geometry of the trench is mathematically implemented beneath the SCR. Accordingly, Langner (2003) proposed a trench profile based on the circular arc on the SCR side of the trench and a seventh-order polynomial

fit to the anchor side of the trench, and Shiri (2014b) examined linear and quadratic exponential functions to generate the trench profile with a desired depth. This mathematical trench insertion leads to contact pressure hotspots and the distortion of the damage profile in the touchdown zone (Shoghi and Shiri 2019, 2020). Randolph et al., (2013) resolved this issue by proposing a new approach called Stepped method. Although this methodology could improve the situation, the contact hotspot was not completely eliminated particularly in the trench mouth where the trench profile makes a relatively sharp angle with the original flat seabed towards the vessel. Alternatively, the trench formation was created within non-linear soil models to resolve any potential hotspot contacts along the TDZ. The nonlinear riser-seabed interaction models such as one proposed by Randolph and Quiggin (2009), called R-Q hereafter, have been used as an alternative solution for cyclic development of trench that prevents forming mismatch between the SCR catenary shape and the seabed in the TDZ. However, studies (e.g., Hejazi and Kimiaei, 2016; Dong and Shiri, 2018) have shown that the ultimate trench is stabilized prematurely through a few cycles, somewhere in between 0.5D to 1D penetration, which is much less than the ranges of 5D trenches observed in the field (Bridge and Howells, 2007). To resolve this limitation, Shiri and Randolph (2010) used extreme values for the non-linear soil model parameters through different analysis steps to push the SCR down the seabed artificially and achieve the target trench depths. However, the strategy was ended to some inconsistencies in created trench profiles as further discussed by Dong and Shiri (2019). The investigation of the trench effect into the fatigue performance of SCR has been mostly conducted based on the mentioned methodologies. However, the beneficial or detrimental effect of the trench is still a point of question that has not been coherently answered by the researchers. Some of the



studies have shown the fatigue life improvement in TDZ due to trench formation (e.g., Langner, 2003; Nakhaei and Zhang, 2008; Sharma and Aubeny, 2011; Elliot et al., 2013b; Randolph et al., 2013; Wang et al., 2016), while other studies have shown a reduced fatigue life (e.g., Giertsen, 2004; Leira, 2004; Shiri and Randolph 2010; Rezazadeh et al., 2012; Shiri, 2014a, b; Zargar 2017). In addition, some studies have obtained scattered results showing improved or reduced fatigue life because of the trench formation (Randolph et al., 2013; Dong and Shiri, 2019; Shoghi and Shiri, 2020). Shoghi and Shiri (2020) conducted a qualitative assessment of the trench effect based on the results reported in the literature and showed that some of these contradictory results are related to the methodology used to implement the trench profile underneath the riser. Considering the above, reliable incorporation of the trench effect in the SCR fatigue analysis through the simplified approaches remains a knowledge gap and needs further investigation.

## **References**

- Al-Janabi, H.A., Aubeny, C.P., Chen, J., and Luo, M. (2019). “Experimental measurement of touchdown zone stiffness for SCR in Gulf of Mexico clay.” In Offshore Technology Conference, 6–9 May, OTC-29504-MS, Houston, Texas, USA.
- API-STD-2RD. (2013). “Standard for riser systems that are part of a floating production system (FPS).” American Petroleum Institute, Washington, DC, USA.
- Aubeny, C. P., Shi, H., and Myrff, J. D. (2005). “Collapse loads for a cylinder embedded in trench in cohesive soil.” *International Journal of Geomechanics*, ASCE, 5(4), 320-325.
- Aubeny, C., and Biscontin, G., (2008). “Interaction model for Steel Compliant Riser on Soft Seabed.” OTC194193, Houston, TX.

- Aubeny, C., and Biscontin, G., (2009). "Seafloor-Riser Interaction Model." *International Journal of Geomechanics* 9(3), 133–141.
- Bridge, C. (2005). "Effects of seabed interaction on steel catenary risers." (Ph.D. thesis). University of Surrey.
- Bridge, C., and Willis, N. (2002), "Steel Catenary Risers—Results and Conclusions from Large Scale Simulations of Seabed Interaction." 14<sup>th</sup> Annual Conference Deep Offshore Technology, Cape Town, South Africa, 40-60.
- Bridge, C., Howells, H. (2007). "Observations and modeling of steel catenary riser trenches." In: The seventeenth international offshore and polar engineering conference, ISOPE 2007, Lisbon, Portugal.
- Bridge, C., Laver, K., Clukey, E., and Evans, T. (2004). "Steel Catenary Riser Touchdown Point Vertical Interaction Models." Offshore Technology Conference, Houston, Texas, USA, OTC16628.
- Brørs, B., 1999. "Numerical modeling of flow and scour at pipelines." *J. Hydraul. Eng.* 125, 511–523.
- Campbell, M. (1999). "The Complexities of Fatigue Analysis for Deepwater Risers." Deepwater Pipeline Conference, New Orleans, USA.
- Clukey, E., Jacobs, P., and Sharma, P.P. (2008) "Investigation of riser seafloor interaction using explicit finite element methods." Offshore Technology Conference, Houston, Texas, OTC19432-MS.
- Clukey, E.C., Zakeri, A., (2017). "Recent Advances in Nonlinear Soil Models for Fatigue Evaluation of Steel Catenary Risers SCRs." Offshore Technology Conference, 1-4 May, Houston, Texas, USA.

Cathie, D. N., Jaeck, C., Ballard, J. C., and Wintgens, J. F. (2005). "Pipeline geotechnics– State of the Art." Proceedings of the international symposium on frontiers in offshore geotechnics, Perth, Australia, 95–114.

Clukey, E. C., Haustermans, L. & Dyvik, R. (2005). "Model tests to simulate riser–soil interaction in touchdown point region." In *Frontiers in offshore geotechnics* (eds S. Gourvenec and M. Cassidy), pp. 651-658. Boca Raton, FL, USA: CRC Press/ Balkema.

Clukey, E. C., Aubeny, C. P., Randolph, M. F., Sharma, P. P., White, D. J., Sancio, R. & Cerkovnik, M. (2017). "A Perspective on the state of knowledge regarding soil-pipe interaction for SCR fatigue assessments." Proceedings of the offshore technology conference, Houston, TX, USA, paper no. OTC 27564.

Chatterjee, S., White, D. J. & Randolph, M. F. (2013). "Coupled consolidation analysis of pipe–soil interactions." *Can. Geotech. J.* 50, No. 6, 609–619.

Clukey, E.C., Zakeri, A., (2017). "Recent Advances in Nonlinear Soil Models for Fatigue Evaluation of Steel Catenary Risers SCRs." Offshore Technology Conference, 1-4 May, Houston, Texas, USA.

Clukey, E. C., Young, A. G., Dobias, J. R. & Garmon, G. R. (2008). "Soil response and stiffness laboratory measurements of SCR pipe/soil interaction." Proceedings of the offshore technology conference, Houston, TX, USA, paper no. OTC 19303.

Cheng, L., Yeow, K., Zang, Z., and Li, F. (2014). "3D scour below pipelines under waves and combined waves and currents." *Coastal Eng.*, 83, 137–149.

DNV-RP-F204, (2017). "Offshore Standard, Riser Fatigue." Recommended practice, Det Norske Veritas.

- Dong, X., Shiri, H. (2018). "Performance of nonlinear seabed interaction models for steel catenary riser, Part I: nodal response." *Ocean Eng.* 154, 153–166.
- Dong, X., Shiri, H. (2019). "Performance of nonlinear seabed interaction models for steel catenary riser, Part II: global response." *Appl. Ocean. Res.* 82, 158-174.
- Draper, S., An, H., Cheng, L., White, D. J., Griffiths, T. (2015). "Stability of subsea pipelines during large storms." *Phil. Trans. R. Soc. A* 373: 20140106. <http://dx.doi.org/10.1098/rsta.2014.0106>.
- Elliott, B. J., Zakeri, A., Barrett, J., Macneill, A., Phillips, R., Clukey, E. C., and Li, G. (2013). "Centrifuge modeling of steel catenary risers at touchdown zone Part I: Development of novel centrifuge experimental apparatus." *Ocean Engineering*, March 1; 60, 200-207. <https://doi.org/10.1016/j.oceaneng.2012.11.012>.
- Elliott, B.J., Zakeri, A., Barrett, J., Hawlader, B., Li. G., Clukey, E.C. (2013). "Centrifuge modeling of steel catenary risers at touchdown zone Part II: assessment of centrifuge test results using kaolin clay." *Ocean. Eng.* 60 (March) 208–218.
- Fuhrman, D. R., Baykal, C., Sumer, B. M., Jacobsen, N. G., and Fredsøe, J. (2014). "Numerical simulation of wave-induced scour and backfilling processes beneath submarine pipelines." *Coastal Eng.*, 94, 10–22.
- Fouzder, A., Zakeri, A., and Hawlader, B. (2012). "Steel catenary risers at touchdown zone - A fluid dynamics approach to the water-riser-soil interaction", 9<sup>th</sup> Int. Pipeline Conf., Calgary, V4, 31-36.
- Giertsen, E., Verley, R., Schröder, K. (2004). "CARISIMA: A Catenary Riser/Soil Interaction Model for Global Riser Analysis." *ASME 2004 23<sup>rd</sup> International Conference on Offshore Mechanics and Arctic Engineering 2004*, pp. 633-640.

Hejazi, R., Kimiaei, M. (2016). “Equivalent linear soil stiffness in fatigue design of steel catenary risers.” *Ocean. Eng.* 111, 493–507.

Hodder, M. White, D. J. & Cassidy, M. J. (2009). “Effect of remolding and reconsolidation on the touchdown stiffness of a steel catenary riser: Observations from centrifuge modelling.” *Proceedings of the offshore technology conference*, Houston, TX, USA, paper no. OTC 19871.

Hodder, M. S., White, D. J. & Cassidy, M. J. (2013). “An effective stress framework for the variation in penetration resistance due to episodes of remoulding and reconsolidation.” *Géotechnique* 63, No. 1, 30-43, <https://doi.org/10.1680/geot.9.P.145>.

Hou, Z., Sahdi, F., Gaudi, C. & Randolph, M. F. (2018). “Evolution of riser–soil stiffness in a soil crust layer.” In *Proceedings of the 1st Vietnam symposium on advances in offshore engineering: energy and geotechnics* (eds M. F. Randolph, D. H. Doan, A. M. Tang, M. Bui and V. N. Dinh), pp. 130–136. Singapore: Springer Nature Singapore.

Howells H. (1995). “Advances in Steel Catenary Riser Design.” 2H OffShore Engineering Ltd, Surrey.

Langner, C. (2003). “Fatigue life improvement of steel catenary risers due to self-trenching at the touchdown point.” *Proceedings of the Offshore Technology Conference*, OTC 15104, May 5-8.

Larsen C. M., Halse K. H., (1997). “Comparison of models for vortex-induced vibrations of slender marine structures.” *Marine Structures* 1997 July; 10(6):413-441. [https://doi.org/10.1016/S0951-8339\(97\)00011-7](https://doi.org/10.1016/S0951-8339(97)00011-7).

- Larsen, B.E., Fuhrman, D.R., Sumer, B.M., (2016). "Simulation of wave-plus-current scour beneath submarine pipelines." *J. Waterw. Port, Coast. Ocean Eng.* 142, 04016003.
- Leeuwestein, W., Bijker, E. W., Peerbolte, E. B., Wind, H. G., (1985). "The Natural Self Burial of Submarine Pipelines." *Behaviour of Offshore Structures*, Elsevier Publishers, pp717-728.
- Leira, B.J., Passano, E., Karunakaran, D., Farnes, K.A., Giertsen, E. (2004). "Analysis guidelines and application of a riser-soil interaction model including trench effects." *Proceedings of the 23<sup>rd</sup> International Conference on Offshore Mechanics and Arctic Engineering OMAE 2004-51527*, 955–962, June 20-25.
- Li, F., Cheng, L., (2000). "Numerical simulation of pipeline local scour with lee-wake effects." *Int. J. Offshore Polar Eng.* 10.
- Li, F., Cheng, L., (2001). "Prediction of lee-wake scouring of pipelines in currents." *J. Waterw. Port, Coast. Ocean Eng.* 127, 106–112.
- Li, F.Z., Dwivedi, A., Low, Y., and Hong, J. (2013). "Experimental investigation on scour under a vibrating catenary riser.", *Journal of Engineering Mechanics*, vol. 139, No. 7.
- Li, F.Z., Low, Y.M. (2012). "Fatigue reliability analysis of a steel catenary riser at the touchdown point incorporating soil model uncertainties." *Appl. Ocean Res.* 38, 100–110.
- Liang, D., Cheng, L., Li, F., (2005). "Numerical modeling of flow and scour below a pipeline in currents: Part II. scour simulation." *Coast. Eng.* 52, 43–62.

Lucassen, R. J., (1984). "Scour underneath submarine pipelines." Rep. No. PL-4 2A, Netherlands Marine Technical Research, Netherlands Industrial Council for Oceanology, Delft Univ. of Technology, Delft, The Netherlands.

Lu, Y., Chiew, Y.-M., (2007). "Seepage effects on dune dimensions." *J. Hydraul. Eng.* 133, 560–563.

Lu, Y., Chiew, Y.-M., Cheng, N.-S., (2008). "Review of seepage effects on turbulent open channel flow and sediment entrainment." *J. Hydraul. Res.* 46, 476–488.

Mao, Y., (1986). "The interaction between a pipeline and an erodible bed. Series Paper No. 39, Institute of Hydrodynamic and Hydraulic Engineering." Technical Univ. of Denmark, Copenhagen, Denmark.

Myrhaug, D., Ong, M. C., Føien, H., Gjengedal, C., and Leira, B. J. (2009). "Scour below pipelines and around vertical piles due to second-order random waves plus current." *Ocean Eng.*, 36(8), 605–616.

Nakhaee, A., Zhang, J., (2008). "Effects of the interaction with the seafloor on the fatigue life of a SCR." Proceedings of the 18<sup>th</sup> International Society of Offshore and Polar Engineers Conference ISOPE-I-08-397; 2008 July 6-11; Vancouver, Canada. pp 87-93.

Ogbeifun, A. M., Oterkus, S., Race, J., Naik, H., Moorthy, D., Bhowmik, S., Ingram, J. (2021). "Vessel relocation solution for steel catenary riser touch down fatigue management." *Ocean Eng.* 237, 109632.

Ogbeifun, A. M., Oterkus, S., Race, J., Naik, H., Moorthy, D., Bhowmik, S., Ingram, J. (2022). "Vessel relocation strategy for multiple steel catenary riser fatigue damage mitigation." *Ocean Eng.* 248, 110493.

Orcina Ltd. (1986). "Orcaflex User Manual." Cumbria, UK.

Palmer, A. (1997). "Geotechnical evidence of ice scour as a guide to pipeline burial depth." *Can. Geotech. J.* 34, No. 6, 1002–1003.

Pesce, C. P., Aranha, J. A. P., and Martins, C. A. (1998). "The Soil Rigidity Effect in the Touchdown Boundary-Layer of a Catenary Riser: Static Problem." Eighth International Offshore and Polar Engineering Conference, Montreal, Canada, 207-213.

Phifer, E. H., Frans, K., Swanson, R. C., Allen, D. W., and Langner, C. G. (1994), "Design And Installation Of Auger Steel Catenary Risers." Offshore Technology Conference, Houston, Texas, USA, OTC7620.

Quintin, H., Legras, J. L., Huang, K., and Wu, M., (2007). "Steel Catenary Riser Challenges and Solutions for Deepwater Applications." Offshore Technology Conference, Houston, Texas, USA, OTC19118.

Randolph, M. F., and White, D. J. (2008) "Pipeline embedment in deep water: processes and quantitative assessment." Offshore Technology Conf., Houston, USA, OTC 19128.

Randolph, M.F., Quiggin, P. (2009). "Non-linear hysteretic seabed model for catenary pipeline contact." In: Proceedings of the 28<sup>th</sup> International Conference on Ocean, Offshore and Arctic Engineering. Honolulu, Hawaii, USA.

Randolph, M.F., Bhat, S., Mekha, B. (2013). "Modeling the touchdown zone trench and its impact on SCR fatigue life." Proceedings of the Offshore Technology Conference 2013, OTC-23975-MS, <https://doi.org/10.4043/23975-MS> May 6-9.

Rezazadeh, K., Shiri, H., Zhang, L., Bai, Y. (2012). "Fatigue generation mechanism in touchdown area of steel catenary risers in nonlinear hysteretic seabed." *Res. J. Appl. Sci. Eng. Technol.* 4 (24), 5591–5601.



- Sumer, B.M., Baykal, C., Fuhrman, D.R., Jacobsen, N.G. & Fredsøe, J., (2014). "Numerical calculation of backfilling of scour holes." Proceedings of the 7<sup>th</sup> International Conference on Scour and Erosion, ICSE-7 Perth.
- Sumer, B. M., Fredsøe, J., (1993). "Self Burial of Pipelines at Span Shoulders." Proceedings of the International Symposium in Offshore and Polar Engineering, I-93-111.
- Sumer, B.M., Fredsøe, J., (1996). "Scour Around Pipelines in Combined Waves and Current." Technical Report American Society of Mechanical Engineers, New York, NY (United States).
- Shiri H., (2010). "Influence of seabed response on fatigue performance of steel catenary risers in touchdown zone." PhD Thesis, University of Western Australia.
- Shiri, H., Randolph, M. (2010). "The influence of seabed response on fatigue performance of steel catenary risers in touchdown zone." In: Proceedings of the 29<sup>th</sup> international conference on offshore mechanics and arctic engineering, OMAE 2010, Shanghai, China, p. 20051.
- Shiri, H. (2014a). "Response of steel catenary risers on hysteretic non-linear seabed." Appl. Ocean. Res. 44 (January), 20–28.
- Shiri, H. (2014b). "Influence of seabed trench formation on fatigue performance of steel catenary risers in touchdown zone." Marine Structure. 36 (April), 1–20.
- Sharma, P.P., Aubeny, C.P. (2011). "Advances in pipe-soil interaction methodology and application for SCR fatigue design." Proceedings of the Offshore Technology Conference OTC-21179-MS.

- Shoghi, R., Shiri, H. (2019). "Modeling touchdown point oscillation and its relationship with fatigue response of steel catenary risers." *Appl. Ocean. Res.* 87, 142-154.
- Shoghi, R., Shiri, H. (2020). "Re-assessment of trench effect on fatigue performance of steel catenary risers in the touchdown zone." *Appl. Ocean Res.* 94, 1-16.
- Smith, H.D., Foster, D.L., (2005). "Modeling of flow around a cylinder over a scoured bed." *J. Waterw. Port, Coast. Ocean Eng.* 131, 14-24
- Staub, C., Bijker, R., (1990). "Dynamic Numerical Models for Sandwaves and Pipeline Self-Burial." *Journal of Coastal Engineering.*
- Tom, J.G., Draper, S., White, D.J., (2018). "Sediment transport and trench development beneath a cylinder oscillating normal to a sandy seabed." *Coastal Engineering* 140, 395-410.
- White, D. J. & Hodder, M. (2010). "A simple model for the effect on soil strength of episodes of remoulding and reconsolidation." *Can. Geotech. J.* 47, No. 7, 821–826.
- Yuan, F., White, D. J. & O'Loughlin, C. D. (2017). "The evolution of seabed stiffness during cyclic movement in a riser touchdown zone on soft clay." *Géotechnique* 67, No. 2, 127–137, <https://doi.org/10.1680/jgeot.15.P.161>.
- Zargar, E., Kimiaei, M., Randolph, M.F. (2019). "A new hysteretic seabed model for riser-soil interaction." *Marine Structures*, 64, 360-378, <https://doi.org/10.1016/j.marstruc.2018.08.002>.
- Wang, K., Low, Y.M. (2016). "Study of seabed trench induced by steel catenary riser and seabed interaction." *Proceedings of the 35<sup>th</sup> International Conference on Ocean, Offshore and Arctic Engineering OMAE 2016-54236.*

Zargar, E. (2017). “New hysteretic seabed model for riser-soil interaction.” PhD Thesis, University of Western Australia.

Zhao, Y., Haveman, C. E., Cribbs, A. R., Miller, J. D. (2015). “Global benefits and operational challenges of vessel relocation, Proceedings of the 34<sup>th</sup> International Conference on Ocean, Offshore and Arctic Engineering OMAE2015 May 31-June 5, St. John's, Newfoundland, Canada.

Zhao, F., Griffiths, T., Shen, W., Draper, S., An, H., Leggoe, J., Carneiro, D., (2015) “Sediment Attractors: Seabed Shear Stress Shadows Around Subsea Pipelines Cause Net Sediment Accretion.” OMAE2015-41651.

Zhou, Z., O’Loughlin, C. D., White, D. J. (2020). “An effective stress analysis for predicting the evolution of SCR-seabed stiffness accounting for consolidation.” Géotechnique 70, No. 5, 448–467. <https://doi.org/10.1680/jgeot.18.P.313>.

## CHAPTER 3

# **Incorporation of Effective Stress Analysis into the Numerical Model of the Steel Catenary Riser; Accounting for Soil Remoulding and Reconsolidation Effect**

Hossein Janbazi<sup>1</sup>, Hodjat Shiri<sup>2</sup>

1: Department of Civil Engineering  
Memorial University of Newfoundland  
e-mail: [hjanbaziokn@mun.ca](mailto:hjanbaziokn@mun.ca)

2: Department of Civil Engineering  
Memorial University of Newfoundland  
e-mail: [hshiri@mun.ca](mailto:hshiri@mun.ca)

This chapter is under review by *Géotechnique*.

## **Abstract**

Steel catenary risers (SCRs) are subjected to some level of environmental loading, resulting in cyclic oscillations in the touchdown zone (TDZ), which strongly affects the fatigue damage accumulation. Over a long time of riser operations, the surrounding soil undergoes a drainage condition due to the minimal TDZ movements, e.g., small motion amplitudes of the floating vessel during the calm weather or limited contact with the seabed due to the vessel relocation. This long-term assessment may recover soil strength associated with excess pore pressure dissipation. However, existing SCR-seabed interaction models used for global analysis of riser are mostly based on the total stress approach and do not account for any drainage conditions, resulting in an underestimation of fatigue damage in design practice. The current study incorporates the effective stress analysis into the numerical model of SCR by defining user-defined elements to determine the SCR-soil stiffness at each increment of dynamic analysis, accounting for the damage accumulation surrounding the pipe during the cyclic motions and reconsolidation process due to the excess pore pressure dissipation during the intervening pause period. Stochastic fatigue analysis will be presented to accurately represent the real response of a riser during its operational lifetime.

## **Keywords**

Steel Catenary Riser, Effective stress analysis, Consolidation, Soil stiffness, Fatigue analysis

### **3.1. Introduction**

Steel Catenary Risers (SCRs) are widely used in offshore oil and gas systems to convey hydrocarbons from deep water seabed to floating vessels. Due to the cyclic environmental loads, e.g., waves, currents, and operation loads from the host vessel, fatigue analysis is crucial for SCR design, especially in two areas of the system, the hang-off point and the touchdown zone (TDZ); the latter being the most challenging issue in SCR design due to the complex riser-seabed-seawater interaction (Bridge, 2005; Randolph & White, 2008; Shiri & Randolph, 2010; Janbazi & Shiri, 2022). Cyclic motions of a catenary riser commonly occur at a rate that induces an undrained loading due to its large movements in TDZ, leading to the remoulding of the surrounding soil due to the progressive generation of positive excess pore water pressure. This soil degradation would be escalated due to the scouring of fluid around the riser and leading to the gradual penetration of the riser, which is mostly developed during the early stages of the riser operation life, first 2-3 years (Thethi & Moros, 2001; Bridge & Howells, 2007; Randolph et al., 2013; Shoghi & Shiri, 2019; Janbazi & Shiri, 2023a). However, the soil might be undergoing a drainage condition over a long-term operation of a SCR, which comes from several factors: e.g., small motion amplitudes due to calm weather or changes in wave directions (Clukey et al., 2017; Al-Janabi et al., 2019), as well as limited contact with the seabed resulting from vessel repositioning according to the vessel relocation plan (Zhao et al., 2015; Ogbeifun et al., 2021 and 2022). This minimal disturbance in the soil allows the pore water pressure gradually dissipates through the seabed, regaining the soil strength during consolidation. The significance of the consolidation process on soil strength has been accepted in the literature, with experimental model tests conducted to demonstrate the recovery of soil stiffness and

strength during pause periods (Hodder et al., 2009; Elliot et al., 2013; Clukey et al., 2017; Yuan et al., 2017; Zhou et al., 2019; Al-Janabi et al., 2019). However, some works showed low values for normalized stiffness even after wait periods (Clukey et al., 2005; Clukey et al., 2008). Moreover, some studies have conducted an effective stress analysis of vertical pipe-seabed interaction based on the analytical effective stress framework to capture both remoulding and reconsolidation effects (White & Hodder, 2010; Hodder et al., 2013; Zhou et al., 2020; Janbazi & Shiri, 2023b). This framework is based on the critical state model (CSM) within interpreting the void ratio – effective stress path for a one-dimensional soil horizon. Although the applicability of this framework has been well captured in both remoulding and reconsolidation effects, all investigations have been limited to a truncated section of a sample pipe/SCR, making it challenging to extrapolate their findings to the fatigue performance of the SCR since the consolidation effect may not be uniform along the entire TDZ. In addition, the variability in SCR-seabed stiffness in the TDZ could possibly result in the formation of a ladle-shaped trench beneath the riser, which could potentially be another factor that affects fatigue performance and has not been considered in prior studies involving the consolidation effect. Therefore, the feasibility of an effective stress framework for analyzing timescales in field conditions with the global analysis of the SCR remains a knowledge gap and needs further investigation. The main features of the current study compared to the previous works that employed an effective stress framework for pipe-seabed interaction have been outlined in Table 3-1.

Table 3-1. List of studies worked on an effective stress framework for pipe-seabed interaction

Study.	Methodology	Model type	Remoulding / Consolidation effect	Trench formation	Fatigue analysis
--------	-------------	------------	-----------------------------------	------------------	------------------

White & Hodder (2010)	Analytical analysis	T-bar penetrometer	Episodic cyclic undrained loading/intervening pause period	No	No
Hodder et al., (2013)					
Zhou et al., (2020)		SCR/shortened segment	Continues cyclic undrained loading /incremental dissipation	Yes/one-dimensional	
Current study	Numerical analysis	SCR/global analysis	Episodic cyclic undrained loading/intervening pause period	Yes/two-dimensional	Yes

The current study aims to establish a time-dependent seabed model by incorporating the effective stress framework into the numerical analysis of SCR through a user-defined element which is coded in FORTRAN as a subroutine within the ABAQUS user element library (UEL), to quantify the realistic simulation of a full-scale SCR during its life history (see Figure 3-1).

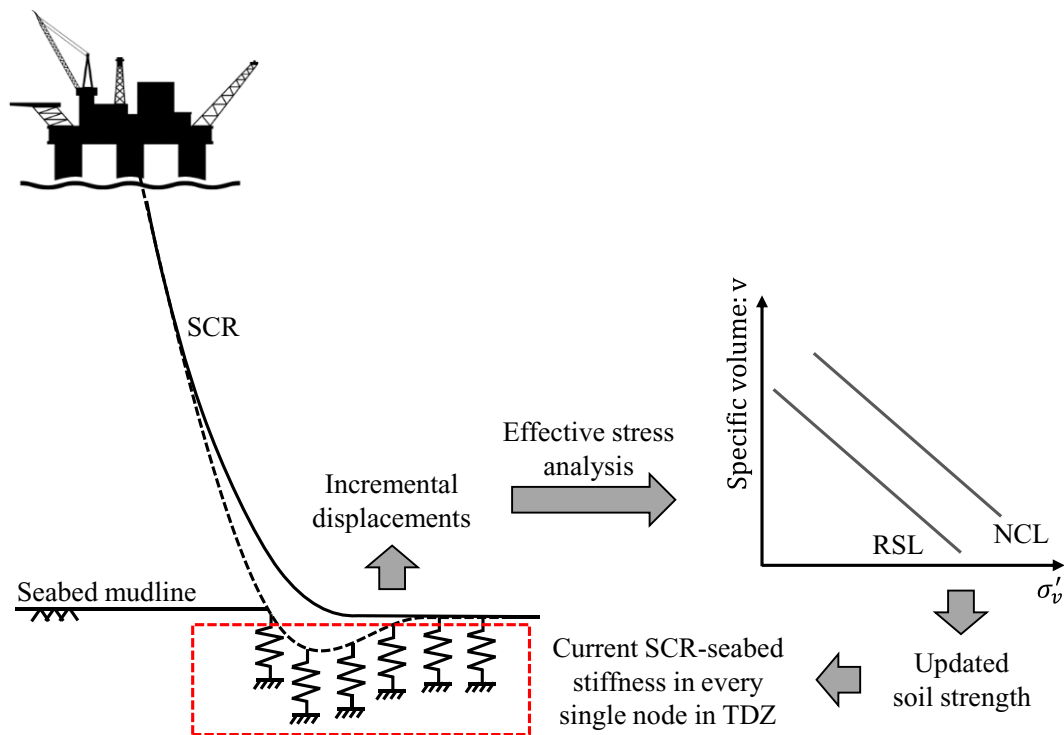




Figure 3-1. Time-dependent SCR-seabed stiffness, accounting for remoulding and consolidation

It is worth noting that the existing non-linear hysteretic soil models used for global analysis of SCRs are based on the total stress approach, representing only cyclic soil strength degradation without consolidation effect (Bridge, 2005; Randolph & Quiggin, 2009; Aubeny & Biscontin, 2008; Clukey & Zakeri, 2017; Dong & Shiri, 2019). This overlooked consolidation effect could lead to an underestimation of fatigue damage in design practice, highlighting the significance of the present study.

### **3.2. Effective Stress Methodology**

The effective stress framework is based on the critical state soil mechanics in which the reduction in effective stress is linked to the generation of excess pore water pressure during undrained loading, and it can be recovered at the lower specific volume of soil horizon associated with the dissipation of excess pore pressure during the intervening pause period.

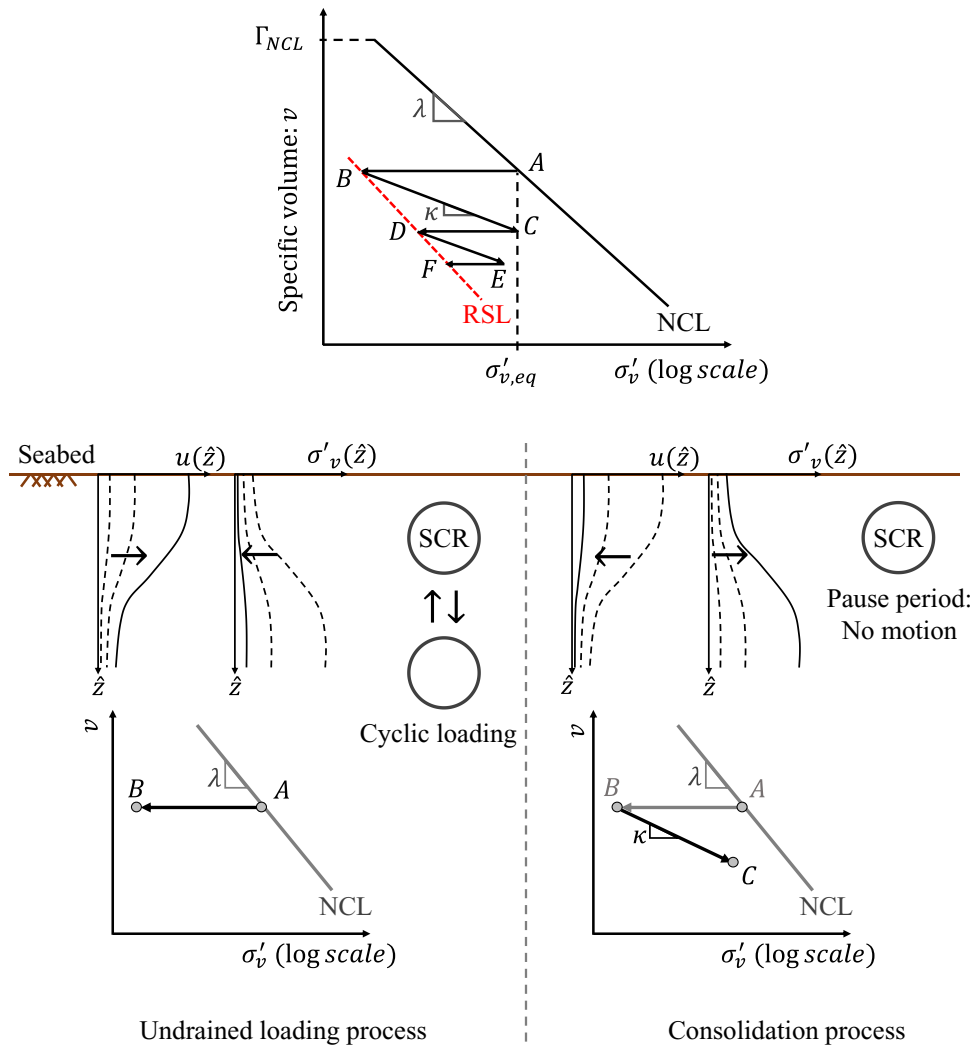


Figure 3-2. Definition of the effective stress framework with the schematic variation of effective stress and excess pore pressure during remoulding and consolidation process

Figure 3-2 illustrates the effective stress-specific volume path of a soil element that is assumed to be intact and may exist on a normal compression line (NCL), point A. During cyclic undrained loading, effective stress is reduced to below the in-situ stress and reaches the remoulded value, e.g., point B. However, the effective stress is regained during drainage conditions due to the excess pore water pressure dissipation, leading to a decreased void ratio, e.g., by path B-C for full consolidation. Further soil disturbance at a lower specific volume causes the effective stress point is progressively migrating

towards a fully remoulded value at the higher value, e.g., the remoulded state line (RSL) is achieved at points D and F for the last two episodes.

### **3.3. Global Analysis of SCR based on Effective Stress Analysis**

The behavior of SCR-soil stiffness variation for each individual node located in TDZ is not uniform and can be affected by specific cyclic displacements and intervening pause periods. This variation can also impact neighbouring nodes, changing the riser embedment, trench depth and overall consolidation effect; highlighting the importance of global analysis for accurately calculating fatigue performance in the TDZ. A novel approach has been developed in the current study to model the seabed vertical reaction force by incorporating effective stress analysis into the global analysis of the riser. As shown in Figure 3-3, a series of user-defined elements were used along the TDZ, which are defined through a UEL subroutine of ABAQUS to represent a riser-seabed interaction model. The stiffness matrix of each element has been calculated by getting the updated vertical resistance ( $q_t$ ), which is in equilibrium with the submerged weight in unit length ( $m_s g$ ). This procedure is called by ABAQUS at every increment of the dynamic analysis.

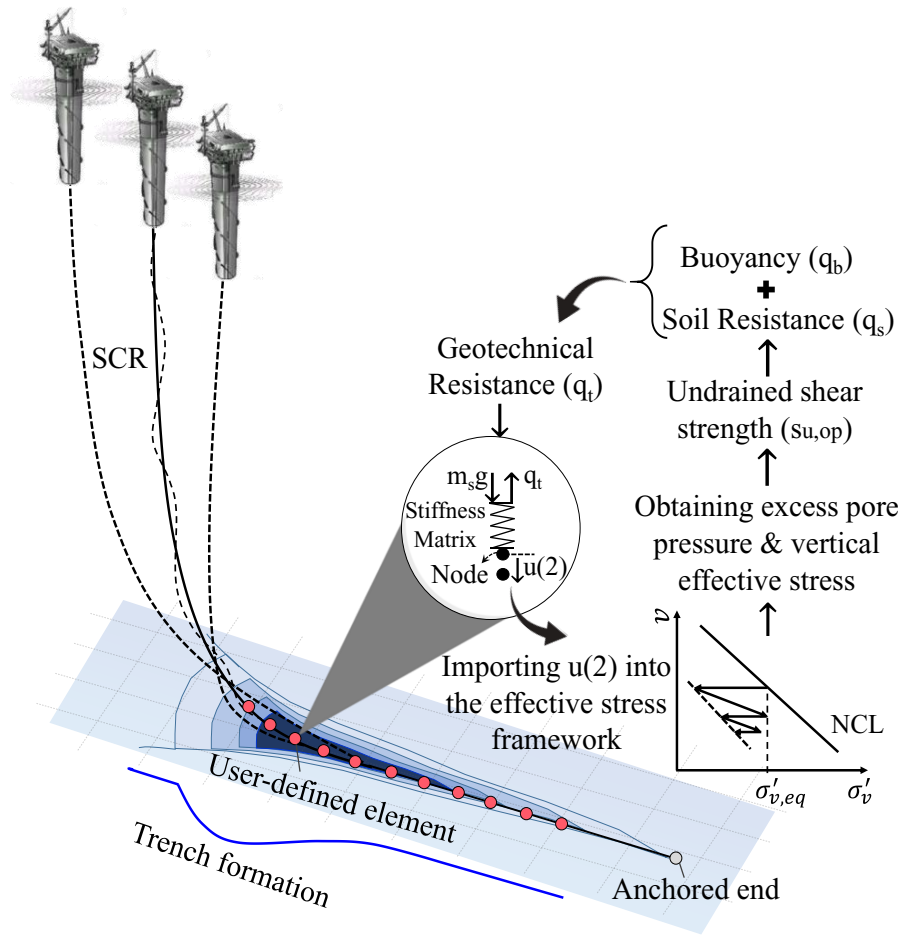


Figure 3-3. Schematic illustration of user-defined elements implemented into the UEL subroutine of Abaqus

The vertical resistance on the SCR elements comprises soil buoyancy forces ( $q_b$ ) and soil resistance ( $q_s$ ) as provided in equations (3-1) and (3-2), which are expressed in kPa.

$$q_t(\hat{z}) = q_b(\hat{z}) + q_s(\hat{z}) \quad (3-1)$$

$$q_t(\hat{z}) = f_b A_s (\rho_{soil} - \rho_{water}) g / D + N_c s_u \quad (3-2)$$

where  $D$  is the outer pipe diameter,  $f_b$  is the soil buoyancy factor,  $\rho_{soil}$  is the saturated density of the soil,  $\rho_{water}$  is the density of water, and  $g$  is the acceleration due to gravity. The parameter of  $A_s$  is the nominal area of the pipe embedded below the seabed mudline, which can be determined by equation (3-3), if  $\frac{z}{D} \leq 0.5$  (Randolph and White, 2008).

$$A_s = \frac{D^2}{4} \left[ \sin^{-1} \left( \sqrt{4 \frac{z_m}{D} \left(1 - \frac{z_m}{D}\right)} \right) - 2 \left(1 - 2 \frac{z_m}{D}\right) \sqrt{\frac{z_m}{D} \left(1 - \frac{z_m}{D}\right)} \right] \quad (3-3)$$

where  $z_m$  is the vertical pipe penetration.

$N_c$  is the soil bearing factor and can be obtained by equation (3-4), in which power law coefficients were assumed by  $a = 6$  and  $b = 0.25$  (Randolph and White, 2008; Aubeny and Biscontin, 2009).

$$N_c = a(\hat{z})^b \quad (3-4)$$

Regarding equation (3-2),  $s_u$  is undrained shear strength given from the effective stress analysis, which will be discussed in the next sections.

### 3.3.1. Generation of Excess Pore Water Pressure

A series of user-defined elements were used along the TDZ with the notation of “ $i$ ”, to represent a riser-seabed interaction model. As shown in Figure 3-4, the current vertical displacement of each user-defined element, Node $_i$ , is defined by a distance from the seabed mudline normalized by the SCR diameter, denoted as  $\hat{z}_{i,m}$ . The current vertical location of the given soil horizon relative to each node, normalized by the diameter, is denoted as  $\hat{\eta}_i$ , and can be obtained by equation (3-5).

$$\hat{\eta}_i = \hat{z}_i - \hat{z}_{i,m} \quad (3-5)$$

where  $\hat{z}_i$  is the given soil depth normalized by the diameter which is located in the vertical path of Node $_i$ . The cycle number is used to quantify the damage accumulation  $N(\hat{z}_i)$  of the surrounding soil, resulting in the progressive generation of excess pore pressure. The depth zone over which the damage is accumulated due to the passage of the pipe is referred to as the influence damage zone,  $\mu(\hat{z}_i)$ , with boundaries extending to a normalized distance,  $\beta$ , mid-depth above and below the user-defined element. A

triangular expression is adopted for  $\mu(\hat{z}_i)$  as provided by equation (3-6). If the soil horizon is outside the influence zone, then  $\mu(\hat{z}_i) = 0$ , which means that the soil horizon is unaffected by the riser displacement.

$$\mu(\hat{z}_i) = \frac{1}{\beta} \left( 1 - \frac{|\hat{\eta}_i|}{\beta} \right) \quad (3-6)$$

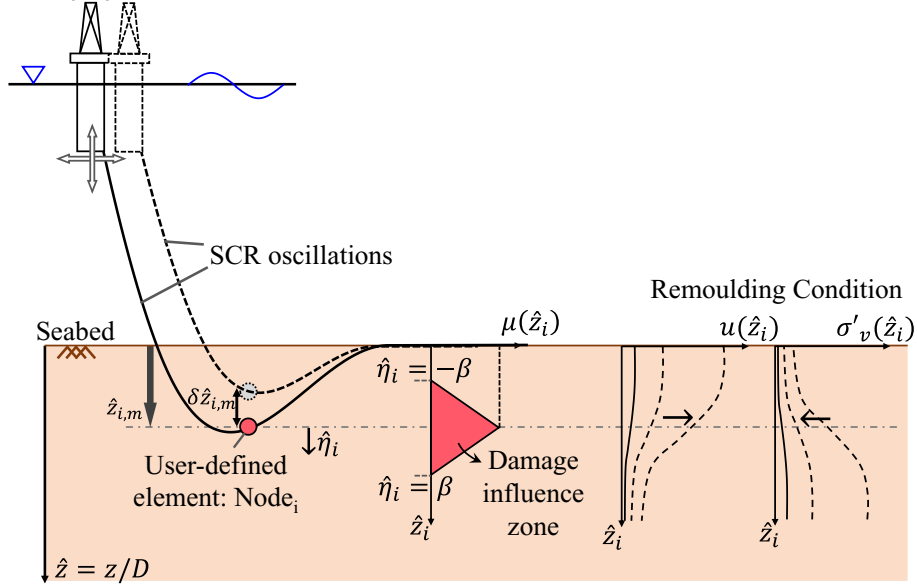


Figure 3-4. Remoulding process for a sample node in TDZ based on the effective stress analysis

As explained earlier, the progressive generation of excess pore pressure is linked to the cumulative soil damage accumulated by cyclic motions of SCR occurring in an undrained condition, as shown in equation (3-7).

$$u(\hat{z}_i) = u_{max}(\hat{z}_i) \left( 1 - a_u e^{-\frac{3N(\hat{z}_i)}{N_{95,u1}}} - (1 - a_u) e^{-\frac{3N(\hat{z}_i)}{N_{95,u2}}} \right) \quad (3-7)$$

where  $N_{95,u1}$  and  $N_{95,u2}$  are the number of cycles required to generate excess pore pressure within 95% of the maximum value;  $a_u$  is a constant parameter used for the rate of excess pore pressure generation. The accumulation of excess pore pressure causes

the effective stress to decrease from an intact to a fully remoulded state; thus, the maximum excess pore pressure is calculated by equation (3-8).

$$u_{max}(\hat{z}_i) = \sigma'_{v0}(\hat{z}_i) - \sigma'_{v,RSL}(\hat{z}_i) \quad (3-8)$$

where  $\sigma'_{v0}(\hat{z}_i)$  is the in-situ vertical effective stress; and  $\sigma'_{v,RSL}(\hat{z}_i)$  is the effective stress in the fully remoulded condition and can be expressed as provided in equation (3-9).

$$\sigma'_{v,RSL}(\hat{z}_i) = \left[ \frac{s_u}{\sigma'_{v0}} \right]_{NC} \frac{\sigma'_{v0}(\hat{z}_i)}{\phi(\hat{z}_i) S_{t,cycle}} \quad (3-9)$$

$$\times \exp \left[ \frac{\Lambda \{ \Gamma_{NCL} - v_{initial}(\hat{z}_i) - \lambda \ln[\sigma'_{v0}(\hat{z}_i)] \}}{\lambda - \kappa} \right]$$

where  $\left[ \frac{s_u}{\sigma'_{v0}} \right]_{NC}$  is the normally consolidated undrained strength ratio,  $\Lambda$  is the plastic volumetric strain ratio, and  $S_{t,cyc}$  is the cyclic sensitivity of the soil.  $\phi$  is the lumped strength parameter and can be determined by equation (3-10).

$$\phi(\hat{z}_i) = k_\phi(\hat{z}_i) \phi_{steady} - [k_\phi(\hat{z}_i) - 1] (1 - e^{-3N(\hat{z}_i)/N_{95,\phi}}) \phi_{steady} \quad (3-10)$$

where  $N_{95,\phi}$  is the number of cycles required to cause a 95% drop from  $k_\phi \phi_{steady}$  to  $\phi_{steady}$  (since  $e^{-3} \approx 0.05$ ). The parameter  $k_\phi$  is equal to  $OCR(\hat{z})^b$ , where  $b$  is a peak strength parameter. It is worth noting that the selection of the  $\phi_{steady}$  value can be achieved by utilizing measured data obtained from experimental tests. An appropriate value of  $\phi_{steady} = 0.6$  was back-calculated by Hodder et al., (2013) through the fitting of three parameters, soil sensitivity, swelling line slope, and remoulded undrained strength, using T-bar model tests.

$N(\hat{z})$  is the cumulative damage, increasing progressively with each SCR-seabed user-defined element (Node<sub>i</sub>) passing through the specific soil horizon, accumulating during

a one-half cycle (Einav and Randolph, 2005). A detailed demonstration of damage accumulation of the surrounding soil in the TDZ can be seen in Figure 3-5.

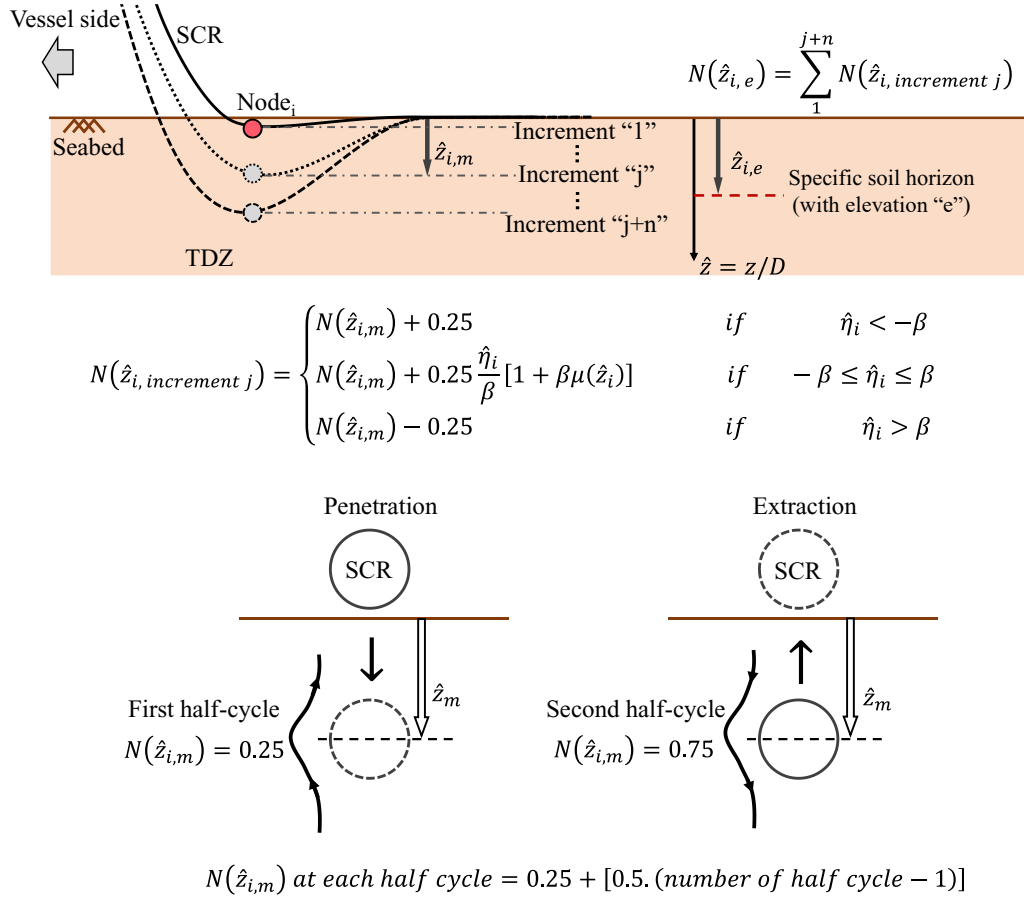


Figure 3-5. Damage accumulation of the surrounding soil with each Node<sub>i</sub> cyclic movement

### 3.3.2. Dissipation of Excess Pore Water Pressure

The excess pore pressure at a given soil horizon dissipates in response to the intervening pause period, decreasing from its initial value,  $u_0$ , to the current excess pore pressure,  $u_c$ , as provided in equation (3-11) (see Figure 3-6).

$$u_c(\hat{z}_i) = (1 - U) \cdot u_0(\hat{z}_i) \quad (3-11)$$

where  $U$  is the degree of dissipation.



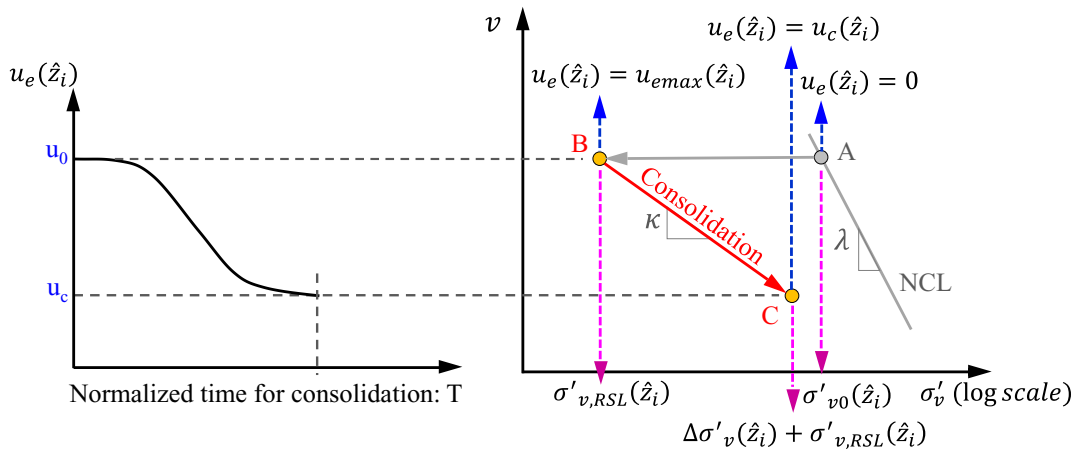


Figure 3-6. Schematic illustration of excess pore pressure dissipation during the consolidation process

The current vertical effective stress of the soil can be linked to the undrained shear strength using the lumped strength parameter, equation (3-12).

$$s_u(\hat{z}_i) = \phi(\hat{z}_i)\sigma'_v(\hat{z}_i) \quad (3-12)$$

The shear strength of the soil at the current location of the riser pipe is governed by the soil strength in the surrounding area, within a normalized distance,  $\alpha$ , below and above the user-defined elements (Node<sub>i</sub>) as illustrated in Figure 3-7(a). The average strength for each node in the TDZ is calculated by a weighted integration of the current soil strength with respect to a strength influence zone,  $v(\hat{z}_i)$  which is defined by a triangular function similar to the cycle number influence function,  $\mu(\hat{z}_i)$ .

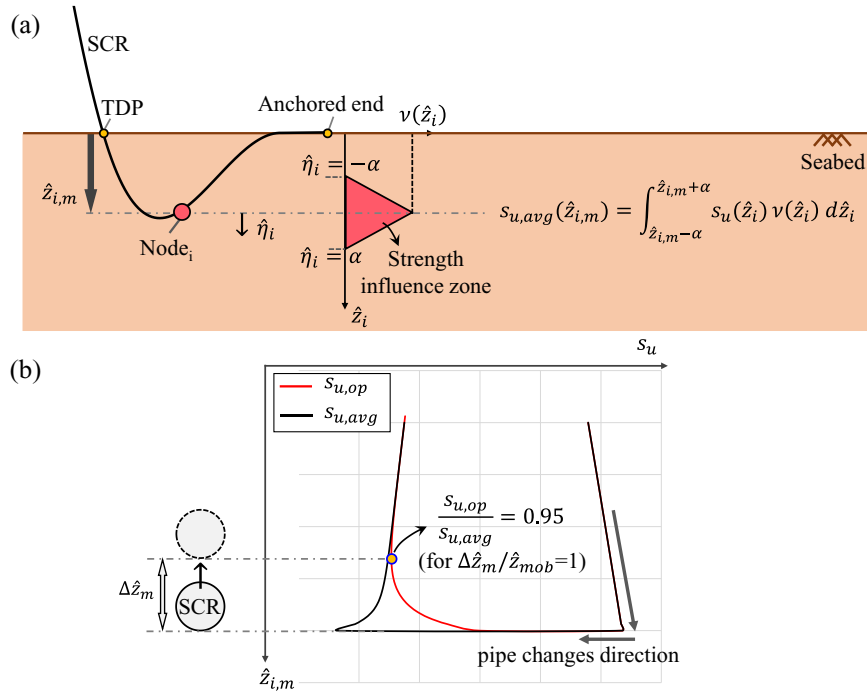


Figure 3-7. Soil strength definition for a sample SCR-seabed user-defined element in the TDZ

- (a) Contribution of the surrounded soil for average strength (b) soil mobilization after the change in pipe direction

As shown in Figure 3-7(b), when the node changes direction, the gradual mobilization of the soil strength is captured by an exponential function, resulting in a reduction of secant stiffness to such an extent that the operative strength asymptotically approaches 95% of the average soil strength within the strength mobilized distance,  $\hat{z}_{mob}$  (equation (3-13)).

$$s_{u,op}(\hat{z}_{i,m}) = s_{u,avg}(\hat{z}_{i,m}) \left[ 1 - e^{-3\left(\frac{\Delta\hat{z}_{i,m}}{\hat{z}_{mob}}\right)} \right] \quad (3-13)$$

where  $\Delta\hat{z}_{i,m}$  is the change in vertical displacement from a reversal point while Node<sub>i</sub> changes its direction to uplift mode.

### 3.4. SCR - Case Study

A global SCR model was constructed in ABAQUS using an example base case from the literature with a length of 2333 m and a water depth of 1800 m located in the Gulf of Mexico (e.g., Bridge, 2005). The model boundary conditions were defined by assuming simple hinge supports at both the anchored end and the hang-off point. The riser pipe was modeled based on the Timoshenko beam theory using PIPE21 elements from the ABAQUS element library, starting from node No. 1 at the anchored end and ending with node No. 828 at the hang-off point attached to the floating vessel. The element length of 1 m was assumed in the TDZ and changed to 5 m for the hanging part. The values for the main parameters of the SCR are summarized in Table 3-2.

Table 3-2. Main parameters of SCR

Parameter	Value
D (m)	0.324
t (m)	0.0205
$\Delta Z$ (m)	1600
A (m <sup>2</sup> )	1.95E-02
I (m <sup>4</sup> )	2.26E-04
m <sub>s</sub> (kg/m)	100
EI (Nm <sup>2</sup> )	4.68E+07
$\theta_{HO}$ (deg)	77.88

The vessel undergoes perturbations to replicate the influence of wave action. In this process, the DISP subroutine in ABAQUS plays a pivotal role in generating each new position of the vessel. This subroutine effectively processes the sea state data applied and the vessel's RAO (Response Amplitude Operator) at every increment of the analysis. The surge, pitch, and heave movements of the vessel, centered at its gravity point, are then transmitted to the attachment point through the DISP subroutine. This transfer of motion causes the riser to undergo sequential lifting and lowering within the

touchdown zone throughout the loading and unloading cycles. As explained earlier, the effective stress analysis has been employed to represent the riser-seabed interaction model using UEL subroutine, which is called by ABAQUS at every increment of the dynamic analysis. The detailed procedure of the SCR numerical analysis is provided in Figure 3-8.

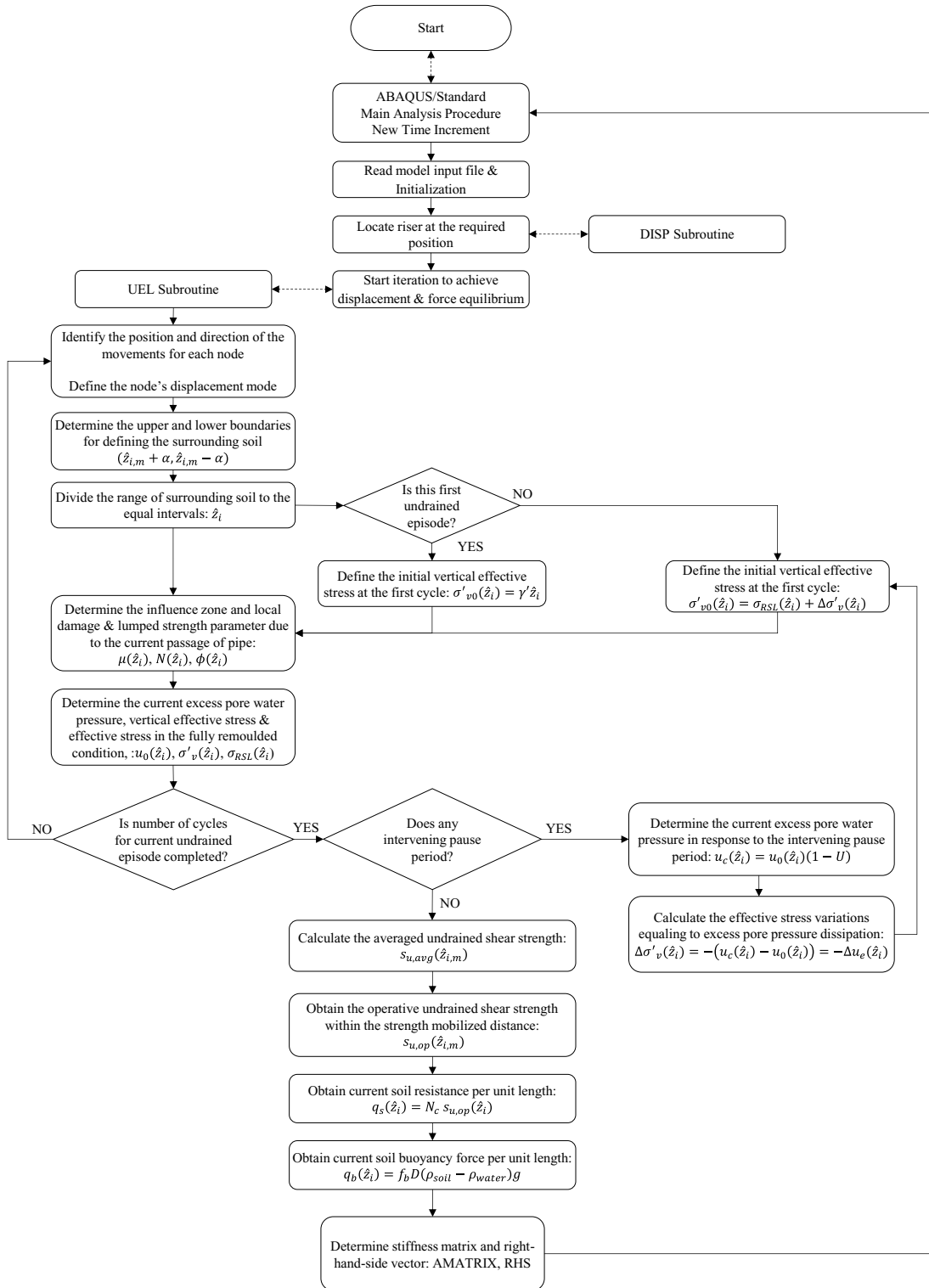


Figure 3-8. ABAQUS main procedure flowchart conducted for the numerical model of SCR. The seabed soil undergoes cyclic disturbance and reconsolidation effects during the riser's service life, resulting in variations in soil strength. To investigate the effects of

the remoulding process, three episodes of undrained cyclic loading (each comprising 200 cycles) were considered in this study within an intervening pause period between every two consecutive episodes to examine the reconsolidation effect. The selection of 200 cycles in each episode was somewhat arbitrary but was made to ensure adequate stabilization of the riser embedment while maintaining reasonable computational time. The coefficient of consolidation was assumed based on the typical properties of soft clay using the equation (3-14), proposed by Gourvenec and White (2010), with Young's modulus  $E' = 2000$  kPa, drained Poisson's ratio  $\nu' = 0.3$ , and permeability  $k = 10^{-5}$  m/day, resulting in a coefficient of consolidation  $c_v = 1$  m<sup>2</sup>/year. This value is also consistent with the recommended values for kaolin clay extracted from Rowe cell consolidation tests conducted by House et al., 2001.

$$c_v = \frac{kE'}{\gamma_w} \frac{(1 - \nu')}{(1 - 2\nu')(1 + \nu')} \quad (3-14)$$

The consolidation effect was investigated by considering 90% dissipation between each two consecutive episodes. The numerical analyses of an embedded pipeline conducted by Chatterjee et al. (2013) showed that an elasto-plastic solution with a range of embedment ratio  $\hat{z}_m = 0.2-0.5$  yields  $T_{90} \sim 1$ . This corresponds to a total pause periods of  $\sim 3$  months, without taking into account any soil berms. The parameters used for effective stress analysis were assumed as listed in Table 3-3.

Table 3-3. Main parameters for the effective stress analysis

Parameter	Sign	Value
Effective unit weight	$\gamma'$	6 kN/m <sup>3</sup>
Specific volume at $\sigma'_v = 1$ kPa	$\Gamma_{NCL}$	3.74
Slope of normal compression line	$\lambda$	0.311
Slope of swelling/reconsolidation line	$\kappa$	0.0667
Peak strength ductility	$N_{95,\phi}$	0.75
Cycle number influence zone extent	$\beta$	1

Plastic volumetric strain ratio	$\Lambda$	0.557
Steady strength parameter	$\phi_{steady}$	0.6
Pore pressure rate parameter	$N_{95,u1}$	0.25
Pore pressure rate parameter	$N_{95,u2}$	11
Pore pressure component parameter	$a_u$	0.77
Strength influence zone extent	$\alpha$	1
Strength mobilized distance	$\hat{z}_{mob}$	1
Soil sensitivity	$S_{t,cycle}$	3.5

The direction of vessel oscillation was chosen based on a study conducted by Kimiaei et al. (2010), which suggested that oscillations in the tangential direction of the local coordinate system at the SCR hang-off point could contribute over 95% to the overall fatigue damage accumulation in the TDZ. Consequently, for this stage of the study, the tangential direction at the hang-off point was selected for vessel oscillation, with  $H_{tan} = 2$  m and  $T = 15$  s, to minimize computational effort. However, later in this paper, realistic oscillations under random waves will also be provided for fatigue analysis. The normalized shape of the SCR within three episodes is presented in Fig. 6(a), which reveals that the soil disturbance caused trench formation at a depth of approximately 1.5 times the riser diameter during episode 1, with this depth remaining relatively constant during the subsequent episodes.

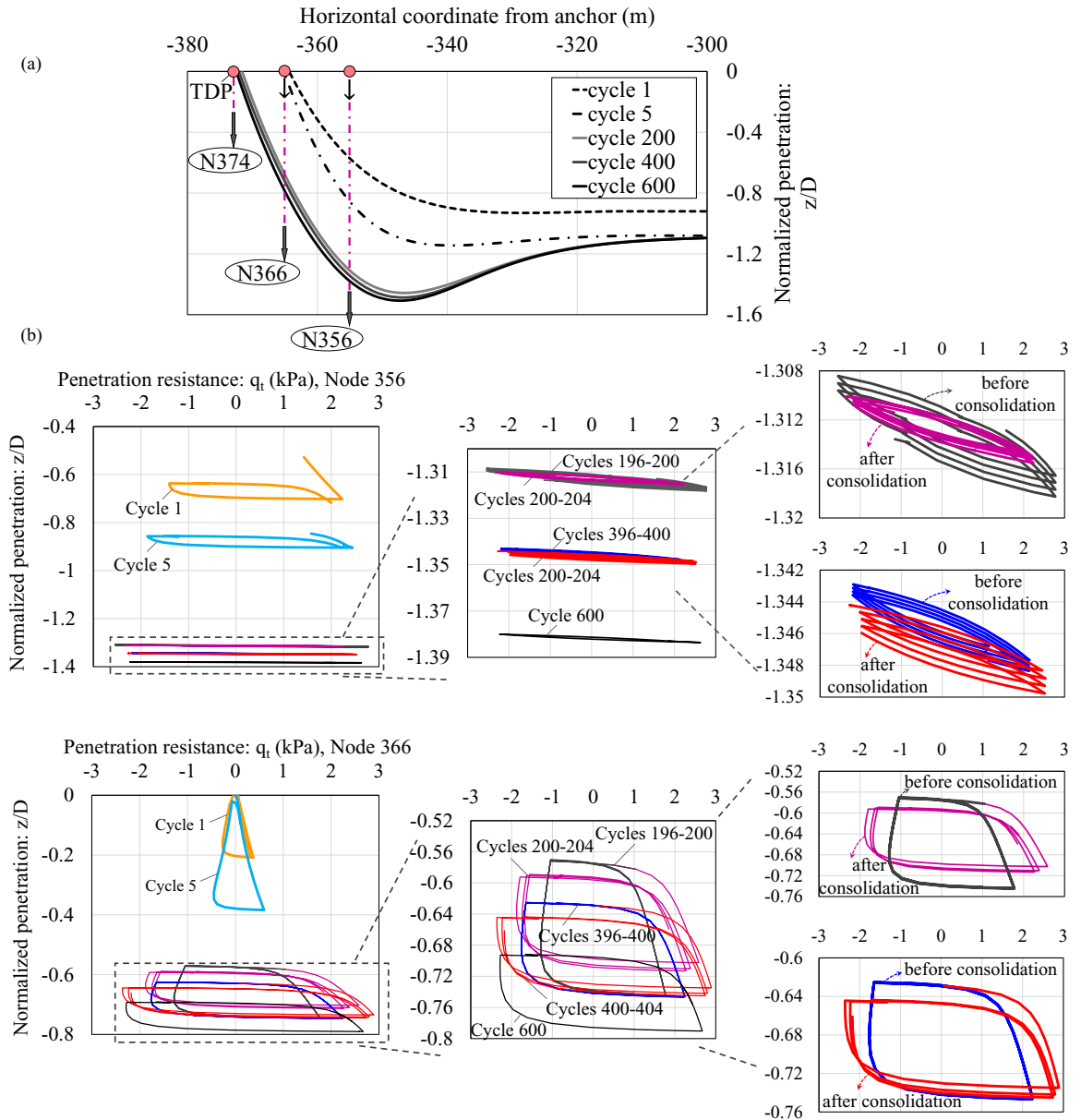


Figure 3-9: Numerical analysis of SCR over 600 cycles based on effective stress analysis: (a) normalized penetration; (b) total resistance-penetration for sample nodes 356, 366

The results of total resistance versus normalized penetration are provided in Fig. 6(b) for two sample nodes in the TDZ, Node 356 and Node 366. It is apparent that there are changes in the slope of the curves during the pause periods as the consolidation occurred (e.g., cycles 200-204 and cycles 400-404), indicating variations in soil stiffness that will be discussed in the next section.



### 3.4.1. SCR-Soil Stiffness in the TDZ

The fatigue performance of SCR is significantly affected by the soil stiffness in the TDZ, which is influenced by any soil resistance during pipe loading and unloading. The concept of soil stiffness can be defined by the normalized unloading secant stiffness,  $K_{sec}$ , which is schematically superimposed in Figure 3-10. The results of the global analysis of SCR have been presented in Figure 3-10 by demonstrating the ratio of the stabilized secant stiffness (at cycle 600) to its initial value for various nodes in the TDZ at a cyclic displacement of  $\Delta z_m/D = 0.0025$ . The figure shows a tendency for soil stiffness recovery due to consolidation effects, with the highest ratio occurring at node 366. The results for this node have also been provided based on the number of cycles. Initially, the normalized secant stiffness is 280, but it drops during the first five cycles to  $\sim 250$ . It then gradually rises as the cycles accumulate, achieving  $\sim 340$  at cycle 200. After two abrupt increases during the intervening pause periods (after cycle 200 and 400), it ultimately stabilizes at cycle 600, exceeding the initial normalized stiffness by a factor of 1.9 (e.g., 2.2 times greater than remoulded value). These findings are consistent with other published works, e.g., Hodder et al. (2009), Clukey et al. (2017), and Zhou et al. (2020).

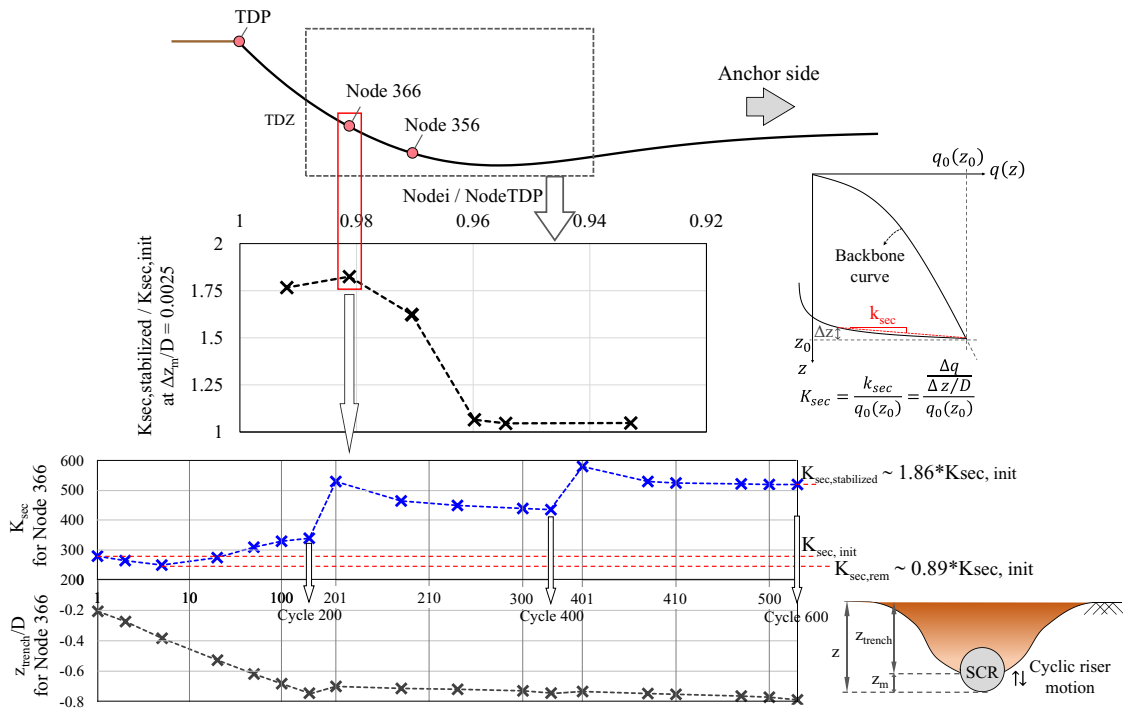


Figure 3-10. Normalized uplift secant stiffness for some nodes in TDZ, with more focus on Node 366

Additionally, the penetration of Node 366 during the 600 cycles has been provided to demonstrate the gradual softening of the soil. It is worth noting that the parameter  $z_{trench}/D$  refers to the trench depth and is different from the cyclic embedment of the riser, which was previously referred to  $z_m$ . It is worth noting that the consolidation effect can be influenced by incorporating various trench depths (Janbazi and Shiri, 2023b).

Figure 3-11 depicts the decline in  $K_{sec}$  with increasing cyclic displacement,  $\Delta z_m/D$ , along with a trend of initially decreasing and then increasing  $K_{sec}$  with cycle number, which is attributed to the initial soil softening and the consolidation-induced hardening. The stiffness degradation can also be captured by existing SCR-seabed stiffness models, as demonstrated by Randolph and Quiggin (2009) (named R-Q model hereafter), which shows the amount of softening over the same loading period as the current model. The following soil properties were considered for the R-Q model: Mudline shear strength:

$s_{u0} = 1$  kPa; Shear strength gradient:  $\rho = 1.2$  kPa/m; Suction ratio:  $f_{suc} = 0.2$ ; Suction decay parameter:  $\lambda_{suc} = 0.5$ ; Re-penetration parameter:  $\lambda_{rep} = 0.5$ .

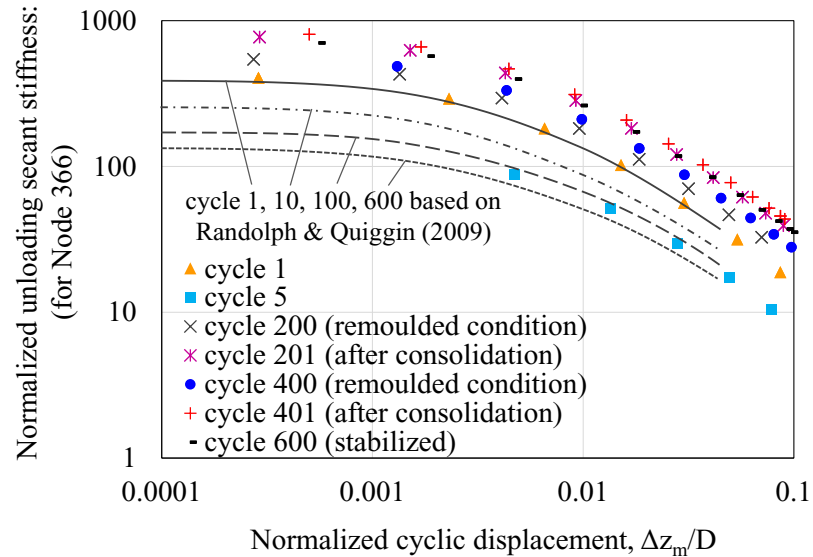


Figure 3-11. Variations in normalized secant stiffness for Node 366 based on the current model and an existing non-linear spring model (R-Q model)

Results confirm that the existing models, e.g., R-Q model, do not account for the regain in stiffness due to consolidation, resulting in a predicted long-term stiffness that is significantly lower than the eventual value obtained in the current study.

### 3.4.2. Validation of UEL subroutine developed for SCR-soil interaction model

The SCR-soil interaction process coded in the UEL subroutine was validated by simulating three episodes of undrained cyclic loading similar to those employed in the T-bar model tests performed by Hodder et al., 2009 at Western Australia University. Each episode comprised 20 cycles, with an intervening pause period of 3.5 hours (equivalent to 1 year at the prototype scale). The T-bar penetrometer, with a diameter of 5 mm corresponding to 0.25 m at the prototype scale, was subjected to cyclic loading

between  $z = -0.75$  m to  $-3$  m with an acceleration level of  $50g$  in a geotechnical centrifuge test.

Figure 3-12 illustrates the consistency between the outcomes of the framework implemented in this study and the previously published research. A measurement of relative soil resistance during cyclic penetration and extraction was used as a degradation factor (DF) to quantify soil degradation caused by cyclic motions. The results indicate that DF progressively decreased to a steady value throughout each cyclic episode, indicating the remoulded state of the soil. However, it subsequently increased as the soil regained its strength after undergoing consolidation.

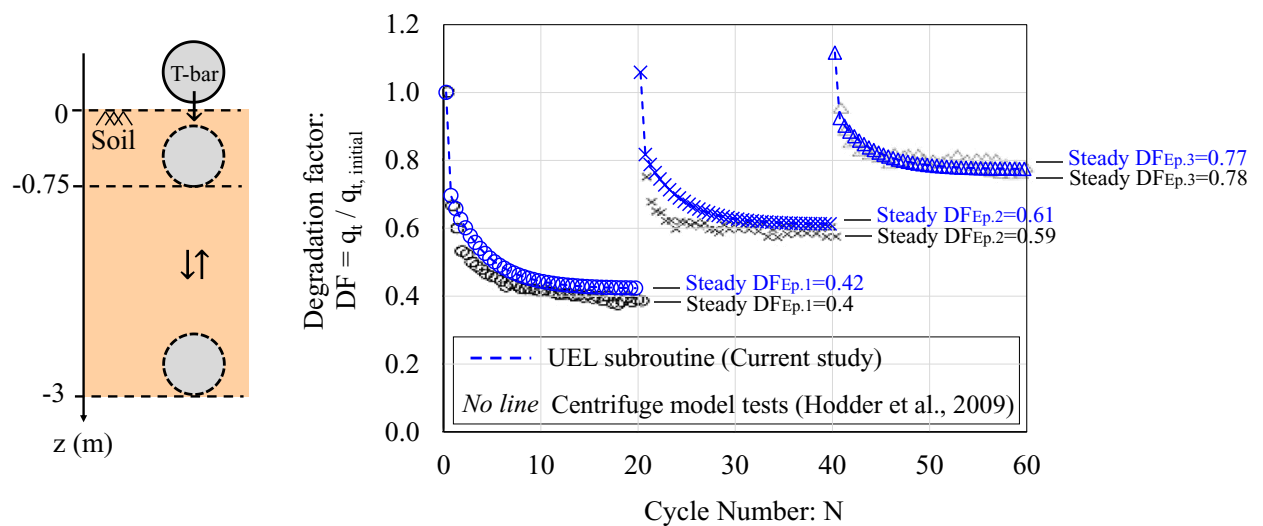


Figure 3-12. Results of degradation factor based on the UEL subroutine developed for SCR-soil interaction model and centrifuge model tests

The same concept of the degradation factor was used for the global analysis of SCR based on the effective stress approach conducted in the current study and also the total stress approach used by the existing non-linear soil models. As shown in Figure 3-13, the value of DF was reported at cycle 600, when the riser had stabilized sufficiently

after undergoing cyclic motions. The corresponding riser embedments were also superimposed for each approach to identify the specific nodes in the TDZ.

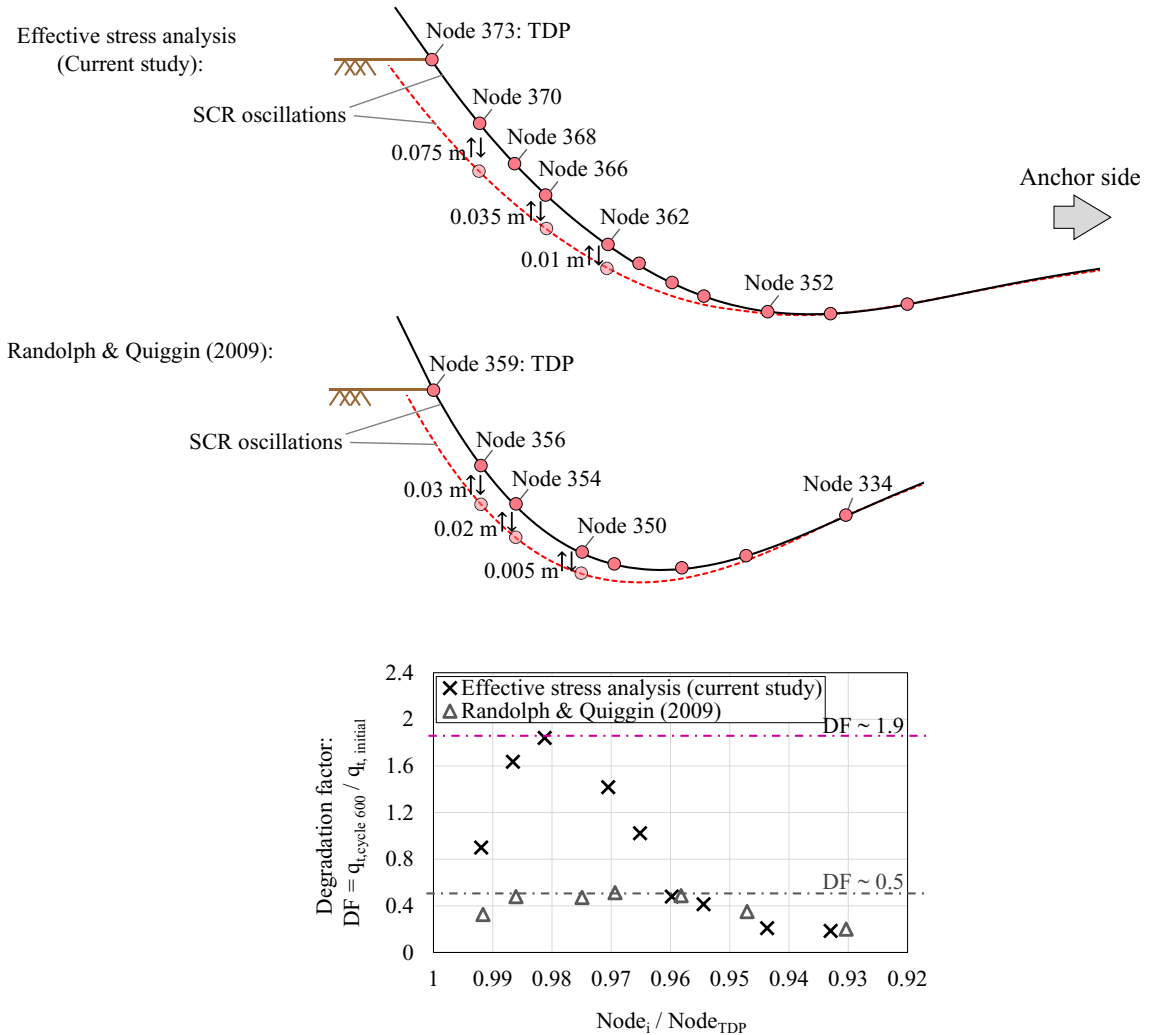


Figure 3-13. Degradation factor at stabilized condition for specific nodes in TDZ, based on the effects stress and total stress approaches

The results presented in Figure 3-13 illustrate that the R-Q model cannot demonstrate any consolidation effect, and the soil resistance decreased during cyclic motions, with an average value of  $DF = 0.5$ , which was much lower than the current prediction. However, the effective stress approach indicates a tendency for soil resistance recovery, exceeding the initial resistance with most nodes in TDZ. Although previous studies have

emphasized the soil regaining due to the consolidation effect, the rate of recovery may differ for each node due to various factors such as its location, cyclic motions of the riser, trench depth, and behavior of adjacent nodes. This finding indicates the importance of including effective stress analysis into the global analysis of the SCR with its entire length in the TDZ.

### **3.4.3. Axial stress range along TDZ**

The variations of axial stress are strongly influenced by the softening and consolidation behaviour of the soil during the riser operation. Therefore, it would be beneficial to present the stress range results across the broad length of the SCR to demonstrate how the position of the critical node shifts due to the effects of remoulding and reconsolidation. According to Figure 3-14, the initial cyclic undrained loading results in gradual riser penetration, leading to a notable stress range. Moreover, there was an additional increase in stress range while the consolidation process was considered. Some minor damage reduction could be observed for the later remoulding process, but the stabilized peak damages were still more than the initial remoulded value by around 9% for this scenario of vessel motion ( $H_{tan} = 2$  m). It can be noted that the initial remoulding process resulted in a further shift of peak fatigue damage towards the vessel, with a horizontal distance of 9 m to the initial SCR shape. This horizontal offset is almost constant for the subsequent cyclic loading.

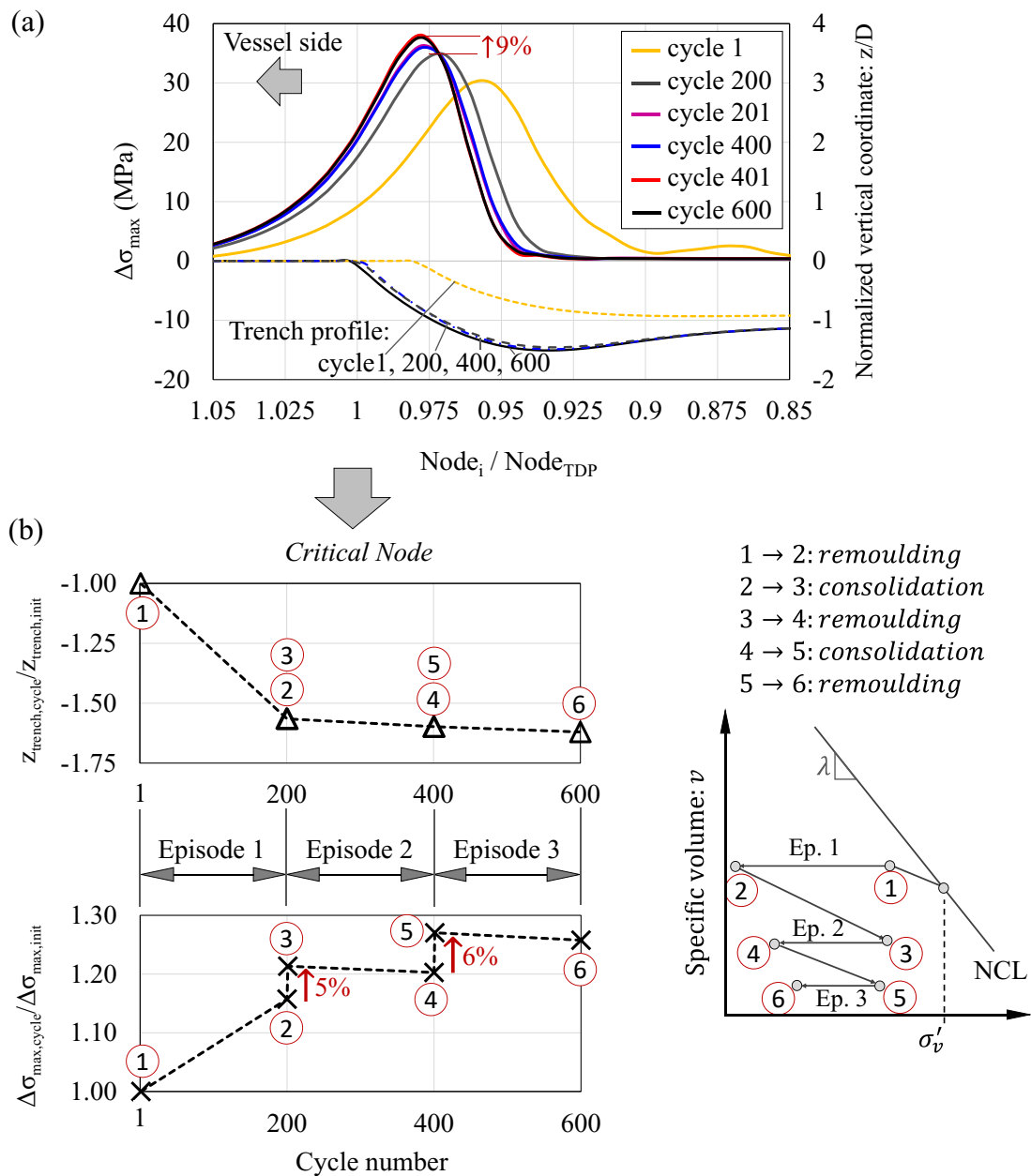


Figure 3-14. Axial stress range and trench formation along the TDZ based on effective stress analysis

Figure 3-14(b) demonstrates the results of maximum trench depth and maximum stress range in TDZ, which is normalized by its initial value. Due to the cyclic undrained loading during the first episode, point 1→2: cycle 1 to 200, the riser significantly penetrated into the seabed, indicating the remoulding process. This riser penetration

causes the  $\Delta\sigma_{max}$  at the end of episode 1 (cycle 200) to be higher than the initial value by almost 16%. It is consistent with some results in the literature indicating that the trenched seabed has a detrimental effect on fatigue damage (Leira, 2004; Shiri and Randolph 2010; Shiri, 2014a, b; Shoghi and Shiri, 2020). After that, the first pause period, point 2→3: cycle 200 to 201, increases the stress range in TDZ by around 5%, without any changes in the riser embedment. The next remoulding process, point 3→4: cycle 201 to 400, results in slight riser penetration, leading to a minor reduction in stress range. A similar trend of increasing and decreasing stress range is observed for the second pause period, point 4→5: cycle 400 to 401, and the latest remoulding process, point 5→6: cycle 401 to 600. It increased by 6% and then slightly decreased to be stabilized within cycle 600.

### **3.5. Stochastic fatigue analysis with incorporation of consolidation effect**

Due to the random nature of the sea states, a stochastic approach was considered for more accurate and less conservative fatigue damage results (Kimiaei, 2017). Two distinct sea states were assumed for stochastic fatigue analysis, e.g., SS3:  $H_s = 2.3$  m,  $T_p = 6.7$  s and SS4:  $H_s = 3.2$  m,  $T_p = 7.8$  s, representing dominant heights of the waves for fatigue performance (Muraleedharan and Kimiaei, 2018). This can be generalized for more sea states considered through the specific offshore fields as it is essential to get the full sea states of the real field data to calculate the fatigue performance of the riser during its whole life history. The vessel excitation is determined by employing Response Amplitude Operators (RAOs) to relate the wave amplitudes to the response amplitudes at the vessel's centre of gravity (CoG), which was then transferred to the hang-off point that has a horizontal and vertical offset from the CoG. This boundary condition was incorporated into the ABAQUS software by means of a DISP subroutine.



A dynamic analysis of the riser comprises three cyclic episodes within 90% degree of dissipation assumed between each two consecutive episodes. The total time for each cyclic episode is 3600 s, resulting in a total 3-hour simulation period to generate the stable loading of irregular waves. As shown in Figure 3-15, annual fatigue damage for the length of the riser in TDZ is provided for two sea states, SS3 and SS4. A SCR and trench profiles are also superimposed on each plot. The findings reveal a noticeable increase in fatigue damage, which is attributed to the consolidation process that was well captured by the effective stress simulation.

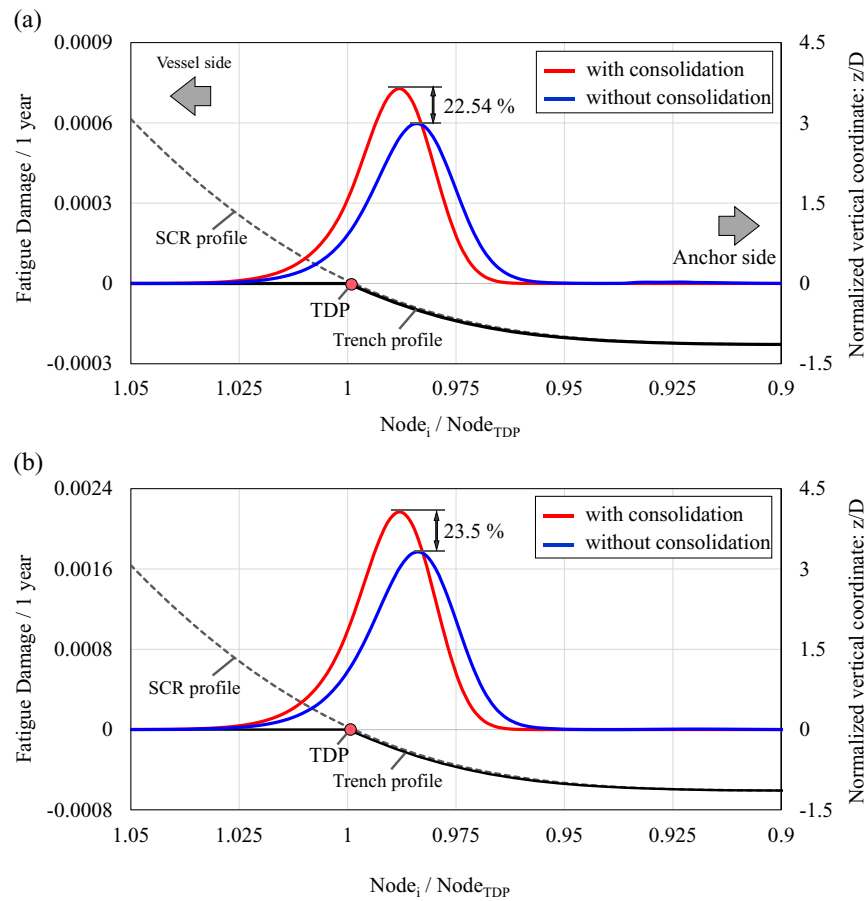


Figure 3-15. Consolidation effect on fatigue performance of SCR with degree of dissipation:

U=90% (a) SS3, (b) SS4

It is obvious that the consolidation process has a detrimental effect on fatigue lifetime, increasing the critical damage by an average of 23%. However, this amount of dissipation,  $U = 90\%$ , may not happen in reality due to the large movements of TDZ during SCR life operation, limiting the potential for full consolidation. Therefore, lower values of  $U$  were also considered to represent partial consolidation. As shown in Figure 3-16, the maximum annual fatigue damage in consolidation cases was normalized by the corresponding peak damage without the consolidation effect and presented for  $U = 50\%$ ,  $70\%$ , and  $90\%$ , equivalent to approximately  $T \sim 0.1, 0.5, 1$ . The assumption regarding excess pore pressure dissipation was derived from a numerical elasto-plastic solution for a pipeline subjected to a maintained load at an embedment depth of  $d/D = 0.5$  (Chatterjee et al., 2013). Accordingly, a schematic illustration is provided in Figure 3-16, where  $c_v$  is the coefficient of consolidation,  $t$  is the total elapsed time of the intervening pause period, and  $T$  is the normalized time for consolidation.

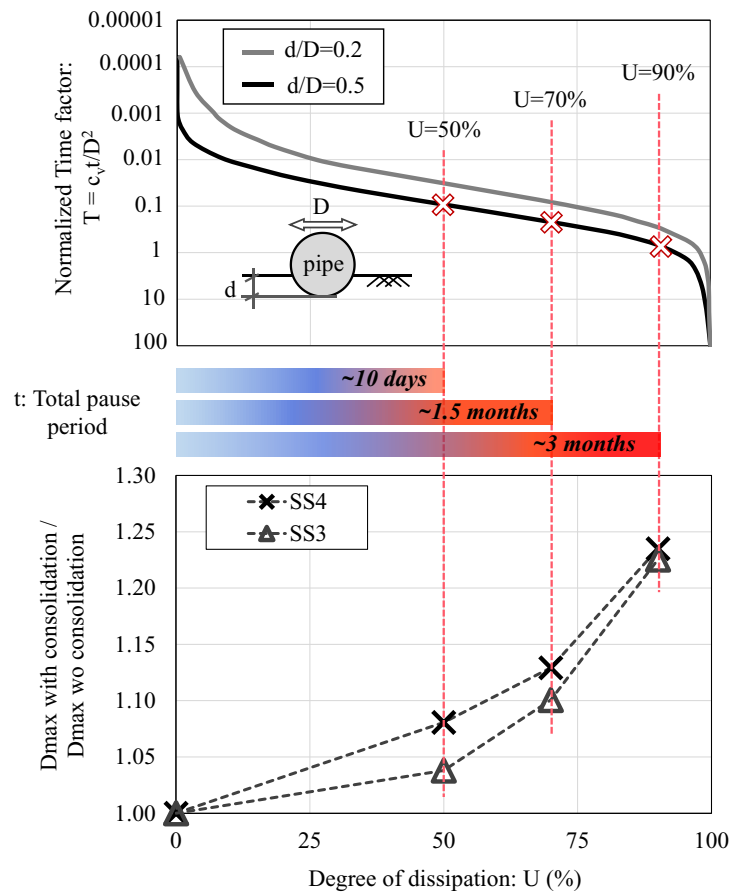


Figure 3-16. Peak fatigue damage variation due to the different dissipation rate

The current analyses confirm that fatigue damage results would be eclipsed detrimentally due to the consolidation effect, despite being insignificant for partial consolidation, with an average of less than 15%.

### 3.6. Conclusion

The riser-seabed interaction model used in the current study is based on the effective stress framework to examine cyclic soil degradation with an intervening pause period that could result in a reliable assessment of fatigue predictions. A global analysis of the steel catenary riser was constructed in ABAQUS within a series of user-defined elements along the TDZ through the UEL subroutine. The soil resistance was determined by updating the stiffness matrix of each element through two phases: i)

undrained loading quantified by the accumulation of damage surrounding the pipe during the cyclic motions of the riser, resulting in excess pore pressure generation and remoulded effective stress, and ii) inactivity periods, where the degree of excess pore water pressure dissipation was modelled to simulate the recovery of effective stress during the consolidation process.

Numerical analysis was first conducted under regular tangential heave amplitude, and results showed that the consolidation effect could recover the soil stiffness of the user-defined elements in TDZ, with the highest value of 86%. Moreover, stochastic fatigue analysis was conducted based on the three-hour dynamic simulations of the two distinct sea states, SS3 and SS4. Considering three different values for  $U$ , the excess pore pressure was partially or fully dissipated to examine the effect of the consolidation process. Results showed that the consolidation effect could generally increase the critical fatigue damage in all consolidation scenarios, with the highest factor of  $\sim 1.23$  in the higher dissipation degree,  $U = 90\%$ .

In summary, the proposed model is able to predict long-term soil stiffness and fatigue performance of subsea risers by capturing both remoulding and reconsolidation effects, which could not be captured by the existing advanced non-linear hysteretic soil models. The applicability of the current model could be further extended for SLWRs which have limited oscillations in the TDZ, improving the occurrence of consolidation.

### **3.7. Acknowledgments**

The authors gratefully acknowledge the financial support of this research by the “Natural Science and Engineering Research Council of Canada (NSERC)” through Discovery program, and the Memorial University of Newfoundland through school of graduate studies funding support.

## References

- Al-Janabi, H.A., Aubeny, C.P., Chen, J., and Luo, M. (2019). “Experimental measurement of touchdown zone stiffness for SCR in Gulf of Mexico clay.” In Offshore Technology Conference, 6–9 May, OTC-29504-MS, Houston, Texas, USA.
- Aubeny, C. & Biscontin, G. (2009). “Seafloor-riser interaction model.” *Int. J. Geomech.* 9, No. 3, 133-144.
- Bridge, C. (2005). “Effects of seabed interaction on steel catenary risers.” (Ph.D. thesis). University of Surrey.
- Bridge, C., Howells, H. (2007). “Observations and modeling of steel catenary riser trenches.” In: The seventeenth international offshore and polar engineering conference, ISOPE2007, Lisbon, Portugal., pp. 803–13.
- Chatterjee, S., White, D. J. & Randolph, M. F. (2013). “Coupled consolidation analysis of pipe–soil interactions.” *Can. Geotech. J.* 50, No. 6, 609–619.
- Clukey, E. C., Haustermans, L. & Dyvik, R. (2005). “Model tests to simulate riser–soil interaction in touchdown point region.” In *Frontiers in offshore geotechnics* (eds S. Gourvenec and M. Cassidy), pp. 651-658. Boca Raton, FL, USA: CRC Press/ Balkema.
- Clukey, E. C., Young, A. G., Dobias, J. R. & Garmon, G. R. (2008). “Soil response and stiffness laboratory measurements of SCR pipe/soil interaction.” *Proceedings of the offshore technology conference, Houston, TX, USA, paper no. OTC 19303.*
- Clukey, E. C., Aubeny, C. P., Randolph, M. F., Sharma, P. P., White, D. J., Sancio, R. & Cerkovnik, M. (2017). “A Perspective on the state of knowledge regarding soil-pipe interaction for SCR fatigue assessments.” *Proceedings of the offshore technology conference, Houston, TX, USA, paper no. OTC 27564.*

- Clukey, E. C. & Zakeri, A. (2017). "Recent advances in non-linear soil models for fatigue evaluation of steel catenary risers SCRs." Proceedings of the offshore technology conference, Houston, TX, USA, paper no. OTC 27627.
- Dong, X., Shiri, H. (2018). "Performance of non-linear seabed interaction models for steel catenary riser, Part I: nodal response." *Ocean Eng.* 154, 153–166.
- Dong, X., Shiri, H. (2019). "Performance of non-linear seabed interaction models for steel catenary riser, Part II: global response." *Appl. Ocean. Res.* 82, 158-174.
- Elliott, B.J., Zakeri, A., Barrett, J., Hawlader, B., Li. G., Clukey, E.C. (2013). "Centrifuge modeling of steel catenary risers at touchdown zone Part II: assessment of centrifuge test results using kaolin clay." *Ocean. Eng.* 60 (March) 208–218.
- Gourvenec, S. M. & White, D. J. (2010). "Elastic solutions for consolidation around seabed pipelines." Proceedings of the offshore technology conference, Houston, TX, USA, paper no. OTC 20554.
- Hodder, M. White, D. J. & Cassidy, M. J. (2009). "Effect of remolding and reconsolidation on the touchdown stiffness of a steel catenary riser: Observations from centrifuge modelling." Proceedings of the offshore technology conference, Houston, TX, USA, paper no. OTC 19871.
- Hodder, M. S., White, D. J. & Cassidy, M. J. (2013). "An effective stress framework for the variation in penetration resistance due to episodes of remoulding and reconsolidation." *Géotechnique* 63, No. 1, 30-43, <https://doi.org/10.1680/geot.9.P.145>.
- House, A., Olivera, J. R. M. S. & Randolph, M. F. (2001). "Evaluating the coefficient of consolidation using penetration tests." *Int. J. Phys. Modelling Geotech.* 1, No. 3, 17–26.

Janbazi, H., Shiri, H. (2022). “An alternative vessel excitation algorithm to incorporate the trench effect into the fatigue analysis of steel catenary risers in the touchdown zone.” *Applied Ocean Research*, 126-103292.

Janbazi, H., Shiri, H. (2023). “A hybrid model to simulate the trench effect on the fatigue analysis of steel catenary risers in the touchdown zone.” *Can. Geotech. J.* Published online, <https://doi.org/10.1139/cgj-2022-0103>.

Janbazi, H., Shiri, H. (2023). “Investigation of trench effect on fatigue response of steel catenary risers using an effective stress analysis.” *Computers and Geotechnics*, 160, 105506, <https://doi.org/10.1016/j.compgeo.2023.105506>.

Kimiaei, M., Randolph, M., Ting, I. (2010). “A parametric study on effects of environmental loadings on fatigue life of steel catenary risers (using a non-linear cyclic riser–soil interaction model).” In: *Proceedings of the 29th International Conference on Ocean, Offshore and Arctic Engineering*, Shanghai, China, Paper OMAE2010-21153.

Leira, B.J., Passano, E., Karunakaran, D., Farnes, K.A., Giertsen, E. (2004). “Analysis guidelines and application of a riser–soil interaction model including trench effects.” *Proceedings of the 23<sup>rd</sup> International Conference on Offshore Mechanics and Arctic Engineering OMAE 2004-51527*, 955–962, June 20-25.

Ogbeifun, A. M., Oterkus, S., Race, J., Naik, H., Moorthy, D., Bhowmik, S., Ingram, J. (2021). “Vessel relocation solution for steel catenary riser touch down fatigue management.” *Ocean Eng.* 237, 109632.

Ogbeifun, A. M., Oterkus, S., Race, J., Naik, H., Moorthy, D., Bhowmik, S., Ingram, J. (2022). “Vessel relocation strategy for multiple steel catenary riser fatigue damage mitigation.” *Ocean Eng.* 248, 110493.

Randolph, M.F., Quiggin, P. (2009). “Non-linear hysteretic seabed model for catenary pipeline contact.” In: Proceedings of the 28th International Conference on Ocean, Offshore and Arctic Engineering. Honolulu, Hawaii, USA.

Randolph, M.F., Bhat, S., Mekha, B. (2013). “Modeling the touchdown zone trench and its impact on SCR fatigue life.” Proceedings of the Offshore Technology Conference OTC-23975-MS, <https://doi.org/10.4043/23975-MS> May 6-9.

Randolph, M. F. & White, D. J. (2008). “Pipeline embedment in deep water: processes and quantitative assessment.” Proceedings of the offshore technology conference, Houston, TX, USA, paper no. OTC 19128.

Shiri, H., Randolph, M. (2010). “The influence of seabed response on fatigue performance of steel catenary risers in touchdown zone.” In: Proceedings of the 29<sup>th</sup> international conference on offshore mechanics and arctic engineering, OMAE 2010, Shanghai, China. 2010, p. 20051.

Shiri, H. (2014a). “Response of steel catenary risers on hysteretic non-linear seabed.” Appl. Ocean. Res. 44 (January), 20–28.

Shiri, H. (2014b). “Influence of seabed trench formation on fatigue performance of steel catenary risers in touchdown zone.” Marine Structure. 36 (April), 1–20.

Shoghi, R., Shiri, H. (2019). “Modeling touchdown point oscillation and its relationship with fatigue response of steel catenary risers.” Appl. Ocean. Res. 87, 142-154.

Shoghi, R., Shiri, H., (2020). “Re-assessment of trench effect on fatigue performance of steel catenary risers in the touchdown zone.” Appl. Ocean Res. 94, 1–16.



Thethi, R., Moros, T., (2001). “Soil interaction effects on simple catenary riser response.” Deepwater Pipeline and Riser Technology Conference, Houston, Texas, USA.

White, D. J. & Hodder, M. (2010). “A simple model for the effect on soil strength of episodes of remoulding and reconsolidation.” *Can. Geotech. J.* 47, No. 7, 821–826.

Yuan, F., White, D. J. & O’Loughlin, C. D. (2017). “The evolution of seabed stiffness during cyclic movement in a riser touchdown zone on soft clay.” *Géotechnique* 67, No. 2, 127-137, <https://doi.org/10.1680/jgeot.15.P.161>.

Zhao, Y., Haveman, C. E., Cribbs, A. R., Miller, J. D. (2015). “Global benefits and operational challenges of vessel relocation.” Proceedings of the 34<sup>th</sup> International Conference on Ocean, Offshore and Arctic Engineering OMAE2015 May 31-June 5, 2015, St. John's, Newfoundland, Canada.

Zhou, Z., O’Loughlin, C. D., White, D. J. (2020). “An effective stress analysis for predicting the evolution of SCR-seabed stiffness accounting for consolidation.” *Géotechnique* 70, No. 5, 448–467 <https://doi.org/10.1680/jgeot.18.P.313>.

## CHAPTER 4

# **Incorporation of the Riser-Seabed-Seawater Interaction Effect into the Trench Formation beneath the Steel Catenary Riser in the Touchdown Zone**

Hossein Janbazi<sup>1</sup>, Hodjat Shiri<sup>2</sup>

1: Department of Civil Engineering  
Memorial University of Newfoundland  
e-mail: [hjanbazirokn@mun.ca](mailto:hjanbazirokn@mun.ca)

2: Department of Civil Engineering  
Memorial University of Newfoundland  
e-mail: [hshiri@mun.ca](mailto:hshiri@mun.ca)

This chapter is under review by *Ocean Engineering*

## **Abstract**

The existing non-linear hysteretic soil models have generally considered Steel Catenary Riser (SCR)-seabed interactions, while the contribution of fluid mechanics as a third key influential factor is often neglected. The present study will be further extended to examine the seawater surrounding the pipe where water mass is displaced during riser oscillations in the Touchdown Zone (TDZ). This investigation aims to explore the interactions between cohesive soil, such as soft clay, and water, which have not been the primary focus of the previous studies. To accomplish this, a comprehensive three-domain analysis will be carried out through the implementation of a Coupled Eulerian-Lagrangian (CEL) analysis methodology, utilizing the ABAQUS software. A parametric study was conducted to observe the impact of water fluid by considering the effects of shear strain rate and soil softening within ranges of soil shear strength. The conventional bearing capacity approach for analyzing pipe penetration is also reviewed, and modifications are presented to account for the effects of water entrainment. The constructed FE model will be enhanced to include load control analysis, simulating the conditions experienced by SCR in the TDZ. This expanded analysis will capture the evolution of the trench profile in the presence of water fluid and also consider the lateral oscillations of the riser, which are critical factors observed in real field operations. The findings indicate that the entrainment of water can fill gaps and alter the shape of the soil structure, leading to a softening effect. This remolding effect is particularly pronounced when coupled with lateral oscillations, resulting in an approximate 60% increase in trench depth.

**Keywords:** Fluid-Pipe-Soil interaction, trench formation, Steel Catenary Riser, Touchdown zone, Water entrainment, Soil erosion

## 4.1. Introduction

Hydrocarbons are extracted from the seabed wellheads and transported to the sea surface through a pipeline called subsea risers. Among the various types of subsea risers, Steel Catenary Risers (SCRs) are considered one of the most efficient systems extensively utilized in deepwater or ultra-deepwater developments. The design of SCRs is significantly influenced by their fatigue performance in the touchdown zone (TDZ), where the risers repeatedly come into contact with the seabed due to environmental cyclic loading, such as wind and waves (Campbell M., 1999; Bridge et al., 2004; Janbazi & Shiri, 2023b). Fatigue studies for SCRs have been traditionally carried out using linear elastic soil (API-ST-2RD 2013; DNV-RP-F204; Pesce 1998). This model simplifies the seabed as a linear spring, often resulting in a conservative approach to fatigue design (Theti and Moros, 2001). However, the initial exploration of SCR technology in the Auger field of the Gulf of Mexico (Phifer et al., 1994) prompted the STRIDE and CARISIMA Joint Industry Projects (JIPs) (2H Offshore Engineering Ltd, 1999-2004) to investigate the necessity for more advanced models that account for the complex interaction between the riser and the seabed. Over the past two decades, considerable progress has been made in the development of non-linear soil models. These models were specifically designed to provide more accurate predictions of SCR-soil interaction, with a particular focus on fatigue assessment within the TDZ. The proposed non-linear soil models for riser-soil interaction consider various load-displacement paths, including initial penetration, uplift, separation, and re-penetration modes of the riser. The formulation of the hysteretic load-displacement behaviour for these different modes has been extensively studied in the literature. One notable study conducted by Bridge and Willis, (2002) involved full-scale harbour tests in Watchet

Harbor, UK, to simulate the behaviour of the bottom 10 meters of the SCR in a water depth of 1000 meters. The force-displacement interaction curve developed in this study captured the non-linear characteristics of soil behaviour through comprehensive testing. The data obtained from these tests were part of the information exchange between the 2H Offshore STRIDE JIP and the CARISIMA JIP. However, the proposed non-linear soil model had limitations in sequentially simulating gradual seabed soil softening and riser embedment. Aubeny and Biscontin (2008) developed a closed hysteretic loop model that effectively simulated the non-linear behaviour of soil, addressing the limitations of previous models by incorporating cyclic softening through unloading and re-loading paths. The proposed model was further improved by Nakhaee and Zhang to represent the trench formation (Nakhaei and Zhang, 2008). Randolph and Quiggin (2009) used a combination of hyperbolic and exponential functions to simulate hysteretic soil behaviour under a vertical oscillating riser. This model was implemented in a commercial riser analysis program, OrcaFlex (Orcina 2010), and also coded through user-defined element subroutine (UEL) within the ABAQUS software to explore the pros and cons for future developments (Shiri and Randolph, 2010; Dong and Shiri, 2018, 2019). Despite the notable advancements made, current SCR-soil models still have limitations in accurately simulating the realistic penetration of the riser into the seabed. These models typically focus on two domains of interaction, the SCR and the soil, often overlooking the contribution of the seawater fluid surrounding the riser pipe as a third influential factor (see Figure 4-1). The significance of three-domain fluid-pipe-soil interaction has been examined in the literature, particularly emphasizing the occurrence of scour beneath the subsea structures. Through comprehensive analyses, it has been established that varying hydraulic gradients have a notable effect

on hydrodynamic forces exerted on the bed surface, thereby influencing sediment transport processes and ultimately impacting the scour pattern around subsea structures (Mao, 1986; Sumer and Fredsøe, 2002; Liang et al., 2005; Larsen et al., 2016; Li et al., 2020). In addition, the impact of water flow on the formation of trenches (Tom et al., 2018) and the experimental investigation of the effects of cyclic motions, such as catenary riser, on underlying scour were also studied (Li et al., 2013). However, the majority of these studies have primarily focused on considering seabed soil as either an impermeable wall (Li and Cheng, 2000, 2001; Liang and Cheng, 2005a; Smith and Foster, 2005; Fuhrman et al., 2014; Larsen et al., 2016) or a medium porous material (Liang et al., 2005b; Lu et al., 2008; Li et al., 2013; Tom et al., 2018; Li et al., 2020), while only a limited number of studies have specifically investigated the influence of water fluid on low porosity soils, such as clay. In order to address this gap, several studies have numerically investigated the three-domain fluid-pipe-soil interaction using cohesive soil models. These investigations revealed notable variations in soil resistance, especially during the suction mode, and a reduction in soil stiffness when water was considered (Clukey et al., 2008; Fouzder et al., 2012). The significance of water fluid entrainment was investigated through physical modelling experiments conducted at the University of Western Australia, utilizing various scenarios of vertical pipe motions within centrifuge model tests using Kaolin clay. The results obtained from these tests revealed that water entrainment could lead to an additional reduction in soil strength, accelerating soil degradation by a factor of approximately 1.6 (Yuan et al., 2017). Subsequent research endeavours have taken inspiration from these experiments and have adjusted soil properties by assuming higher soil sensitivity to account for the effects of fluid in the degradation of clay soils (Zhou et al., 2020). While certain studies

have investigated the influence of water fluid in cohesive soil, further investigations are needed to address the knowledge gaps regarding sediment transport during riser oscillations and the evolution of trench morphology within a comprehensive three-domain analysis.

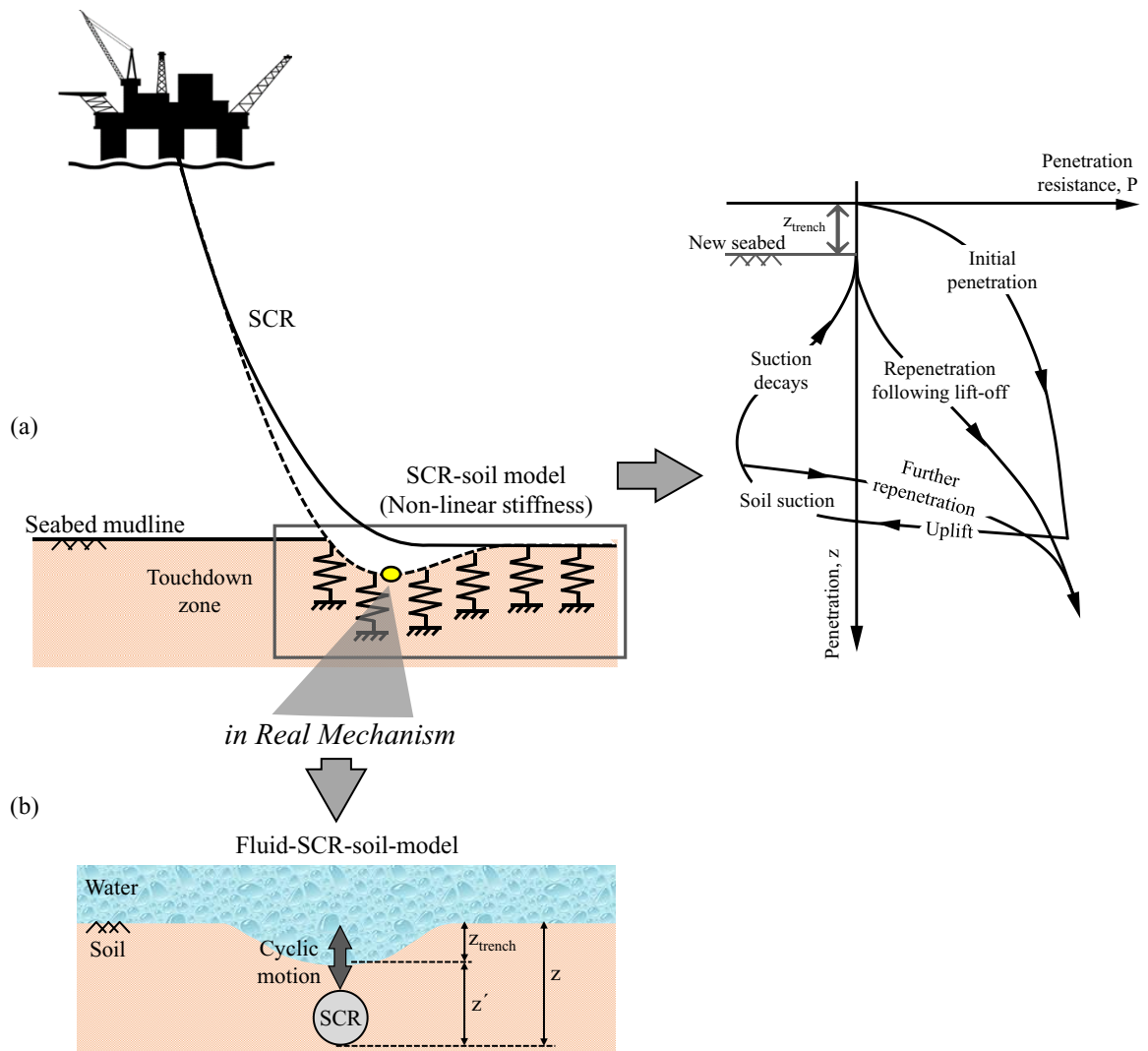


Figure 4-1. Steel Catenary Riser system: (a) typical SCR-soil interaction model during vertical cyclic motions; (b) SCR-seabed-seawater interaction defined in the current study

The current study is taking further steps to address two important objectives: i) soil erosion due to the combined water fluid and bed softening, and ii) the contribution of seawater fluid in the generation of trench formation. A Coupled Eulerian-Lagrangian (CEL) analysis was conducted using the ABAQUS finite element software to simulate

the erosion mechanisms and the reduction of soil resistance caused by water entrainment. A modified Mohr-Coulomb (MMC) soil model was developed through a VUSDFLD subroutine to properly simulate the soil softening and shear strain rate of seabed soil in an Eulerian domain. Furthermore, a global analysis of SCR was conducted to determine realistic load limit ranges in the TDZ, which were subsequently used as input data for load control analysis in localized CEL simulations. The proposed model integrates the kinematics of seawater fluid to provide a comprehensive insight into the limitations inherent in the existing SCR-soil models.

#### **4.2. Large Deformation Finite Element Technique**

Cyclic motion of the floating vessel leads to vertical and lateral displacement of the riser in the TDZ, and it could be accounted as a large deformation problem, which generally cannot be modelled with the Lagrangian framework due to its excessive mesh distortion and convergence issues. Numerous numerical models have been documented in the literature for simulating the vertical movement of pipelines in diverse soil conditions, utilizing large deformation analyses. One such technique is the Arbitrary Lagrangian–Eulerian (ALE) method, which has been explored in previous studies (Clukey et al., 2008; Merifield et al., 2009). In the ALE approach, the number of elements and nodes remains constant, while the nodal positions can be updated over time to generate a deformed mesh. While mesh distortion can generally be controlled in small strain problems, it becomes challenging to entirely eliminate mesh tangling and convergence issues, particularly in extreme cases. This issue could be resolved by using “remeshing and interpolation techniques with small strain” (RITSS) technique, which has been used by a number of researchers to calculate the vertical pipe penetration (e.g., Hu and Randolph 1998; Barbosa-Cruz and Randolph 2005; Chatterjee et al. 2012a) and lateral



resistance (e.g., Wang et al. 2010; Chatterjee et al. 2012b; Dong et al., 2021). The Coupled-Eulerian Lagrangian (CEL) is another FE technique for large deformation problems (Pike et al., 2010; Dutta et al., 2014) that has been performed in the current study. The nodes of the element are fixed in the space and Eulerian material flows through the elements. This means that the Eulerian elements can contain varying amounts of material, ranging from partially filled to 100% filled, or they can be void if there is no material present. This method uses an explicit time integration scheme, avoiding convergence issues due to the significant level of contact and material softening during the riser-seabed interaction. The numerical procedure employed in the current study has been extensively discussed in subsequent sections, providing a comprehensive overview of the methodology and its implementation.

#### **4.2.1. Numerical Model**

Figure 4-2 depicts the numerical model employed in this study, comprising three main components: the pipe, water fluid, and seabed soil. The pipe cross section is modelled as a rigid body in Lagrangian framework, which undergoes both vertical and lateral movements. Further details on the range of displacement and load control conditions for different pipe motion scenarios will be provided later in the subsequent sections. The water fluid and soil are modeled as Eulerian materials using EC3D8R elements with element size of  $0.020 \text{ m} \times 0.020 \text{ m}$ . Since Abaqus CEL analysis supports three-dimensional geometries, the plane strain condition is simulated by considering only one element in the axial direction of the pipe. This approach allows for an accurate representation of the system while reducing computational complexity.

The in-situ shear strength of soil was assumed to increase linearly with any depth according to the  $s_{u0} = s_{um} + kz$ , where  $s_{um}$  is the undrained shear strength of clay at the

mudline,  $k$  is the strength gradient, and  $z$  is the depth of the soil horizon. It is worth noting that the temperature was defined in Abaqus/CAE as a dummy variable, which was incorporated into the the VUSDFLD subroutine to represent the linear variation of  $s_{u0}$ .

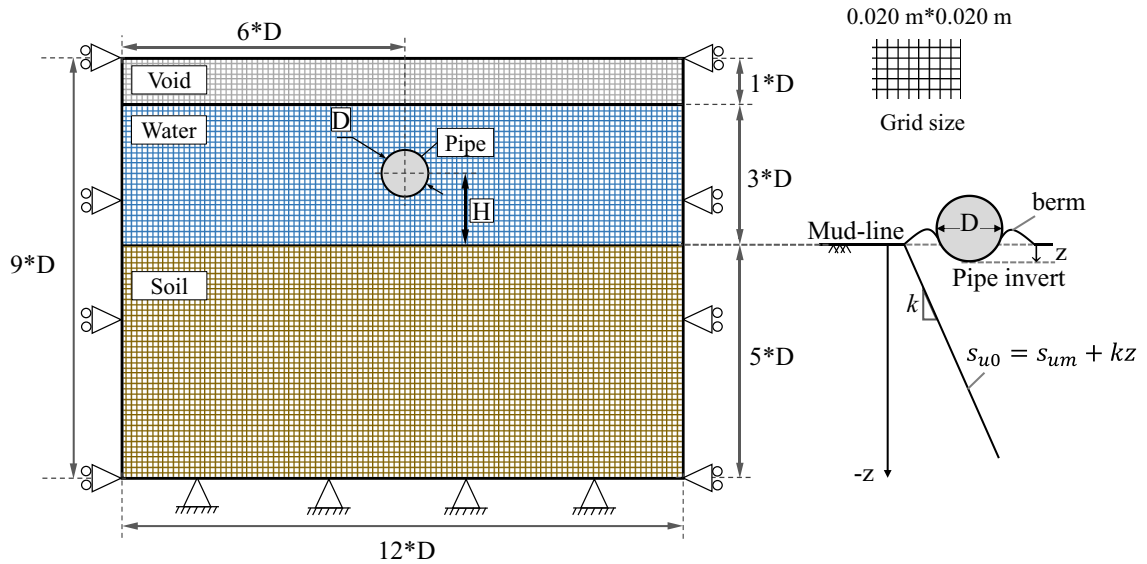


Figure 4-2. Schematic illustration of CEL model: Three-domain model with boundary conditions

Zero velocity boundary conditions were enforced on the normal direction of all vertical faces to constrain the Eulerian materials within the domain. Additionally, the bottom edge was constrained in both the vertical and horizontal directions. General contact was defined between the Eulerian and Lagrangian surfaces to prevent material flow onto the Lagrangian surface and to account for any discrepancies in mesh size between the two surfaces. At the interfaces between the pipe, soil, and fluid, both tangential and normal interactions were considered. A friction coefficient ( $\alpha$ ) ranging from 0 to 1 is commonly assumed to govern the tangential interaction for the pipe-soil interface. It was assumed as  $\alpha = 0$  in the current study, representing the smooth condition. The maximum shear resistance ( $\tau_{max}$ ) was determined based on  $\tau_{max} = (1/S_f) \times s_{um}$  as provided in the literature

(Chatterjee, 2012a), where  $s_{um}$  is the undrained shear strength at the mudline, and  $S_t$  is the soil sensitivity. Furthermore, a “hard” contact condition was assumed for the normal interaction at the pipe-soil interface.

An incompressible water fluid was utilized in the analysis, characterized by a density ( $\rho_w$ ) of 1025 kg/m<sup>3</sup>, an Equation of State (EoS) was defined based on the Us-Up with a  $c_0 = 1450$  m/s, and a viscosity ( $\mu$ ) of 0.001 Pa·s. For the pipe-fluid interface, zero friction was assumed in the tangential direction, indicating a lack of resistance to sliding between the pipe and fluid surfaces. However, a “hard” contact condition was enforced in the normal direction, preventing any penetration between the pipe and fluid components.

### **4.3. Seabed soil strain rate and softening effects**

The in situ shear strength tests have revealed that real soils exhibit strain-rate dependency of shear strength and also gradual softening in strength as they are remoulded. These characteristics have a significant impact on vertical soil resistance, but they are often overlooked by existing plasticity soil models. The significance of these effects has been highlighted in the theoretical studies of deep penetration problems (Einav & Randolph, 2005; Zhou & Randolph, 2007, 2009) and also pipe penetration resistance (Chatterjee et al., 2012a; Dutta et al., 2014). It is important to consider these aspects in order to accurately capture the behaviour of soils and effectively modelling the soil resistance in numerical analyses. In the current analyses, the effects of strain rates and strain softening on the soil resistance were incorporated by modifying the elastic-perfectly plastic Mohr-Coulomb soil model. The undrained shear strength was modified based on the rate of maximum shear strain ( $\dot{\gamma}_{max}$ ) and the accumulated absolute maximum plastic shear strain ( $\xi$ ), as shown in equation (4-1). This

modification allows for the quantification of the enhancement in shear strength due to high strain rates and the reduction in shear strength due to strain softening.

$$s_u = \left[ 1 + \mu \log \left( \frac{\max(\dot{\gamma}_{max}, \dot{\gamma}_{ref})}{\dot{\gamma}_{ref}} \right) \right] \times [\delta_{rem} + (1 - \delta_{rem})e^{-3\xi/\xi_{95}}] s_{u0} \quad (4-1)$$

where  $\dot{\gamma}_{ref}$  is the reference shear strain rate usually taken as  $3 \times 10^{-6} s^{-1}$  ( $\sim 1\%/h$ ) (Wang et al., 2010).  $s_{u0}$  is the in situ undrained shear strength at the reference shear strain rate and prior to any softening;  $\mu$  is the rate of strength increase per log cycle with a typical value ranging from 0.05–0.2 (Einav and Randolph 2005; Lehane et al. 2009).  $\delta_{rem}$  is the ratio of fully remoulded and initial shear strength and obtained by the inverse of sensitivity of soil. The maximum plastic shear strain rate at a given location is defined by the equation (4-2), where  $\Delta\varepsilon_1$  and  $\Delta\varepsilon_3$  are the major and minor principal plastic strain components, and  $\Delta t$  is the time increment.

$$\dot{\gamma}_{max} = \frac{\Delta\varepsilon_1 - \Delta\varepsilon_3}{\Delta t} \quad (4-2)$$

$\xi$  is determined by the accumulation of the absolute maximum plastic shear strain from the first to the current increment, and  $\xi_{95}$  represents the value of  $\xi$  for 95% shear strength degradation, which is typically varied between 10 and 50 (Randolph, 2004). A VUSDFLD subroutine was coded to to modify the undrained soil strength at each increment of the dynamic analysis, taking into account the shear strain and softening. The Young's modulus of the soil was adjusted accordingly based on the relation  $E = 500s_u$ .

#### 4.3.1. Parametric study to validate the FE model

A series of analyses were performed using the CEL approach to validate the numerical model. Initially, analyses were performed assuming ideal soil behavior, neglecting

strain rate effects and soil softening. Subsequently, the combined effects of strain rate and soil softening were considered. Two scenarios of vertical pipe-seabed interaction were considered in these analyses. The first scenario involves a rigid pipe being vertically inserted into the soil, while the second scenario considers the same situation but with the inclusion of water entrainment. These scenarios were based on the pipeline model tests with a 20 mm diameter corresponding to 1 m at the prototype scale, performed at an acceleration level of 50g in a geotechnical centrifuge test at Western Australia University (Yuan et al., 2017). The seabed soil used in the physical model was kaolin clay, which was normally consolidated from slurry in a centrifuge with a submerged weight of  $\gamma' = 6 \text{ kN/m}^3$ . A piezoball penetrometer was used to measure the intact undrained shear strength, which was linearly increased at a rate of 0.9 kPa/m (in prototype depth unit) over the depth range with a negligible intercept at the seabed mudline.

To examine the influence of strain rate and softening, a series of numerical simulations with the broad ranges of  $\mu$  and  $\zeta_{95}$  were carried out ( $\mu = 0.05, 0.1, 0.2$ ;  $\zeta_{95} = 10, 50$ ), followed by a comparison with the results of a centrifuge model test. The analyses also included the ideal soil to represent a scenario without any strain rate and softening effects. A total of 14 simulations were provided for two scenarios of pipe motions while considering the presence or absence of water entrainment. In order to expedite the computation time, only a half-cycle of pipe penetration was initially considered. According to Figure 4-3, it was observed that the values of  $\mu = 0.05$  and 0.1, within the range of  $\zeta_{95} = 10$ , exhibited a satisfactory level of agreement with the centrifuge model tests. Consequently, these specific values were selected to generate results for three

half-cycles, thereby validating the outcomes for both extraction and subsequent penetration in cycle 2.

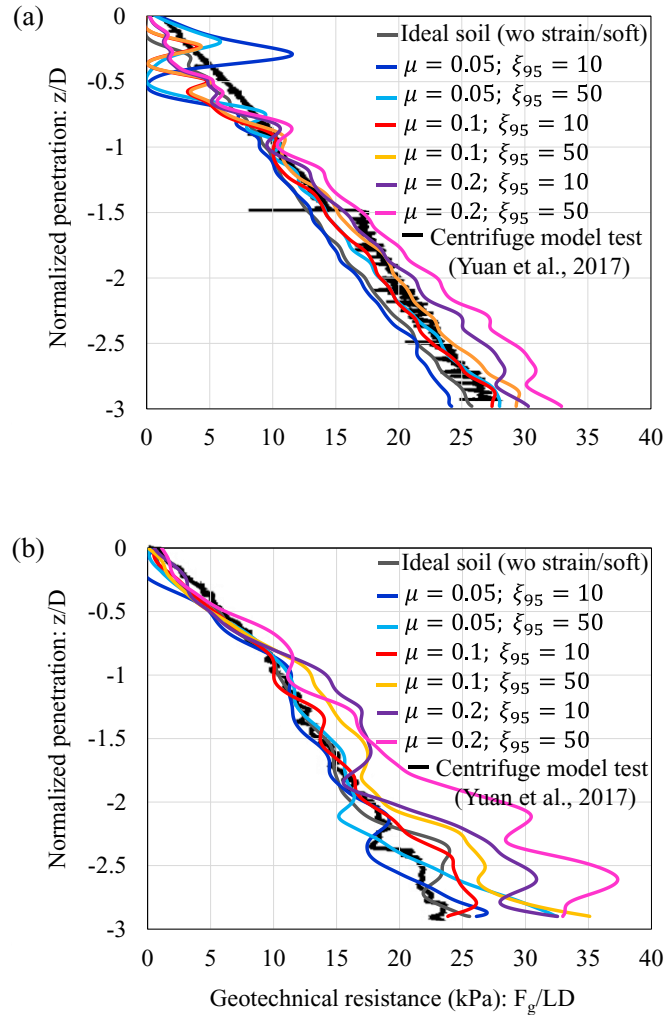


Figure 4-3. Penetration resistance for the first one-half cycle: (a) without water entrainment, (b) with water entrainment

As shown in Figure 4-4, the pipe starts to move downward from the seabed mudline and then cyclically displaced between  $z/D = -1.5$  and  $-3$ , demonstrating completely buried into the soil, and no water interaction was considered. However, as illustrated in Figure 4-5, a modification was made to the upper displacement limit, which was adjusted to  $z/D = 1$  above the original mudline. This adjustment allowed water entrainment to take place during each cycle as the pipe penetrated and emerged from

the seabed. The geotechnical resistance was used for comparing the results with the centrifuge modelling study to choose a set of values ( $\mu$ ,  $\xi_{95}$ ) that matched with the finding of the published work. The geotechnical resistance ( $F_g$ ) is considered as the sum of the soil resistance and a component due to the soil buoyancy force as the pipe becomes embedded into the soil, as provided in equations (4-3), which are expressed in Newton.

$$F_g(z) = F_s(z) + F_b(z) \quad (4-3)$$

The vertical pipe velocity was assumed as 0.125 m/s for all the parametric analyses. It is noting that the results of centrifuge tests are provided for 200 cycles, while two cycles were considered for validation purposes due to the significant computational time required for the CEL simulations.

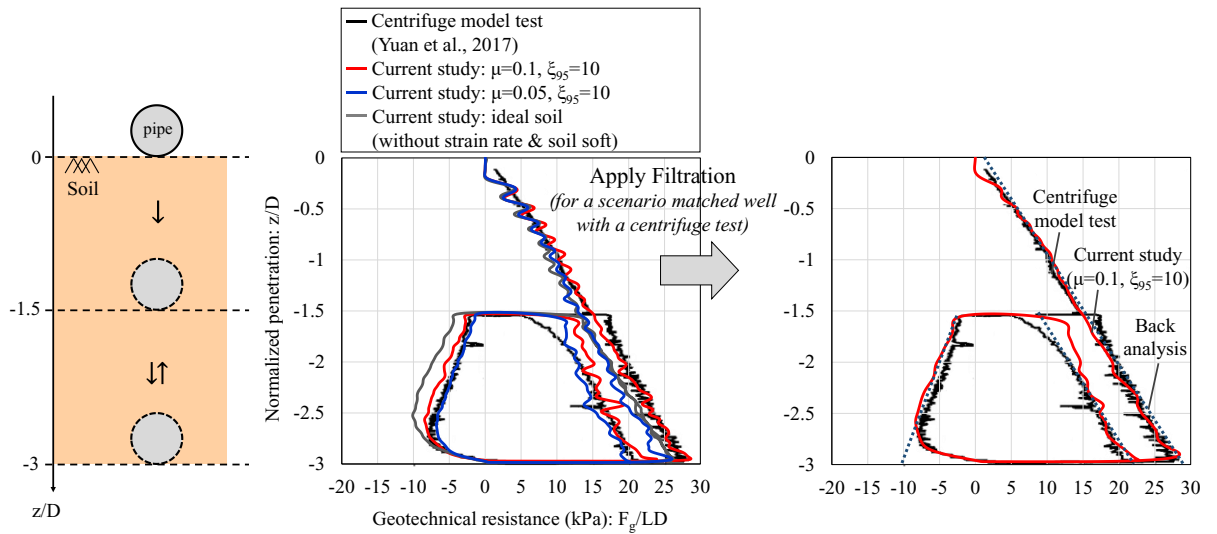


Figure 4-4. Vertical resistance obtained from CEL and centrifuge model test without water entrainment

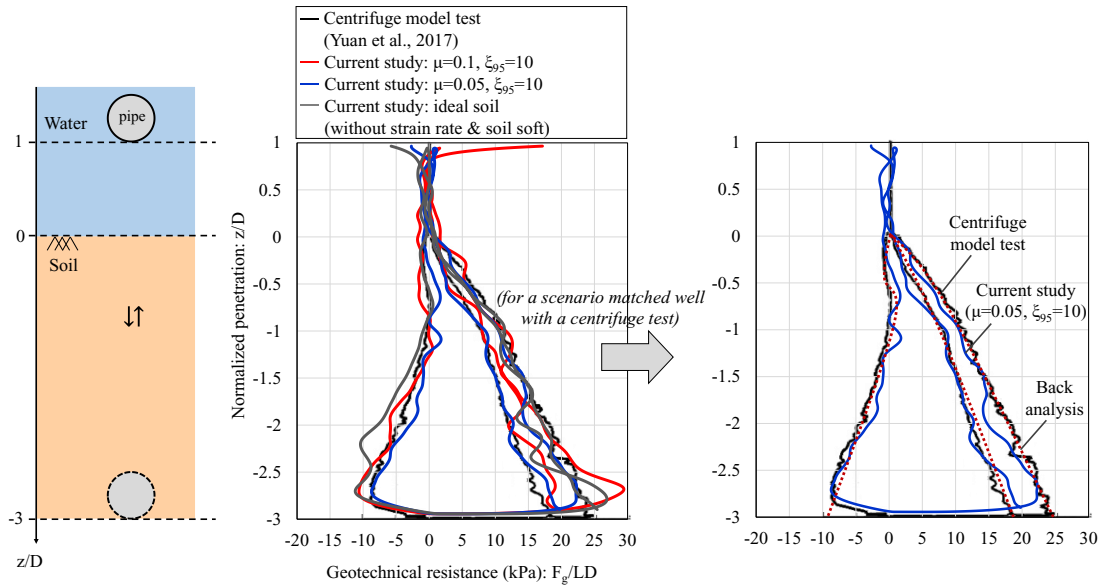


Figure 4-5. Vertical resistance obtained from CEL and centrifuge model test with water entrainment

The results confirm that both the strain rate and softening effects have a significant impact on the vertical resistance in both scenarios of pipe motion, particularly during the second cycle of penetration. It should be noted that in an ideal soil, the vertical resistance would remain constant during this second cycle. In order to better represent the results, a suitable Butterworth filtration was applied to the scenarios that demonstrated good agreement with the experimental measurements. This included the use of the values  $\mu = 0.1$  and  $\zeta_{95} = 10$  for the first scenario, which involved purely soil conditions, and  $\mu = 0.05$  and  $\zeta_{95} = 10$  for the scenario with water entrainment. These specific parameter values are considered as the base case hereafter, affirming the validity and reliability of the CEL approach employed for the subsequent analyses.

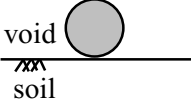
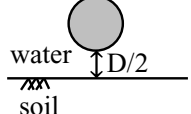
#### 4.4. FE Analysis for a Case Study

The FE models in this section involved displacement control analyses, where the pipe oscillated vertically between lower and upper displacement limits with zero lateral



movements. Table 4-1 provides the scenarios conducted for two different cases of interactions, with and without water entrainment.

Table 4-1. Summary of pipe motion scenarios used for displacement control analysis

Scenario	upper cyclic limit	lower cyclic limit	water entrainment	Schematic pipe configuration
DISP1	$z/D = 0$	$z/D = -0.5$	NO	void  soil
DISP2	$z/D = +0.5$	$z/D = -0.5$	YES	water  soil

The pipe diameter ( $D$ ) was taken as 0.5 m in these simulations, representing an example of SCR diameter (Zhou et al., 2020). The submerged unit weight of the soil was assumed as  $\gamma' = 5.5 \text{ kN/m}^3$ , a typical value for deep-water seabed sediments (Chatterjee et al., 2012a; Zhou et al., 2020). A parametric study was conducted, involving variations in the in-situ undrained shear strength properties, including the  $s_{um}$  and  $k$  values as specified in Table 4-2. These variations were performed for each scenario, resulting in a total of 12 different simulations.

Table 4-2. Naming of FE simulations within different shear strength properties

in-situ undrained shear strength $s_{u0} \text{ (kPa)} = s_{um} + kz$	Water entrainment scenario	
	NO	YES
	Case No.	
$0 + 0.9z$	DISP1-1	DISP2-1
$0.5 + 1.8z$	DISP1-2	DISP2-2
$1 + 2.7z$	DISP1-3	DISP2-3
$2 + 3.6z$	DISP1-4	DISP2-4
$6 + 1.8z$	DISP1-5	DISP2-5
$10 + 0.9z$	DISP1-6	DISP2-6

The Pipe motion was vertically moved in three half-cycles: i) Penetration mode, ii) uplift mode, and iii) re-penetration mode. The variation of normalized vertical geotechnical resistance,  $F_g/DLs_{u0}$  ( $s_{u0}$  is the in-situ undrained shear strength at the invert of the pipe), with non-dimensionalized pipe embedment,  $z/D$ , are plotted in Figure 4-6 for different scenarios. The results show that water entrainment had a minimal effect during the first half-cycle, with only a slight reduction in the vertical resistance within the soft clay cases (e.g., DISP2-1, DISP2-2, DISP2-3, DISP2-4) and no changes observed for stiff cases (DISP2-5, DISP2-6). In pure soil cases, the downward movement of the pipe during the initial penetration mode resulted in the formation of a stabilized trench. This trench formation can be attributed to the high load range applied to the soil, which is a consequence of the displacement control analyses. As the suction force is minimal and reaches zero in stiff soil cases (DISP1-4, DISP1-5, and DISP1-6), there is no tendency for the soil mass to move upward. Consequently, the contact between the pipe and the soil is lost during the subsequent penetration mode. However, the presence of water at the pipe-seabed interface creates an additional suction force by allowing free water to enter the gaps around the pipe section, causing the soil mass to move upward.

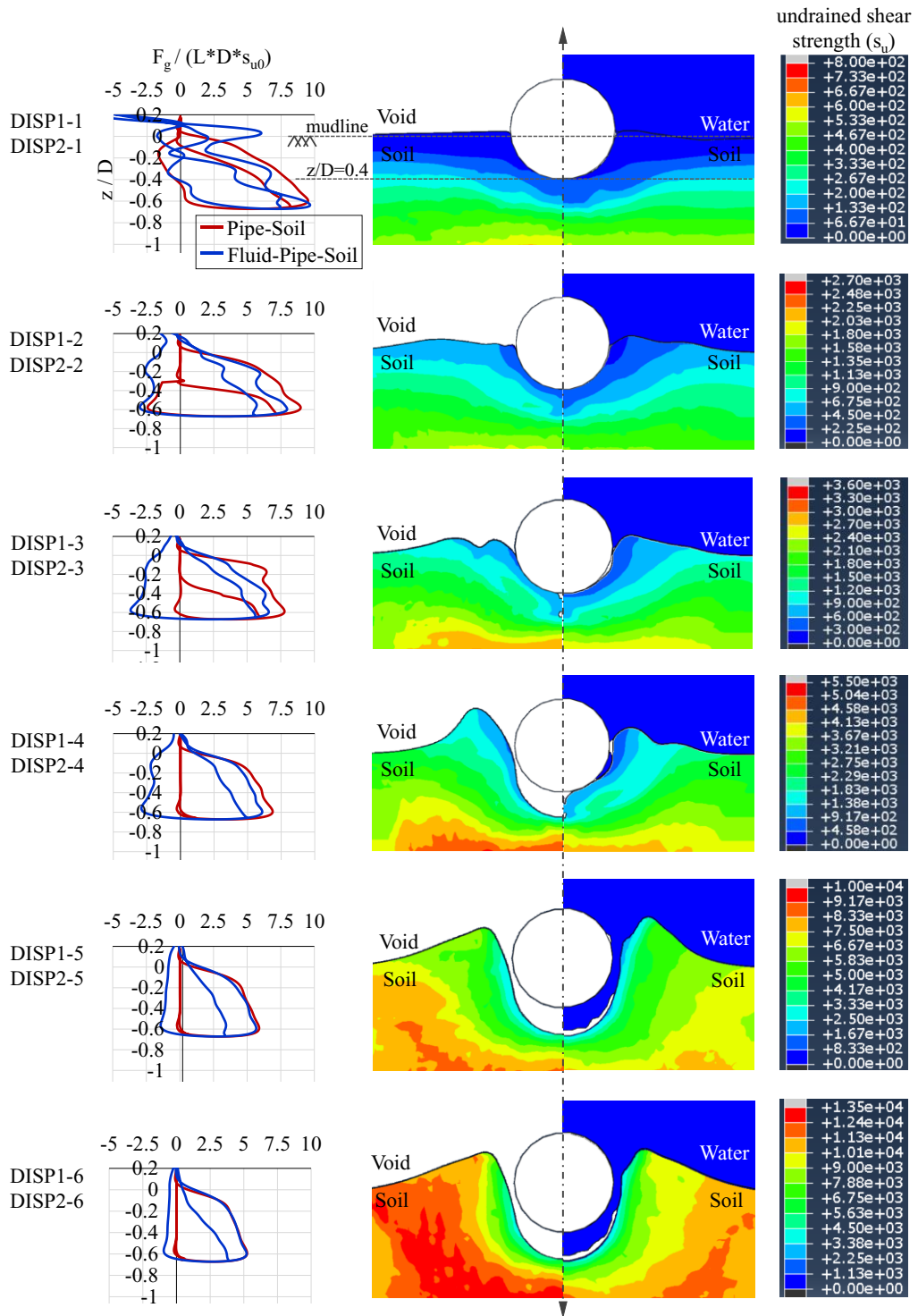


Figure 4-6. Normalized geotechnical resistance for pipe-soil and fluid-pipe-soil interaction

A contour representation of the undrained shear strength has been schematically superimposed in Figure 4-6 for the specific moment when the pipe is positioned at  $z/D$

= -0.4 during the re-penetration mode. The representation illustrates that the presence of water can influence various soil layers by reducing the undrained shear strength.

As noted earlier, the vertical geotechnical resistance may be considered as the sum of two components, soil resistance and extra buoyancy force as the pipe penetrates into the soil, which are expressed in N/m in equation (4-4).

$$q_g(z) = N_c S_{u0} D + f_b A_s \gamma' \quad (4-4)$$

The first term on the right side denotes the soil resistance based on the bearing capacity failure, indicating that the soil resistance is sufficient to resist the load applied by the pipeline.  $N_c$  is the soil bearing factor and can be obtained by equation (4-5).

$$N_c = a \left( \frac{z}{D} \right)^b \quad (4-5)$$

where “ $a$ ” and “ $b$ ” are the power law parameters.

As indicated in equation (4-4), the second term defined as extra buoyancy force, which has been created due to the higher density of the soil sediment compared to the seawater. This buoyancy force would be enhanced by a soil buoyancy factor,  $f_b$ , which accounts for the local heave effect of the soil adjacent to the pipe. The parameter of  $A_s$  is the nominal area of the pipe embedded below the seabed mudline, which can be determined by the following equation (Randolph and White, 2008).

$$A_s = \begin{cases} \frac{D^2}{4} \left[ \sin^{-1} \left( \sqrt{4 \frac{z}{D} \left( 1 - \frac{z}{D} \right)} \right) - 2 \left( 1 - 2 \frac{z}{D} \right) \sqrt{\frac{z}{D} \left( 1 - \frac{z}{D} \right)} \right] & \text{if } \frac{z}{D} \leq 0.5 \\ \frac{\pi D^2}{4} \left( 1 - \left[ \sin^{-1} \left( \sqrt{4 \frac{z}{D} \left( 1 - \frac{z}{D} \right)} \right) - 2 \left( 1 - 2 \frac{z}{D} \right) \sqrt{\frac{z}{D} \left( 1 - \frac{z}{D} \right)} \right] \right) & \text{if } 0.5 < \frac{z}{D} < 1 \\ \frac{\pi D^2}{4} & \text{if } \frac{z}{D} \geq 1 \end{cases} \quad (4-6)$$

where  $z$  is the vertical depth of penetration. The local heave effect surrounding the pipe causes that the real embedment area is greater than the nominal area ( $A_s$ ), leading to have the factor of buoyancy force,  $f_b$ , greater than unity. As shown in Figure 4-7(a), the Eulerian Volume Fraction (EVF) is schematically provided for different numerical analyses, including both pipe-soil and fluid-pipe-soil interactions at the specific depth,  $z/D = -0.4$ , during the first cycle of penetration. It is worth noting that the local and nominal embedment can be changed over time due to the water fluid flow and soil erosion, but the selection for  $f_b$  is typically conducted through the first penetration process (Randolph and White, 2008).

It can be seen that the level of soil surrounding the pipe is slightly reduced while fluid entrained into the soft clays, e.g., in Cases DISP2-1, and DISP2-2, while this level of exposure remains unchanged for other scenarios. As shown in Figure 4-7(b), the reasonable range of  $f_b$  has been selected for each scenario with the assistance of recommended values suggested by the previous studies (Randolph and White, 2008; Chatterjee et al., 2012a).

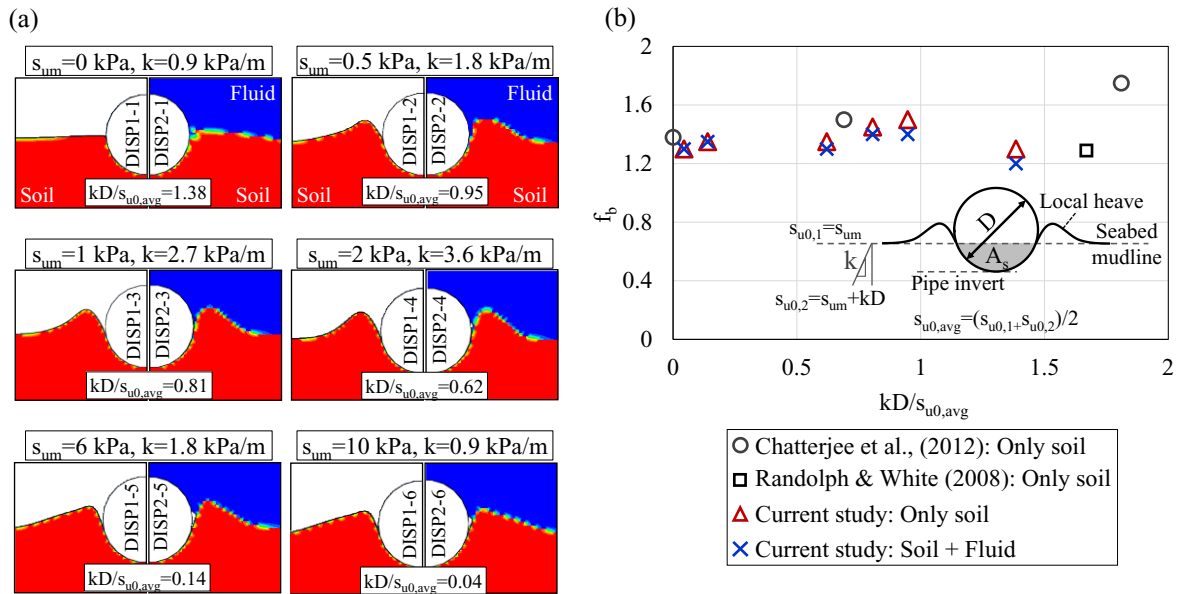


Figure 4-7. (a) Schematic illustration of soil heave during  $z/D = -0.4$  with and without water entrainment; (b) the selected values for  $f_b$

It is essential to quantify the vertical geotechnical resistance using theoretical expressions, which is very helpful for routine design purposes. As explained earlier, the bearing capacity failure can be used for predicting soil resistance, which can be added to the buoyancy force effects to provide a reasonable estimation of the geotechnical resistance. As shown in equation (4-5), the power law relationship is developed within two parameters, “ $a$ ” and “ $b$ ” with the function of pipe embedment. The significance of the values for the power law coefficients is highlighted in the literature. Aubeny et al., (2005) presented fitting coefficients for two different  $kD/s_{um} = 0, \infty$  and then plotted best-fit curves for the ranges of soil between them. Their analysis solely focused on a "wished-in-place" (WIP) pipe configuration, thereby disregarding any alterations in soil geometry or the formation of heave during continuous penetration.

Additionally, the effects of strain rate and soil softening were not incorporated into the soil shear strength. Merifield et al. (2008) presented the results for WIP scenario using

uniform soil and subsequently extended their solutions to include the "Pushed-in-place" (PIP) case in a later publication (Merifield et al., 2009). The shortcomings of the previous studies were resolved later by Chatterjee et al., (2012a). They assumed a wide range of undrained shear strength with accounting for strain rate and soil softening to highlight the power law parameter's variations based on the different soil behavior. Although appropriate values of  $a$  and  $b$  were proposed by fitting to power law curves for different ranges of  $s_{um}$  and  $k$ , their investigation only focused on the pipe-soil domain, neglecting the water fluid as a third influential key parameter. The current study extends the previous works by establishing a three-domain model of fluid-pipe-soil interaction with an appropriate range of  $s_{um}$  and  $k$ , in order to investigate the influence of water entrainment on the power law coefficients. The main features of the current study compared to the previous works have been outlined in Table 4-3.

Table 4-3. Main Features of the current study compared to the previous works on power law coefficients

Studies	Pipe-soil friction*	power law parameters		Strain rate & soil softening effects	Water entrainment	Comments
		a	b			
Aubeny et al., (2005)	S	5.42	0.29	NO	NO	WIP
	R	7.41	0.37			
Merifield et al. (2008)	S	5.6	0.32	NO	NO	WIP
	R	7.4	0.4			
Merifield et al. (2009)	S	5.3	0.25	NO	NO	PIP
	R	7.1	0.33			
Chatterjee et al., (2012a)	$\alpha = 0.31$	6.81	0.25	YES	NO	PIP
Present study	S	see Figure 4-9		YES	YES	PIP

\* (S:  $\alpha = 0$ ); (R:  $\alpha = 1$ )

An appropriate range of values for parameters  $a$ ,  $b$  was chosen to fit the theoretical outcomes of the vertical resistance, as determined by equation (4-5), with the numerical results obtained from the CEL analyses. The graphical representation of this alignment is illustrated in Figure 4-8 using a dashed line labeled as the “Theoretical method” for pure soil conditions without any water entrainment. This was adjusted to account for the fluid-pipe-soil conditions, and a new representation in the form of a black line was introduced, named as “Theoretical method-Modified”.



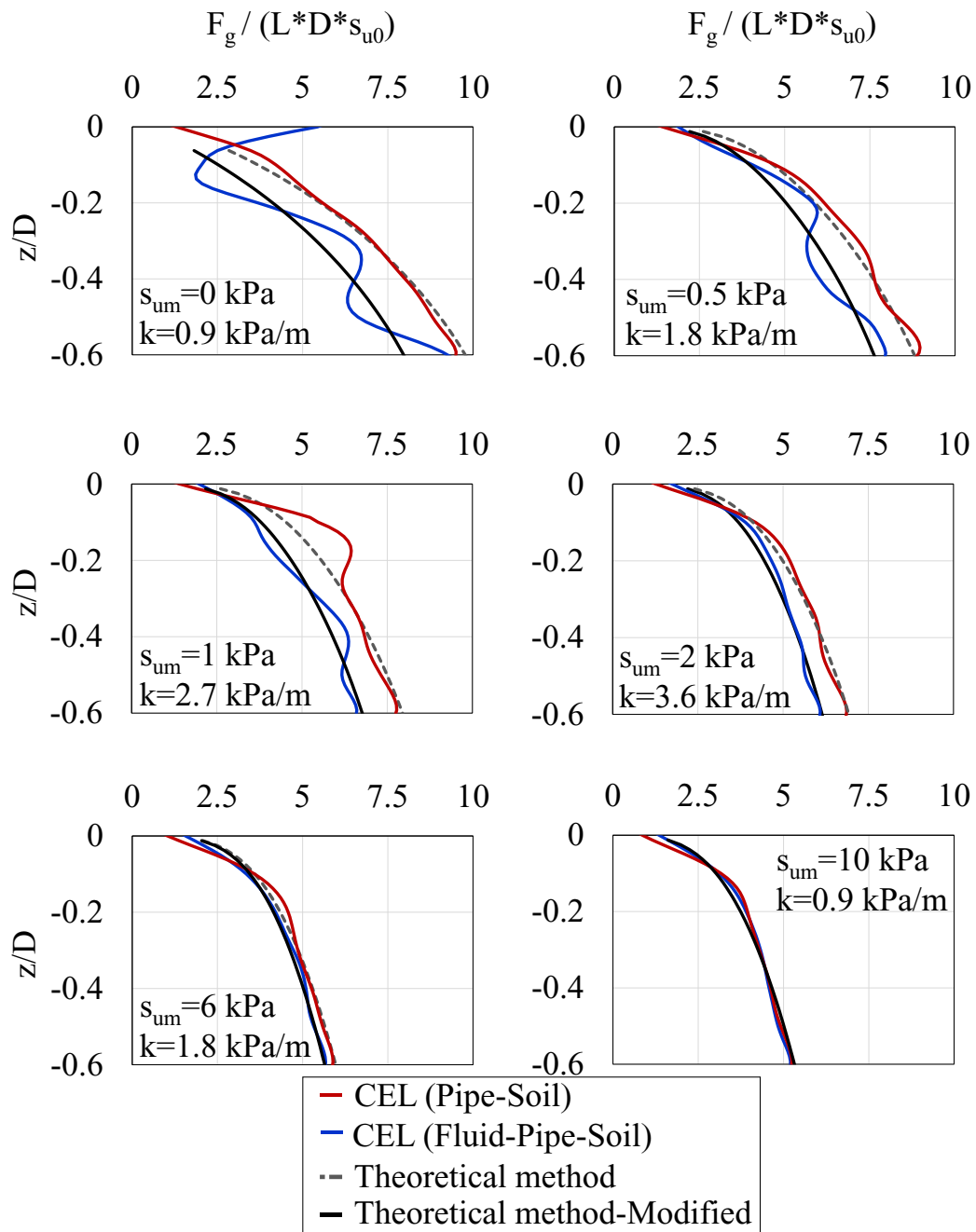


Figure 4-8. Fitting vertical resistance in the CEL method with the theoretical method

The values of  $a$  and  $b$  were extracted in each case scenario and plotted against the averaged shear strength form to establish a generalized relationship applicable to various soil depths. As shown in Figure 4-9, the findings indicate a noticeable decrease of approximately 20% in the range of values for  $a$  when the soil experienced erosion due to water entrainment.

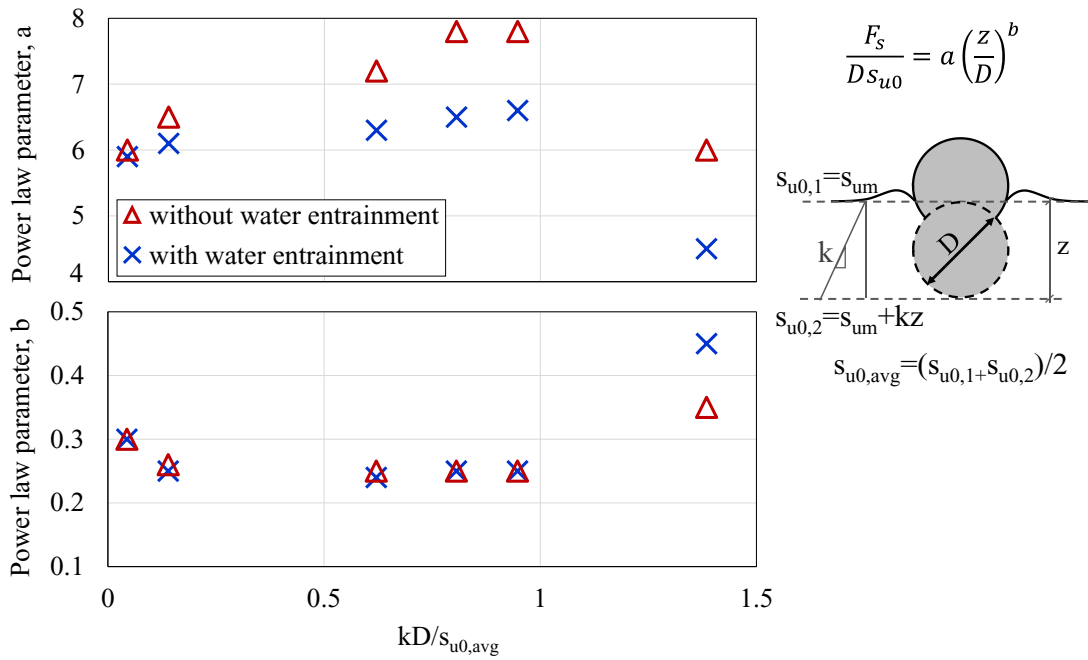


Figure 4-9. Derived values for bearing capacity factors, with and without water entrainment. However, the values for  $b$  remained relatively constant, with the exception of one scenario involving very soft clay. This accomplishment offers valuable insights for potential modifications to the existing parameter values commonly employed in design practices.

#### 4.5. Contribution of water entrainment and lateral movements in trench formation

The existing global analysis of SCRs makes use of both linear and non-linear soil models to determine the vertical contact force, experienced by a catenary riser or pipeline while in contact with the seabed soil. A simple linear spring assumption does not account for any variations in soil response during repeated cycles or soil softening, leading to inaccurate fatigue damage outcomes (Thethi and Moros, 2001; Randolph et al., 2013). Efforts to address uncertainties related to linear stiffness have previously been focused on introducing hysteretic non-linear soil models, which employ a combination of hyperbolic and exponential functions of SCR-soil stiffness during the

four main phases of riser motion: a) initial penetration, b) uplift, c) suction, and d) re-penetration (e.g., Randolph and Quiggin, 2009; Aubeny and Bisconting, 2009). A schematic illustration of the linear and hysteretic non-linear soil models is provided in Figure 4-10. It is worth noting that the cyclic soil remoulding due to the cyclic motion of SCR is not the sole mechanism responsible for riser embedment. Other mechanisms may also increase the riser penetration by scraping the seabed soil, such as seabed erosion caused by combined vortices generated by subsea currents and the presence of seawater entrapped between the oscillating riser and the trench that predominantly occur during the early stages of the riser production life (first 2 to 3 years) (Janbazi & Shiri, 2023a). Despite the limited number of studies on these mechanisms in the literature, they still need deeper investigation to better understand and model the riser-seabed-seawater interaction.

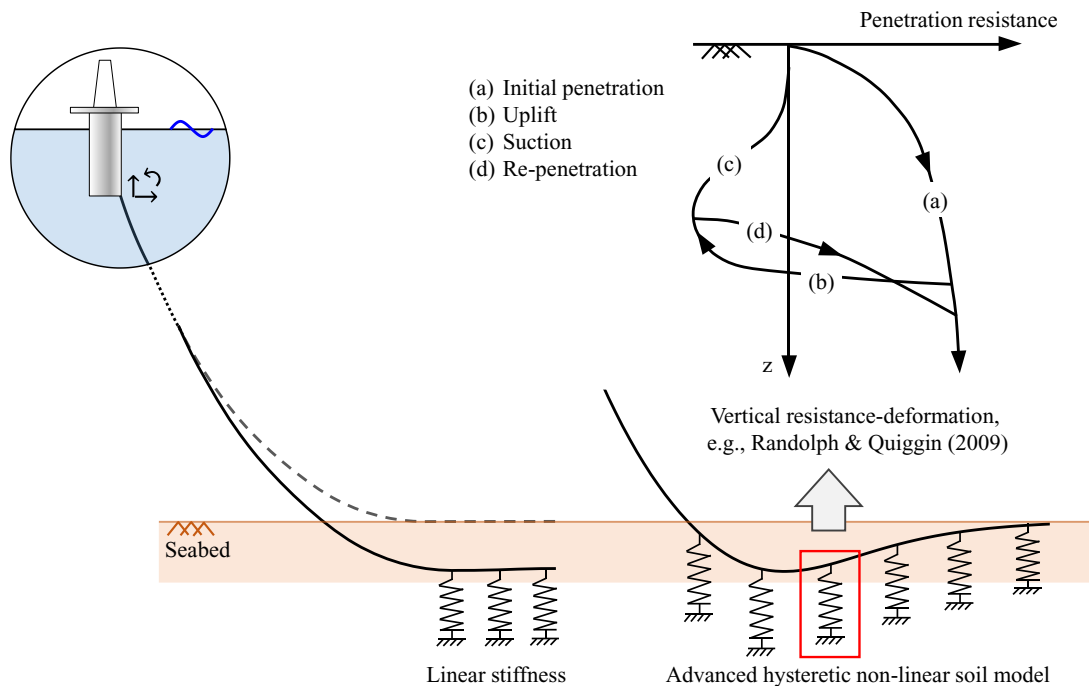


Figure 4-10. Existing methods commonly used for global analysis of SCRs

A global SCR model was developed in the current study by integrating the advanced non-linear soil model (R-Q) into ABAQUS through a UEL subroutine. The vessel excitation under the environmental loads was coded into a DISP user subroutine to provide the cyclic motions of the riser in the TDZ. The aim was to use the results obtained from the global FE model for defining the range of riser oscillations and load limits within the TDZ, which were subsequently incorporated into a local CEL model to analyze the behavior of the pipe cross-section in a more detailed and accurate manner. The key parameters of the SCR and soil properties used for the global simulation of SCR are summarized in Table 4-4.

Table 4-4. Main parameters of the soil properties and SCR used for global analysis

Parameter	Sign	Value
Mud-line shear strength (kPa)	$s_{u0}$	0.5
Shear strength gradient (kPa/m)	$k$	1.8
Saturated soil density (kg/m <sup>3</sup> )	$\rho_{soil}$	1560
Power law parameters	$a, b$	6, 0.25
Suction ratio	$f_{suc}$	0.4
Suction decay parameter	$\lambda_{suc}$	0.4
Re-penetration parameter	$\lambda_{rep}$	0.2
Soil buoyancy factor	$f_b$	1.5
SCR outer diameter (m)	$D$	0.5
pipe wall thickness (m)	$t$	0.0315
water depth (m)	$\Delta Z$	1600
cross-section area (m <sup>2</sup> )	$A_s$	4.63E-02
submerged weight (kg/m)	$m_s$	237

Figure 4-11(a) illustrates the profile of the trench that forms beneath the riser within the normalized cyclic oscillations during the initial cycles of riser simulations. The vessel oscillation was chosen as  $H_{tan} = 4.5$  m and  $T = 15$  s in the tangential direction of the local coordinate system at the SCR hang-off point (Kimiæi et al., 2010). This vessel-induced excitation resulted in vertical displacement within the TDZ, ranging from 0.2-0.3 times the diameter of the pipe.

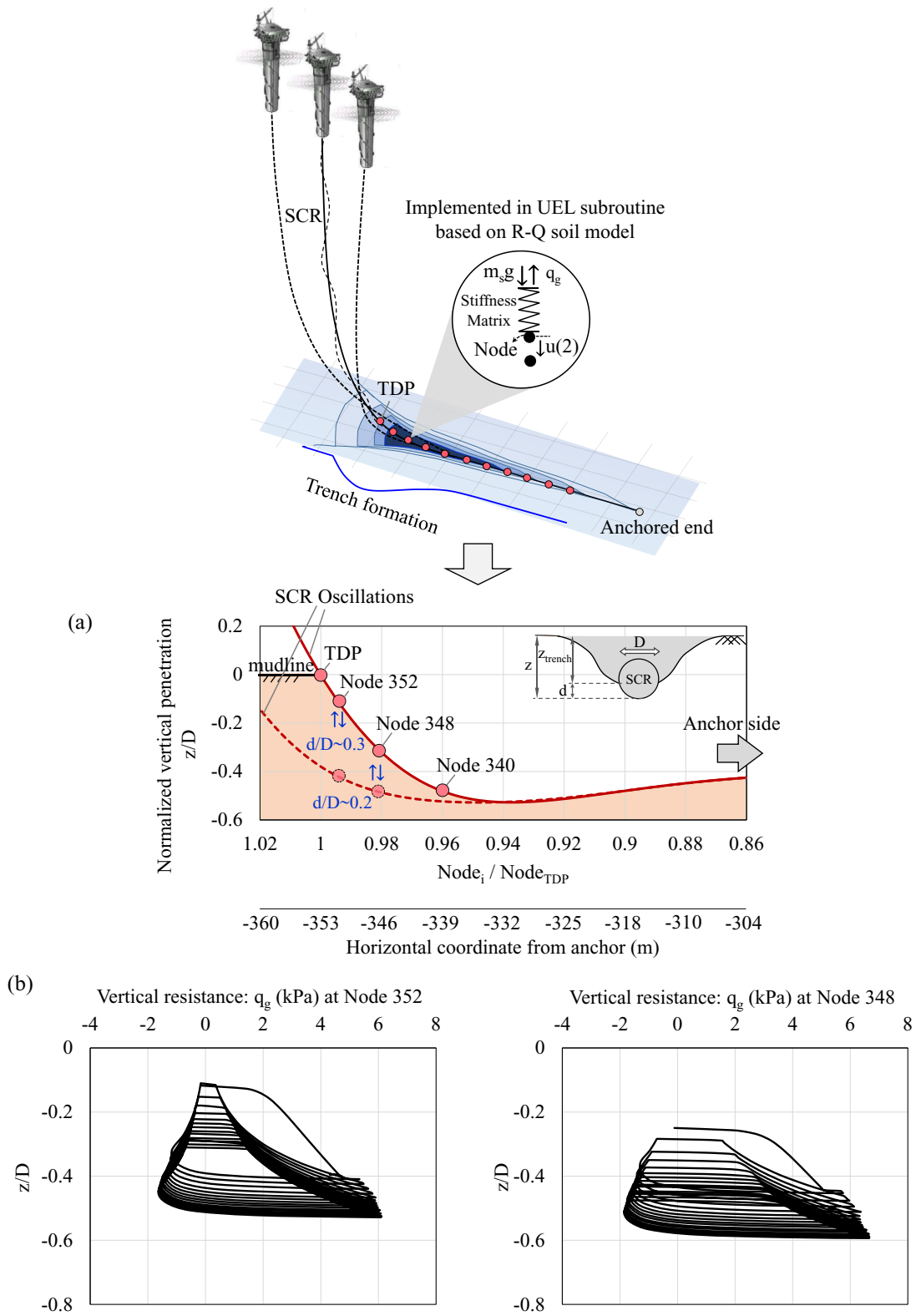


Figure 4-11. (a) SCR profile in the TDZ; (b) The range of riser oscillations and soil resistance for sample nodes in the TDZ

The results of vertical geotechnical resistance versus normalized penetration are provided in Figure 4-11(b) for two sample nodes in the TDZ, Node 348 and Node 352. It is apparent that the soil disturbance caused trench formation at a maximum depth of approximately 0.6 times the riser diameter over 15 cycles when the riser had sufficiently stabilized after undergoing cyclic motions.

Based on the findings given from the global analysis of SCR, a combination of displacement and load control analyses have been employed into the CEL model of the pipe cross-section by defining a specified downward load limit of 7 kPa within normalized vertical oscillation of 0.2, respectively setting the lower and upper displacement limits. A schematic representation of these limits is provided in Figure 4-12, which was implemented in the VUAMP subroutine.

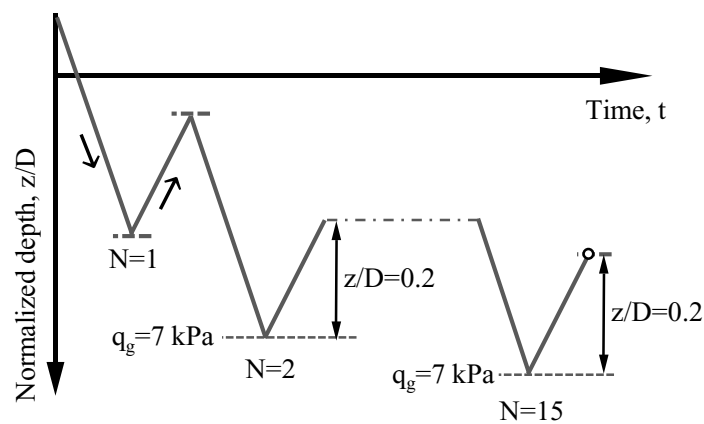
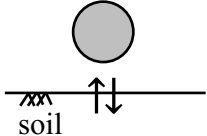
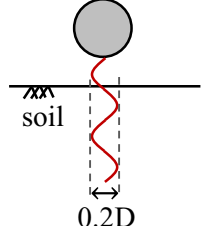
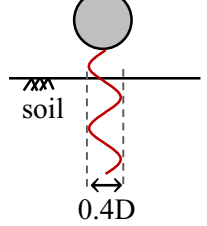


Figure 4-12. Time history of vertical displacement defined with load control analysis

It is worth noting that current touchdown models for SCRs are predominantly based on the investigations involving purely vertical loading and movement. However, several studies have addressed the inclusion of lateral movements, as observed in real-field scenarios (Oliphant et al., 2009; Al-Janabi et al., 2020). Therefore, two distinct ranges were considered to account for these lateral oscillations, leading to the transformation

of the vertical pipe motion into a sinusoidal pattern path. Table 4-5 provides a summary of pipe scenarios, which have been categorized into six simulations.

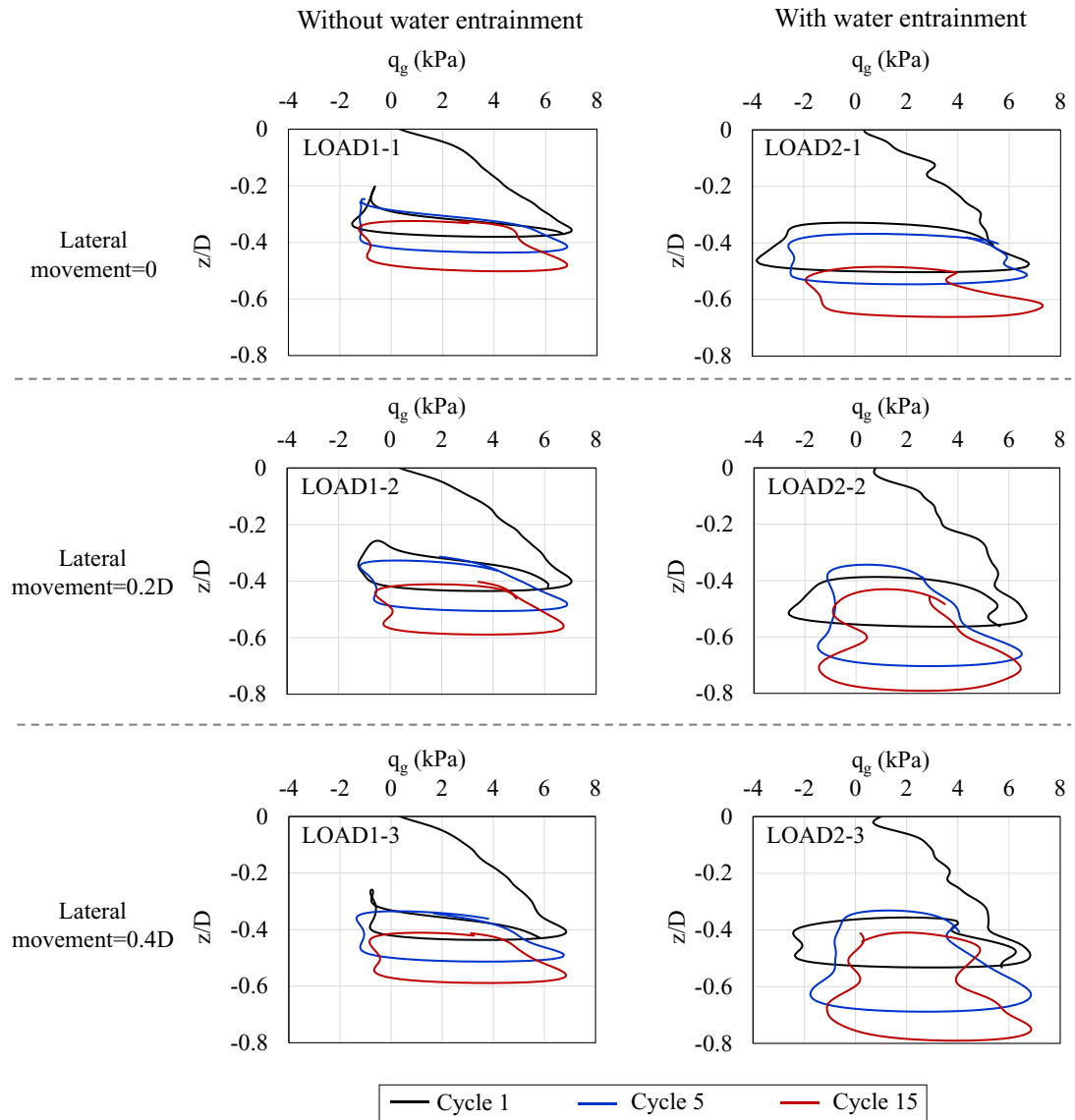
Table 4-5. Summary of pipe motion scenarios used for load control analysis

Scenario	water entrainment	upper / lower cyclic limits	Lateral oscillations	Schematic pipe configuration
LOAD1-1	NO	See Figure 4-12	NO	
LOAD2-1	YES			
LOAD1-2	NO		YES	
LOAD2-2	YES			
LOAD1-3	NO			
LOAD2-3	YES			

The vertical geotechnical resistance in selected cycles, 1, 5, 15, is illustrated in Figure 4-13, highlighting the effects of lateral movement, water entrainment, and trench evolution. The vertical limit for each cycle is determined by the load limit of  $q_g = 7 \text{ kPa}$ , equivalent to  $F_g = 110 \text{ N}$ . The utilization of a load limit enables the modeling of two-dimensional trench evolution, where the displacement attained in each cycle is controlled by the changing soil strength and trench depth. The reduction in soil strength resulting from soil softening becomes apparent throughout the 15 cycles, leading to a gradual increase in the pipe embedment achieved in each cycle.

It is important to emphasize that the scenario LOAD1-1, which corresponds to the global analysis of the SCR depicted in Figure 4-11, exhibits a lower riser embedment

compared to the sample nodes acquired by R-Q soil model. This discrepancy can be attributed to the catenary-induced force exerted by the SCR in the TDZ, leading to a deeper trench depth, a phenomenon that cannot be captured by the local CEL model.



	maximum trench depth (z/D) at cycle 15		maximum trench depth (Normalized by pipe-soil scenario, without lateral)	
	Without water entrainment	With water entrainment	Without water entrainment	With water entrainment
without lateral	-0.50	-0.66	1.00	1.32
lateral=0.2D	-0.59	-0.79	1.17	1.57
lateral=0.4D	-0.59	-0.79	1.17	1.57

Figure 4-13. Evolution of vertical trench depth in response to the effects of lateral movement and water entrainment



According to Figure 4-13, the inclusion of water fluid showed a notable enhancement in trench evolution, resulting in a 32% increase in the maximum vertical depth when no lateral movements were present. However, it is important to consider that these results are based on a limited number of 15 cycles due to computational time constraints in the current study, and the influence of the fluid may be more significant in higher cycles. Moreover, the moderate-amplitude lateral movement serves as an additional factor contributing to the reduction in vertical penetration resistance, thereby accelerating the rate of embedment with each cycle. By cycle 15, in the scenario of pure soil condition, the depth of embedment reaches  $z/D = 0.6$ , whereas without any lateral cycles, this depth would be around 0.5. It is noteworthy that the influence of lateral movement becomes slightly more significant when water entrainment is considered, leading to an improved depth of  $z/D = 0.8$  from 0.6. A summary of these highlights has been provided in a table superimposed within the Figure 4-13. The maximum trench depth was also normalized by the corresponding cycle observed in the pipe-soil interaction model without lateral movement. The results clearly indicate a total improvement of approximately 57% in the maximum trench depth when water fluid is considered in conjunction with lateral movements, which has been neglected in existing advanced non-linear soil models commonly used for SCR-seabed interaction.

The movement of the pipe can displace the surrounding soil, leading to the formation of voids or gaps between the pipe and the soil, as well as the creation of raised mounds or ridges of soil around the pipeline, known as berms. The berms around the pipeline play a crucial role in ensuring stability and support for the pipeline system by serving as a protective barrier, effectively preventing excessive movement and potential harm to the pipeline. As depicted in Figure 4-14, the presence of water fluid further

contributes to the formation and development of the berms. The flow of water can infiltrate the gaps, exerting supplementary pressure on the soil, which consequently causes the soil to be washed away or displaced. Over a period of time, this phenomenon not only leads to the gradual deepening of the trenches but also extends the progression of the berms area by carrying away soil particles in a lateral direction.

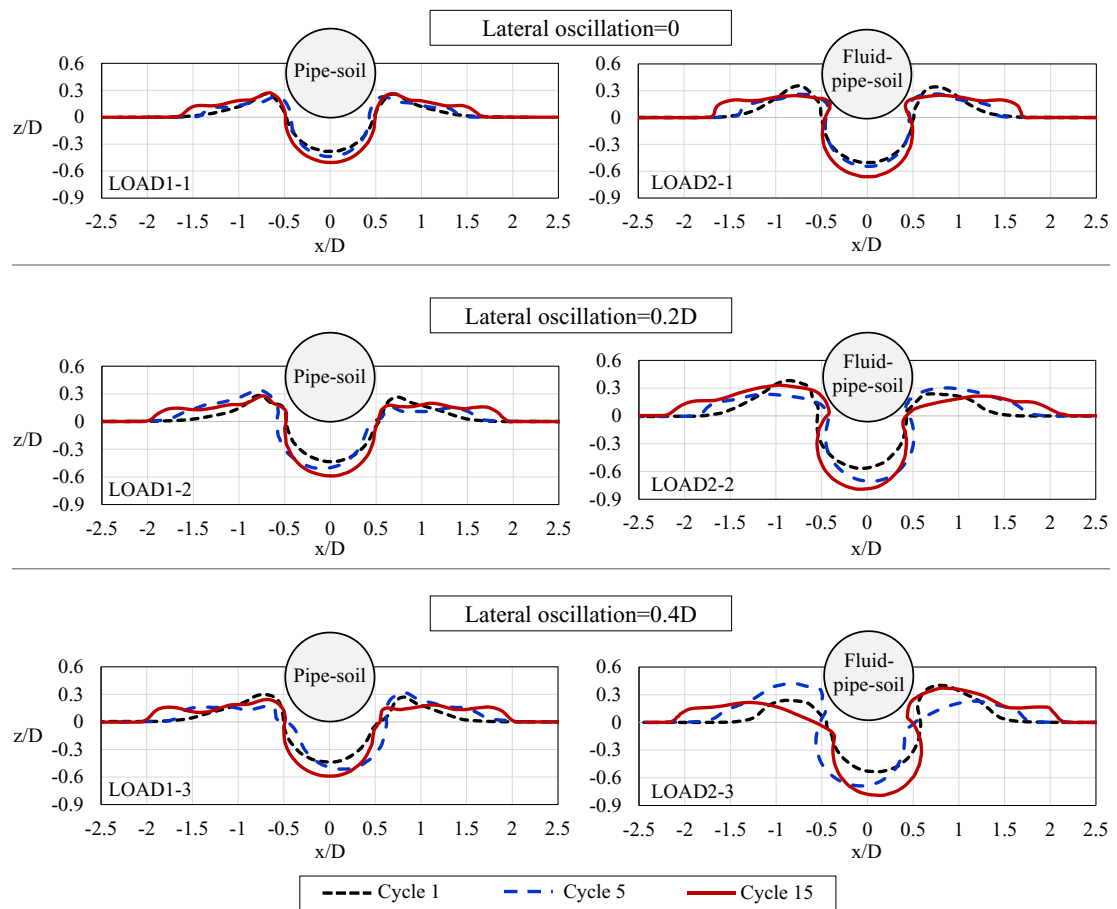


Figure 4-14. Evolution of seabed profile and berm formation surrounding pipeline

The velocity vectors of the fluid at different instances during a cycle are depicted in Figure 4-15 using arrows, with the arrow size representing a scale of  $0.25 \text{ m/s}$  at its largest. This schematic representation provides valuable insights into fluid flow dynamics. It is evident that the movement of the fluid has the potential to displace the

surrounding soil mass, particularly in situations where there is lateral movement of the pipe.

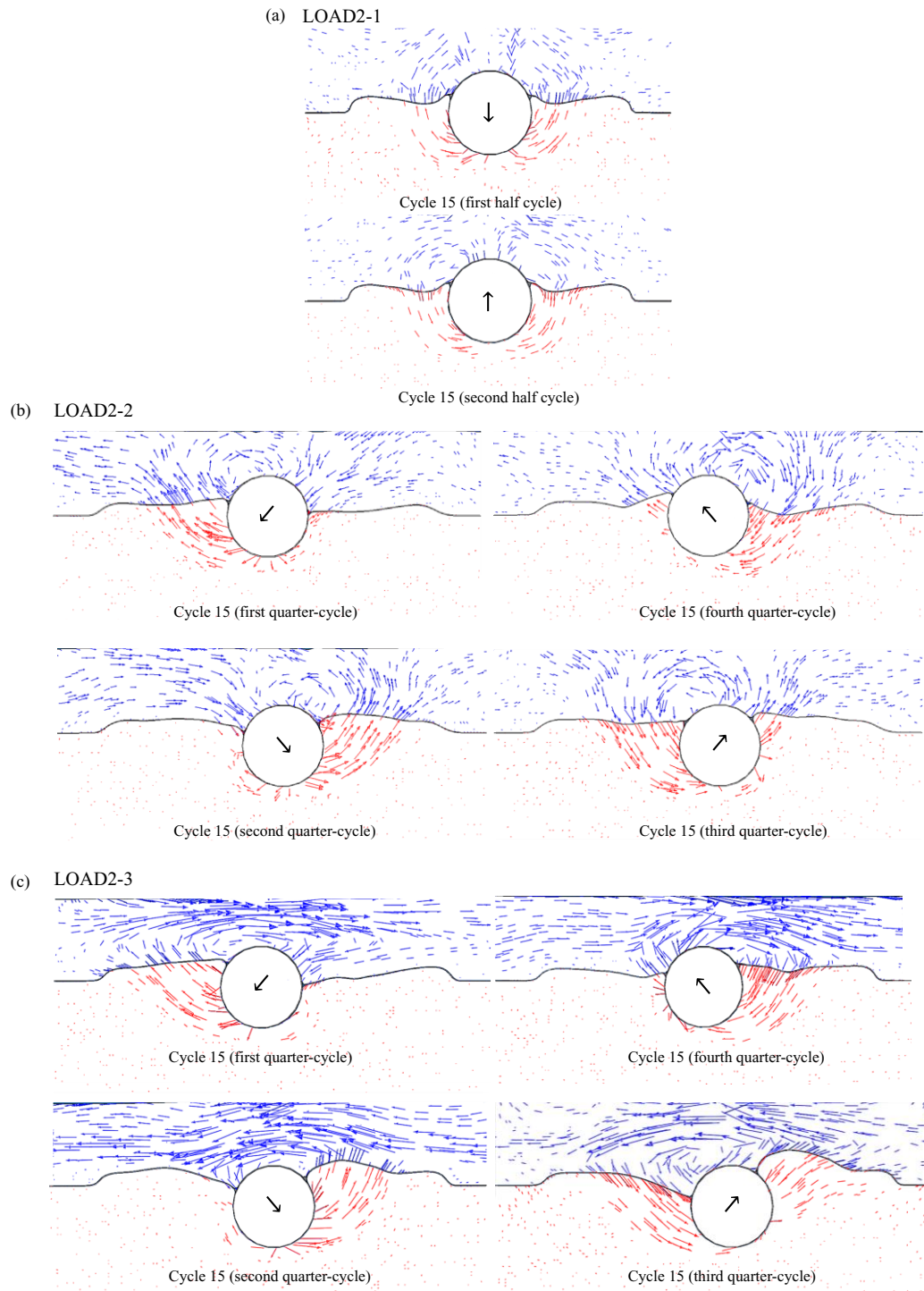


Figure 4-15. Fluid velocity vectors in the scale of  $0.25 \text{ m/s}$  within the largest arrow for (a) without lateral movements; (b) lateral oscillation= $0.2D$ ; (c) lateral oscillation= $0.4D$

Despite the relatively lesser extent of sediment transportation in clay compared to non-cohesive soils like sand due to the fluid flow, the dynamic behaviour of vortices and the movement of water into and out of gaps between riser and soil can cause the mobilization of the soil mass, resulting in soil erosion and potentially leading to trench formation. The analyses confirm that the presence of water fluid can gradually alter the seabed profile and change the soil properties, e.g., degradation factor, affecting riser performance in the TDZ. Thus, understanding pipe-soil-seawater interaction can be essential to evaluate the soil behaviour beneath the riser, especially in shallow water area where the flow of currents are becoming more significant to increase the soil erosion and scouring field.

#### **4.6. Conclusion**

As noted in the literature, the existing non-linear hysteretic soil models commonly used to evaluate the fatigue performance of steel catenary risers (SCRs) in the touchdown zone (TDZ) focus only on the interaction between the pipe and soil, disregarding the potential fluid entrainment that can occur during the operational life of SCRs. This oversight can lead to inaccuracies in predicting the formation of the trench beneath the riser and underestimating the rate of soil softening, leading to over/under estimate long-term fatigue damage in the TDZ.

In the current study, the simulation of a large deformation problem is conducted using the Coupled Eulerian-Lagrangian (CEL) technique in the Abaqus finite element (FE) software. The Eulerian model encompasses two domains: water and soil, which interact with the rigid pipe model represented as the Lagrangian domain. To accurately capture the behavior of the soil, a modified Mohr-Coulomb model is employed with the incorporation of the strain rate and softening model for the undrained shear strength of

the clay. The performance of the FE model is validated against the centrifuge test results, confirming the accuracy and reliability of the numerical analysis in simulating the water entrainment phenomenon. An appropriate range of bearing capacity factors is taken into account in order to align the theoretical results of vertical resistance with the numerical findings while considering the variations in the geometry of the seabed surface or heave effects. Accordingly, certain modifications were suggested for the power law factors when water entrainment occurs.

The constructed FE model was further improved to include load control analysis, simulating the conditions encountered by SCR in the TDZ. The pipe penetration was controlled by a maximum resistance of  $7 \text{ kPa}$ , to accurately capture the evolution of trench formation. Furthermore, lateral oscillations were incorporated as well to provide a reliable representation of the real field operation. The findings reveal that water flow can penetrate into the gaps, exerting additional pressure on the soil, resulting in erosion or soil displacement. This occurrence not only causes the trench beneath the pipeline to deepen gradually but also extends erosion of the surrounding berms by carrying soil particles away in a lateral direction.

The flow of water can infiltrate the gaps, exerting supplementary pressure on the soil, which consequently causes the soil to be washed away or displaced. Over a cyclic motion, this phenomenon not only leads to the gradual deepening of the trench but also extends the progression of the berms area by carrying away soil particles in a lateral direction. The impact of water entrainment has the potential to worsen when combined with lateral oscillations, leading to an estimated 60% increase in the depth of the trench, which has been neglected in the existing non-linear SCR-soil models.

## **Acknowledgments**

The authors gratefully acknowledge the financial support of this research by the “Natural Science and Engineering Research Council of Canada (NSERC)” through Discovery program, and the Memorial University of Newfoundland through school of graduate studies funding support.

## **References**

- Al-Janabi, H.A., Aubeny, C.P., Chen, J., and Luo, M. (2020). “Experimental measurement of monotonic and cyclic lateral resistance of risers and pipelines in Gulf of Mexico clays.” *Can. Geotech. J.* 57, 1534–1549.
- API-STD-2RD. (2013). “Standard for riser systems that are part of a floating production system (FPS).” American Petroleum Institute, Washington, DC, USA.
- Aubeny, C. P., Shi, H. & Murff, J. D. (2005). “Collapse load for a cylinder embedded in trench in cohesive soil.” *Int. J. Geomech.* 5, No. 4, 320–325.
- Aubeny, C., and Biscontin, G., (2008). “Interaction model for Steel Compliant Riser on Soft Seabed.” OTC194193, Houston, TX.
- Barbosa-Cruz, E.R., and Randolph, M.F. (2005). “Bearing capacity and large penetration of a cylindrical object at shallow embedment.” In *Proceedings of the 1<sup>st</sup> International Symposium on Frontiers in Offshore Geotechnics (ISFOG)*. pp. 615–621. doi:10.1201/NOE0415390637.ch67.
- Bridge, C., Laver, K., Clukey, E., and Evans, T. (2004), “Steel Catenary Riser Touchdown Point Vertical Interaction Models.” *Offshore Technology Conference*, Houston, Texas, USA, OTC16628.

Bridge, C., and Willis, N. (2002). “Steel Catenary Risers—Results and Conclusions from Large Scale Simulations of Seabed Interaction.” 14<sup>th</sup> Annual Conference Deep Offshore Technology, Cape Town, South Africa, 40-60.

Campbell, M. (1999). “The Complexities of Fatigue Analysis for Deepwater Risers.” Deepwater Pipeline Conference, New Orleans, USA.

Chatterjee, S., Randolph, M.F., White, D., 2012a. The effects of penetration rate and strain softening on the vertical penetration resistance of seabed pipelines. *Géotechnique*, vol. 62, no. 7, p. 573.

Chatterjee, S., White, D., Randolph, M.F., (2012b). “Numerical simulations of pipe-soil interaction during large lateral movements on clay.” *Géotechnique*, vol. 62, no. 8, p. 693.

Clukey, E., Jacobs, P., and Sharma, P.P. (2008). “Investigation of riser seabed interaction using explicit finite element methods.” Offshore Technology Conference, Houston, Texas, OTC19432-MS.

Dong, X., Shiri, H., (2018). “Performance of non-linear seabed interaction models for steel catenary riser, Part I: nodal response.” *Ocean Eng.* 154, 153–166.

Dong, X., Shiri, H., (2019). “Performance of non-linear seabed interaction models for steel catenary riser, Part II: global response.” *Appl. Ocean. Res.* 82, 158-174.

Dong, X., Zhang, W., Shiri, H., Randolph, M.R., (2021). “Large deformation coupled analysis of embedded pipeline – Soil lateral interaction.” *Marine Structures* 78, 102971.

DNV-RP-F204, (2017). “Offshore Standard, Riser Fatigue. Recommended practice.” Det Norske Veritas.

- Dutta, S., Hawlader, B., Phillips, R., (2014). "Finite element modeling of partially embedded pipelines in clay seabed using Coupled Eulerian–Lagrangian method." *Can. Geotech. J.* 52: 58–72, <https://doi.org/10.1139/cgj-2014-004>.
- Einav, I. & Randolph, M. F. (2005). "Combining upper bound and strain path methods for evaluating penetration resistance." *Int. J. Numer. Methods Engng* 63, No. 14, 1991–2016.
- Fouzder, A., Zakeri, A., and Hawlader, B. (2012). "Steel catenary risers at touchdown zone - A fluid dynamics approach to the water-riser-soil interaction." 9<sup>th</sup> Int. Pipeline Conf., Calgary, V4, 31-36.
- Fuhrman, D.R., Baykal, C., Sumer, B.M., Jacobsen, N.G., Fredsøe, J., (2014). "Numerical simulation of wave-induced scour and backfilling processes beneath submarine pipelines." *Coast. Eng.* 94, 10–22.
- Hu, Y., and Randolph, M.F. (1998). "Deep penetration of shallow foundations on non-homogeneous soil." *Soils and Foundations*, 38(1): 241–246. doi:10.3208/sandf.38.241.
- Kimiaei, M., Randolph, M., Ting, I. (2010). "A parametric study on effects of environmental loadings on fatigue life of steel catenary risers (using a nonlinear cyclic riser–soil interaction model)." In: *Proceedings of the 29th International Conference on Ocean, Offshore and Arctic Engineering*, Shanghai, China, Paper OMAE2010-21153.
- Janbazi, H., Shiri, H., (2023a). "A hybrid model to simulate the trench effect on the fatigue analysis of steel catenary risers in the touchdown zone." *Can. Geotech. J.* Published online, <https://doi.org/10.1139/cgj-2022-0103>.



- Janbazi, H., Shiri, H. (2023b). "Investigation of trench effect on fatigue response of steel catenary risers using an effective stress analysis." *Computers and Geotechnics*, 160, 105506, <https://doi.org/10.1016/j.compgeo.2023.105506>.
- Larsen, B.E., Fuhrman, D.R., Sumer, B.M., (2016). "Simulation of wave-plus-current scour beneath submarine pipelines." *J. Waterw. Port, Coast. Ocean Eng.* 142, 04016003.
- Lehane, B., O'Loughlin, C., Gaudin, C., and Randolph, M. (2009). "Rate effects on penetrometer resistance in kaolin." *Géotechnique*, 59(1): 41–52.  
[doi:10.1680/geot.2007.00072](https://doi.org/10.1680/geot.2007.00072).
- Li, F.Z., Dwivedi, A., Low, Y., and Hong, J. (2013). "Experimental investigation on scour under a vibrating catenary riser." *Journal of Engineering Mechanics*, vol. 139, No. 7.
- Li, Y., Ong, M.C., Fuhrman, D.R., Larsen, B.E., (2020). "Numerical investigation of waveplus-current induced scour beneath two submarine pipelines in tandem." *Coast. Eng.* 156, 103619.
- Li, F., Cheng, L., (2000). "Numerical simulation of pipeline local scour with lee-wake effects." *Int. J. Offshore Polar Eng.* 10.
- Li, F., Cheng, L., (2001). "Prediction of lee-wake scouring of pipelines in currents." *J. Waterw. Port, Coast. Ocean Eng.* 127, 106–112.
- Liang D., Cheng, L., Li, F., (2005a). "Numerical modeling of flow and scour below a pipeline in currents Part I. Flow simulation." *Coastal Engineering* 52 25-42.
- Liang D., Cheng, L., Li, F., (2005b). "Numerical modeling of flow and scour below a pipeline in currents Part II." *Coastal Engineering* 52 43-62.

Lu, Y., Chiew, Y.M., Cheng, N.S., (2008). “Review of seepage effects on turbulent open channel flow and sediment entrainment.” *J. Hydraul. Res.* 46, 476–488.

Mao, Y., (1986). “The interaction between a pipeline and an erodible bed.” PhD thesis, Technical University of Denmark, Lyngby, Denmark.

Merifield, R. S., White, D. J. & Randolph, M. F. (2008). “The ultimate undrained resistance of partially embedded pipelines.” *Geotechnique* 58, No. 6, 461–470, <http://dx.doi.org/10.1680/geot.2007.00097>.

Merifield, R.S., White, D.J., and Randolph, M.F. (2009). “Effect of surface heave on response of partially embedded pipelines on clay.” *Journal of Geotechnical and Geoenvironmental Engineering*, 135(6): 819–829. doi:10.1061/(ASCE)GT. 1943-5606.0000070.

Nakhaee, A., Zhang, J., (2008). “Effects of the interaction with the seafloor on the fatigue life of a SCR.” *Proceedings of the 18<sup>th</sup> International Society of Offshore and Polar Engineers Conference ISOPE-I-08-397*, July 6-11, 87–93.

Oliphant, J., Maconochie, A., White, D., and Bolton, M. (2009). “Trench interaction forces during lateral SCR movement in deepwater clays.” In *Proceedings of the Offshore Technology Conference, OTC-19944*, Houston, Texas, USA.

Orcina Ltd. (1986). “Orcaflex User Manual.” Cumbria, UK.

Pesce, C. P., Aranha, J. A. P., and Martins, C. A. (1998). “The Soil Rigidity Effect in the Touchdown Boundary-Layer of a Catenary Riser: Static Problem.” *Eighth International Offshore and Polar Engineering Conference ISOPE-I-98-130*; 1998 May 24-29; Montreal, Canada, 207-213.

Phifer, E. H., Frans, K., Swanson, R. C., Allen, D. W., and Langner, C. G. (1994). "Design And Installation Of Auger Steel Catenary Risers." Offshore Technology Conference, Houston, Texas, USA, OTC7620.

Pike, K., Duan, G., Sun, J., and Jukes, P. (2010). "Comprehensive FEA of thermal mitigation buoyancy module (TMBM)-soil interaction using the coupled Eulerian-Lagrangian (CEL) method." In Proceedings of the 28th International Conference on Ocean, Offshore and Arctic Engineering, OMAE 2009, Honolulu, Hawaii, 31 May – 5 June 2009. pp. 865–870. doi: 10.1115/OMAE2010-20885.

Randolph, M. F. (2004). "Characterization of soft sediments for offshore applications." Keynote lecture. Proc. 2nd Int. Conf. on Site Characterization, Porto, Portugal 1, 209–231. Rotterdam, The Netherlands: Millpress Science Publishers.

Randolph, M.F., Bhat, S., Mekha, B. (2013). "Modeling the touchdown zone trench and its impact on SCR fatigue life." Proceedings of the Offshore Technology Conference 2013, OTC-23975-MS, <https://doi.org/10.4043/23975-MS> May 6-9.

Randolph, M. F. & White, D. J. (2008). "Pipeline embedment in deep water: process and quantitative assessment." Proceedings of the offshore technology conference, Houston, paper OTC 19128.

Randolph, M.F., Quiggin, P. (2009). "Nonlinear hysteretic seabed model for catenary pipeline contact." In: Proceedings of the 28th International Conference on Ocean, Offshore and Arctic Engineering. Honolulu, Hawaii, USA.

Shiri, H., Randolph, M., (2010). "The influence of seabed response on fatigue performance of steel catenary risers in touchdown zone." In: Proceedings of the 29<sup>th</sup>

international conference on offshore mechanics and arctic engineering, OMAE 2010, Shanghai, China, p. 20051.

Sumer, B.M., Fredsbe, J., (2002). “The Mechanics of Scour in the Marine Environment.” World Scientific, Singapore.

Smith, H.D., Foster, D.L., (2005). “Modeling of flow around a cylinder over a scoured bed.” *J. Waterw. Port, Coast. Ocean Eng.* 131, 14–24.

Thethi, R., Moros, T., (2001). “Soil interaction effects on simple catenary riser response.” Deepwater Pipeline and Riser Technology Conference, Houston, Texas, USA.

Tom, J.G., Draper, S., White, D.J., (2018). “Sediment transport and trench development beneath a cylinder oscillating normal to a sandy seabed.” *Coastal Engineering* 140, 395-410.

Wang, D., White, D. J., and Randolph, M. F., (2010). “Large-Deformation Finite Element Analysis of Pipe Penetration and Large-Amplitude Lateral Displacement.” *Can. Geotech. J.*, 47(8), pp. 842–856.

Yuan, F., White, D. J. & O’Loughlin, C. D. (2017). “The evolution of seabed stiffness during cyclic movement in a riser touchdown zone on soft clay.” *Géotechnique* 67, No. 2, 127–137, <https://doi.org/10.1680/jgeot.15.P.161>.

Zhou, H. & Randolph, M. F. (2007). “Computational techniques and shear band development for cylindrical and spherical penetrometers in strain-softening clay.” *Int. J. Geomech.* 7, No. 4, 287–295.

Zhou, H. & Randolph, M. F. (2009). “Resistance of full-flow penetrometers in rate-dependent and strain-softening clay.” *Géotechnique* 59, No. 2, 79–86, <http://dx.doi.org/10.1680/geot.2007.00164>.

Zhou, Z., O’Loughlin, C. D., White, D. J. (2020). “An effective stress analysis for predicting the evolution of SCR-seabed stiffness accounting for consolidation.” *Géotechnique* 70, No. 5, 448–467 <https://doi.org/10.1680/jgeot.18.P.313>.

## CHAPTER 5

# **An Alternative Vessel Excitation Algorithm to Incorporate the Trench Effect into the Fatigue Analysis of Steel Catenary Risers in the Touchdown Zone**

Hossein Janbazi<sup>1</sup>, Hodjat Shiri<sup>2</sup>

1: Department of Civil Engineering  
Memorial University of Newfoundland  
e-mail: [hjanbaziokn@mun.ca](mailto:hjanbaziokn@mun.ca)

2: Department of Civil Engineering  
Memorial University of Newfoundland  
e-mail: [hshiri@mun.ca](mailto:hshiri@mun.ca)

This chapter was published in *Applied Ocean Research*.

<https://doi.org/10.1016/j.apor.2022.103292>

## **Abstract**

Cyclic penetration of steel catenary risers (SCR) into the seabed in the touchdown zone (TDZ) results in the formation of trenches several diameters deep, which has a significant impact on the riser fatigue life. Two main approaches have been proposed in the literature to incorporate the trench effect into the SCR's fatigue analysis, i.e., i) the insertion of a mathematically expressed trench profile into the touchdown zone, ii) cyclic trench formation using non-linear hysteretic riser-seabed interaction models. It has been repeatedly reported in the literature that the first approach leads to non-realistic pressure hot spots and damage profile distortion, particularly in the trench mouth; and the second approach suffers from premature stabilization of the hysteretic models resulting in limited embedment much less than the observed trench depths. In this study, an alternative vessel excitation algorithm called equivalent motion method (EMM) was introduced to incorporate the trench effect in the fatigue analysis. An equation was proposed for a given riser resting on an elastic seabed to obtain an equivalent vessel motion amplitude on a rigid seabed with the same cyclic damage. The study showed that the proposed EMM is able to predict the maximum cross-sectional stress range with an accuracy of over 90% in the majority of load cases. As an alternative solution, the proposed EMM was found to be a promising basis for further extension into the non-linear hysteretic riser-seabed interaction.

**Keywords:** Steel catenary riser; trench effect; equivalent motion method; maximum stress range; fatigue analysis; numerical modeling

## 5.1. Introduction

Steel Catenary Risers (SCRs) are extensively used in offshore developments to convey hydrocarbons from the seabed to different hosting vessels. Due to the cyclic vessel oscillations, fatigue damage accumulation is quite significant in the two areas of SCRs, i.e., the hang-off point, where the riser is connected to the vessel, and the touch down zone (TDZ), where the SCR has a cyclic interaction with the seabed soil (Bridge, 2005; Randolph and White, 2008; Aubeny et al., 2015; Clukey et al., 2017). The latter aspect is probably the most challenging issue in SCR engineering design because of the complex riser-seabed-seawater interaction that results in a trench formation underneath the SCR and affects the fatigue life in the TDZ (Bridge et al., 2005; Langford and Aubeny, 2008; Sharma and Aubeny, 2011; Wang and Low, 2016; Clukey and Zakeri, 2017).

The trench formation, several riser diameter deep, has been recorded and proven by remote operating vehicles (ROV) surveys (Thethi and Moros, 2001; Bridge and Howells, 2007). The significance of trench effect on fatigue performance of SCRs in the TDZ has been broadly investigated in the literature (Liu, 2018; Shoghi and Shiri, 2019, 2020). However, there is still no coherent agreement on the beneficial or detrimental effect of trench formation on fatigue. Some of the studies have observed fatigue life improvement by gradual trench formation (Elliot et al., 2013; Randolph and Bhat, 2013; Nakhaei and Zhang, 2008; Langner, 2003; Wang et al., 2016). Some other studies have shown the fatigue damage increasing due to trench formation (Shiri and Randolph 2010; Shiri, 2014b; Zargar 2017; Leira, 2004; Giertsen, 2004). Shoghi and Shiri (2019, 2020) conducted a comprehensive study to compare the observations in the literature and propose a framework to assess the trench effect on fatigue. Besides the



significant effect of the second-order motions, the authors showed that the methodology undertaken to incorporate the trench effect can completely distort the results of fatigue analysis. This finding was in agreement with earlier observations in the literature (Randolph et al., 2013; Dong and Shiri, 2019). There are two main approaches in the literature that has been used for incorporation of trench effect in fatigue analysis: a) insertion of a mathematically expressed trench profile in the TDZ (e.g., Langner, 2003; Li and Low, 2012; Randolph et al., 2013; Shiri, 2014b; Wang et al., 2016), b) automative trench formation using non-linear hysteretic riser-seabed interaction models (e.g., Nakhaei and Zhang, 2008; Shiri and Randolph, 2010, Shiri 2014a). Either of these methodologies has pros and cons. The mathematical trench insertion leads to contact pressure hotspots and the distortion of the damage profile particularly in the trench mouth (Shoghi and Shiri 2019, 2020). Randolph et al., (2013) resolved this issue by proposing new approach called Stepped method. Although this methodology could improve the situation, the contact hotspot was not completely eliminated particularly in the trench mouth. The non-linear riser-seabed interaction models are prematurely stabilized with a limited amount of riser embedment (less than 1D) (Aubuney and Biscontin, 2008; Randolph and Quiggin, 2009) and do not explicitly model the trench (Zargar, 2017; Dong and Shiri, 2018). Efforts have been made in the literature to address some of these challenges mostly by introducing simplified methodologies to obtain the fatigue damage of riser with considering linear and non-linear features of the seabed (Wang et al., 2013; Clukey and Zakeri, 2017; Chen et al., 2019). Moreover, equivalent linear stiffness was used instead of the complex plastic seabed to provide a fast estimation of the fatigue life in the touchdown zone (e.g., Hejazi and Kimiaei, 2016). In the simplified method, equivalent linear soil stiffness provides similar results of stress

range that non-linear soil model created. However, the reliable incorporation of the trench effect in the SCR fatigue analysis through the simplified approaches still remains a knowledge gap and needs further investigations.

In this study, a new vessel excitation algorithm called equivalent motion method (EMM) was developed to incorporate the trench effect in fatigue analysis and to overcome the pre-mature stabilization of the riser embedment in the existing non-linear riser-seabed interaction models and to resolve the contact pressure hotspots when the mathematical trenches are used. The proposed solution was investigated by focusing on the equivalent vessel oscillations on a rigid seabed corresponding to the linear elastic seabed with the same peak fatigue damage (see Figure 5-1).

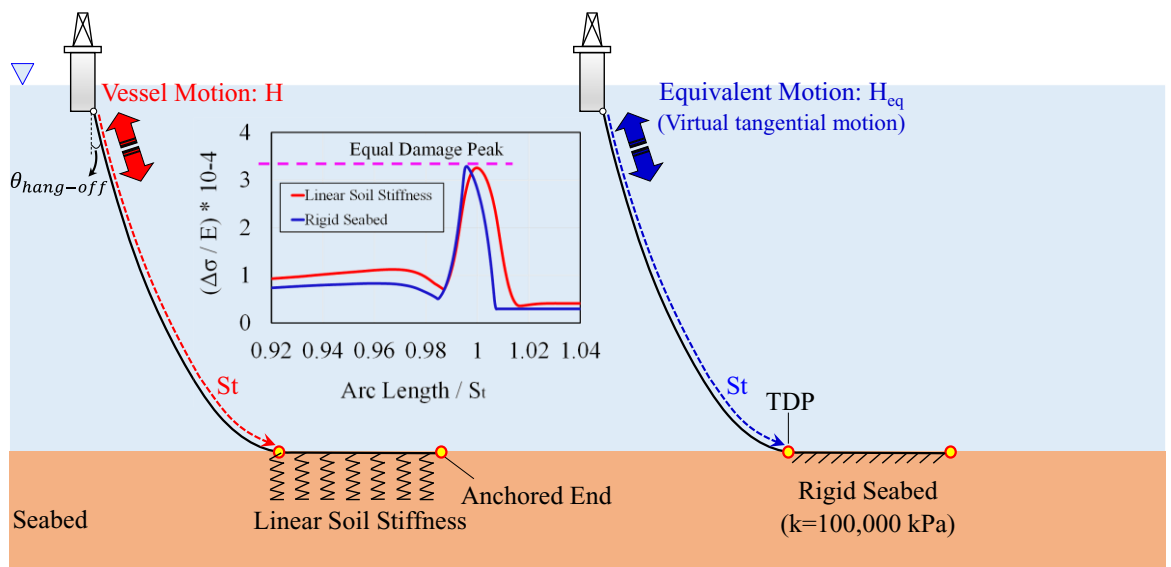


Figure 5-1. Schematic representation of the concept behind the EMM proposed in the current study

The idea was to explore whether this is possible to oscillate the vessel in a rigid seabed with a predefined motion pattern to result in the same damage accumulation that has been obtained from a given linear elastic seabed. This idea was proposed on the basis

of the earlier studies showing the significance of the touchdown point oscillation and its relation with the seabed stiffness (i.e., Shoghi and Shiri 2019, 2021).

To facilitate the study, the maximum cross-sectional stress range was investigated as the primary interest in fatigue damage accumulation (Queau et al., 2013; Hejazi and Kimiaei, 2016). OrcaFlex (Orcina, 2010) software was used to perform comprehensive numerical analyses of the riser oscillating in the linear elastic seabed with a range of soil stiffness and the riser oscillating in the rigid seabed with a range oscillation amplitudes. The results were matched to obtain a relationship between the maximum dynamic stress range in the linear elastic seabed and the corresponding vessel oscillation amplitude in the rigid seabed resulting in the same stress range. To minimize the computational effort and facilitate data handling difficulties, only the heave motions on the tangential local coordinate system at the SCR attachment point were considered which is known to be the major contributor to the fatigue damage accumulation (Kimiaei, 2010). The study showed that the peak dynamic stress range (indicating the fatigue damage) in the linear elastic seabed can be approximated by using the same riser on the rigid seabed but with a virtual vessel motion algorithm that was obtained in the current study. This approach can be extended in future studies to the seabed with non-linear plastic response. Thus, the methodology can be potentially used for incorporation of the trench effect in fatigue analysis resolving the aforementioned challenges.

## **5.2. Numerical Model**

### **5.2.1. Model configuration**

The numerical model was constructed in OrcaFlex (Orcina, 2010). Two example base case SCRs (BC1 and BC2) from the literature (Quéau et al., 2014a) were used to facilitate model validation. The BC1 is a SCR with 1600 m length suspended from a

semisubmersible in 1000 m water depth at the Gulf of Mexico (GoM). The BC2 is an altered version of the BC1 with a different set of structural parameters. Figure 5-2 schematically shows the configuration of model SCR with parameters summarized in Table 5-1.

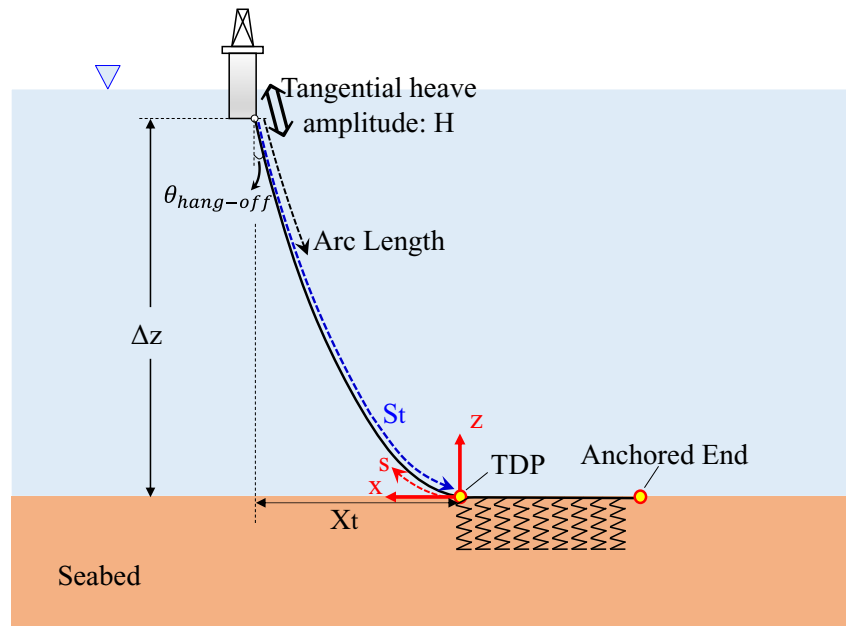


Figure 5-2. 2D view of SCR configuration

Linear elements based on the theory of elasticity were used to model the SCR, which are represented by a lumped mass model in OrcaFlex. The boundary conditions were defined by assuming simple hinge supports both at the anchored end and at the hang off point. The riser-seabed interaction was defined using a simple elastic spring.

Table 5-1. SCR model parameters (BC1 and BC2)

Parameter	Sign (unit)	Value (BC1)	Value (BC2)
Outer diameter	$D_o$ (m)	0.228	0.4572
Wall thickness	$t$ (m)	0.025	0.0305
Water depth	$\Delta Z$ (m)	982	2000
Moment of inertia	$I$ ( $m^4$ )	8.34E-05	9.35E-04
Submerged weight	$m_s$ (kg/m)	83.31	152.68
Bending stiffness	$EI$ ( $Nm^2$ )	1.77E+07	1.98E+08
Hang off angle	$\theta_{HO}$ (deg)	9.83	11.00

Displacement controlled dynamic analyses were conducted by applying harmonic heave vessel oscillations in the tangential direction of the local coordinate system at the attachment point (see Figure 5-2). This direction was found by Kimiaei et al. (2010) to contribute by more than 93% to the accumulated fatigue damage. The performance of current models were verified through comparisons with the results published by Quéau et al., 2014a (see Figure 5-3 and Figure 5-4).

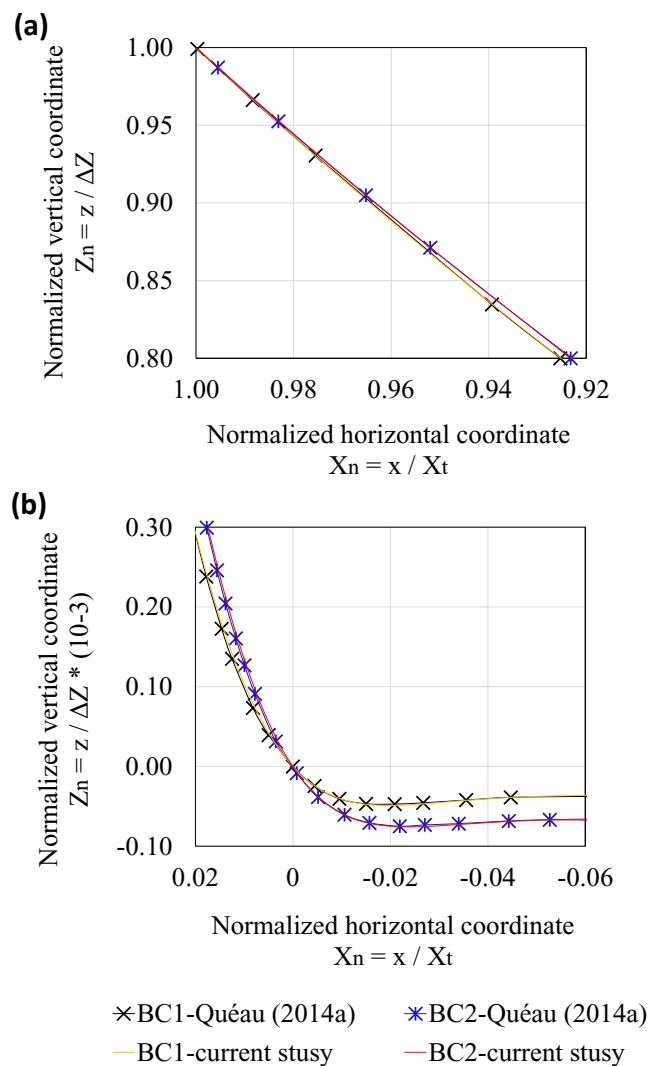


Figure 5-3. Comparison of the normalized SCR shape of the current base cases with the published work (Quéau et al., 2014a): (a) zoom around the HOP; and (b) zoom around the

TDP

Normalized shapes of the SCRs (BC1 and BC2) around the hang-off point and TDZ are shown in Figure 5-3, plotted with the normalized vertical coordinate ( $Z_n = z / \Delta z$ ) versus the normalized horizontal coordinate ( $X_n = x / X_t$ ) of the nodes. Noted that  $\Delta z$  is the water depth,  $X_t$  is the horizontal offset from TDP to the hang-off point,  $z$  and  $x$  are the vertical and horizontal coordinates of the nodes measured from the TDP, as illustrated in Figure 5-2. Moreover, normalized axial stress distributions in the TDZ are shown in Figure 5-4, where normalized arc length  $S_n = s / S_t$  is used for the horizontal axis and  $S_t$  is defined as suspended length of the riser in equilibrium condition (arc length from hang-off point to TDP).

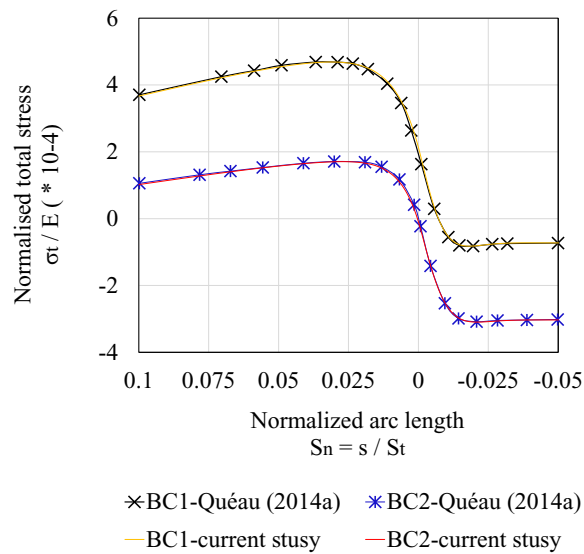


Figure 5-4. Comparison of the normalized stress of the current base cases with the published work (Quéau et al., 2014a), zoom around the TDP

According to Figure 5-3 and Figure 5-4, the results of the current numerical model are in agreement with the published work (Quéau et al., 2014a), so the validity of the constructed model in OrcaFlex is verified.

### 5.2.2. Fatigue damage assessment

The wave-induced fatigue damage is calculated by the following set of equations and superposed by using the Miner-Palmgren methods (DNV-RP-F204, 2017). Fatigue damage assessment is based on the S-N curve method (Figure 5-5), in which the number of stress cycles to failure ( $N$ ) is related to the total stress range ( $\Delta\sigma$ ) with the constant factors that are expressed as follows (DNV-RP-F204, 2017).

$$N = \bar{a}(\Delta\sigma^{-m}) \quad (5-1)$$

where  $\bar{a}$  and  $m$  are empirical factors and determined by fatigue test data.

Equation (5-1) can be established as following.

$$\log(N) = \log(\bar{a}) - m \log(\Delta\sigma) \quad (5-2)$$

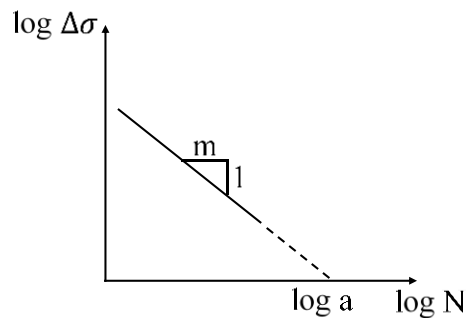


Figure 5-5. S–N curve for fatigue analysis

The Palmgren–Miner’s rule is used to estimate the damage caused by the different stress ranges.

$$D = \sum_i \frac{n(\Delta\sigma_i)}{N(\Delta\sigma_i)} \quad (5-3)$$

Where  $n(\Delta\sigma_i)$  is the number of stress cycles with range  $\Delta\sigma_i$  and  $N(\Delta\sigma_i)$  is the number of stress cycles to failure as expressed by Equation (5-1).

It is worth noting that total stress range is calculated by the following set of equations from total axial stress ( $\sigma$ ) comprising the direct tensile stress ( $\sigma_a$ ) and bending stress ( $\sigma_m$ ) (DNV-RP-F204, 2017).

$$\sigma = \sigma_a \pm \sigma_m \quad (5-4)$$

$$\sigma_a = \frac{T_w}{A} \quad (5-5)$$

$$\sigma_m = \frac{MD_o}{2I} \quad (5-6)$$

$$\Delta\sigma = \sigma_{max} - \sigma_{min} \quad (5-7)$$

where  $T_w$  and  $M$  are the wall tension and bending moment, respectively. Other parameters including  $A$ ,  $D_o$  and  $I$  are structural characteristics of the riser and defined as cross-section area, outer diameter, and moment inertia. As seen in equation (5-3), the damage is mainly dependant on  $\Delta\sigma$ . Therefore, to facilitate the current study and minimize the computational effort,  $\Delta\sigma$  was investigated as the key output instead of going through a full fatigue damage assessment.

### 5.3. Concept of the proposed methodology

Using a single regular wave ( $H = 1$  m and  $T = 15$  s), a series of analyses were conducted on seabed with different stiffness ranging from 1 to 100,000 kPa. Then the second series of analyses were conducted on a rigid seabed ( $k = 100,000$  kPa) but using different values of tangential heave amplitudes (from 0 to 1 m). The results were combined and shown in Figure 5-6 to find the seabed stiffness and vessel amplitudes resulting in equal cross-sectional damage. Accordingly, maximum stress ranges of an example riser (BC1) were reported against two horizontal axes, plotting through different motion amplitudes in rigid seabed on the lower axis, and different linear stiffness from very



soft (1 kPa) to the rigid seabed within  $H = 1$  m on the top axis. As seen in Figure 5-6, the study showed that the cross-sectional damage on a given seabed stiffness corresponds to a distinct motion amplitude on the rigid seabed. This triggered the idea of finding an equation to give the equivalent motion amplitude ( $H_{eq}$ ) on a rigid seabed corresponding to a target damage on a given elastic seabed, which will be more investigated in the next sections. Therefore, instead of modelling a trench in the touchdown zone, one may use the proposed idea by altering the vessel excitation and obtain the same damage results, while by-passing the aforementioned challenges of pressure hot spots or premature penetration stabilization severally reported in the literature.

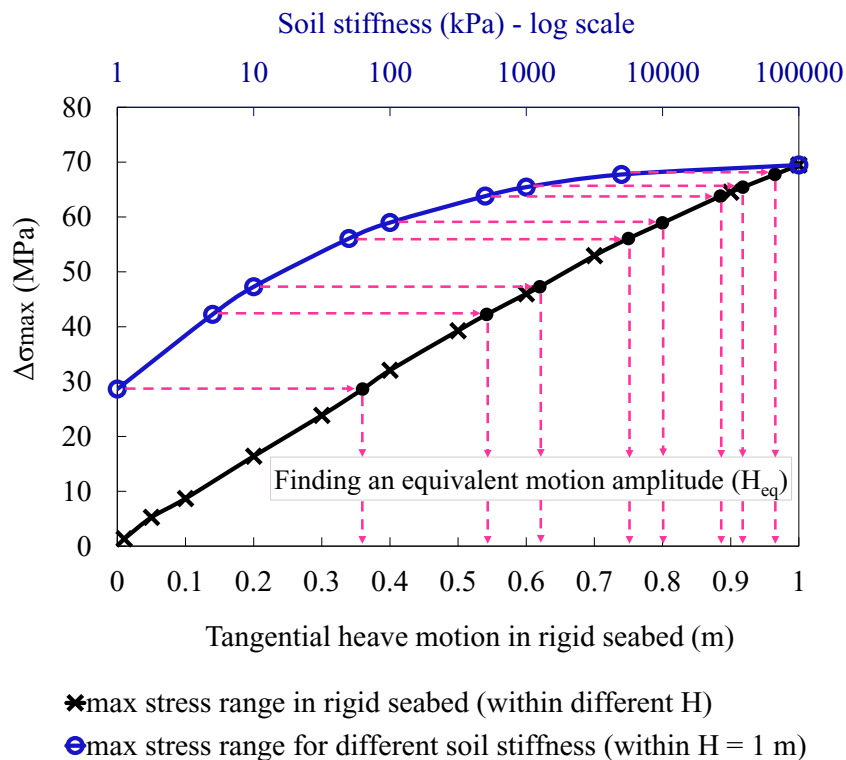


Figure 5-6. Relation between linear soil and rigid seabed to find equivalent motion amplitudes

Figure 5-7 provides a schematic insight into the EMM concept, where an equivalent motion amplitude in the rigid seabed is determined resulting in the same maximum

damage obtained from the linear soil models. The left side of the Figure 5-7 shows dynamic analyses of BC1 with different linear soil stiffness, where the motion parameters are identical for all of cases ( $H = 1$  m and  $T = 15$  s). In the right side, the dynamic analyses of the BC1 were conducted on the rigid seabed ( $k = 100,000$  kPa) with different motion amplitudes to reach the same maximum stress range that obtained by each of the given linear soil models. As can be seen from the graphs shown in the middle of the Figure 5-7, the peak stress range obtained from each linear stiffness is equal to the corresponding rigid seabed with a distinct motion amplitude. For example, the maximum stress range for the linear stiffness of  $k = 1$  kPa, with dynamic motion amplitude of  $H = 1$  m is equal to the maximum stress range of the same riser on the rigid seabed, if the motion amplitude is changed to  $H = 0.36$  m. Similarly, the maximum stress range for the  $k = 5$  kPa can be predicted, if motion amplitude in the rigid seabed is changed to the  $H = 0.54$  m.

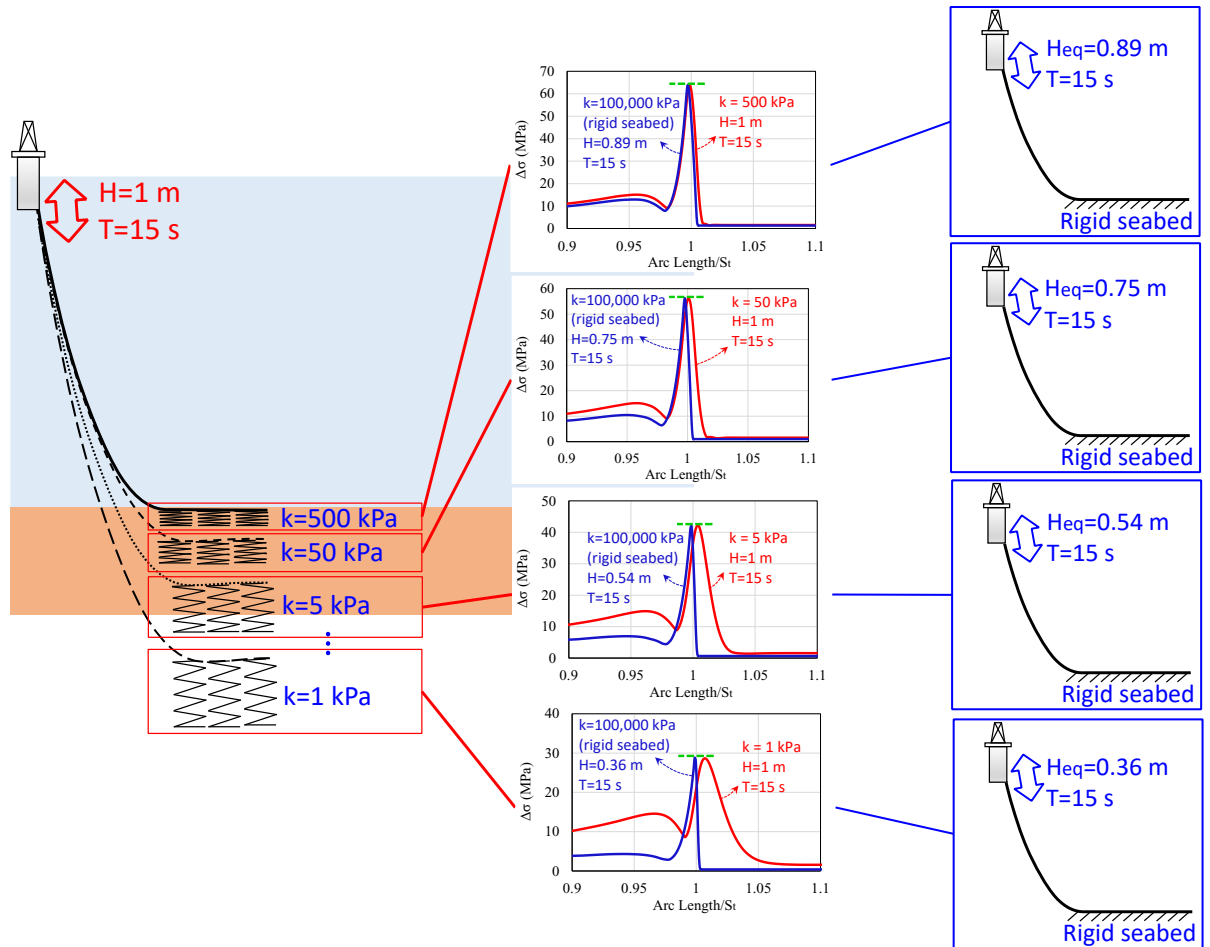


Figure 5-7. Same peak damage results for linear soil models and rigid seabed by defining

EMM

Table 5-2. Equivalent motion amplitudes for one scenario of motion in different linear stiffness

Linear soil model (within $H = 1\text{ m}$ )		Rigid seabed
$k$ (kPa)	$\Delta\sigma_{\max}$ (MPa)	Equivalent motion amplitude $H_{eq}$ (m)
1	28.63	0.36
5	42.24	0.54
10	47.27	0.62
50	56.07	0.75
100	58.98	0.80
500	63.79	0.89
1000	65.43	0.92
5000	67.74	0.97
100,000	69.46	1

Detailed results have been provided in Table 5-2. For each case of soil stiffness, an equivalent motion amplitude can be approached in the rigid seabed, which represents similar  $\Delta\sigma_{max}$  that linear soil models created in the  $H = 1$  m.

As shown in Table 5-2, as soil stiffness increases the maximum stress range would be increased, which this trend is consistent with the other published works (e.g., Quéau et al., 2014a). In addition, the equivalent motion amplitudes increase while soil becomes stiffer.

#### **5.4. Analysis procedure and the trends observed**

To expand the conceptual approach discussed above and build the database for extraction of EMM equation which will be proposed in the next section, a series of numerical analysis were conducted using OrcaFlex to simulate the BC1 and BC2 risers for five different linear elastic seabed stiffness, i.e., 5, 10, 50, 100, and 500 kPa. The risers in each case were analysed for eighteen different amplitudes of tangential heave vessel motions in a range of 0.15 to 5.1 m and four ranges of wave periods including 5, 10, 15, and 20 s totalling 720 different cases (360 cases for each, BC1 and BC2). The axial dynamic stress variation range was extracted and stored as a database (see Table 5-11). Moreover, iterative analyses were conducted on the rigid seabed (a seabed stiffness of 100,000 kPa) to determine the corresponding tangential heave motion amplitudes for a set of given periods (i.e., 5, 10, 15, and 20 s), resulting in equivalent maximum stress ranges obtained from the linear elastic seabed. According to Figure 5-8 and Figure 5-9, a total number of 200 cases with a coincidence margin of less than 1% were determined for BC1 and BC2 configurations in the rigid seabed, and used for finding the equivalent motion amplitudes.

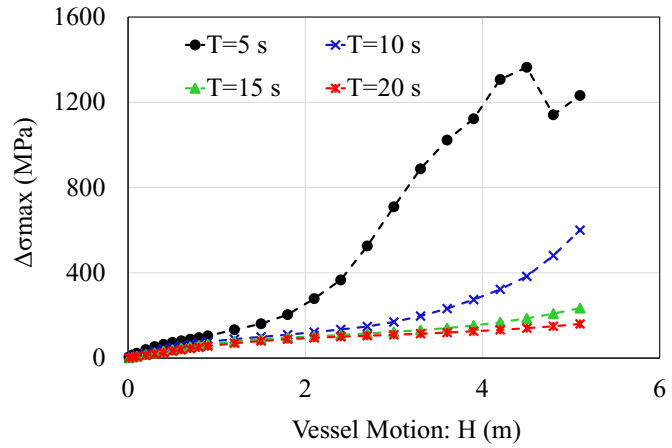


Figure 5-8. Maximum stress range of BC1 in rigid seabed through different vessel motions and periods

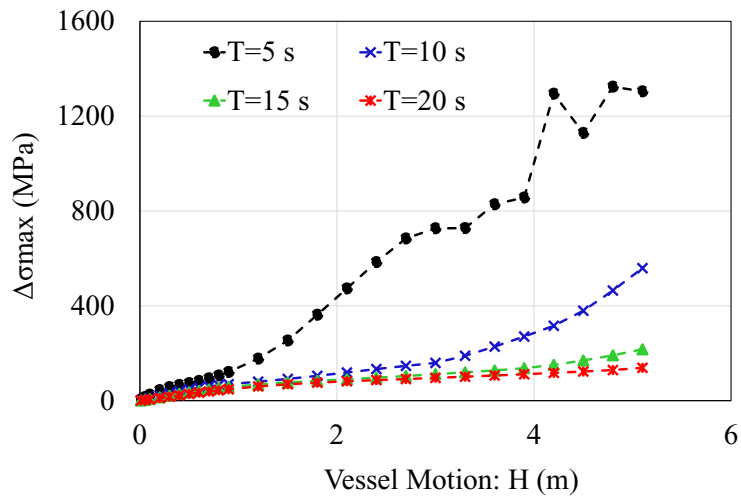


Figure 5-9. Maximum stress range of BC2 in rigid seabed through different vessel motions and periods

It was also found in Figure 5-8 and Figure 5-9 that by shifting from a wave period of 5 s to 20 s, the riser response becomes more static and results in lower  $\Delta\sigma_{max}$ , despite the fact that the lower period may cause more dynamic effects due to the indication of resonance in the system.

To evaluate the applicability of the EMM, it is necessary to conduct dynamic simulation of risers through rigid seabed within calculated equivalent motion amplitudes to confirm this approach can predict similar results with the linear soil model (LM). Table 5-3 and Table 5-4 show a sample of summarized key outputs including maximum dynamic stress variation range, the TDP location in equilibrium condition ( $S_t$ ), and the location of peak damage ( $arcL_{crit}$ ) for five different heave motions and a period of 15 s.

Table 5-3. Results of LM analysis and EMM (model case: BC1)

Groups	LM				EMM				Relative difference (EMM to LM)		
	H (m)	$S_t$ (m)	critical point		$H_{eq}$ (m)	$S_t$ (m)	critical point		in $S_t$ (%)	critical point	
			$arcL_{crit}$ (m)	$\Delta\sigma_{max}$ (MPa)			$arcL_{crit}$ (m)	$\Delta\sigma_{max}$ (MPa)		in $arcL_{crit}$ (%)	in $\Delta\sigma_{max}$ (%)
Group 1 k=5 kPa	0.9	1164	1168.5	38.07	0.48	1175	1173.5	38.04	0.95	0.43	-0.08
	1.8	1164	1169.5	70.44	1.03	1175	1171.5	70.52	0.95	0.17	0.11
	2.7	1164	1166.5	93.76	1.72	1175	1167.5	93.71	0.95	0.09	-0.05
	3.6	1164	1161.5	117.65	2.79	1175	1159.5	117.61	0.95	-0.17	-0.03
	4.5	1164	1151.5	151.12	3.85	1175	1151.5	150.64	0.95	0.00	-0.32
Group 2 k=10 kPa	0.9	1166	1169.5	42.73	0.55	1175	1173.5	42.83	0.77	0.34	0.23
	1.8	1166	1169.5	76.43	1.17	1175	1170.5	77.02	0.77	0.09	0.77
	2.7	1166	1166.5	99.36	1.97	1175	1165.5	99.36	0.77	-0.09	0.00
	3.6	1166	1159.5	123.59	3.02	1175	1158.5	123.54	0.77	-0.09	-0.04
	4.5	1166	1150.5	159.97	4.04	1175	1149.5	159.73	0.77	-0.09	-0.15
Group 3 k=50 kPa	0.9	1170	1171.5	51.25	0.68	1175	1172.5	51.24	0.43	0.09	-0.02
	1.8	1170	1169.5	85.75	1.42	1175	1169.5	85.5	0.43	0.00	-0.29
	2.7	1170	1164.5	107.46	2.35	1175	1163.5	107.37	0.43	-0.09	-0.08
	3.6	1170	1157.5	132.06	3.33	1175	1155.5	131.97	0.43	-0.17	-0.07
	4.5	1170	1148.5	172.6	4.27	1175	1147.5	172.46	0.43	-0.09	-0.08
Group 4 k=100 kPa	0.9	1171	1171.5	54.12	0.72	1175	1172.5	54.21	0.34	0.09	0.17
	1.8	1171	1169.5	88.24	1.5	1175	1168.5	88.29	0.34	-0.09	0.06
	2.7	1171	1163.5	109.51	2.44	1175	1162.5	109.46	0.34	-0.09	-0.05
	3.6	1171	1156.5	134.2	3.39	1175	1154.5	133.98	0.34	-0.17	-0.16
	4.5	1171	1148.5	175.92	4.33	1175	1147.5	175.18	0.34	-0.09	-0.42
Group 5 k=500 kPa	0.9	1173	1171.5	58.87	0.8	1175	1172.5	58.89	0.17	0.09	0.03
	1.8	1173	1168.5	91.97	1.64	1175	1167.5	92.29	0.17	-0.09	0.35
	2.7	1173	1162.5	112.65	2.58	1175	1161.5	112.58	0.17	-0.09	-0.06
	3.6	1173	1155.5	137.61	3.5	1175	1154.5	137.48	0.17	-0.09	-0.09
	4.5	1173	1147.5	181.09	4.41	1175	1146.5	180.49	0.17	-0.09	-0.33

Table 5-4. Results of LM analysis and EMM (model case: BC2)

Groups	LM				EMM				Relative difference (EMM to LM)		
	H (m)	S <sub>i</sub> (m)	critical point		H <sub>eq</sub> (m)	S <sub>i</sub> (m)	critical point		in S <sub>i</sub> (%)	critical point	
			arcL <sub>crit</sub> (m)	Δσ <sub>max</sub> (MPa)			arcL <sub>crit</sub> (m)	Δσ <sub>max</sub> (MPa)		in arcL <sub>crit</sub> (%)	in Δσ <sub>max</sub> (%)
Group 1 k=5 kPa	0.9	2418	2426.5	30.44	0.42	2438	2437.5	30.31	0.83	0.45	-0.41
	1.8	2418	2429.5	56.85	0.89	2438	2433.5	56.90	0.83	0.16	0.08
	2.7	2418	2425.5	78.76	1.58	2438	2428.5	78.95	0.83	0.12	0.25
	3.6	2418	2419.5	103.84	2.68	2438	2417.5	103.85	0.83	-0.08	0.01
	4.5	2418	2356.5	134.41	3.81	2438	2403.5	134.07	0.83	1.99	-0.26
Group 2 k=10 kPa	0.9	2423	2429.5	34.95	0.49	2438	2436.5	34.89	0.62	0.29	-0.19
	1.8	2423	2430.5	63.06	1.05	2438	2432.5	63.41	0.62	0.08	0.55
	2.7	2423	2425.5	85.36	1.87	2438	2425.5	85.38	0.62	0.00	0.01
	3.6	2423	2418.5	110.90	2.96	2438	2414.5	110.79	0.62	-0.17	-0.10
	4.5	2423	2413.5	138.82	3.94	2438	2401.5	138.51	0.62	-0.50	-0.22
Group 3 k=50 kPa	0.9	2429	2432.5	43.41	0.63	2438	2435.5	43.78	0.37	0.12	0.85
	1.8	2429	2430.5	72.79	1.35	2438	2430.5	73.07	0.37	0.00	0.39
	2.7	2429	2423.5	94.82	2.30	2438	2421.5	94.76	0.37	-0.08	-0.06
	3.6	2429	2414.5	119.91	3.31	2438	2410.5	119.92	0.37	-0.17	0.01
	4.5	2429	2399.5	152.20	4.22	2438	2397.5	152.15	0.37	-0.08	-0.04
Group 4 k=100 kPa	0.9	2431	2433.5	46.15	0.68	2438	2435.5	46.33	0.29	0.08	0.39
	1.8	2431	2430.5	75.49	1.45	2438	2429.5	75.79	0.29	-0.04	0.40
	2.7	2431	2422.5	97.25	2.41	2438	2420.5	97.27	0.29	-0.08	0.02
	3.6	2431	2413.5	122.12	3.39	2438	2409.5	122.09	0.29	-0.17	-0.02
	4.5	2431	2398.5	156.24	4.28	2438	2396.5	155.88	0.29	-0.08	-0.23
Group 5 k=500 kPa	0.9	2435	2433.5	50.88	0.77	2438	2434.5	51.04	0.12	0.04	0.30
	1.8	2435	2429.5	79.53	1.62	2438	2427.5	79.67	0.12	-0.08	0.17
	2.7	2435	2420.5	100.84	2.55	2438	2418.5	100.78	0.12	-0.08	-0.06
	3.6	2435	2410.5	125.09	3.50	2438	2407.5	125.13	0.12	-0.12	0.03
	4.5	2435	2396.5	162.58	4.38	2438	2395.5	162.19	0.12	-0.04	-0.24

The results presented in Table 5-3 and Table 5-4 show that the EMM is capable of well predicting the critical damage point on the riser with a negligible error of 0.77% and 0.43% on the maximum stress range and critical location for BC1, and 0.85% and 0.5% for BC2. The location of critical node determined from EMM is in a  $\mp$  0.5% difference from corresponding cases in LM. This shows that the EMM can well predict the location of the critical node as well. Furthermore, the arc length of the TDP in equilibrium condition ( $S_i$ ) is sensitive to the seabed stiffness. EMM that uses a rigid seabed gives

higher  $S_t$ ; therefore, the value of  $S_t$  in EMM is always greater than the corresponding LM. The difference of the  $S_t$  between these two methods is varied from 0.17% to 0.95% for BC1 and 0.12% to 0.83% for BC2, respectively, while moving from stiff to soft soil (i.e., from 500 to 5 kPa).

It would be useful to investigate the effects of input parameters (soil stiffness and motion characteristics) on the equivalent motions to trace an appropriate relationship between these parameters. Table 5-11 shows that the maximum stress ranges in both BC1 and BC2 are increased for higher heave amplitudes and decreased for higher values of wave periods. As expected, the soil stiffness showed a great influence on the stress range, whereas the stress range is significantly decreased for the softer seabed. These results are in agreement with earlier observations (e.g., Bridge, 2005; Quéau, 2015). As shown in Table 5-11, there are cases from BC2 in which the maximum stress range is beyond the upper boundary of  $\Delta\sigma_{\max}$  in the rigid seabed with identical wave period (e.g., the wave period of 5 s). The equivalent motions for these cases are not provided. Table 5-11 shows some exceptions for the observed trends, when a relatively high motion amplitudes happens within a short period (e.g.,  $T = 5$  s), as well as in very low amplitudes with long periods (e.g.,  $T = 15$  s &  $T = 20$  s). These ranges are considered less-realistic seastates (Quéau, 2015).

Considering above, to propose a logical relationships between the equivalent motions and the key parameters including seabed stiffness, motion amplitude and wave period, a realistic range of motion characteristics (Quéau, 2015; Randolph et al., 2013), shown in Table 5-5 were selected for further mathematical analysis and curve fit in the next section.



Table 5-5. Ranges of input parameters considered for predicting simplified equation

Parameter	selected range	
Motion (tangential heave amplitudes and periods)	T=10 s	$0.9 \leq H \leq 3$
	T=15 s	$0.9 \leq H \leq 5.1$
	T=20 s	$1.2 \leq H \leq 5.1$
Linear soil stiffness	k = 10, 50, 100, 500 kPa	

The selected reasonable range will prevent unnecessary difficulties of inaccuracies in curve fit for non-realistic ranges of data.

### 5.5. Obtaining a curve fit for equivalent vessel motions

Figure 5-10 shows the equivalent vessel motions and the corresponding curve fits that have been extracted from Table 5-11.

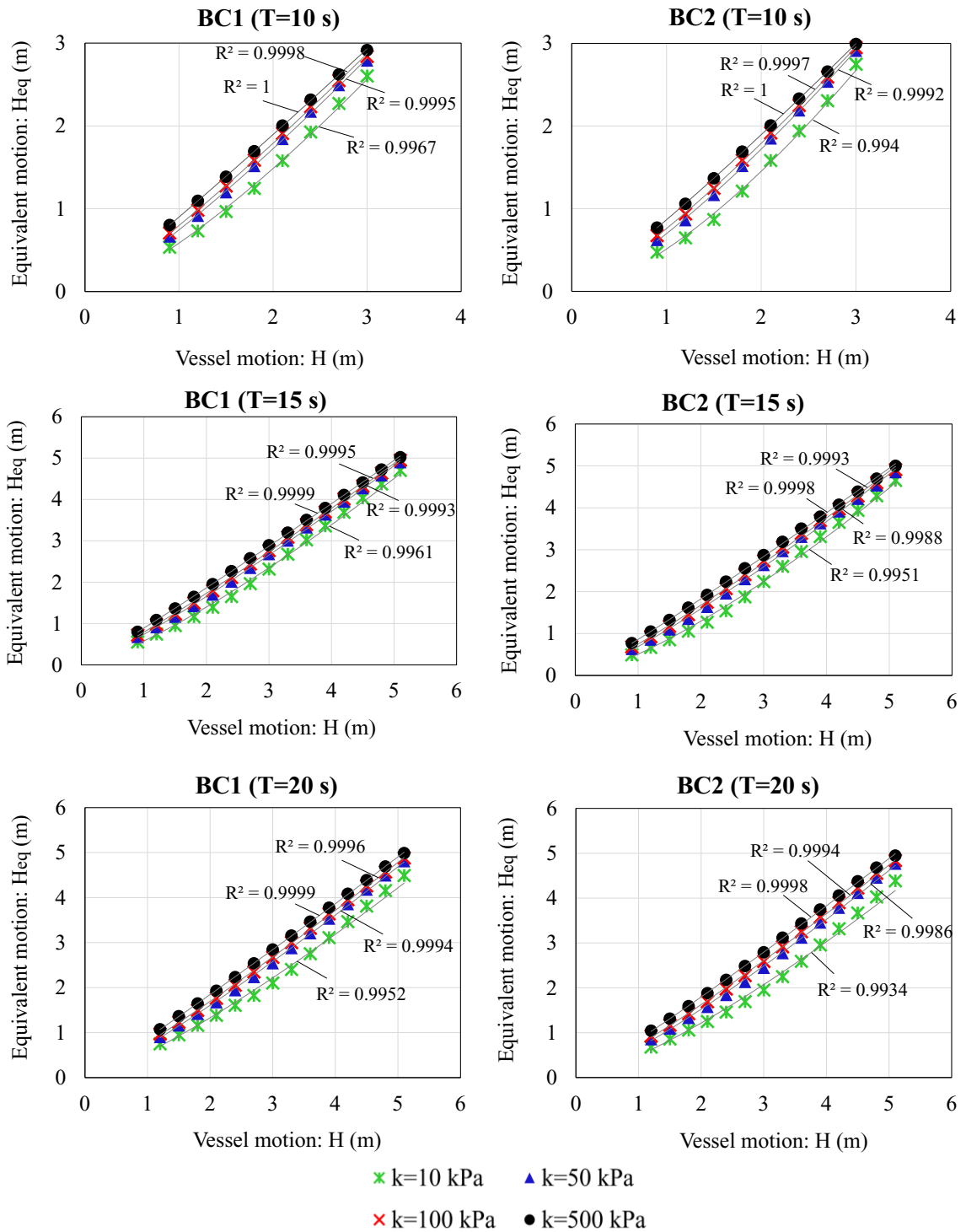


Figure 5-10. Variations of equivalent motions ( $H_{eq}$ ) against vessel amplitudes (H) through different soil stiffness and periods

The results for various seabed stiffness and wave periods in BC1 and BC2 risers show that a strong curve fit in the form of a power regression can be proposed as follows:

$$\text{Equivalent Motion Amplitude} = H_{eq} = a_1 \left( \frac{H_N}{T_N^{0.1}} \right)^{a_2} \cdot \left( \frac{T_N^{0.2}}{H_N^3} \right) \cdot H \quad (5-8)$$

where  $H$  is the heave amplitude in the tangential direction at the hang-off point,  $H_N$  and  $T_N$  are the normalized heave amplitude and normalized period in the linear soil models (normalized  $H$  and  $T$  by 1 m and 1 s, respectively).

Equation (5-8) can be expressed in another form as follow:

$$H_{eq} = a_1 \left( \frac{H_N^{a_2-3}}{T_N^{10-a_2}} \right) * H = A_1 * H, \quad \text{where} \quad A_1 = a_1 \left( \frac{H_N^{a_2-3}}{T_N^{10-a_2}} \right) \quad (5-9)$$

The proposed regression turns to be linear with increasing soil stiffness, whereas the coefficient of  $A_1$  approaches to the unity for a rigid seabed (e.g.,  $k = 100,000$  kPa).

“ $a_1$ ” and “ $a_2$ ” are non-dimensional coefficients that mathematically be obtained as a function of structural characteristics of riser and the soil stiffness.

$$a_1 = \frac{0.0598 \ln(\lambda_1) - 2.61}{(\lambda_2)^{0.11}} \quad (5-10)$$

$$a_2 = \frac{(\lambda_2)^{0.07}}{0.011 \ln(\lambda_1) - 0.4} \quad (5-11)$$

where  $\lambda_1$  and  $\lambda_2$  are defined as:

$$\lambda_1 = \left( \frac{ED}{P} \right)^3 \frac{kA \Delta Z}{T_0 L} \quad (5-12)$$

$$\lambda_2 = \frac{k}{E}$$

where  $D$  is the outer diameter of riser;  $E$  is the Young's modulus;  $P$  is the unit submerged weight;  $k$  is the soil stiffness;  $A$  is the cross-sectional area of riser;  $T_0$  is the tension of riser;  $\Delta Z$  is the vertical difference between the hang-off point and the seabed; and  $L$  is the length of the riser.

For the selected ranges of parameters listed in Table 5-5, the values of  $H_{eq}$  in the rigid seabed for BC1 and BC2 were calculated using the proposed curve fit. Then the maximum stress ranges corresponding to the calculated equivalent motions were determined. Summary of this procedure provided through the flow chart illustrated in Figure 5-11.

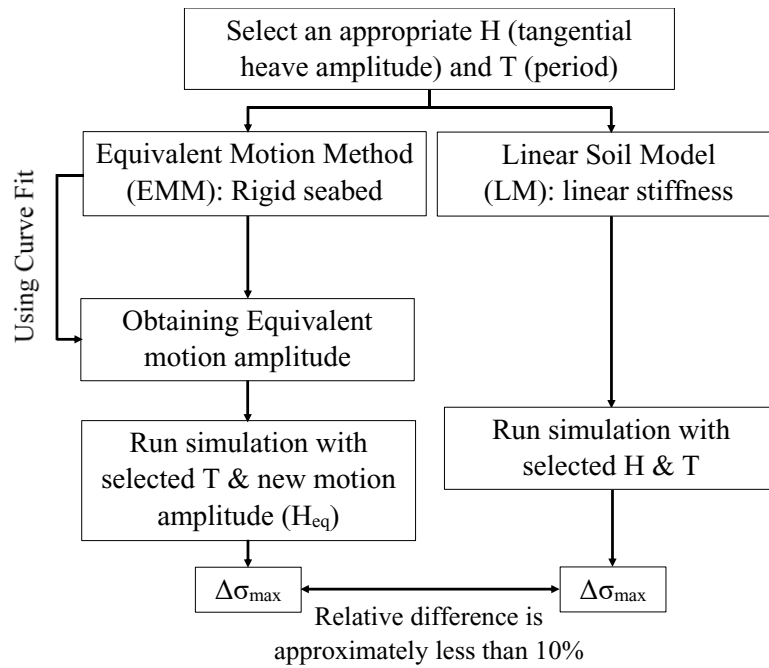


Figure 5-11. Summary of the procedure to find max stress range based on the EMM and LM

Table 5-6. Results obtained directly from linear soil models and proposed curve fit within the relative difference in  $\Delta\sigma_{\max}$  (in BC1)

		Linear soil models				Estimated Results from Proposed Equation								Relative difference in $\Delta\sigma_{\max}$ (%)			
H (m)	T (s)	$\Delta\sigma_{\max}$ (MPa)				$H_{eq}$ (m)				$\Delta\sigma_{\max}$ (MPa)				soil stiffness (kPa)			
		soil stiffness (kPa)				soil stiffness (kPa)				soil stiffness (kPa)				soil stiffness (kPa)			
		10	50	100	500	10	50	100	500	10	50	100	500	10	50	100	500
0.9	10	53.8	63.5	66.4	71.2	0.54	0.77	0.85	0.97	53.8	69.6	73.7	79.5	0.05	9.62	11.07	11.63
1.2	10	67.6	77.4	80.2	84.8	0.77	1.05	1.14	1.27	69.4	83.0	86.6	91.6	2.68	7.27	8.01	8.11
1.5	10	79.5	89.1	91.7	95.6	1.02	1.34	1.44	1.58	81.6	93.9	97.2	102.3	2.64	5.47	6.07	7.05
1.8	10	90.7	100.1	102.6	106.3	1.28	1.63	1.73	1.88	91.8	104.1	107.7	113.3	1.23	4.02	4.97	6.59
2.1	10	102.3	111.7	114.3	118.0	1.55	1.93	2.03	2.19	101.3	115.0	119.1	125.4	-1.00	2.94	4.20	6.23
2.4	10	115.0	124.8	127.3	130.8	1.83	2.23	2.33	2.49	111.4	127.1	131.5	138.4	-3.17	1.80	3.25	5.78
2.7	10	129.0	138.7	141.3	144.7	2.13	2.53	2.63	2.79	122.9	140.4	145.3	154.4	-4.71	1.19	2.83	6.71
3	10	143.9	154.8	158.2	163.7	2.43	2.83	2.94	3.08	135.6	157.9	165.0	177.3	-5.75	1.97	4.32	8.31
0.9	15	42.7	51.3	54.1	58.9	0.49	0.71	0.78	0.90	38.5	53.6	57.9	64.3	-9.86	4.65	7.00	9.18
1.2	15	55.7	65.2	68.0	72.8	0.70	0.97	1.05	1.18	53.1	67.7	71.4	77.2	-4.69	3.92	5.01	6.02
1.5	15	66.8	76.5	79.2	83.7	0.93	1.24	1.33	1.47	65.8	79.2	82.4	87.2	-1.49	3.58	3.99	4.18
1.8	15	76.4	85.8	88.2	92.0	1.17	1.50	1.60	1.75	76.6	88.5	90.9	94.6	0.18	3.17	3.02	2.83
2.1	15	84.6	93.4	95.7	99.1	1.42	1.78	1.88	2.03	85.5	95.3	97.5	100.7	1.01	2.04	1.91	1.62
2.4	15	92.1	100.4	102.5	105.7	1.68	2.05	2.16	2.31	92.8	101.2	103.4	106.6	0.68	0.79	0.82	0.84
2.7	15	99.4	107.5	109.5	112.6	1.94	2.33	2.43	2.58	98.9	107.1	109.4	112.8	-0.47	-0.30	-0.14	0.11
3	15	106.8	115.0	117.1	120.2	2.22	2.61	2.71	2.86	104.7	113.4	115.8	119.4	-2.00	-1.33	-1.14	-0.66
3.3	15	114.9	123.2	125.4	128.4	2.50	2.90	2.99	3.14	110.8	120.4	122.8	126.7	-3.50	-2.28	-2.08	-1.33
3.6	15	123.6	132.1	134.2	137.6	2.79	3.18	3.27	3.41	117.6	128.0	130.6	134.7	-4.83	-3.08	-2.71	-2.12
3.9	15	133.2	142.2	144.8	148.8	3.08	3.47	3.56	3.68	125.2	136.5	139.3	144.2	-5.97	-4.00	-3.82	-3.14
4.2	15	144.5	155.8	158.8	163.5	3.38	3.76	3.84	3.96	133.8	147.3	150.8	156.1	-7.37	-5.44	-5.08	-4.54
4.5	15	160.0	172.6	175.9	181.1	3.69	4.05	4.12	4.23	144.3	160.7	164.3	169.9	-9.77	-6.91	-6.61	-6.19
4.8	15	178.9	192.8	196.6	202.6	4.00	4.34	4.41	4.50	158.2	176.9	180.9	186.7	-11.59	-8.26	-8.00	-7.83
5.1	15	201.2	217.2	221.3	227.6	4.32	4.64	4.69	4.77	175.2	196.4	200.4	206.1	-12.93	-9.58	-9.44	-9.44
1.2	20	47.4	56.1	59.0	63.8	0.66	0.92	1.00	1.12	42.3	56.7	60.3	66.0	-10.89	1.00	2.20	3.35
1.5	20	58.1	67.8	70.7	75.4	0.87	1.17	1.25	1.39	54.3	68.1	71.5	76.2	-6.57	0.42	1.20	1.17
1.8	20	67.8	77.2	79.9	84.4	1.10	1.42	1.51	1.66	64.8	77.3	80.5	84.7	-4.35	0.10	0.75	0.41
2.1	20	76.0	85.3	87.8	91.5	1.33	1.68	1.78	1.92	74.1	85.3	88.2	91.4	-2.52	0.06	0.45	-0.14
2.4	20	83.2	91.8	94.0	97.3	1.57	1.94	2.04	2.19	82.2	91.7	93.7	96.5	-1.16	-0.13	-0.32	-0.82
2.7	20	89.4	97.4	99.3	102.3	1.82	2.20	2.30	2.45	89.3	96.8	98.5	101.0	-0.08	-0.62	-0.82	-1.31
3	20	95.0	102.4	104.4	107.1	2.08	2.47	2.57	2.71	94.6	101.3	102.8	105.0	-0.44	-1.14	-1.56	-1.93
3.3	20	100.3	107.6	109.5	112.1	2.34	2.73	2.83	2.97	99.3	105.4	106.8	109.0	-1.04	-2.08	-2.39	-2.71
3.6	20	105.6	112.9	114.8	117.5	2.61	3.00	3.10	3.23	103.5	109.5	111.1	113.4	-2.00	-3.04	-3.28	-3.51
3.9	20	111.3	118.7	120.7	123.5	2.89	3.28	3.36	3.49	107.8	114.1	115.6	118.0	-3.19	-3.95	-4.21	-4.45
4.2	20	117.5	125.1	127.2	130.1	3.17	3.55	3.63	3.75	112.3	119.0	120.6	123.0	-4.38	-4.91	-5.20	-5.45
4.5	20	124.3	132.2	134.2	137.5	3.46	3.82	3.90	4.01	117.4	124.4	126.0	128.4	-5.55	-5.88	-6.14	-6.57

4.8	20	131.7	140.2	142.4	146.0	3.75	4.10	4.17	4.27	123.0	130.4	132.0	134.4	-6.62	-6.95	-7.36	-7.96
5.1	20	140.1	149.7	152.2	156.0	4.05	4.38	4.44	4.52	129.3	137.2	138.7	141.0	-7.74	-8.35	-8.86	-9.62

Table 5-7. Results obtained directly from linear soil models and proposed curve fit within the relative difference in  $\Delta\sigma_{\max}$  (in BC2)

		Linear soil models				Estimated Results from Proposed Equation								Relative difference in $\Delta\sigma_{\max}$ (%)			
H (m)	T (s)	$\Delta\sigma_{\max}$ (MPa)				$H_{eq}$ (m)				$\Delta\sigma_{\max}$ (MPa)				Relative difference in $\Delta\sigma_{\max}$ (%)			
		soil stiffness (kPa)				soil stiffness (kPa)				soil stiffness (kPa)				soil stiffness (kPa)			
		10	50	100	500	10	50	100	500	10	50	100	500	10	50	100	500
0.9	10	46.1	56.2	59.2	64.1	0.47	0.71	0.79	0.91	46.2	61.3	65.0	70.2	0.23	9.05	9.79	9.49
1.2	10	57.6	68.1	71.0	75.4	0.70	0.99	1.08	1.22	60.6	73.0	76.2	81.4	5.11	7.16	7.36	7.89
1.5	10	68.4	79.3	82.3	86.8	0.94	1.28	1.38	1.54	71.2	83.5	87.3	93.4	4.09	5.31	6.10	7.55
1.8	10	80.9	92.6	95.6	100.1	1.20	1.58	1.68	1.85	80.5	95.2	99.9	107.3	-0.51	2.85	4.59	7.14
2.1	10	95.5	107.4	110.5	114.8	1.48	1.88	1.99	2.16	90.9	108.9	114.2	122.2	-4.77	1.45	3.39	6.43
2.4	10	111.7	123.4	126.3	130.2	1.77	2.19	2.31	2.48	103.5	123.7	129.1	137.0	-7.33	0.22	2.27	5.19
2.7	10	129.0	139.7	142.2	145.1	2.07	2.51	2.63	2.79	117.6	138.6	143.6	150.8	-8.83	-0.81	1.05	3.99
3	10	149.0	155.9	157.4	159.3	2.38	2.84	2.95	3.11	132.6	152.7	157.3	170.3	-11.00	-2.04	-0.04	6.92
0.9	15	35.0	43.4	46.2	50.9	0.43	0.65	0.73	0.84	31.2	44.7	48.8	54.6	-10.80	3.00	5.67	7.22
1.2	15	45.4	54.9	57.9	62.7	0.63	0.91	1.00	1.13	43.6	57.5	60.8	66.0	-3.98	4.58	5.00	5.35
1.5	15	54.7	64.6	67.5	72.0	0.86	1.18	1.27	1.42	55.1	67.7	70.6	74.7	0.60	4.82	4.64	3.76
1.8	15	63.1	72.8	75.5	79.5	1.09	1.45	1.55	1.71	64.5	75.5	78.1	81.7	2.30	3.69	3.41	2.73
2.1	15	70.5	80.0	82.5	86.4	1.34	1.73	1.84	2.00	72.6	82.2	84.6	88.1	2.89	2.73	2.51	2.02
2.4	15	77.8	87.2	89.7	93.4	1.61	2.02	2.13	2.29	79.3	88.5	90.9	94.6	1.94	1.46	1.32	1.36
2.7	15	85.4	94.8	97.3	100.8	1.88	2.31	2.42	2.58	85.5	95.0	97.6	101.5	0.17	0.21	0.35	0.70
3	15	93.5	102.8	105.2	108.7	2.16	2.60	2.71	2.87	91.7	102.1	104.7	108.8	-1.83	-0.73	-0.47	0.14
3.3	15	101.9	111.2	113.5	116.8	2.46	2.91	3.01	3.17	98.6	109.6	112.3	116.3	-3.31	-1.44	-1.05	-0.41
3.6	15	110.9	119.9	122.1	125.1	2.76	3.21	3.31	3.46	106.0	117.4	120.1	124.0	-4.42	-2.07	-1.67	-0.86
3.9	15	120.1	128.7	130.7	133.6	3.08	3.52	3.62	3.75	114.0	125.6	128.3	132.5	-5.10	-2.39	-1.87	-0.76
4.2	15	129.4	137.7	140.4	145.2	3.40	3.83	3.92	4.05	122.3	135.0	138.2	144.1	-5.47	-1.99	-1.60	-0.77
4.5	15	138.8	152.2	156.2	162.6	3.73	4.15	4.23	4.34	131.7	148.8	153.1	160.0	-5.15	-2.25	-2.03	-1.59
4.8	15	156.5	172.2	176.9	183.9	4.06	4.47	4.54	4.64	144.7	167.7	172.6	179.8	-7.55	-2.64	-2.44	-2.25
5.1	15	180.8	196.0	201.0	208.3	4.41	4.79	4.85	4.93	163.9	190.9	196.0	202.7	-9.36	-2.58	-2.50	-2.66
1.2	20	37.6	46.2	48.9	53.7	0.59	0.86	0.94	1.07	33.2	46.3	49.7	54.9	-11.68	0.17	1.48	2.13
1.5	20	46.3	55.7	58.6	63.3	0.80	1.11	1.20	1.34	43.9	56.3	60.0	64.4	-5.15	1.10	2.33	1.69
1.8	20	54.3	64.0	66.8	71.3	1.02	1.36	1.46	1.62	52.9	65.1	68.2	72.0	-2.54	1.71	1.99	0.97
2.1	20	61.5	71.0	73.7	77.9	1.26	1.63	1.73	1.89	61.7	72.3	74.8	78.1	0.35	1.79	1.41	0.33
2.4	20	67.9	77.2	79.7	83.4	1.50	1.90	2.01	2.17	69.3	78.3	80.3	83.2	1.99	1.42	0.82	-0.16
2.7	20	73.8	82.6	84.9	88.3	1.76	2.17	2.28	2.44	75.4	83.3	85.1	87.7	2.16	0.86	0.20	-0.68
3	20	79.2	87.7	89.9	93.1	2.02	2.45	2.56	2.72	80.7	87.8	89.5	92.0	1.82	0.12	-0.46	-1.22
3.3	20	84.5	92.8	95.1	98.3	2.30	2.74	2.84	3.00	85.4	92.2	93.9	96.4	0.99	-0.67	-1.21	-1.93
3.6	20	89.9	98.4	100.5	103.5	2.58	3.02	3.13	3.27	89.8	96.9	98.5	100.9	-0.10	-1.56	-1.99	-2.48
3.9	20	95.8	103.9	105.8	108.8	2.88	3.31	3.41	3.55	94.5	101.6	103.1	105.4	-1.34	-2.21	-2.52	-3.09

4.2	20	101.6	109.5	111.6	114.6	3.18	3.61	3.70	3.83	99.3	106.3	108.0	110.4	-2.22	-2.93	-3.23	-3.70
4.5	20	107.4	115.8	117.8	120.6	3.48	3.91	3.99	4.11	104.3	111.8	113.4	115.6	-2.94	-3.47	-3.77	-4.16
4.8	20	114.0	122.2	124.1	126.8	3.80	4.21	4.28	4.39	109.8	117.5	118.9	120.9	-3.73	-3.87	-4.21	-4.67
5.1	20	120.8	128.8	130.7	134.1	4.12	4.51	4.58	4.67	115.8	123.2	124.7	126.6	-4.17	-4.31	-4.61	-5.56

---

As seen in Table 5-6 and Table 5-7, in the majority of cases, the relative difference between the maximum stress ranges obtained from numerical simulations, and the proposed curve fit is less than 10%. However, the difference reaches to 11% to 13% in some of the cases (e.g., 11.1% and 11.6%, for BC1 with  $H = 0.9$  m,  $T = 10$  s,  $k = 100$  kPa, and  $k = 500$  kPa; and 11.6% and 12.9% for BC1 while  $H = 4.8$  m,  $H = 5.1$  m,  $T = 15$  s, and  $k = 10$  kPa).

### 5.5.1. Verification of the proposed curve fit

A new case study (BC3) was conducted to verify the performance of the proposed curve fit in the prediction of the stress range through the EMM. The BC3 was selected to have completely different structural characteristics compared with BC1 and BC2, to assess the general performance of the proposed solution. The structural characteristics of BC3 are presented in Table 5-8 (Bridge, 2005).

Table 5-8. Main parameters of BC3

Parameter	Sign (unit)	Value (BC3)
Outer diameter	$D_o$ (m)	0.324
Wall thickness	$t$ (m)	0.0205
Water depth	$\Delta Z$ (m)	1600
Moment of inertia	$I$ (m <sup>4</sup> )	2.26E-04
Submerged weight	$m_s$ (kg/m)	100
Bending stiffness	$EI$ (Nm <sup>2</sup> )	4.68E+07
Hang off angle	$\theta_{HO}$ (deg)	12.12

The prediction results were obtained for both the critical node with the peak stress range and the entire length of the riser.

#### 5.5.1.1. Peak stress range in critical nodes

Different tangential heave motions with three different wave periods were applied to the BC3 and the maximum stress ranges were obtained from a series of numerical analyses with four linear soil stiffness (e.g.,  $k = 10, 50, 100,$  and  $500$  kPa). The equivalent motions ( $H_{eq}$ ) on the rigid seabed corresponding to each vessel amplitude ( $H$ ) in the linear soil models were



calculated by the proposed curve fit. Then, the dynamic simulations on the rigid seabed ( $k = 100,000$  kPa) were performed using the calculated equivalent motions to obtain the maximum stress range. Figure 5-12 compares the results of maximum stress range that were obtained from both approaches, directly analysis of LM and simplified EMM. Detailed results are provided in Table 5-9.

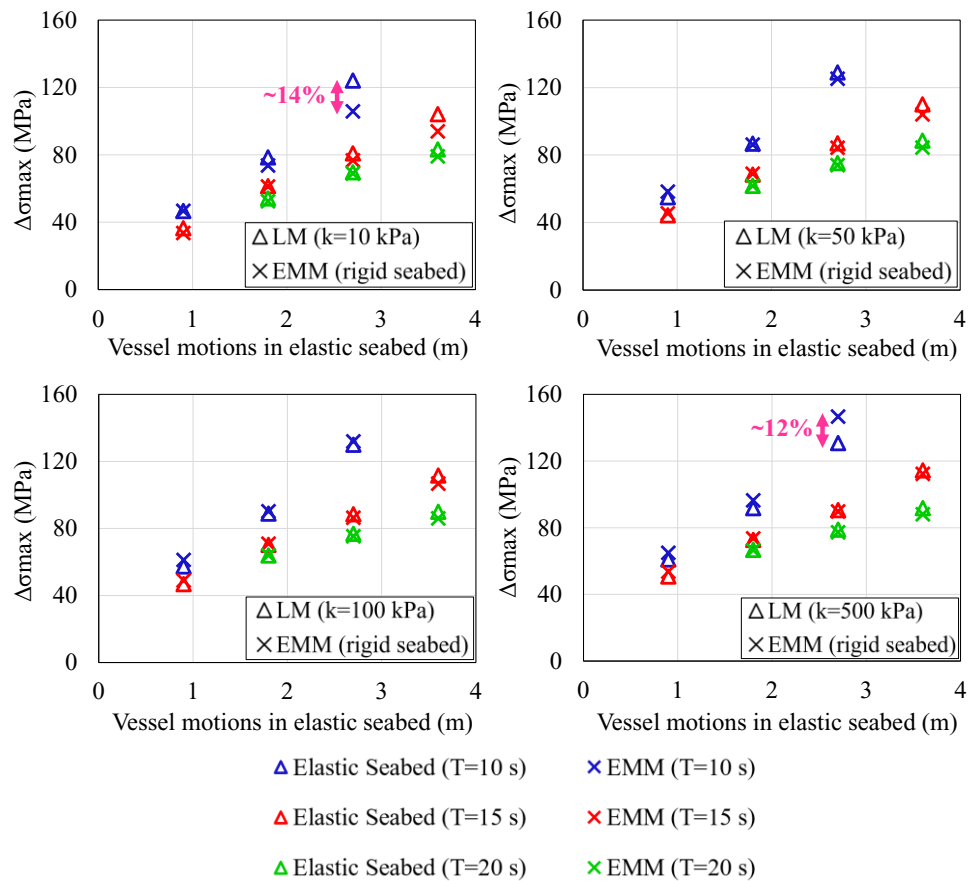


Figure 5-12. Results of maximum stress range based on the elastic seabed and EMM (for BC3)

Table 5-9. Results obtained directly from linear soil models and proposed equation within the relative difference in  $\Delta\sigma_{\max}$  (in BC3)

		Linear soil models				Estimated Results from Proposed Equation				Relative difference in $\Delta\sigma_{\max}$ (%)			
		$\Delta\sigma_{\max}$ (MPa)				$\Delta\sigma_{\max}$ (MPa)							
		soil stiffness (kPa)				soil stiffness (kPa)				soil stiffness (kPa)			
H (m)	T (s)	10	50	100	500	10	50	100	500	10	50	100	500
0.9	10	46.6	55.0	57.3	60.9	46.7	58.3	61.1	64.9	0.30	6.04	6.60	6.65
1.8	10	78.5	86.8	88.8	91.7	73.6	86.2	90.2	96.4	-6.24	-0.62	1.55	5.11
2.7	10	124.1	128.9	129.9	130.7	105.8	125.2	131.9	146.6	-14.78	-2.84	1.58	12.19
0.9	15	36.4	44.3	46.7	50.7	33.6	45.5	48.9	53.6	-7.69	2.90	4.60	5.71
1.8	15	61.4	68.4	70.1	72.7	61.2	68.9	70.8	73.5	-0.31	0.80	0.94	1.08
2.7	15	80.8	87.0	88.4	90.5	76.7	84.3	86.3	89.7	-5.08	-3.08	-2.33	-0.81
3.6	15	104.1	110.0	111.5	114.4	93.9	104.1	106.7	112.3	-9.75	-5.33	-4.24	-1.78
1.8	20	54.1	61.7	63.8	66.7	52.4	61.7	63.9	66.5	-3.09	-0.02	0.24	-0.25
2.7	20	69.6	75.3	76.8	78.8	68.9	74.0	75.3	77.2	-0.89	-1.74	-1.90	-2.02
3.6	20	83.2	88.5	89.9	91.7	79.1	84.4	85.9	88.0	-4.96	-4.64	-4.47	-4.04

It was observed that the peak stress range predicted by the proposed curve fit are in a reasonable agreement with the numerical model simulating the linear elastic seabed. A difference of less than 10% was observed in the majority of cases. However, there were some exceptions, such as the case with  $H = 2.7$  m,  $T = 10$  s with  $k = 10$  kPa and  $k = 500$  kPa, where the EMM slightly underestimates and overestimates the peak stress range by around 14% and 12%, respectively.

### 5.5.1.2. Stress range in the entire length of SCR

As discussed earlier, the basis of the proposed EMM is using the critical node of the riser, where the maximum stress range occurs. The critical node is the primarily important point from a design perspective. However, it is worth examining the performance of the proposed method for the prediction of damage throughout the riser as well. For this purpose, motion amplitudes of 0.9, 1.8, 2.7, and 3.6 m were considered with a wave period of 15 s. The corresponding equivalent motions were obtained from the proposed curve fit. Figure 5-13 shows the results of stress ranges throughout the entire length of the SCR using the EMM and LM.

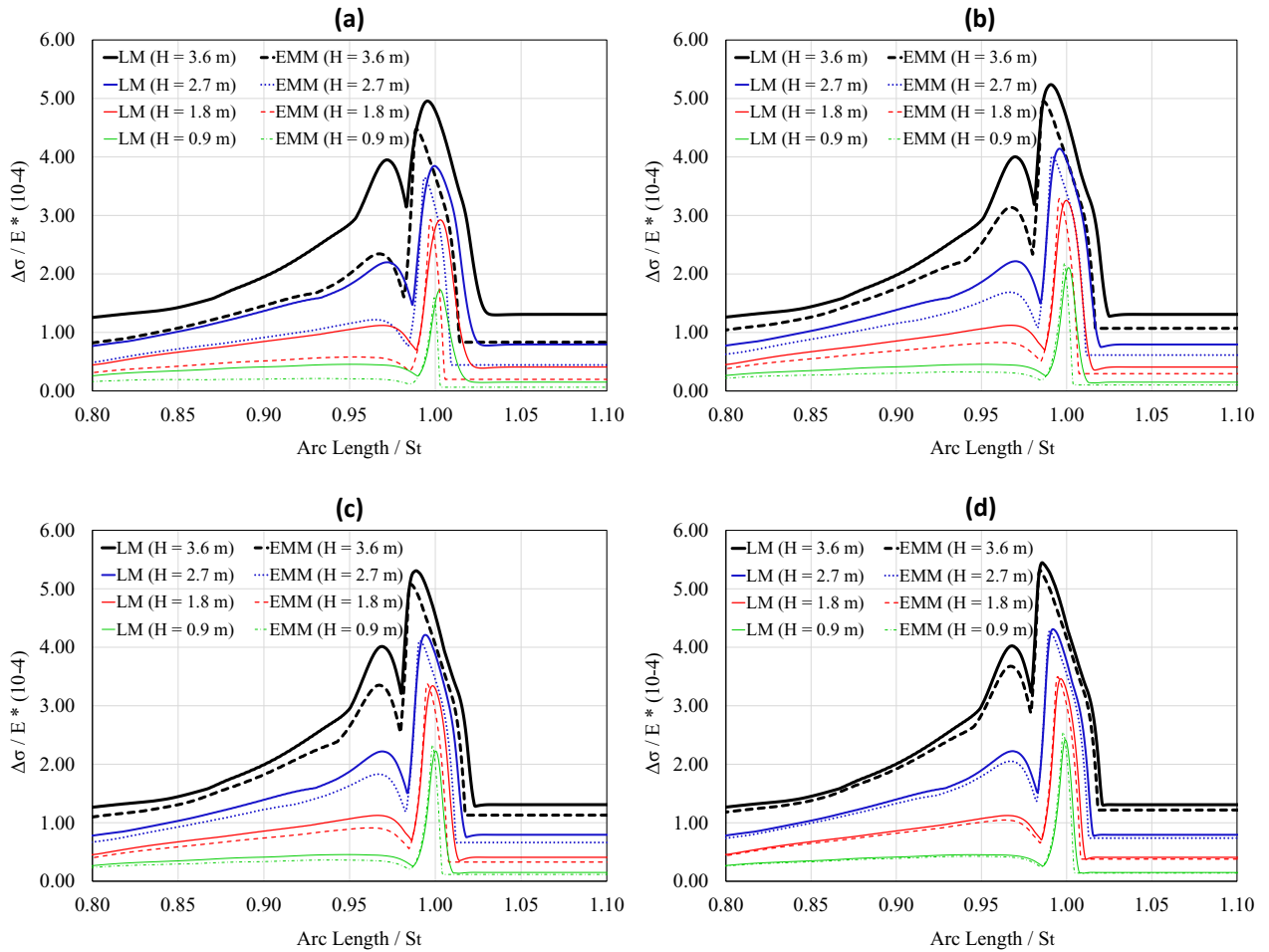


Figure 5-13. Stress range for the entire length of BC3 based on the EMM and LM: (a)  $k=10$  kPa; (b)  $k=50$  kPa; (c)  $k=100$  kPa; (d)  $k=500$  kPa

As originally developed, it was observed that the simplified EMM has its best performance in the peak point of the stress range with a reduced level of accuracy in the other parts of the riser (see Figure 5-13). However, even throughout the riser, the proposed solution gives a reasonable prediction of the damage when seabed becomes harder. While the seabed stiffness is decreased, the EMM starts slightly underestimating the stress range compared with the LM results. These differences become larger when the motion amplitude increases.

### 5.5.2. EMM performance in fatigue analysis

Further to verifying the successful performance of the EMM for harmonic individual waves, the model was examined through a wider deterministic fatigue analysis with the representing

sea states from the wave scatter diagram given in Table 5-10 (Gulf of Mexico, Shiri and Randolph, 2010), where the riser BC3 is geographically located. The S-N curve constants, explained in section 2.2, were assumed to be  $m = 3$ ;  $\log \bar{a} = 20.61$ . The earlier studies show that the contribution of the out-of-plane riser motions to the total fatigue damage is negligible (Martin and White, 2012; Yuan et al., 2017). Therefore, in this study, the sea states was applied in-plane that is the main source of damage accumulation involving only the top and bottom fibres of the riser section.

Table 5-10. Manipulated wave scatter diagram for a 30 year service life in Gulf of Mexico (Shiri and Randolph, 2010)

Sea State ID	H <sub>s</sub> (m)	T <sub>z</sub> (s)	n applied	Sea State ID	H <sub>s</sub> (m)	T <sub>z</sub> (s)	n applied
1	0.5	4.2	18011291	16	8	9.1	3389
2	1	4.6	71370445	17	8.5	9.3	3011
3	1.5	5	48449608	18	9	9.5	1822
4	2	5.4	25187856	19	9.5	9.7	1395
5	2.5	5.8	13529335	20	10	9.9	1070
6	3	6.1	7473660	21	10.5	10.1	1246
7	3.5	6.5	3080495	22	11	10.2	566
8	4	6.9	1631014	23	11.5	10.4	928
9	4.5	7.3	583770	24	12	10.6	544
10	5	7.7	363725	25	12.5	10.7	813
11	5.5	8	114700	26	13	10.9	712
12	6	8.4	33676	27	13.5	11	877
13	6.5	8.5	16907	28	14	11.2	262
14	7	8.7	10864	29	14.5	11.3	343
15	7.5	8.9	5421	30	15	11.5	420

The damage results were superposed using Miner's rule to calculate the total cumulative fatigue damage for the given soil stiffness of 10, 50, 100 and 500 kPa. Figure 5-14 shows the results of total fatigue damage for a linear soil model as well as corresponding results obtained by the proposed method (EMM). The results shows that the EMM can simulate the accumulative fatigue damage with an average difference of less than 12%.

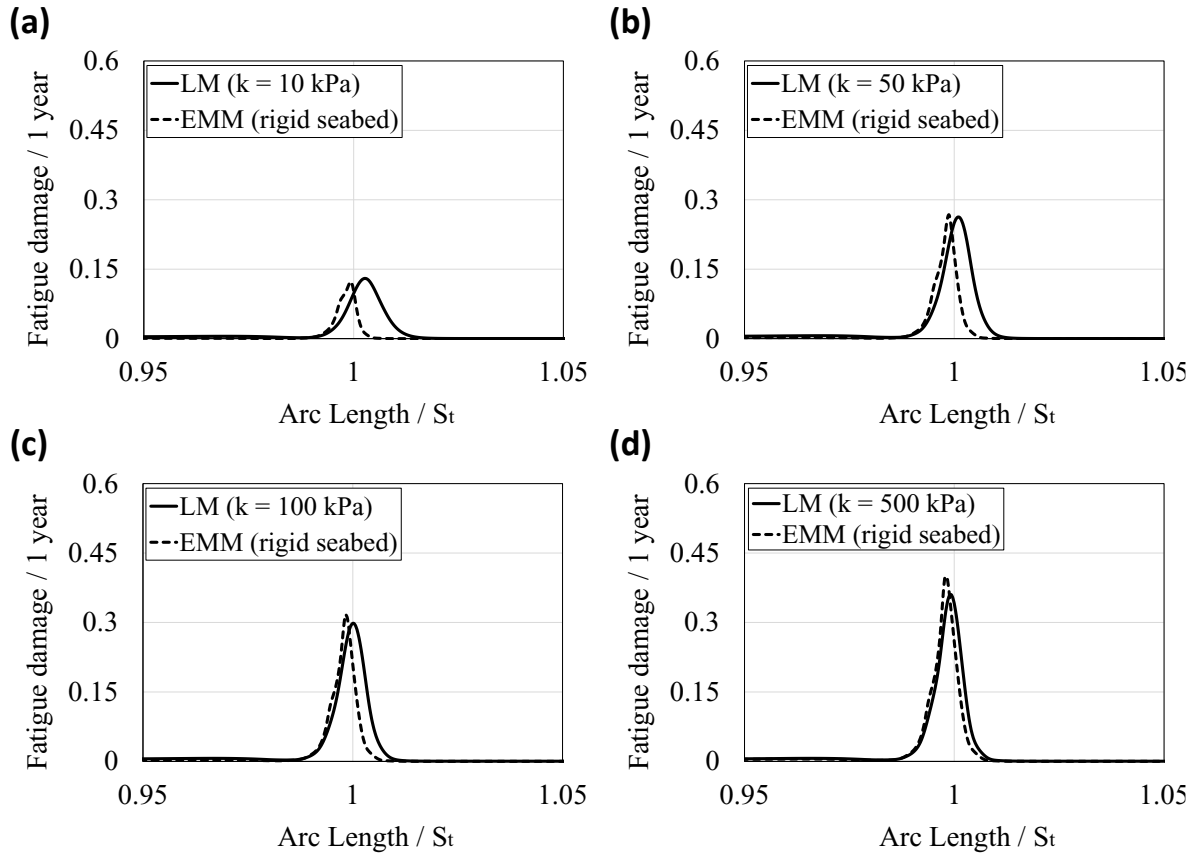


Figure 5-14. Fatigue damage for sample riser (BC3) based on the EMM and LM: (a)  $k=10$  kPa; (b)  $k=50$  kPa; (c)  $k=100$  kPa; (d)  $k=500$  kPa

Overall, the study showed that the proposed EMM could be considered as a potential methodology to predict the stress range of riser in the linear seabed with reasonable accuracy. Although the current study was limited to the linear elastic seabed, the methodology can be further extended in future studies for extraction of the equivalent motions to the non-linear hysteretic seabed interaction conditions resolving the challenges of existing methodologies for incorporation of the trench effect in fatigue analysis.

## 5.6. Conclusion

A methodology called the equivalent motion method (EMM) was developed by introducing an alternative vessel excitation algorithm on a rigid seabed to produce a target peak damage that was obtained from the same riser on a linear elastic seabed. Harmonic heave motions in the tangential direction of the local coordinate system at the hang-off point were considered

and the maximum cyclic stress range and its location were predicted using an EMM equation extracted from a comprehensive set of analyses. A deterministic fatigue analysis was also conducted to examine the EMM performance in a wider perspective. The damage distribution along the riser was also examined. Several interesting observations were made as follows:

- The EMM was found to be an appropriate basis for an alternative methodology with an accuracy of over 90% in most of the cases to incorporate the linear soil model into the fatigue analysis of the SCR in the touchdown zone.
- The equivalent motion amplitude (given through the rigid seabed) is increased for higher values of the seabed stiffness. By gradual shifting from soft to stiff soil, the value of the maximum stress range is also increased.
- For a given vessel amplitude and soil stiffness, by increasing the wave period, the equivalent motion amplitude is decreased, except the loading cases with non-realistic sea states.
- For a given wave period, higher motion amplitude resulted in a higher equivalent motion with a sharper increasing rate for lower seabed soil stiffness magnitudes.

This simplified alternative solution was aimed to incorporate the trench effect into the fatigue analysis of steel catenary risers in the touchdown zone for resolving any pressure hot spots and premature stabilization problems repeatedly reported in the literature (Randolph and Bhat, 2013; Shiri 2014b, Shoghi and Shiri, 2020). Thus, extended studies need to be conducted to investigate the application of the proposed methodology to the non-linear hysteretic riser-seabed interaction scenarios.

## **Acknowledgments**

The authors gratefully acknowledge the financial support of this research by the “Natural Science and Engineering Research Council of Canada (NSERC)” through Discovery program, and the Memorial University of Newfoundland through school of graduate studies funding support.

Table 5-11. Results of maximum stress range and corresponding equivalent motions through different groups of soil stiffness

H (m)	BC1				Equivalent motion amplitude H <sub>eq</sub> (m)				BC2				Equivalent motion amplitude H <sub>eq</sub> (m)				
	$\Delta\sigma_{\max}$ (MPa)				T=5 s	T=10 s	T=15 s	T=20 s	$\Delta\sigma_{\max}$ (MPa)				T=5 s	T=10 s	T=15 s	T=20 s	
	T=5 s	T=10 s	T=15 s	T=20 s					T=5 s	T=10 s	T=15 s	T=20 s					
k=5 kPa	0.15	15.3	8.4	6.0	4.6	0.05	0.05	0.06	0.07	19.0	6.7	4.5	3.5	0.07	0.06	0.07	0.06
	0.3	28.1	16.5	12.1	9.5	0.13	0.13	0.14	0.14	35.8	14.0	9.6	7.4	0.15	0.13	0.14	0.14
	0.6	50.1	33.0	25.0	20.3	0.27	0.30	0.31	0.31	68.5	27.9	20.2	15.8	0.43	0.27	0.28	0.28
	0.9	70.3	48.1	38.1	31.5	0.46	0.46	0.48	0.48	104.7	40.1	30.4	24.5	0.79	0.40	0.42	0.43
	1.2	94.9	61.4	50.1	42.4	0.79	0.64	0.66	0.66	148.6	50.9	40.0	33.0	1.05	0.54	0.57	0.59
	1.5	131.2	73.1	60.9	52.6	1.18	0.84	0.84	0.84	202.1	61.1	48.8	41.0	1.30	0.71	0.73	0.74
	1.8	179.9	84.3	70.4	61.9	1.63	1.08	1.03	1.03	259.0	72.9	56.9	48.5	1.52	0.99	0.89	0.91
	2.1	240.9	95.7	78.8	70.2	1.95	1.39	1.22	1.22	296.6	86.5	64.3	55.5	1.62	1.36	1.09	1.09
	2.4	320.9	108.1	86.5	77.4	2.24	1.75	1.45	1.42	324.1	101.6	71.4	61.9	1.69	1.72	1.30	1.26
	2.7	422.7	121.8	93.8	83.9	2.51	2.10	1.72	1.63	473.2	117.7	78.8	67.8	2.10	2.07	1.58	1.45
	3	506.7	136.6	101.2	89.7	2.66	2.45	2.05	1.84	566.2	142.6	86.7	73.4	2.35	2.60	1.93	1.67
	3.3	560.6	164.8	109.1	95.2	2.76	2.93	2.42	2.11	947.0	172.1	95.0	78.7	3.96	3.13	2.31	1.92
	3.6	680.6	196.9	117.7	100.6	2.95	3.30	2.79	2.42	1374.9	205.6	103.8	84.1	0.00	3.43	2.68	2.22
	3.9	738.0	235.2	127.0	106.1	3.05	3.62	3.15	2.78	1084.2	243.3	113.1	89.7	4.06	3.71	3.04	2.58
4.2	930.8	284.0	137.2	112.1	3.40	3.96	3.49	3.16	1173.4	287.6	122.6	95.7	4.57	4.01	3.41	2.95	
4.5	981.1	354.7	151.1	118.7	3.51	4.36	3.85	3.53	1268.8	342.0	134.4	101.7	4.71	4.32	3.81	3.32	
4.8	1047.7	441.2	171.1	125.9	3.67	4.68	4.25	3.90	1381.2	403.2	153.6	107.8	3.93	4.58	4.24	3.69	
5.1	1220.2	546.3	196.2	133.9	5.06	4.96	4.63	4.25	1690.0	461.1	176.2	114.6	-	4.79	4.59	4.05	
k=10 kPa	0.15	17.7	9.7	6.8	5.2	0.07	0.06	0.07	0.08	19.1	7.9	5.2	4.0	0.07	0.07	0.08	0.07
	0.3	32.4	18.9	13.7	10.8	0.16	0.16	0.16	0.16	35.9	16.4	11.0	8.5	0.15	0.15	0.16	0.15
	0.6	56.7	37.5	28.3	23.0	0.33	0.35	0.35	0.36	68.6	32.5	23.4	18.2	0.43	0.31	0.32	0.33
	0.9	78.6	53.8	42.7	35.5	0.57	0.54	0.55	0.55	107.3	46.1	35.0	28.2	0.81	0.47	0.49	0.50
	1.2	105.8	67.6	55.7	47.4	0.92	0.73	0.75	0.75	159.5	57.6	45.4	37.6	1.10	0.65	0.67	0.68
	1.5	138.7	79.5	66.8	58.1	1.26	0.97	0.95	0.95	225.9	68.4	54.7	46.3	1.39	0.87	0.85	0.86
	1.8	192.9	90.7	76.4	67.8	1.72	1.25	1.17	1.16	303.3	80.9	63.1	54.3	1.64	1.21	1.05	1.06
	2.1	261.1	102.3	84.6	76.0	2.03	1.58	1.39	1.38	365.7	95.5	70.5	61.5	1.81	1.58	1.27	1.25
	2.4	345.8	115.0	92.1	83.2	2.33	1.93	1.65	1.60	430.1	111.7	77.8	67.9	1.98	1.94	1.54	1.46
	2.7	476.9	129.0	99.4	89.4	2.61	2.27	1.97	1.83	524.7	129.0	85.4	73.8	2.24	2.31	1.87	1.69
	3	620.8	143.9	106.8	95.0	2.86	2.60	2.32	2.10	549.8	149.0	93.5	79.2	2.31	2.75	2.24	1.95
	3.3	760.6	167.8	114.9	100.3	3.09	2.97	2.68	2.40	657.1	182.2	101.9	84.5	2.62	3.23	2.60	2.25
	3.6	883.1	201.0	123.6	105.6	3.29	3.33	3.02	2.75	1045.6	220.2	110.9	89.9	4.03	3.54	2.96	2.59
	3.9	942.7	241.0	133.2	111.3	3.42	3.66	3.36	3.11	1009.3	262.3	120.1	95.8	4.00	3.84	3.31	2.95



	4.2	962.4	292.2	144.5	117.5	3.47	4.01	3.69	3.47	1158.8	308.0	129.4	101.6	4.55	4.15	3.65	3.32
	4.5	953.3	367.0	160.0	124.3	3.45	4.42	4.04	3.81	1484.2	362.0	138.8	107.4	-	4.42	3.94	3.67
	4.8	1043.2	458.4	178.9	131.7	3.66	4.73	4.37	4.16	1334.2	436.2	156.5	114.0	-	4.70	4.29	4.03
	5.1	1167.7	570.2	201.2	140.1	4.89	5.02	4.70	4.49	1545.9	514.6	180.8	120.8	-	4.96	4.65	4.38
	0.15	22.6	12.4	8.5	6.5	0.10	0.09	0.10	0.10	23.7	10.3	6.8	5.2	0.09	0.10	0.10	0.10
	0.3	40.7	23.9	17.1	13.6	0.21	0.21	0.21	0.21	42.5	21.4	14.3	11.0	0.19	0.20	0.20	0.20
	0.6	67.4	45.7	34.8	28.5	0.43	0.44	0.44	0.44	68.4	41.1	29.8	23.4	0.43	0.41	0.41	0.41
	0.9	90.4	63.5	51.3	43.2	0.73	0.67	0.68	0.67	106.6	56.2	43.4	35.4	0.80	0.62	0.63	0.63
	1.2	119.3	77.4	65.2	56.1	1.06	0.92	0.91	0.90	161.0	68.1	54.9	46.2	1.11	0.86	0.85	0.85
	1.5	150.9	89.1	76.5	67.8	1.39	1.20	1.17	1.16	246.7	79.3	64.6	55.7	1.47	1.17	1.09	1.09
	1.8	201.0	100.1	85.8	77.2	1.78	1.52	1.42	1.42	352.3	92.6	72.8	64.0	1.77	1.52	1.35	1.33
	2.1	275.4	111.7	93.4	85.3	2.09	1.84	1.70	1.68	461.1	107.4	80.0	71.0	2.07	1.85	1.64	1.58
	2.4	363.2	124.8	100.4	91.8	2.39	2.17	2.02	1.94	565.1	123.4	87.2	77.2	2.35	2.19	1.96	1.84
	2.7	515.6	138.7	107.5	97.4	2.68	2.49	2.35	2.24	636.4	139.7	94.8	82.6	2.56	2.54	2.30	2.13
	3	691.0	154.8	115.0	102.4	2.97	2.79	2.68	2.54	791.4	155.9	102.8	87.7	3.49	2.91	2.64	2.45
	3.3	873.4	180.4	123.2	107.6	3.28	3.12	3.01	2.88	865.0	187.1	111.2	92.8	3.91	3.28	2.97	2.77
	3.6	1017.7	213.0	132.1	112.9	3.59	3.44	3.33	3.21	771.9	225.8	119.9	98.4	3.43	3.58	3.31	3.12
	3.9	1087.3	252.1	142.2	118.7	3.79	3.74	3.64	3.53	897.3	267.7	128.7	103.9	3.93	3.88	3.63	3.46
	4.2	1054.6	300.3	155.8	125.1	3.70	4.06	3.95	3.86	1157.3	312.5	137.7	109.5	4.54	4.18	3.91	3.79
	4.5	1118.1	378.7	172.6	132.2	3.89	4.48	4.27	4.18	1069.9	371.7	152.2	115.8	4.05	4.46	4.22	4.12
	4.8	1284.4	475.0	192.8	140.2	4.16	4.78	4.59	4.49	1236.8	454.9	172.2	122.2	4.67	4.77	4.53	4.46
	5.1	1247.8	591.7	217.2	149.7	4.10	5.08	4.90	4.81	1436.7	544.8	196.0	128.8		5.06	4.85	4.77
	0.15	24.3	13.4	9.2	7.1	0.11	0.10	0.11	0.11	25.9	11.3	7.4	5.6	0.10	0.10	0.11	0.11
	0.3	43.3	25.6	18.4	14.6	0.23	0.23	0.23	0.22	45.7	23.2	15.6	11.9	0.21	0.22	0.22	0.21
	0.6	70.5	48.4	37.1	30.5	0.46	0.47	0.47	0.47	71.1	43.9	32.0	25.2	0.46	0.44	0.44	0.45
	0.9	93.8	66.4	54.1	45.8	0.77	0.71	0.72	0.72	106.9	59.2	46.2	37.8	0.80	0.67	0.68	0.68
	1.2	122.6	80.2	68.0	59.0	1.09	0.98	0.98	0.97	163.1	71.0	57.9	48.9	1.12	0.94	0.92	0.92
	1.5	153.7	91.7	79.2	70.7	1.42	1.28	1.24	1.23	249.9	82.3	67.5	58.6	1.49	1.25	1.17	1.17
	1.8	202.3	102.6	88.2	79.9	1.79	1.59	1.50	1.50	357.5	95.6	75.5	66.8	1.79	1.59	1.45	1.42
	2.1	276.7	114.3	95.7	87.8	2.09	1.91	1.79	1.76	466.2	110.5	82.5	73.7	2.08	1.92	1.75	1.69
	2.4	364.4	127.3	102.5	94.0	2.39	2.23	2.12	2.05	578.3	126.3	89.7	79.7	2.38	2.25	2.07	1.97
	2.7	520.1	141.3	109.5	99.3	2.69	2.55	2.44	2.35	666.0	142.2	97.3	84.9	2.65	2.59	2.41	2.27
	3	700.0	158.2	117.1	104.4	2.98	2.84	2.77	2.67	693.2	157.4	105.2	89.9	2.76	2.95	2.73	2.59
	3.3	879.4	184.6	125.4	109.5	3.29	3.16	3.09	3.00	763.5	187.9	113.5	95.1	3.41	3.29	3.06	2.91
	3.6	1028.2	217.7	134.2	114.8	3.62	3.48	3.39	3.32	1083.6	226.7	122.1	100.5	4.06	3.59	3.39	3.25
	3.9	1117.8	257.7	144.8	120.7	3.89	3.78	3.70	3.64	850.6	268.7	130.7	105.8	3.83	3.89	3.70	3.58
	4.2	1080.2	304.8	158.8	127.2	3.77	4.09	4.01	3.95	984.1	313.6	140.4	111.6	3.99	4.18	3.97	3.90
	4.5	1169.0	380.4	175.9	134.2	4.89	4.49	4.33	4.26	1165.7	375.4	156.2	117.8	4.56	4.48	4.28	4.22
	4.8	1130.2	477.7	196.6	142.4	3.91	4.79	4.64	4.57	1218.5	459.6	176.9	124.1	4.64	4.78	4.60	4.55

	5.1	1133.9	594.4	221.3	152.2	3.92	5.09	4.95	4.88	1523.4	549.0	201.0	130.7	5.07	4.91	4.84
	0.15	27.5	15.3	10.4	8.0	0.13	0.12	0.12	0.12	30.0	13.2	8.6	6.6	0.12	0.12	0.12
	0.3	48.0	28.9	20.8	16.5	0.26	0.26	0.26	0.25	50.9	26.6	17.9	13.8	0.25	0.25	0.25
	0.6	75.4	52.8	41.1	34.0	0.52	0.52	0.53	0.52	76.7	48.6	36.0	28.6	0.53	0.51	0.50
	0.9	98.9	71.2	58.9	50.1	0.84	0.80	0.80	0.80	113.4	64.1	50.9	42.2	0.85	0.77	0.77
	1.2	127.3	84.8	72.8	63.8	1.14	1.10	1.08	1.07	169.6	75.4	62.7	53.7	1.16	1.06	1.05
	1.5	157.8	95.6	83.7	75.4	1.46	1.39	1.36	1.36	252.7	86.8	72.0	63.3	1.50	1.37	1.32
	1.8	203.5	106.3	92.0	84.4	1.80	1.69	1.64	1.65	360.7	100.1	79.5	71.3	1.80	1.69	1.62
	2.1	278.3	118.0	99.1	91.5	2.10	2.00	1.95	1.93	471.6	114.8	86.4	77.9	2.09	2.01	1.92
	2.4	365.5	130.8	105.7	97.3	2.40	2.32	2.26	2.23	583.5	130.2	93.4	83.4	2.40	2.33	2.24
k=500 kPa	2.7	523.9	144.7	112.6	102.3	2.70	2.62	2.58	2.54	679.8	145.1	100.8	88.3	2.69	2.66	2.55
	3	706.5	163.7	120.2	107.1	2.99	2.92	2.89	2.85	723.5	159.3	108.7	93.1	2.98	2.99	2.87
	3.3	883.4	191.3	128.4	112.1	3.29	3.24	3.20	3.16	727.0	188.9	116.8	98.3	3.04	3.30	3.19
	3.6	1033.0	224.9	137.6	117.5	3.63	3.54	3.50	3.47	828.0	227.7	125.1	103.5	3.60	3.60	3.50
	3.9	1122.9	265.8	148.8	123.5	3.90	3.84	3.79	3.78	857.7	269.9	133.6	108.8	3.90	3.90	3.79
	4.2	1084.9	314.8	163.5	130.1	3.79	4.15	4.11	4.08	988.4	315.3	145.2	114.6	3.99	4.19	4.07
	4.5	1372.7	382.5	181.1	137.5	0.00	4.50	4.41	4.39	1213.0	378.1	162.6	120.6	4.63	4.49	4.38
	4.8	1097.9	480.5	202.6	146.0	3.83	4.80	4.72	4.69	1097.9	463.4	183.9	126.8	4.07	4.80	4.69
	5.1	1156.0	598.5	227.6	156.0	4.85	5.10	5.02	4.99	1644.8	555.0	208.3	134.1	5.09	5.00	4.95

## Reference

Aubeny, C., and Biscontin, G., (2008). “Interaction model for Steel Compliant Riser on Soft Seabed.” OTC194193, Houston, TX.

Aubeny, C., White, T., Langford, T., Meyer, V. & Clukey, E. (2015). “Seabed stiffness model for steel catenary risers.” In *Frontiers in offshore geotechnics III* (ed. V. Meyer), pp. 351–356.

Bridge, C., (2005). “Effects of seabed interaction on steel catenary risers.” (Ph.D. thesis). University of Surrey.

Bridge, C., Howells, H. (2007). “Observations and modeling of steel catenary riser trenches.” In: *The seventeenth international offshore and polar engineering conference, ISOPE 2007*, Lisbon, Portugal.

Chen, J., Newlin, J.A., Luo, M., Zhang, H., Hadley, C.J., Hu, S. (2019). “Practice of Riser-Soil Interactions at Touch Down Zones for Steel Catenary Risers.” *Offshore Technology Conference*, 6-9 May, Houston, Texas.

Clukey, E. C., Aubeny, C. P., Randolph, M. F., Sharma, P. P., White, D. J., Sancio, R. & Cerkovnik, M. (2017). “A Perspective on the state of knowledge regarding soil-pipe interaction for SCR fatigue assessments.” *Proceedings of the offshore technology conference*, Houston, TX, USA, paper no. OTC 27564.

Clukey, E.C., Zakeri, A. (2017). “Recent Advances in Nonlinear Soil Models for Fatigue Evaluation of Steel Catenary Risers SCRs.” *Offshore Technology Conference*, 1-4 May, Houston, Texas, USA.

- DNV-RP-F204, (2017). Offshore Standard, Riser Fatigue, Det Norske Veritas.
- Dong, X., Shiri, H. (2018). “Performance of nonlinear seabed interaction models for steel catenary riser, Part I: nodal response.” *Ocean Eng.* 154, 153–166.
- Dong, X., Shiri, H. (2019). “Performance of nonlinear seabed interaction models for steel catenary riser, Part II: global response.” *Appl. Ocean. Res.* 82, 158-174.
- Elliott, B.J., Zakeri, A., Barrett, J., Hawlader, B., Li. G., Clukey, E.C. (2013). “Centrifuge modeling of steel catenary risers at touchdown zone Part II: assessment of centrifuge test results using kaolin clay.” *Ocean. Eng.* 60 (March) 208–218.
- Giertsen, E., Verley, R., Schroder, K. (2004). “CARISIMA: A Catenary Riser/Soil Interaction Model for Global Riser Analysis.” *ASME 2004 23rd International Conference on Offshore Mechanics and Arctic Engineering 2004*, pp. 633-640.
- Hejazi, R., Kimiaei, M. (2016). “Equivalent linear soil stiffness in fatigue design of steel catenary risers.” *Ocean. Eng.* 111, 493–507.
- Kimiaei, M., Randolph, M., Ting, I. (2010). “A parametric study on effects of environmental loadings on fatigue life of steel catenary risers (using a nonlinear cyclic riser–soil interaction model).” In: *Proceedings of the 29th International Conference on Ocean, Offshore and Arctic Engineering*, Shanghai, China, Paper OMAE2010-21153.
- Langford, T. and Aubeny, C. (2008). “Model tests for steel catenary riser in marine clay.” *Proceedings of the Offshore Technology Conference*, Paper 19495, Houston, USA.

Langner, C. (2003). "Fatigue life improvement of steel catenary risers due to self-trenching at the touchdown point." Proceedings of the Offshore Technology Conference, OTC 15104, May 5-8.

Leira, B.J., Passano, E., Karunakaran, D., Farnes, K.A., Giertsen, E. (2004). "Analysis guidelines and application of a riser-soil interaction model including trench effects." Proceedings of the 23rd International Conference on Offshore Mechanics and Arctic Engineering OMAE 2004-51527, 955–962, June 20-25.

Liu, J. (2018). "Numerical modelling of seabed trench and its effect on the structural response of steel catenary riser." PhD Thesis University of Western Australia.

Li, F.Z., Low, Y.M. (2012). "Fatigue reliability analysis of a steel catenary riser at the touchdown point incorporating soil model uncertainties." Appl. Ocean Res. 38, 100–110.

Martin, C.M., White, D.J. (2012). "Limit analysis of the undrained capacity of offshore pipelines." Géotechnique 62 (9) 847–863.

Nakhaee, A., Zhang, J., (2008). "Effects of the interaction with the seafloor on the fatigue life of a SCR." Proceedings of the 18th International Society of Offshore and Polar Engineers Conference ISOPE-I-08-397; 2008 July 6-11; Vancouver, Canada. pp 87-93.

Orcina, (2010). OrcaFlex User Manual 11. UK. <[www.orcina.com](http://www.orcina.com)>

Quéau, L.M., Kimiaei, M., Randolph, M.F. (2013). "Dimensionless groups governing response of steel catenary risers." Ocean Eng. 74, 247–259.

Quéau, L.M., Kimiaei, M., Randolph, M.F. (2014a). “Analytical estimation of static stress range in steel catenary risers at touchdown area and its application with dynamic amplification factors.” *Ocean. Eng.* 88, 63–80.

Quéau, L.M. (2015). “Estimating the fatigue damage of steel catenary risers in the touchdown zone.” (Ph.D. thesis), The University of Western Australia.

Randolph, M.F., Quiggin, P. (2009). “Non-linear hysteretic seabed model for catenary pipeline contact.” In: *Proceedings of the 28<sup>th</sup> International Conference on Ocean, Offshore and Arctic Engineering*. Honolulu, Hawaii, USA.

Randolph, M. F., and White, D. J. (2008) “Pipeline embedment in deep water: processes and quantitative assessment.” *Offshore Technology Conf.*, Houston, USA, OTC 19128.

Randolph, M.F., Bhat, S., Mekha, B. (2013). “Modeling the touchdown zone trench and its impact on SCR fatigue life.” *Proceedings of the Offshore Technology Conference 2013*, OTC-23975-MS, <https://doi.org/10.4043/23975-MS> May 6-9.

Sharma, P.P., Aubeny, C.P. (2011). “Advances in pipe-soil interaction methodology and application for SCR fatigue design.” *Proceedings of the Offshore Technology Conference* OTC-21179-MS.

Shiri, H., Randolph, M. (2010). “The influence of seabed response on fatigue performance of steel catenary risers in touchdown zone.” In: *Proceedings of the 29th international conference on offshore mechanics and arctic engineering*, OMAE 2010, Shanghai, China, p. 20051.

Shiri, H. (2014a). "Response of steel catenary risers on hysteretic non-linear seabed." *Appl. Ocean. Res.* 44 (January), 20–28.

Shiri, H. (2014b). "Influence of seabed trench formation on fatigue performance of steel catenary risers in touchdown zone." *Marine Structure.* 36 (April), 1–20.

Shoghi, R., Shiri, H. (2019). "Modeling touchdown point oscillation and its relationship with fatigue response of steel catenary risers." *Appl. Ocean. Res.* 87, 142-154.

Shoghi, R., Shiri, H. (2020). "Re-assessment of trench effect on fatigue performance of steel catenary risers in the touchdown zone." *Appl. Ocean Res.* 94, 1–16.

Shoghi, R., Pesce, C. P., Shiri, H. (2021). "Influence of trench geometry on fatigue response of steel catenary risers by using a boundary layer solution on a sloped seabed." *Ocean Eng.* 221, 108447.

Thethi, R., Moros, T. (2001). "Soil interaction effects on simple catenary riser response." *Deepwater Pipeline and Riser Technology Conference*, Houston, Texas, USA.

Wang, K., Low, Y.M. (2016). "Study of seabed trench induced by steel catenary riser and seabed interaction." *Proceedings of the 35th International Conference on Ocean, Offshore and Arctic Engineering OMAE2016-54236*, June 19-24.

Wang, K., Xue, H., Tang, W., Guo, J. (2013). "Fatigue analysis of steel catenary riser at touch-dwon point based on linear hysteretic riser-soil interaction model." *Ocean. Eng.* 68, 102–111.

Yuan, F., White, D. J., O'Loughlin, C.D. (2017). "The evolution of seabed stiffness during cyclic movement in a riser touchdown zone on soft clay." *Géotechnique* 67 (2) 127–137.

Zargar, E. (2017). “New hysteretic seabed model for riser-soil interaction.” PhD Thesis, University of Western Australia.



## CHAPTER 6

### **A hybrid model to simulate the trench effect on the fatigue analysis of steel catenary risers in the touchdown zone**

Hossein Janbazi<sup>1</sup>, Hodjat Shiri<sup>2</sup>

1: Department of Civil Engineering  
Memorial University of Newfoundland  
e-mail: [hjanbazirokn@mun.ca](mailto:hjanbazirokn@mun.ca)

2: Department of Civil Engineering  
Memorial University of Newfoundland  
e-mail: [hshiri@mun.ca](mailto:hshiri@mun.ca)

This chapter was published in *Canadian Geotechnical Journal*.

<https://doi.org/10.1139/cgj-2022-010>

## **Abstract**

The gradual trench formation of steel catenary risers (SCRs) in the touchdown zone (TDZ) is known to significantly affect the SCR's fatigue life. However, there is still no coherent agreement amongst the researchers on the beneficial or detrimental effects of the trench on fatigue. Recent studies have shown that a potential source of contradictory fatigue results could be the methodology to incorporate the trench in the numerical simulations. Since the predefined mathematical trench profiles create non-realistic contact pressure hot spots in the seabed, and the nonlinear hysteretic seabed interaction models may cause premature trench stabilization, both methods distort the damage distribution. To resolve these problems, a new model called Hybrid Trench Model (HTM) has been developed in this study by combining the linear soil stiffness and nonlinear hysteretic seabed interaction model. This hybrid model provides an equivalent stiffness distribution in the touchdown zone to simulate the trench profile obtained from a nonlinear riser-seabed interaction model. HTM's capability in developing deep trenches, e.g. 5D, was examined along with perfect compatibility with the natural catenary shape of the riser, exhibiting the reliability of this method to incorporate the trench effect into the fatigue analysis.

**Keywords:** Steel Catenary Riser, Nonlinear soil model, Equivalent soil stiffness, Trench model, Fatigue analysis

## 6.1. Introduction

Steel catenary risers (SCRs) are among the most cost-effective systems widely used in offshore oil and gas developments to convey hydrocarbons from the seabed well to the floating structure. The design of SCR is strongly affected by the fatigue performance in the touchdown zone (TDZ), where the dynamic motion of the SCR contacts cyclically with the seabed (Campbell, 1999; Bridge, 2005; Randolph and White, 2008; Clukey et al., 2011; Sharma and Aubeny, 2011; Aubeny et al., 2015; Clukey et al., 2017; Dong and Shiri, 2019). This can lead to remoulding and softening of the soil in TDZ and result in a several-diameter-deep trench formation, as observed by remote operating vehicles (ROV) (Thethi and Moros, 2001; Bridge, 2005; Bridge and Howells, 2007). The significance of trench impact on the fatigue response of SCRs is widely accepted in the literature. However, the beneficial or detrimental effect of the trench is still a point of question that has not been coherently answered by the researchers. Some of the studies have shown the fatigue life improvement in TDZ due to trench formation (e.g., Langner, 2003; Nakhaei and Zhang, 2008; Sharma and Aubeny, 2011; Elliot et al., 2013; Randolph et al., 2013; Wang et al., 2016), while other studies have shown a reduced fatigue life (e.g., Giertsen, 2004; Leira, 2004; Shiri and Randolph 2010; Rezazadeh et al., 2012; Shiri, 2014a, b; Zargar 2017). Also, some studies have obtained scattered results showing improved or reduced fatigue life because of the trench formation (Randolph et al., 2013; Dong and Shiri, 2019; Shoghi and Shiri, 2020). The studies published on the trench effect on fatigue have mainly used two different approaches: (i) artificial insertion of the trench through mathematical formulation (e.g., Langner, 2003; Clukey et al., 2007; Sharma and Aubeny, 2011; Li and Low, 2012;

Randolph et al., 2013; Wang et al., 2016), (ii) automatic development of the trench using advanced nonlinear hysteretic soil models (e.g., Nakhaei and Zhang, 2008; Shiri and Randolph, 2010; Shiri 2014a, b; Zargar, 2017). Shoghi and Shiri (2020) conducted a qualitative assessment of the trench effect based on the results reported in the literature and showed that some of these contradictory results are related to the methodology used to implement the trench profile underneath the riser.

There are some inconsistencies between the natural catenary shape of the riser and the trenches created by mathematical expressions, leading to hotspots of contact pressure and distortion of the stress distribution in TDZ (Sharma and Aubeny, 2011; Randolph et al., 2013; Shiri, 2014b). To resolve this issue, Randolph et al. (2013) proposed a new approach called the Stepped method that could improve the situation but not eliminate the contact pressure hot spots, particularly in the trench mouth where the trench profile makes a relatively sharp angle with the original flat seabed towards the vessel. Advanced nonlinear riser-seabed interaction models have been used as an alternative solution for the cyclic development of trenches to prevent the mismatch between the SCR catenary shape and the seabed profile in TDZ (e.g., Aubeny and Biscontin, 2009; and Randolph and Quiggin, 2009). These models use different functions of soil stiffness to represent four main episodes of riser motions: (a) initial penetration, (b) uplift, (c) suction, and (d) re-penetration. However, the cyclic trench formation is stabilized prematurely through a few oscillations achieving an embedment of 0.5D to 1D (Hejazi and Kimiaei, 2016; Dong and Shiri, 2018). This is much less than the ranges of 3.5D to 5D trenches observed in the field (Bridge and Howells, 2007). To resolve this limitation, Shiri and Randolph (2010) used extreme values

for the nonlinear soil model parameters through different analysis steps to achieve the target trench depths. However, the strategy ended in inconsistencies in created trench profiles, as further discussed by Dong and Shiri (2019). Efforts were made to resolve the limitations of these models (e.g., Randolph et al., 2013; Zargar et al., 2019; Shoghi and Shiri, 2021; Janbazi and Shiri, 2022). However, there is still a need for developing simple but robust methodologies to reliably incorporate the trench effect into the fatigue analysis of the SCRs. In this study, a new model called Hybrid Trench Model (HTM) was proposed that combines the linear soil stiffness and a typical nonlinear hysteretic riser-seabed interaction model. For nonlinear riser-seabed interaction, the model developed by Randolph and Quiggin (2009) was used, which is probably the most popular model in the literature. This model, which is called “R-Q”, is a built in model in OrcaFlex software used worldwide for global riser analysis. Using the combination of a linear elastic approach and the R-Q model a nonlinear equation was extracted for the distribution of equivalent stiffness along the SCR in TDZ. This resulted in generating a target trench profile in an elastic seabed that can be solely obtained from the nonlinear hysteretic riser-seabed interaction models (see Figure 6-1).



the literature (e.g., Shiri, 2014b): (1) touchdown point (TDP) where the SCR reaches the nominal level of the seabed, (2) trench bottom point (TBP) defined as the maximum depth of the trench profile, and (3) trench surface point (TSP) where the SCR essentially reaches the zero gradient towards the anchored end of the riser. Figure 6-2(b) shows the incremental penetration of the sample riser with a nonlinear soil model, such as one proposed by Randolph and Quiggin (2009), called R-Q hereafter. As the embedment gradually increases, TDP moves toward the vessel, and TBP moves down with a different depth, but TSP is less affected. These three points (TDP, TBP, and TSP) specify the trench's depth and longitudinal profile.

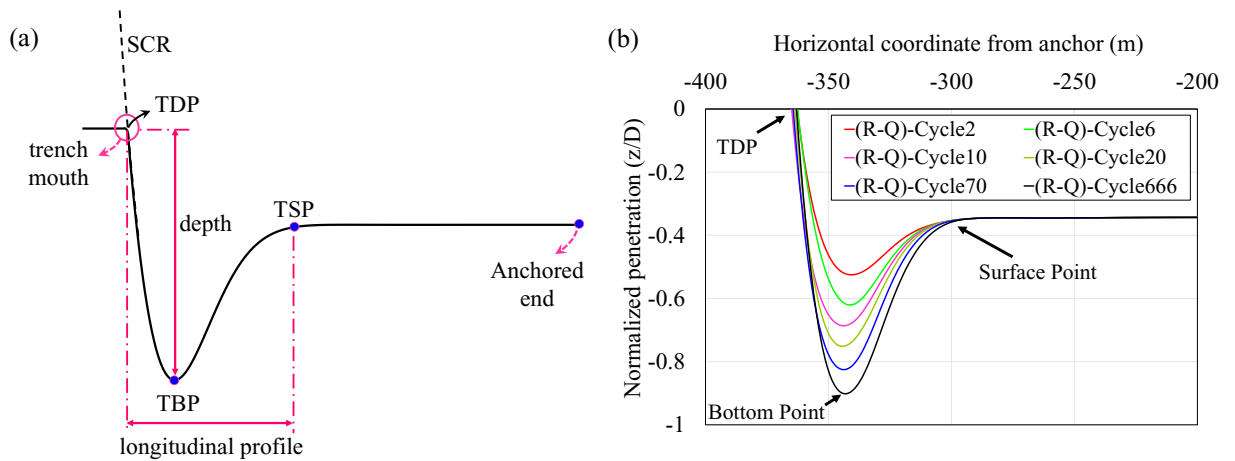


Figure 6-2. Configuration of the trenched seabed: (a) trench profile with some key points; (b) incremental embedment of riser (R-Q model)

According to the riser embedment profile shown in Figure 6-2, assuming a single linear elastic soil stiffness in TDZ causes unrealistic penetration and curvatures in the trench curve (inside the ladle) and the pipeline part resting on the seabed (see Figure 6-3(a)). In reality, the soil stiffness varies throughout TDZ due to experiencing different cycles and degrees

of remoulding, leading to trenched profiles with several diameter depths. This triggered the idea of finding an equivalent stiffness to result in a more realistic trench profile, as explained earlier. As shown in Figure 6-3(b), two patterns of linear soil stiffness along the riser in TDZ were introduced, leading to the target riser embedment that is usually obtained from nonlinear hysteretic riser-seabed interaction models. The reduction in soil stiffness was defined by pattern 1 to simulate the depth of the ladle shape, and pattern 2 represented the horizontal translation of soil stiffness in TDZ to adjust the surface point of the trench.



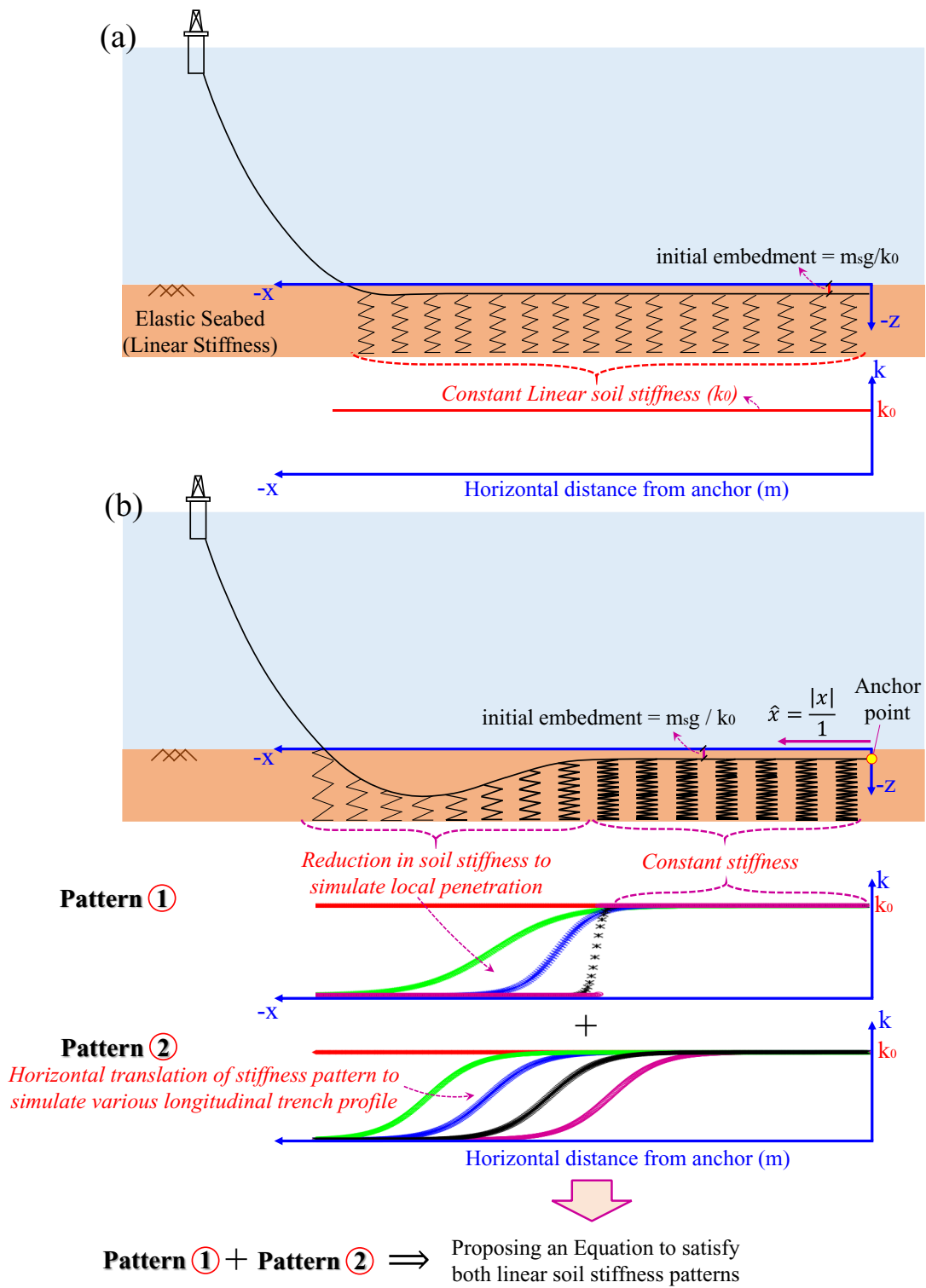


Figure 6-3. Schematic soil stiffness changing from linear to the equivalent stiffness: (a) linear stiffness; (b) equivalent stiffness

To satisfy both stiffness patterns mentioned above, a nonlinear equation was proposed to factorize the linear seabed stiffness in every single node contacting with the seabed, which is provided in equation (6-1) and named as equivalent stiffness.

$$k_{eq} = \frac{k_0}{1 + [\alpha \cdot \exp(\alpha \cdot (\hat{x} - \eta))]} \quad (6-1)$$

where  $k_0$  is defined as reference stiffness used for creating the initial embedment of the riser, as shown in equation (6-2).

$$k_0 = \frac{m_s g}{z_0} \quad (6-2)$$

where  $z_0$  is the initial riser embedment under its submerged weight ( $m_s g$ ). The value of  $z_0$  can be calculated from the backbone curve comprising the soil resistance and the soil buoyancy force, as shown in equation (6-3). For more details about the soil behaviour during the initial penetration, refer to Randolph and Quiggin (2009).

$$P_u = N_c S_u D + f_b A_{disp} \cdot (\rho_{soil} - \rho_{water}) \cdot g \quad (6-3)$$

where  $P_u(z)$  is the ultimate soil penetration resistance,  $N_c(z/D)$  is the soil bearing factor,  $S_u$  is the undrained shear strength,  $D$  is the outer pipe diameter,  $f_b$  is the soil buoyancy factor,  $A_{disp}$  is the nominal area of the pipe that is below the seabed tangent plane,  $\rho_{soil}$  is the saturated density of the soil,  $\rho_{water}$  is the density of water, and  $g$  is the acceleration due to gravity.

Regarding equation (6-1), the parameter  $\hat{x}$  is the absolute value of the horizontal coordinate of each node from the anchored end normalized by 1 m (as shown in Figure 6-3(b)). Moreover, the depth correlation factor ( $\alpha$ ) and longitudinal adjustment factor ( $\eta$ ) are

dimensionless parameters related to the bottom and surface points of the trench, respectively.

### 6.2.1. Numerical model of riser

A global SCR model was constructed in ABAQUS using an example SCR adopted from a published case in the literature to facilitate comparisons (i.e., Bridge, 2005; Shiri, 2014a).

Figure 6-4 schematically illustrates the modelled SCR with a length of 2333 m and a water depth of 1800 m located in the Gulf of Mexico.

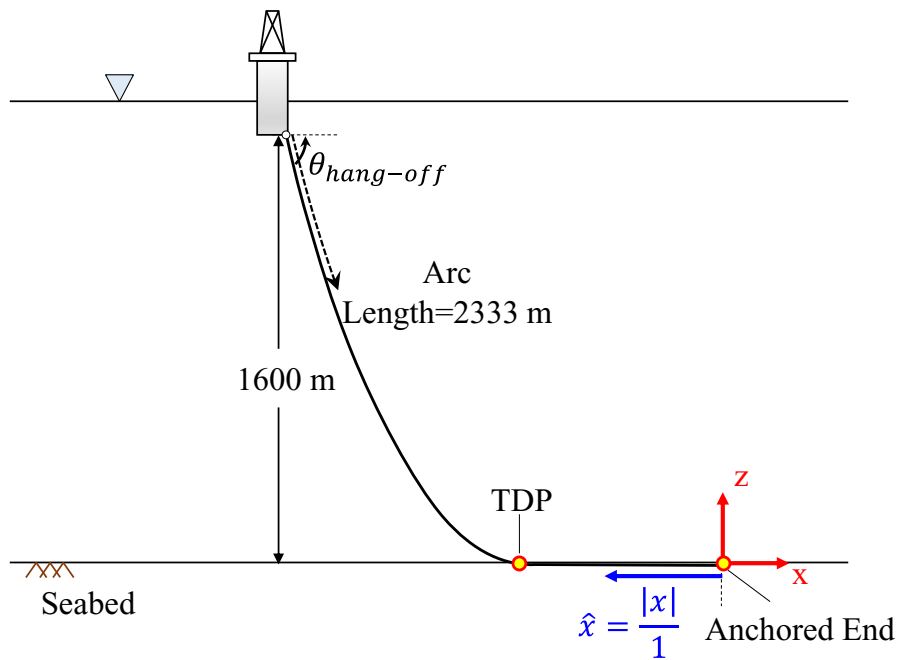


Figure 6-4. The global geometry of SCR modelled by ABAQUS

The PIPE21 elements from the ABAQUS element library were used to model the SCR with an element length of 1 m in TDZ and 5 m in the catenary part. The model boundary conditions were defined by assuming simple hinge supports at both the anchored end and the hang-off point. The vessel excitation under the environmental loads was coded into a

DISP user subroutine in ABAQUS for displacement-controlled analyses. Table 6-1 presents the main structural characteristics of the SCR.

Table 6-1. Main parameters of SCR

Parameter	Value
Do (m)	0.324
t (m)	0.0205
$\Delta Z$ (m)	1600
$A_s$ (m <sup>2</sup> )	1.95E-02
I (m <sup>4</sup> )	2.26E-04
$m_s$ (kg/m)	100
EI (Nm <sup>2</sup> )	4.68E+07
$\theta_{HO}$ (deg)	77.88

### 6.2.2. Sensitivity analysis of the dimensionless parameters

A series of numerical analyses were conducted on a riser based on the equivalent stiffness implemented in the UEL subroutine of ABAQUS. Each dimensionless parameter defined in the equivalent soil stiffness (see equation (6-1)) was changed independently to observe its effects on the trench profile. In the first group of analyses, only the depth correlation factor was changed taking the values of 0, 0.01, 0.1, 0.2, 0.5, and 1 within the constant value for longitudinal adjustment factor,  $\eta = 310$ . In the second group of analyses, different values of  $\eta$  were chosen,  $\eta = 310, 290, 270, 250, 230$ , with the same  $\alpha$  ( $\alpha = 0.1$ ). Figure 6-5 and Figure 6-6 show the soil stiffness patterns obtained from the equivalent stiffness equation within the results of riser penetration obtained from the equilibrium analysis of the riser based on the HTM method.

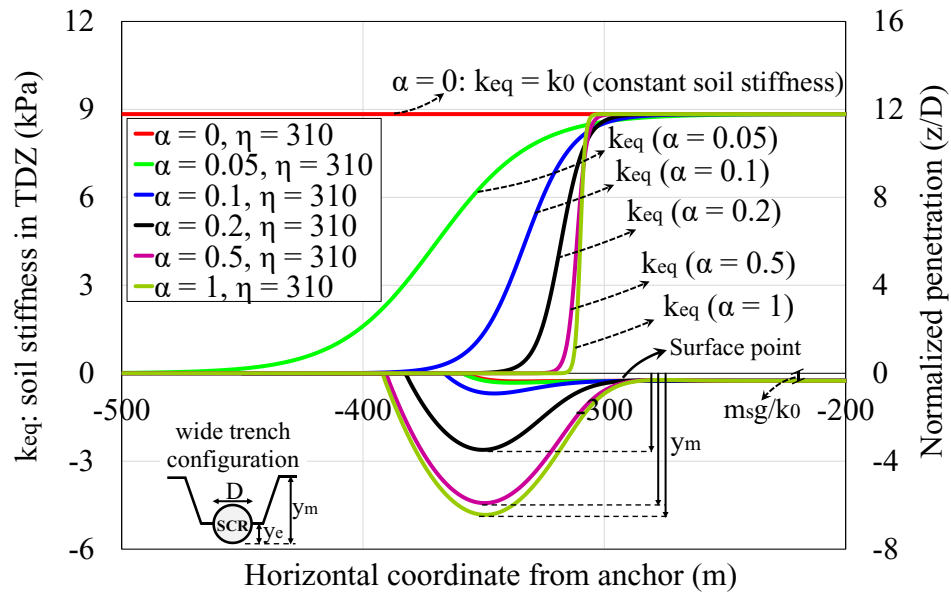


Figure 6-5. Sensitivity analysis of  $\alpha$  with the constant  $\eta$

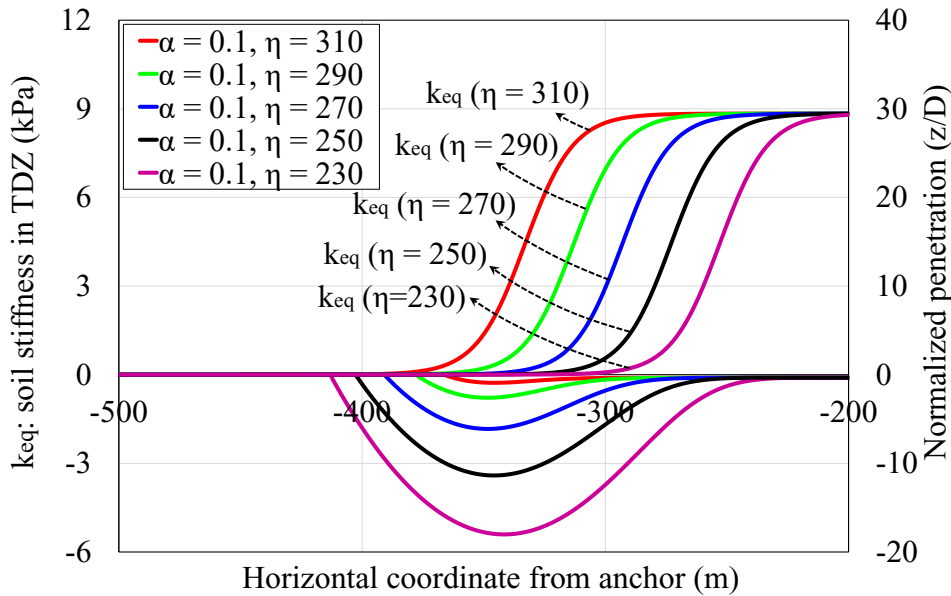


Figure 6-6. Sensitivity analysis of  $\eta$  with the constant  $\alpha$

As illustrated in Figure 6-5, results show that the various depth correlation factors, from 0 to 1, represent soil stiffness reduction in TDZ, corresponding to the cyclic stiffness degradation occurring in reality. This implies that the gradual penetration of the riser into the seabed where TDP moves slightly towards the vessel side and surface point appears to

remain unchanged. Moreover, several values for  $\eta$  were used to translate the soil stiffness pattern in TDZ for adjusting the surface point depending on the seabed type (stiff or soft soil). The analyses confirmed that the trench profiles were entirely compatible with the natural shape of the riser. This compatibility eliminates any pressure hot spots along the trench length and premature stabilization problems repeatedly reported in the literature (Randolph et al., 2013; Shiri, 2014b, Shoghi and Shiri, 2020).

### 6.3. Verification of the Hybrid Trench Model (HTM)

The performance of the proposed hybrid trench model was verified against the nonlinear hysteretic riser-seabed interaction model developed by Randolph and Quiggin (2009), both in terms of the trench profile and cyclic stress range. As explained earlier, a global SCR model was constructed in ABAQUS, and the R-Q riser-seabed interaction model along with the hybrid trench model were coded to user-defined elements using UEL subroutine. The developed model in UEL subroutine of ABAQUS allowed full access to the riser-seabed interaction models that are usually limited in subsea pipe software like OrcaFlex (Orcina, 2010).

#### 6.3.1. Verification of trench profile

The cyclic embedment of the riser was obtained using both HTM and the R-Q model. Table 6-2 shows the R-Q model parameters for seabed interaction.

Table 6-2. Input parameters for the R-Q nonlinear soil model

Description	sign	value
Mud-line shear strength (kPa)	$s_{u0}$	0., 0.5, 1
Shear strength gradient (kPa/m)	$\rho$	1
Saturated soil density (kg/m <sup>3</sup> )	$\rho_{soil}$	1500
Power law parameter	$a$	6

Power law parameter	<b>b</b>	0.25
Normalized maximum stiffness	<b>K</b>	200
Suction ratio	$f_{suc}$	0.3
Suction decay parameter	$\lambda_{suc}$	0.5
Re-penetration parameter	$\lambda_{rep}$	0.5
Soil buoyancy factor	$f_b$	1.5

As shown in Table 6-2, the ranges of mudline shear strength with small values ( $s_{u0} = 0, 0.5, 1$  kPa) were adopted for the R-Q model representing very soft clay usually found in deep water regions (Randolph, 2004; Hejazi and Kimiaei, 2016). An individual harmonic wave with an amplitude of  $H = 3.3$  m and a period of  $T = 15$  s was applied in the tangential direction of the local coordinate system at the riser attachment point.

To verify the functionality of the HTM in simulating the similar trench profiles created by the R-Q model, the appropriate values of  $\alpha$  and  $\eta$  were adopted for the equivalent stiffness distribution proposed in equation (6-1). Figure 6-7, Figure 6-8, and Figure 6-9 show a good agreement between the trench profiles simulated by HTM and those obtained from the R-Q model. These results show that the parameter  $\eta$  remained constant for a given mudline shear strength, while different values of  $\alpha$  were used to simulate the target riser embedment. The choice of 666 cycles shown in the relevant figures was somewhat arbitrary but adopted to ensure that the trench of the R-Q soil model had stabilized and that the depth of penetration no more increased with a higher number of cycles.

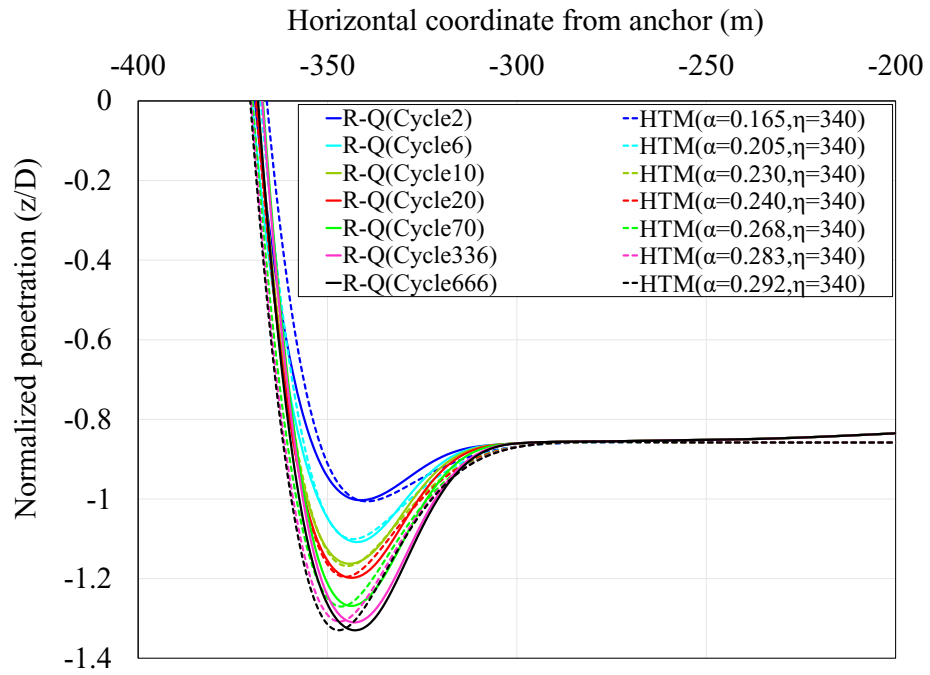


Figure 6-7. Cyclic embedment of the R-Q model and gradual penetration of the HTM ( $s_{u0} = 0$

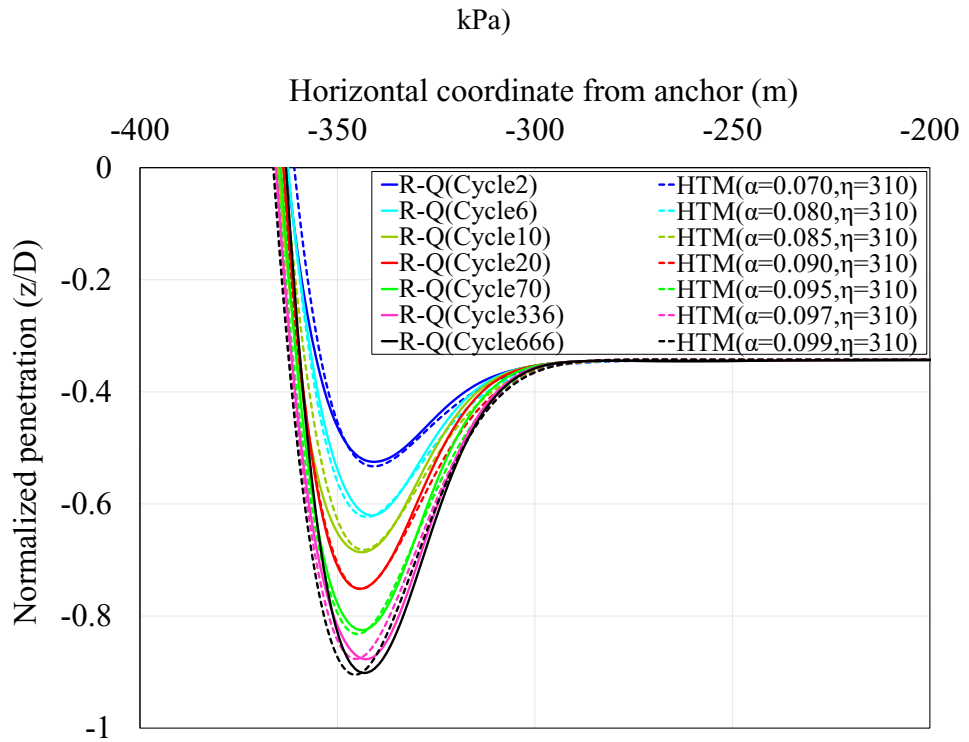


Figure 6-8. Cyclic embedment of the R-Q model and gradual penetration of the HTM ( $s_{u0} = 0.5$

kPa)



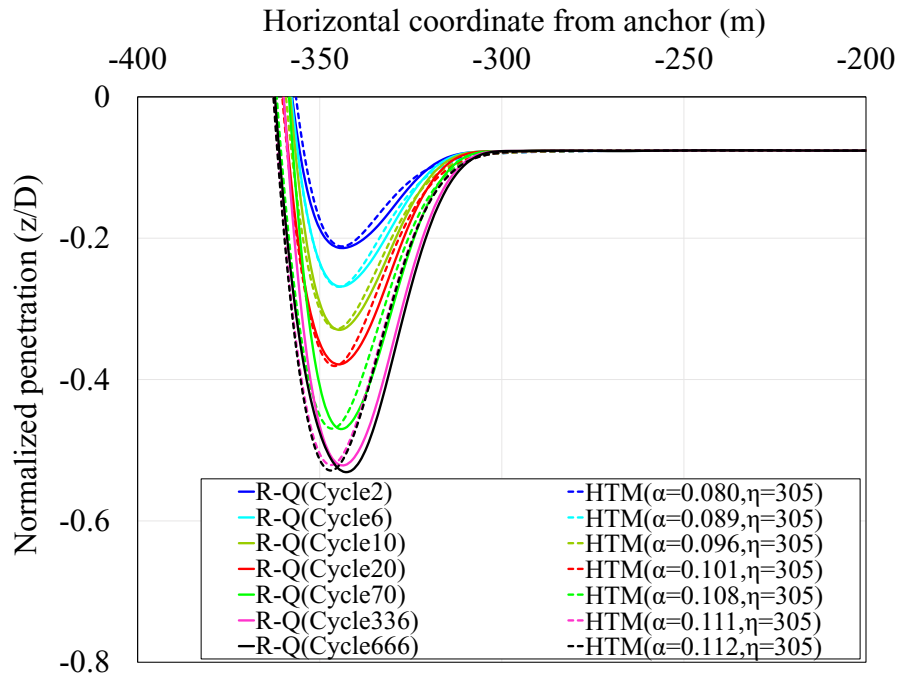


Figure 6-9. Cyclic embedment of the R-Q model and gradual penetration of the HTM ( $s_{u0} = 1$  kPa)

These results show that the depth correlation factor,  $\alpha$ , has a direct relationship with the maximum trench depth. It means that by selecting different values for  $\alpha$ , from small to large, the gradual deepening of the trench can be simulated by moving TDP towards the vessel, moving TBP downward, and keeping TSP almost in the same position.

To better understand the role of  $\alpha$  in the gradual deepening of the riser, the individual values of  $\alpha_i$  were normalized by  $\alpha_{min}$  leading to the similar trench profile obtained from a given riser in each group of the R-Q model (i.e.,  $s_{u0} = 0, 0.5, 1$  kPa, and  $\rho = 1$  kPa/m), where “ $i$ ” refers to each trench profile corresponding to the given number of cycles. As seen in Fig. 10, an appropriate curve that fits in the form of linear regressions can be obtained between  $\alpha_i/\alpha_{min}$  and the normalized maximum depth of the trench for all three groups. It is noted that the value of  $\eta$  modifies the slope of these curve fits.

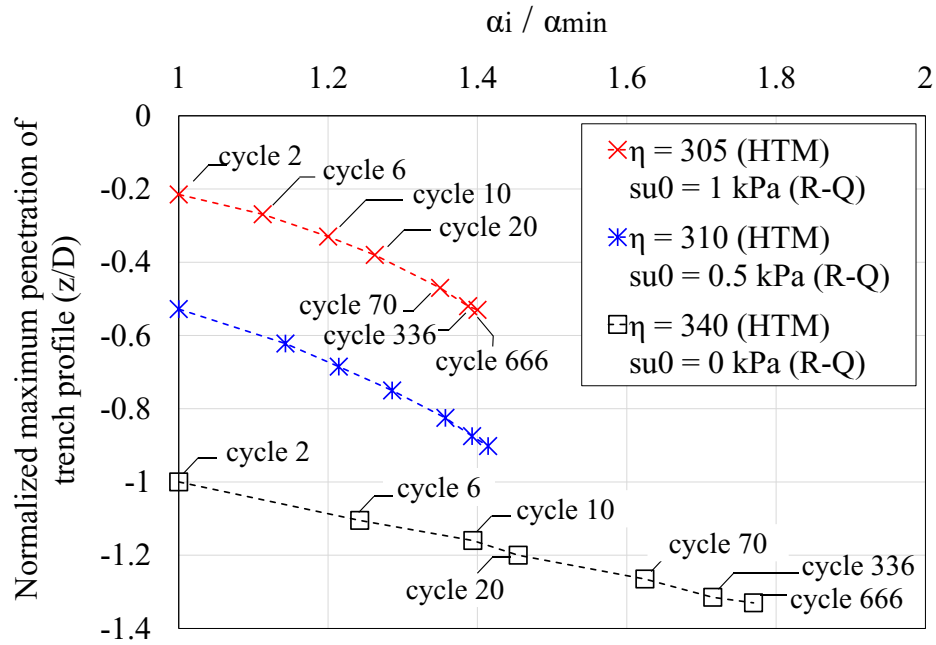


Figure 6-10. Maximum depth of penetration and variations of  $\alpha$  through a number of cycles  
 More detailed investigations are required to extract curve fits that achieve satisfactory agreement between HTM and the R-Q model. Such curve fits could be used to propose simplified frameworks for daily engineering practices. However, this was beyond the scope of the current study.

### 6.3.2. Verification of cyclic axial stress range

The range of cyclic cross-sectional (axial) stress is the primary input to determine the fatigue damage and is calculated by the following set of equations (DNV-RP-F204, 2017):

$$\sigma = \sigma_a \pm \sigma_m \quad (6-4)$$

$$\sigma_a = \frac{T_w}{A} \quad (6-5)$$

$$\sigma_m = \frac{MD_o}{2I} \quad (6-6)$$

$$\Delta\sigma = \sigma_{max} - \sigma_{min} \quad (6-7)$$

where  $\sigma$  is the total axial stress,  $\sigma_a$  is the tensile stress,  $\sigma_m$  is the bending stress,  $T_w$  is the wall tension,  $M$  is the bending moment,  $A$  is the cross-section area,  $D_o$  is the outer diameter,  $I$  is the moment inertia, and  $\Delta\sigma$  is the total stress range.

HTM was examined to predict the total cyclic stress range, and the results were compared with the R-Q model. A series of dynamic analyses were conducted based on the three groups of tangential heave motions, including  $H = 2, 3.3,$  and  $4.5$  m with  $T = 15$  s. This direction was found by Kimiaei et al. (2010) to contribute by more than 93% to the accumulated fatigue damage. Dynamic analysis was conducted when the trench profile was stabilized after 666 cycles in R-Q model. After reaching this point, the soil stiffness was switched to the linear stiffness,  $k = 300$  kPa, representing the common range of soil stiffness assumed for the Gulf of Mexico (e.g., Randolph et al., 2013). Figure 6-11 shows the flowchart of the overall analysis conducted in ABAQUS to evaluate the applicability of HTM in predicting the trench formation and cyclic stress range of SCR in the R-Q model.

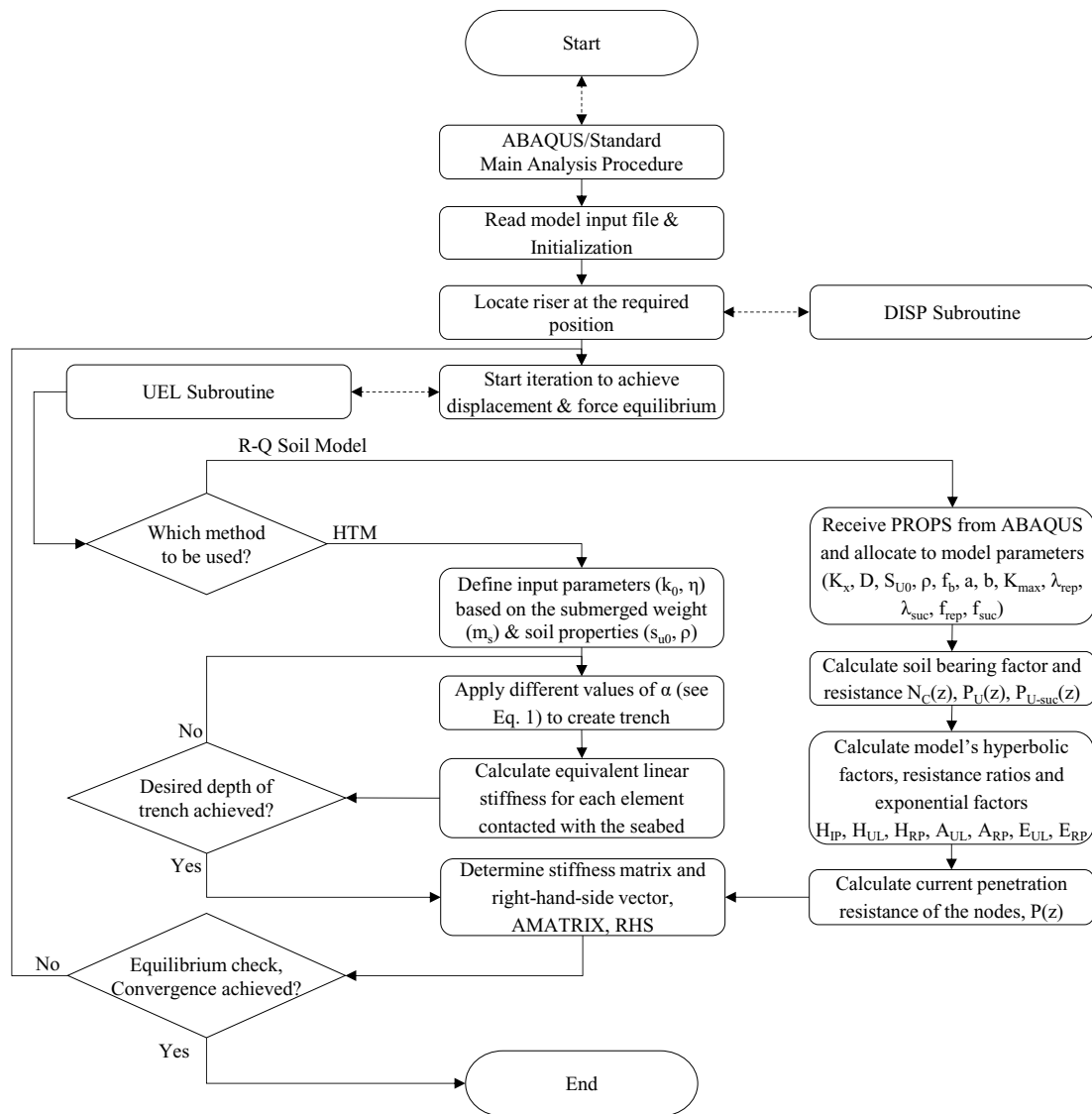


Figure 6-11. The flowchart of ABAQUS main procedure conducted for HTM and R-Q model. As shown in Figure 6-12, Figure 6-13, and Figure 6-14, there is a good agreement between HTM and R-Q in the total cyclic stress range. In these figures,  $x_{TDP}$  is the horizontal coordinate between TDP and anchored end, and  $x$  and  $z$  are the horizontal and vertical axes located at the anchor point (see Figure 6-4).

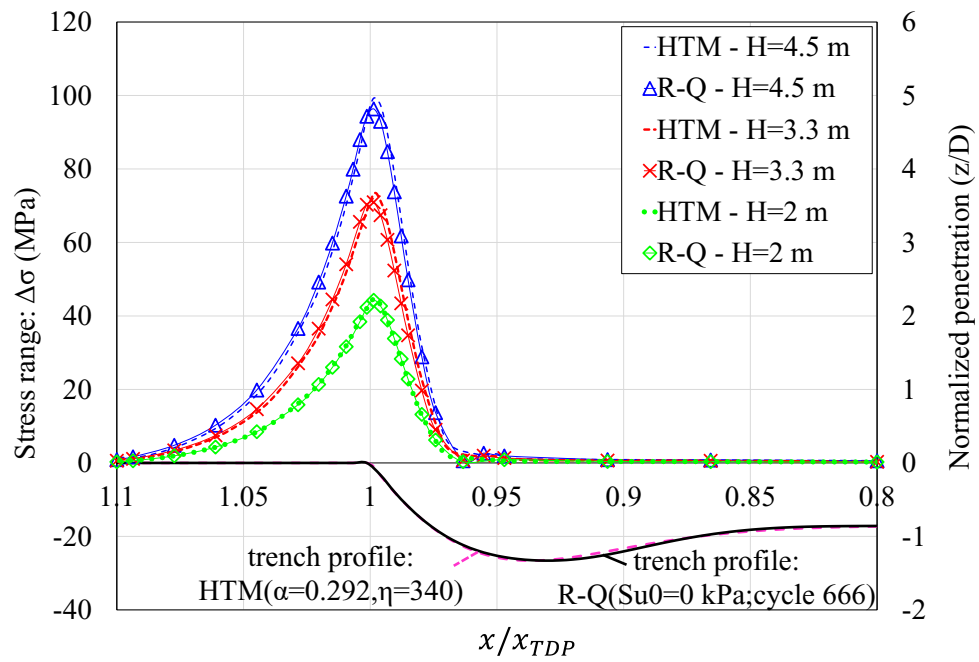


Figure 6-12. Total stress range in TDZ based on the R-Q ( $s_{u0} = 0$  kPa) and HTM ( $\alpha = 0.292$ ,  $\eta = 340$ )

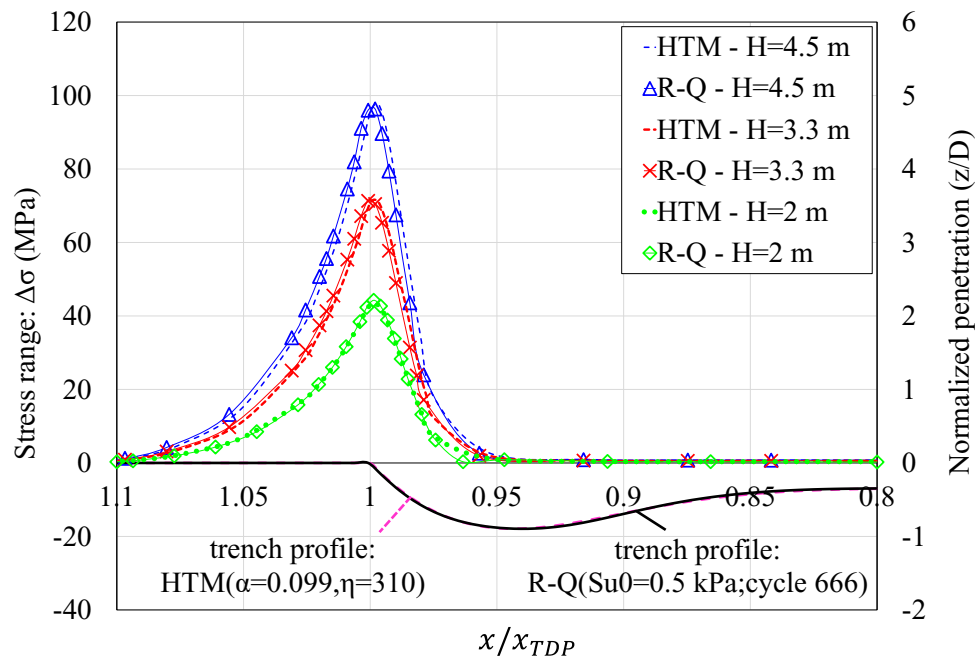


Figure 6-13. Total stress range in TDZ based on the R-Q ( $s_{u0} = 0.5$  kPa) and HTM ( $\alpha = 0.099$ ,  $\eta = 310$ )

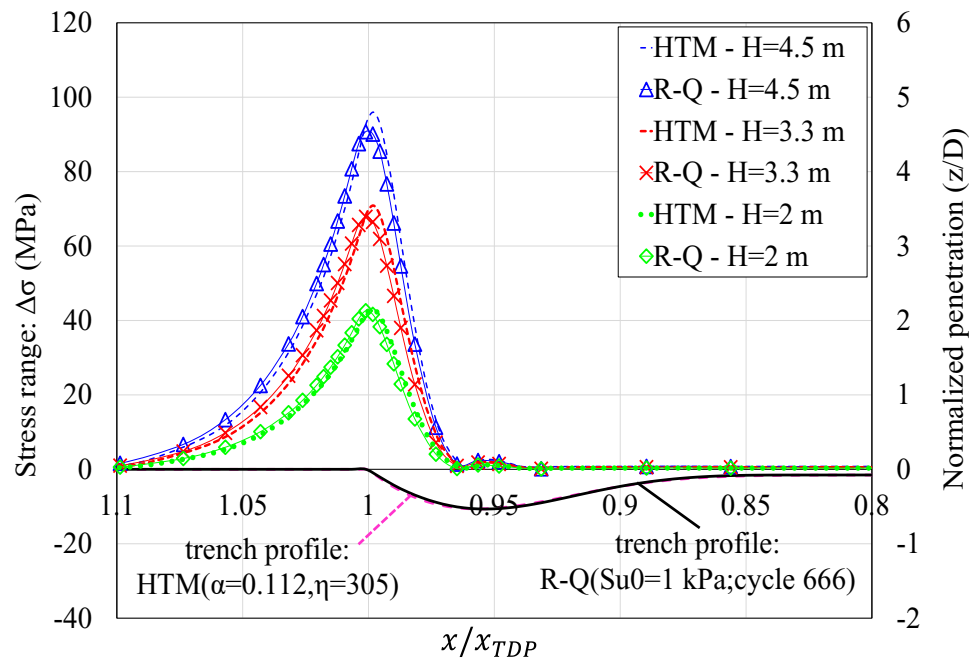


Figure 6-14. Total stress range in TDZ based on the R-Q ( $s_{u0} = 1$  kPa) and HTM ( $\alpha = 0.112$ ,  $\eta = 305$ )

Results of the maximum stress range and its location ( $x_{critical}$ : horizontal coordinate from the critical node to the anchor point) are summarized in Table 6-3.

Table 6-3. Comparison between HTM and the R-Q soil model in the critical point

R-Q				HTM			Relative difference HTM to R-Q (%)		
$s_{u0}$ (kPa)	$\Delta\sigma_{max}$ (MPa)			$\Delta\sigma_{max}$ (MPa)			$\Delta\sigma_{max}$ (MPa)		
	H=2 m	H=3.3 m	H=4.5 m	H=2 m	H=3.3 m	H=4.5 m	H=2 m	H=3.3 m	H=4.5 m
0	44.27	70.96	96.35	44.70	73.16	99.25	0.96	3.10	3.01
0.5	43.50	71.32	96.35	43.34	71.28	97.55	-0.38	-0.06	1.25
1	42.60	67.87	90.75	43.04	70.88	95.96	1.04	4.44	5.75

R-Q				HTM			Relative difference HTM to R-Q (%)		
$s_{u0}$ (kPa)	$x_{critical}$			$x_{critical}$			$x_{critical}$		
	H=2 m	H=3.3 m	H=4.5 m	H=2 m	H=3.3 m	H=4.5 m	H=2 m	H=3.3 m	H=4.5 m
0	-368	-368	-368	-370	-370	-370	0.54	0.54	0.54
0.5	-365	-365	-364	-366	-366	-365	0.27	0.27	0.27
1	-359	-359	-359	-362	-362	-362	0.84	0.84	0.84

It is clear that HTM shows good functionality both in terms of accurate prediction of the critical node with the maximum stress range and the cyclic stress range for the entire length of the riser in TDZ. The analyses confirm that HTM is capable of well predicting the maximum stress ranges with a maximum difference of 5.75% compared with the nonlinear soil model (R-Q). Moreover, the location of the critical node determined from HTM is in good agreement with the corresponding results from R-Q with a coincidence margin of less than 1%.

#### **6.4. Creation of deep trenches by the hybrid model**

As explained earlier, the penetration profiles created by the hysteretic nonlinear riser-soil interaction models (e.g., R-Q model) rapidly deepen and stabilize somewhere between 0.5D and 1D within a few cycles. This stabilization depth is lower than the trench depth ranges reported from the ROV surveys, e.g. 3.5D to 5D (Bridge et al., 2005). Hence, it is worth examining the capability of the HTM to simulate the formation of deep trenches. For this purpose, a higher value of  $\alpha$  with  $\eta = 310$  was assumed ( $\eta = 310$  corresponds to the  $s_{u0} = 0.5$  kPa and  $\rho = 1$  kPa/m) to provide deep trenching with 5D depth. The created trench was compared with the other existing trenches developed by other approaches, including mathematical trench expressions proposed by Langner (2003) and Shiri (2014b) and also automatic development of the trench presented by Shiri and Randolph (2010). Langner (2003), proposed a trench profile based on the circular arc on the SCR side of the trench and a seventh-order polynomial fit to the anchor side of the trench. Shiri (2014b) examined linear and quadratic exponential functions to generate the trench profile with the desired depth (the quadratic exponential expression was used in this study). In the Shiri and

Randolph (2010) method, severe sea state was applied to the vessel by adopting extreme and unreal values for nonlinear soil model parameters ( $\lambda_{rep}, f_{suc}$ ) to artificially push the SCR down the seabed. As shown in Figure 6-15, the trench created by Shiri and Randolph (2010) has a wide longitudinal profile where its trench mouth was highly shifted to the vessel side, and it violates the ratio of the trench's length to depth.

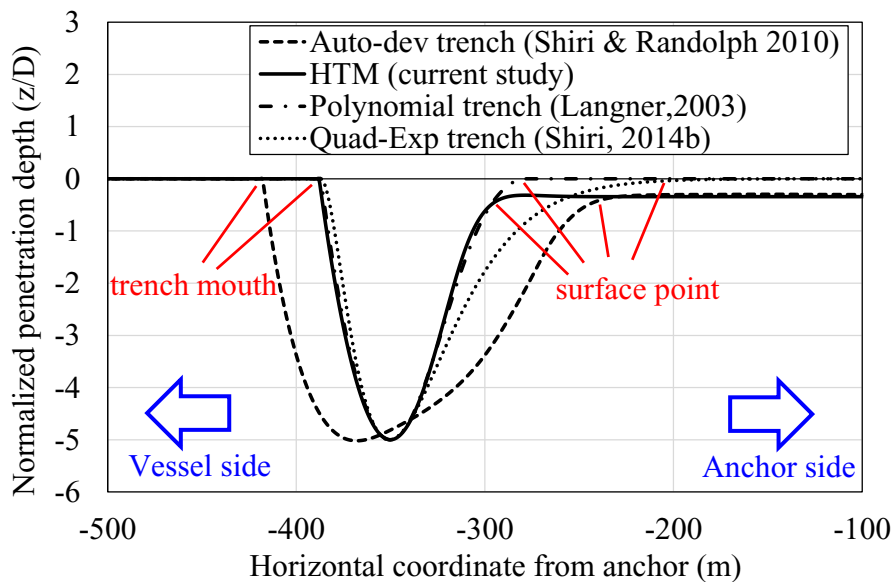


Figure 6-15. Comparison of different trench types

Figure 6-16 shows the results of the riser's contact force in its equilibrium condition based on the four different types of the trenched seabed, including Langner's trench (2003), Shiri's trench (2014b), Shiri and Randolph approach (2010) and HTM. The trenched analyses were considered based on the linear soil stiffness ( $k = 300$  kPa) due to the real range of seabed sediments in the Gulf of Mexico (Randolph et al., 2013) and its conservative predictions. There are some inconsistencies between the riser and seabed in the mathematical trench profiles, which come from the incompatibility of the riser's natural catenary shape with the proposed trench geometry. As shown in Figure 6-16(b) and (c), the



SCR ends up suspended over the deepest part of the trenched seabed, with a significant contact hotspot towards the vessel end of the trench, altering the contact force distribution in TDZ. Alternatively, the trench profile generated by HTM was perfectly consistent with the natural curvature of the SCR in TDZ leading to removing any local contact pressure (see Figure 6-16(a)). The trench proposed by Shiri and Randolph (2010) was compatible with the riser catenary shape as well, but the unusual values of nonlinear soil model parameters (assuming  $f_{suc} = 0.05$ ,  $\lambda_{rep} = 2$ ) have a significant influence on the trench longitudinal geometry where the trench mouth shifted remarkably to the vessel side, and the surface point moved slightly away from the vessel (see Figure 6-16(d)). This significant shifting leads to unreliable results that Dong and Shiri, (2019a) discussed in detail.

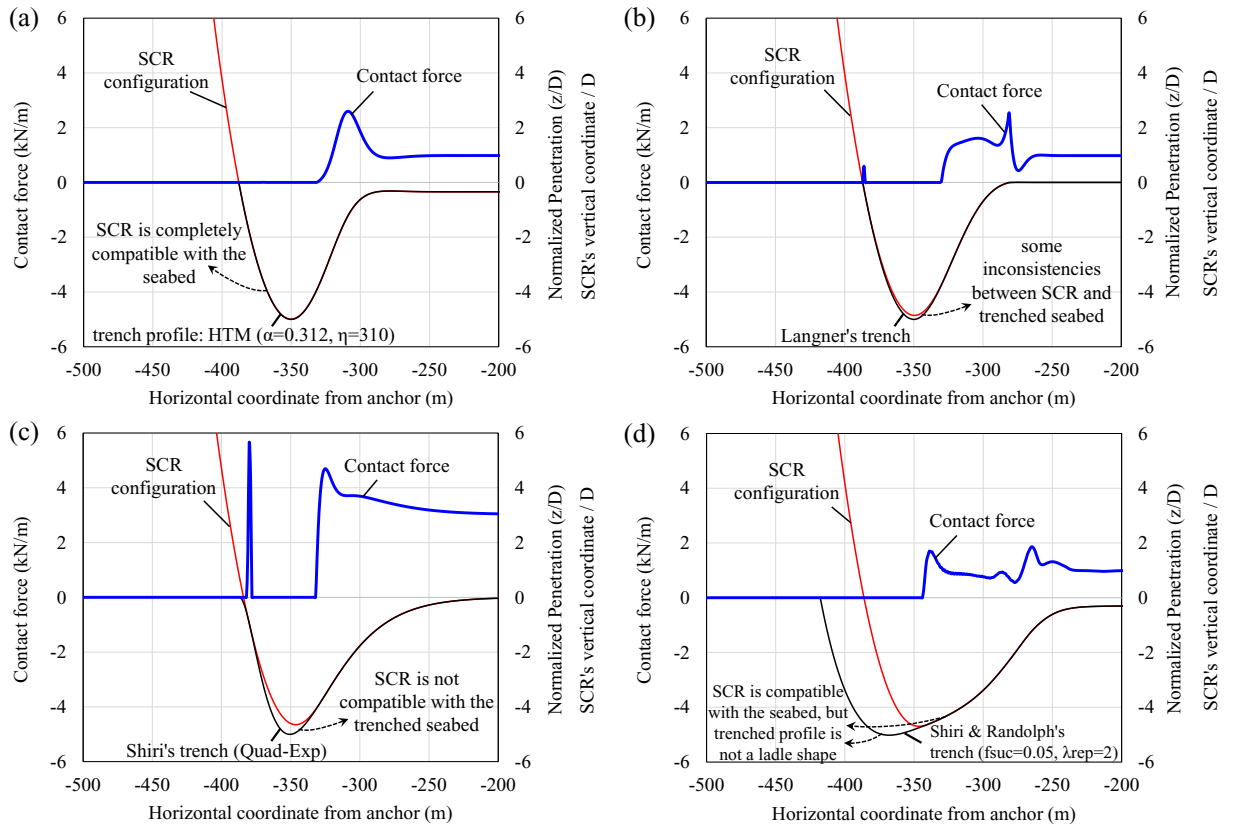


Figure 6-16. Contact force of riser in equilibrium condition, 5D trenched seabed with  $k = 300$  kPa:

- (a) HTM; (b) Langner's trench; (c) Shiri's trench; (d) Shiri and Randolph's trench

Using a single tangential heave amplitude ( $H = 2$  m and  $T = 15$  s), a series of dynamic analyses were conducted on the riser with the different trenched seabed. As seen in Figure 6-17, there are some high contact forces near the TDP in three types of trenches, including HTM, Langner, and Shiri's trench, which comes from the contact of the riser with the trench mouth during the cyclic motions of the riser.

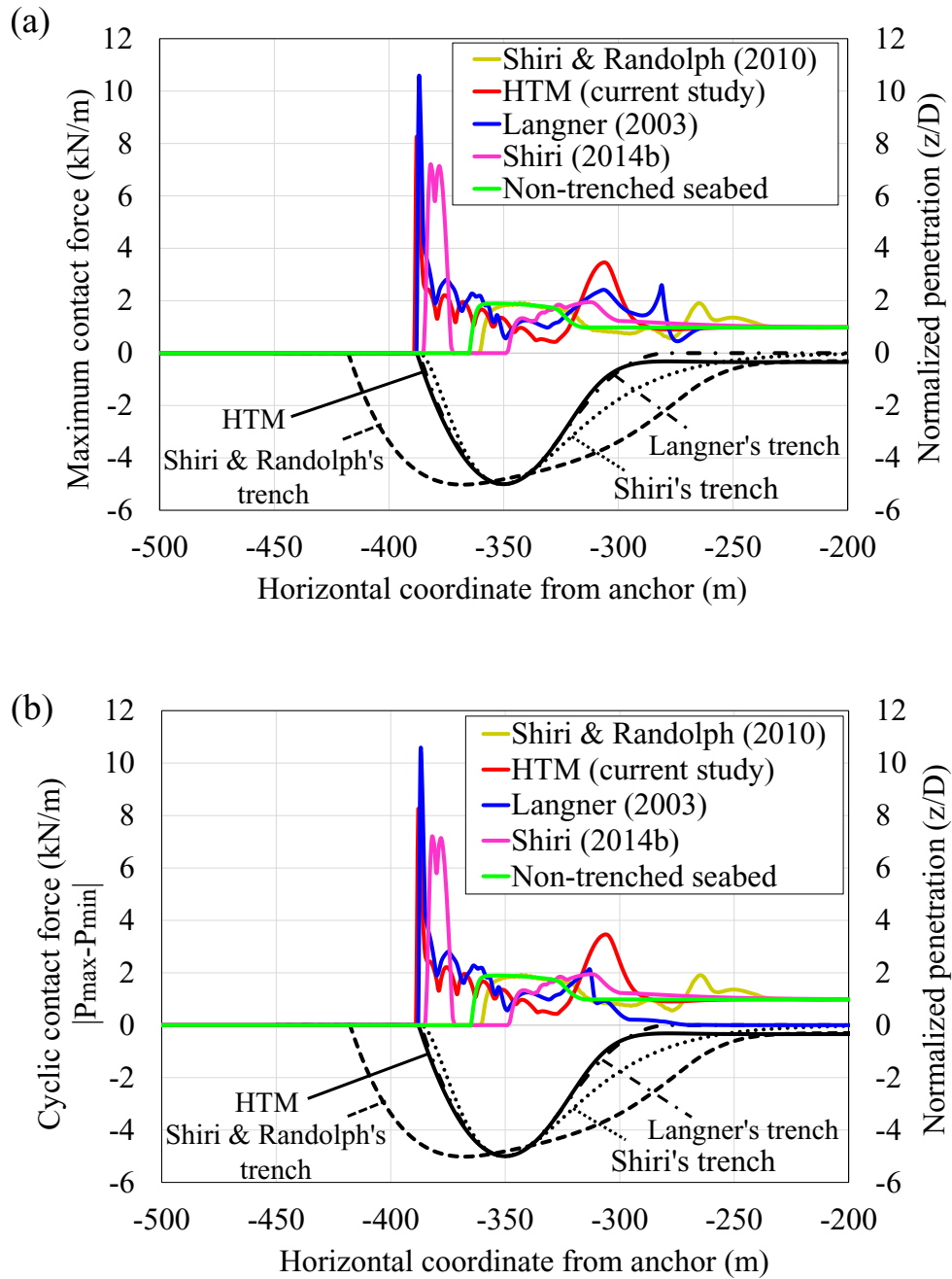


Figure 6-17. Cyclic contact force in TDZ under  $H = 2$  m and  $T = 15$  s: (a) maximum values; (b) cyclic

To better understand the response of the riser around TDP, the snapshots of vertical coordinate and contact force of the riser in the far and near offset were performed based on

the HTM, and Shiri and Randolph's trench. Although the trench profile that the HTM generated was completely compatible with the seabed (as shown in Figure 6-16(a)), the riser inevitably came into contact with the trench mouth due to its large fluctuations in TDZ and consequently leading to the local pressure hotspot (see Figure 6-18(a)). However, SCR's cyclic motions did not come into contact with the leading edge of the trench in the Shiri and Randolph's approach, and there is no local contact pressure (see Figure 6-18(b)).

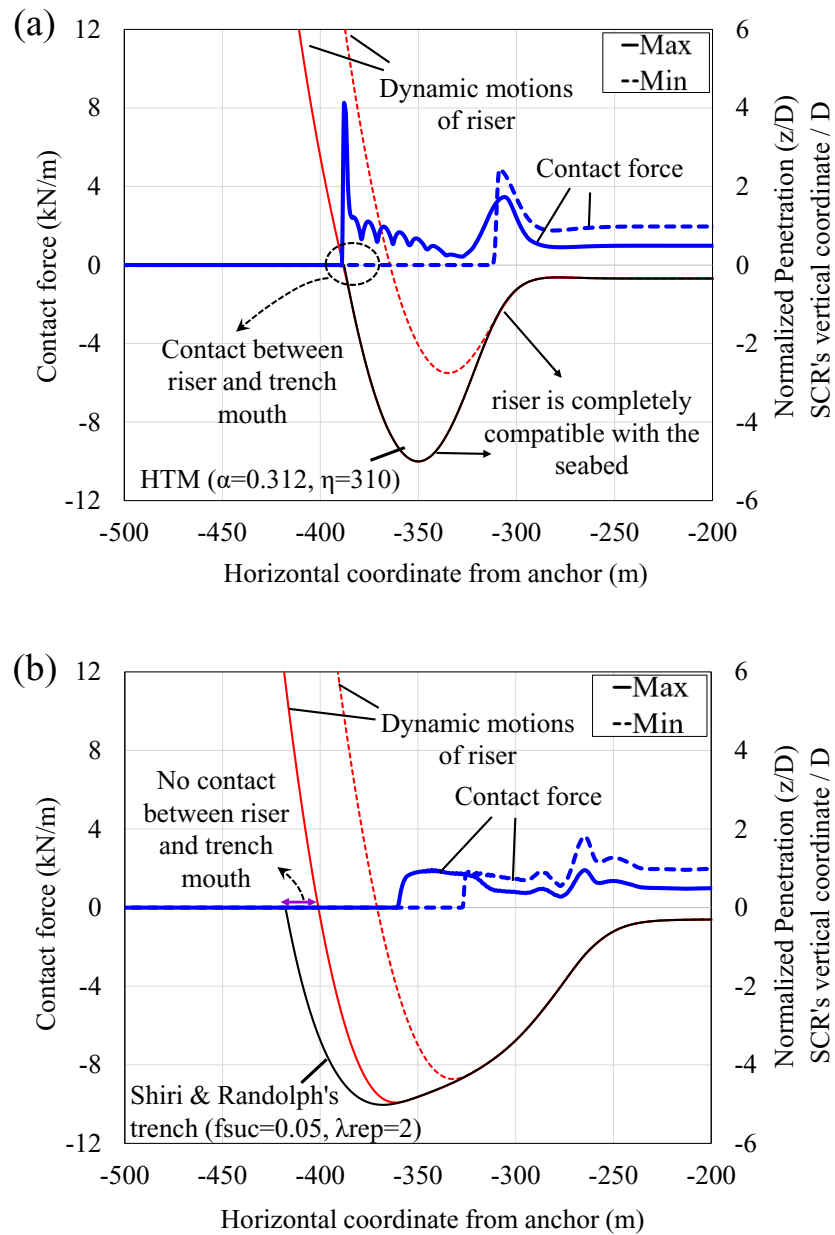


Figure 6-18. Cyclic fluctuations of SCR in TDZ under  $H = 2$  m and  $T = 15$  s by: (a) HTM; (b) Shiri and Randolph's trench

Furthermore, the results of bending moment and total axial stress are presented in Figure 6-19 and Figure 6-20. Results show the peak value of the bending variation or stress range is driven by the response of the riser in the vicinity of the trench edge nearest the vessel.

Depending on the riser perturbations, any local contact with the trench mouth can distort the bending moment variation and, consequently, the stress distributions in TDZ. These results are consistent with the other published works, e.g., Randolph et al. (2013), and Shoghi and Shiri (2020). It is worth mentioning that the results for Shiri and Randolph's trench (2010) are no longer controlled by the leading edge of the trench due to its unusual trench profile, and the riser has not touched the trench mouth during its near or offset position (refer to Figure 6-18(b)).

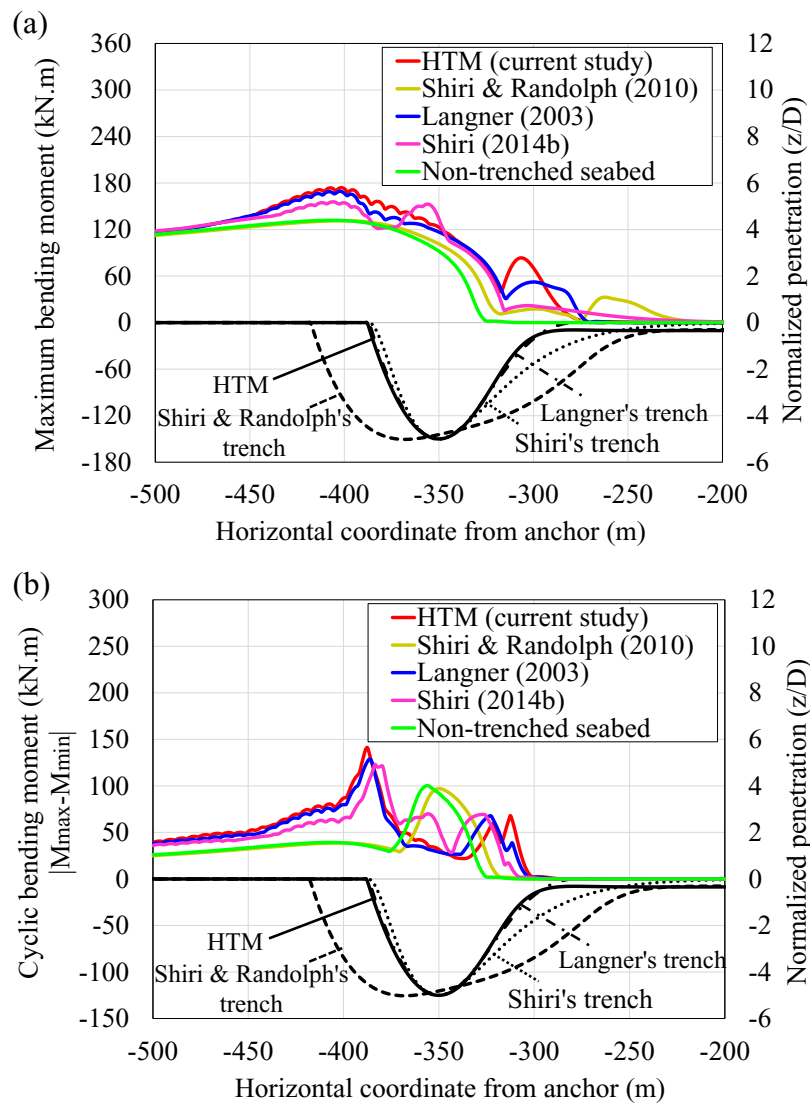


Figure 6-19. Cyclic bending moment in TDZ under  $H = 2$  m and  $T = 15$  s: (a) maximum values;  
 (b) cyclic variations

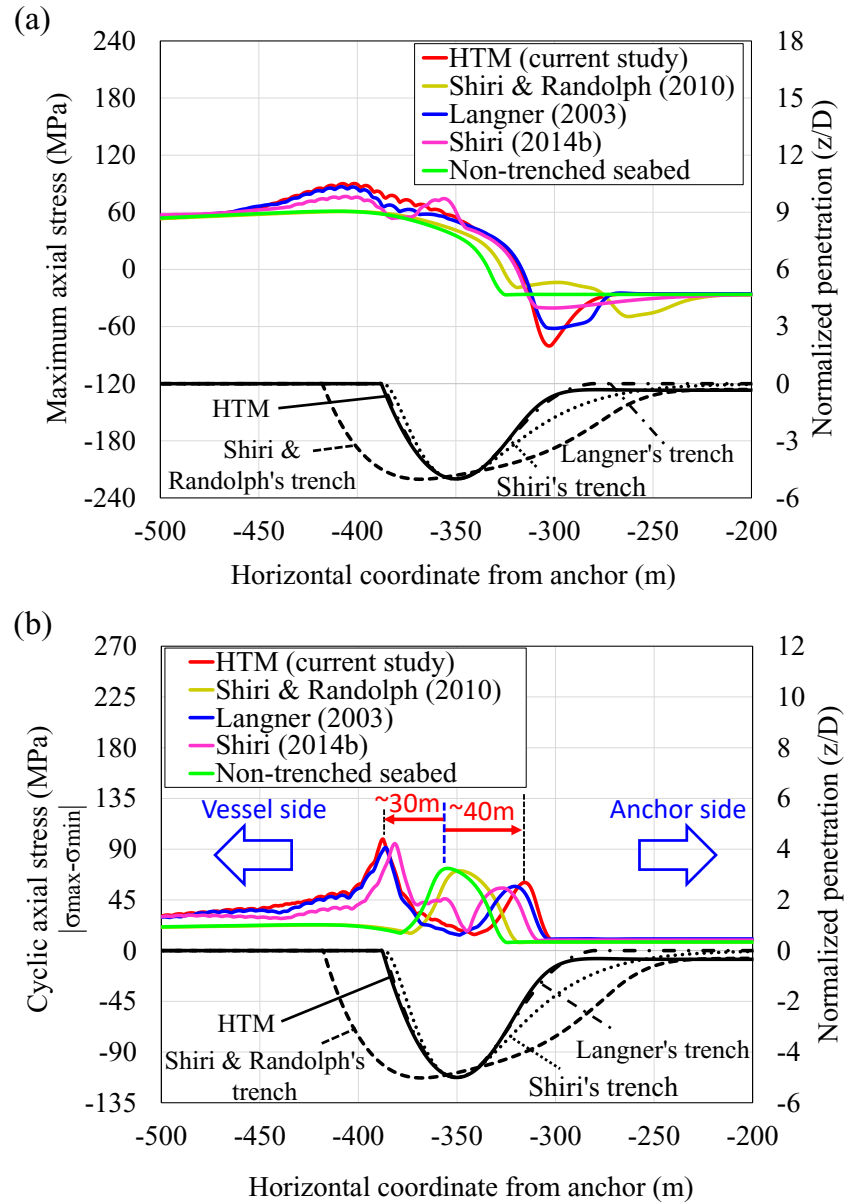


Figure 6-20. Cyclic total axial stress in TDZ under  $H = 2$  m and  $T = 15$  s: (a) maximum values;  
 (b) cyclic variations

Moreover, it was observed that the trenched seabed produced a further shift of a peak stress range towards the anchor side and vessel side with a horizontal offset of 40 m and 30 m to the non-trenched condition (as shown by the red arrows in Figure 6-20(b)). It is interesting to have a closer look at these two peaks in the damage results of the trenched seabed, which will be further assessed in the next section.

### 6.5. Incorporation of the trench into the fatigue analysis

To further explore the effect of the trenched seabed on the fatigue analysis, a series of riser dynamic analyses were conducted on the flat and trenched seabed within six different amplitudes of the tangential heave motions in a range of 0.1 to 1.6 m (see Table 6-4) and considering the linear soil stiffness of 300 kPa.

Table 6-4. Ranges of motions amplitude for fatigue analysis

Tangential heave amplitude (m)	Period (s)
0.1	10
0.3	
0.6	
0.9	15
1.2	
1.6	

The resulting contact force and stress range were plotted in two columns provided in Figure 6-21 and Figure 6-22. A summary of the maximum stress range and its location is superimposed in each subplot. Moreover, the maximum stress range was normalized by the corresponding maximum values in the non-trenched condition and provided in the same plot. Due to the given vessel motions assumed based on the regular waves, the ranges of stress were considered instead of full analysis of fatigue damage.



Results show that the HTM, Langner and Shiri's trench profiles decreased maximum stress range in most of the load cases, including  $H = 0.1, 0.3, 0.6, 0.9$  and  $1.2$  m, even though their contact forces were almost in the higher range compared to the non-trenched condition. This damage reduction was around 20-30% for the lower load cases ( $H = 0.1$  and  $0.3$  m), and it became around 5% for others ( $H = 0.6, 0.9$  and  $1.2$  m). However, there was an increase in the maximum stress range (around 10 to 15%) while motion amplitude was increased to  $H = 1.6$  m.

The analyses confirm that a similar damage distribution is observed in all ranges of motion amplitudes, including two peaks of fatigue damage in both trench edges, the leading edge towards the vessel side and the trailing edge towards the anchor side. It is observed that the left peak is the governing factor in finding the influence of the trench on fatigue performance due to its dominant magnitude. It is susceptible to the potential distortion arising from unexpected contact pressure hotspots at the trench mouth. As explained earlier, HTM uses a smart approach in generating a trench profile that is completely compatible with the natural catenary shape of the riser. However, the trench mouth still causes raising the contact force abruptly, although it is slightly less than the results of mathematical trench insertions.

The results presented in Figure 6-21 and Figure 6-22 show that the trenched seabed is beneficial for fatigue performance in the lower amplitudes of the vessel motions due to the fewer TDP oscillations and, consequently, lower impact of the contact pressure hotspot at the trench mouth. However, the effect of the trench could possibly be detrimental if motion amplitudes become extreme, resulting in abrupt contact hotspots in the trench mouth. These

findings presumably imply why different authors have reported contradictory results for the effect of the trench on fatigue damage.

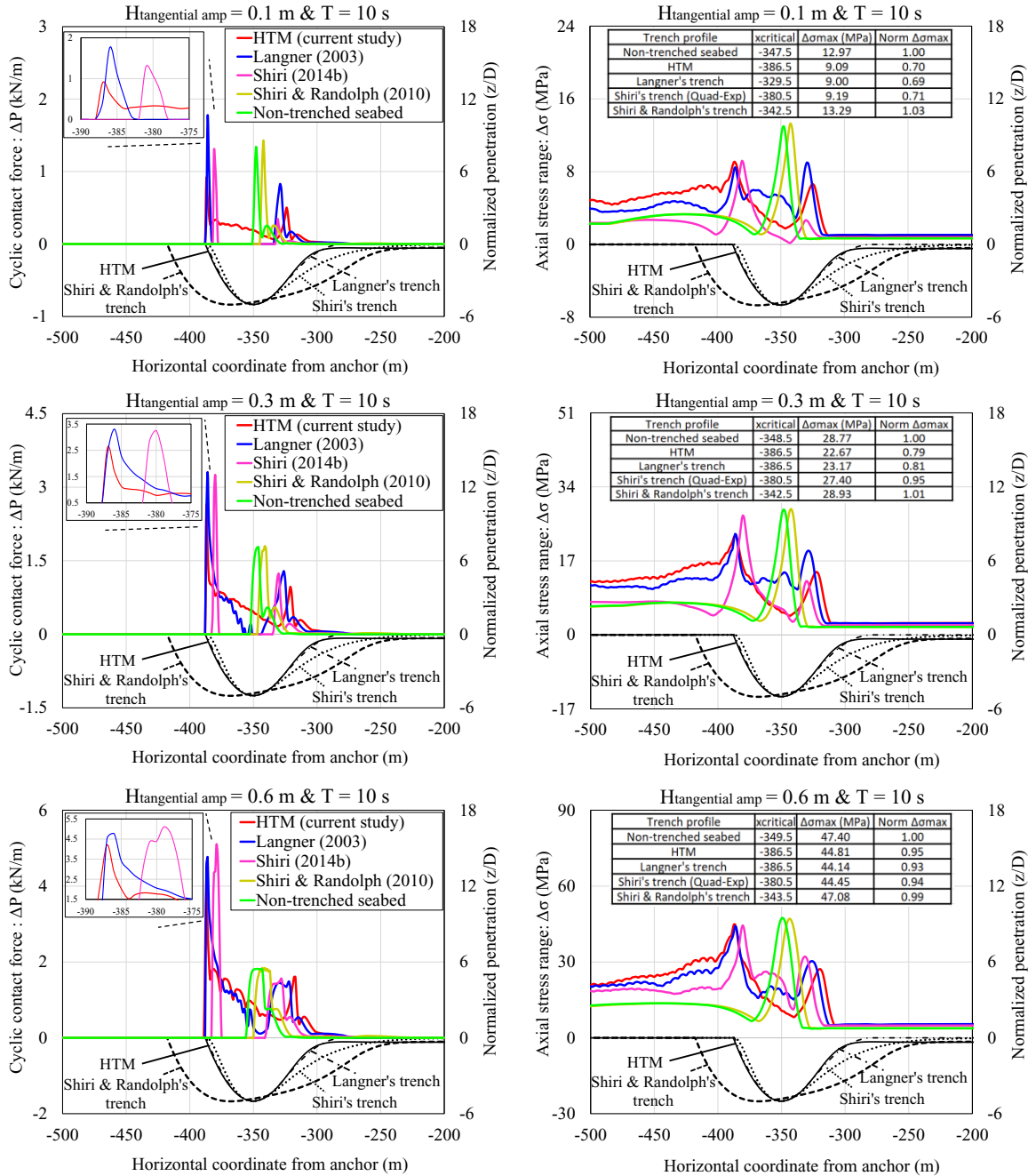


Figure 6-21. Cyclic contact force and axial stress range in TDZ under (H = 0.1, 0.3, 0.6 m & T = 10 s)

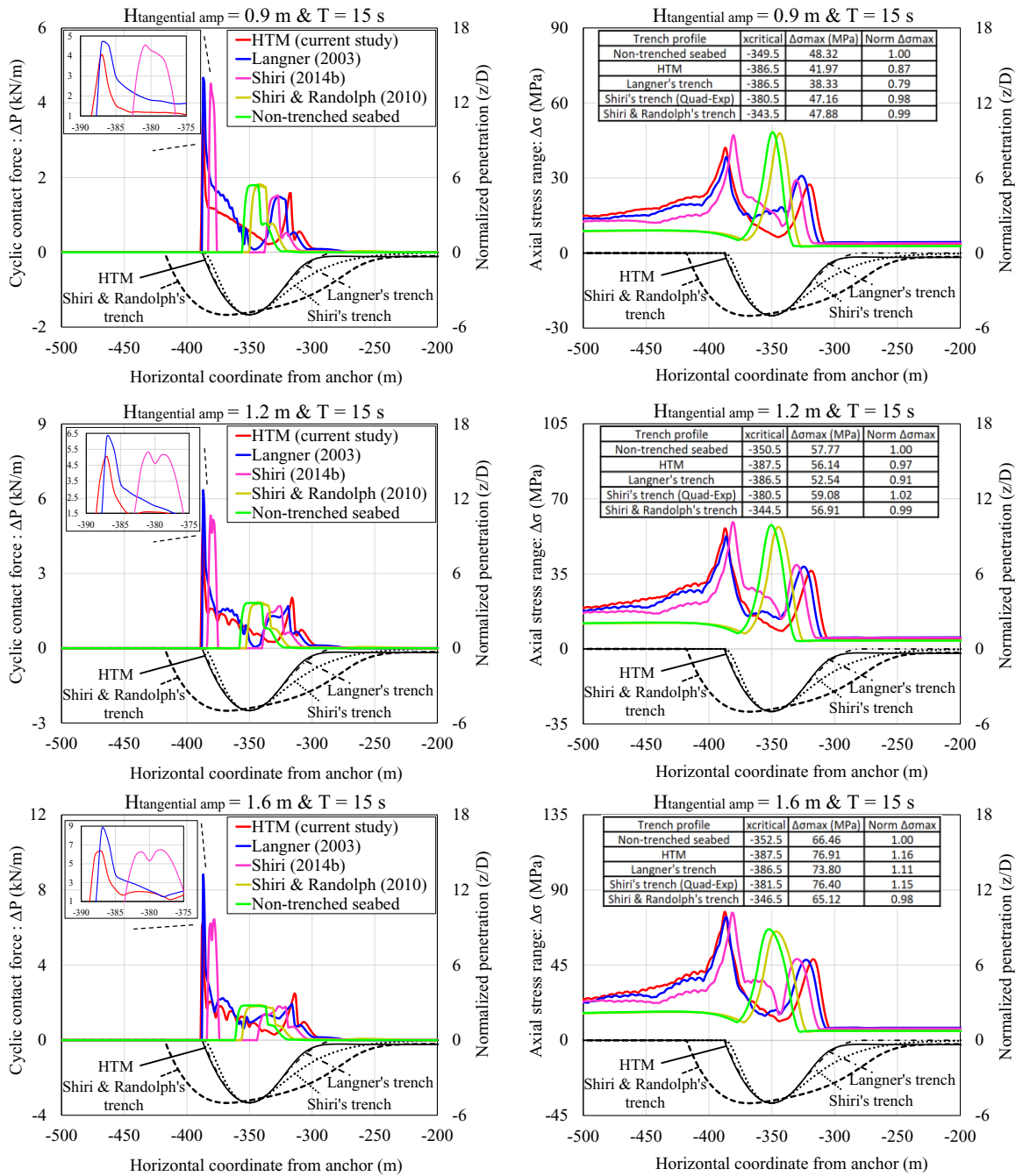


Figure 6-22. Cyclic contact force and axial stress range in TDZ under ( $H = 0.9, 1.2, 1.6$  m &  $T = 15$  s)

Figure 6-21 and Figure 6-22 show that the results of axial stress range have two peaks in trenched conditions. Apparently, the right peak damage is always less than the maximum damage in the non-trenched seabed being independent from the vessel motion amplitudes. It appears that the trench formation has a positive influence on the fatigue life if any contact pressure in the trench mouth is removed. It is worth mentioning that the trenched seabed (HTM, Langner and Shiri's trench) results in a further shift of peak fatigue damage towards the vessel, with a horizontal offset of 30 to 40 m to the maximum damage in the non-trenched condition. This horizontal offset may probably be shifted to the anchor side, approximately around 60 to 70 m (or around 30 m to the right side of the peak damage in the non-trenched case), if the sharp trench mouth is eliminated. These results are in good agreement with the findings of Shoghi and Shiri (2020), who emphasized that the whole distribution of fatigue damage in TDZ should be assessed, not TDP alone.

## **6.6. Conclusion**

As highlighted in the literature, the consistency of the riser natural catenary with the inserted trench profile is an important issue to consider in order to prevent potential contact pressure hot spots in the seabed that may distort damage profiles. Also, the existing nonlinear soil models usually suffer from “numerical premature stabilization” and cannot create deep trenches (e.g., 3.5D to 5D as observed in the field). These are likely the key reasons behind the contradictory results published on the trench effect on SCR fatigue life. The main contribution of this study is developing an alternative methodology to incorporate

the trench effect into the fatigue analysis by resolving the problem of pressure hot spots and premature stabilization. A simplified Hybrid Trench Model (HTM) was developed by defining an equivalent vertical stiffness along the riser nodes contacting with the seabed to achieve the same trench profile obtained from a hysteretic nonlinear riser-seabed interaction model such as the R-Q model. It was demonstrated that the longitudinal trench geometry and gradual trench deepening that the nonlinear soil model created during different cycles could be estimated with the appropriate values of two dimensionless parameters,  $\alpha$  and  $\eta$ , embedded in HTM (see equation (6-1)). The results of the stress range were in good agreement with the R-Q model, with a maximum relative difference of 5.75% in the maximum stress range. Moreover, HTM was able to generate the desired depth of penetration where the trenched seabed was completely consistent with the SCR catenary shape. This automatic trench creation can be an appropriate approach to guarantee the prevention of contact hotspots along the trench profile, particularly inside the ladle shape. However, cyclic oscillations of TDP resulted in contact with the trench edge towards the vessel side, and consequently, pressure hotspots were created at the trench mouth.

Damage analysis of the trenched seabed was conducted under the different tangential vessel motions, and the results showed that a 5D deep trench might decrease or increase the fatigue damage, depending on the magnitude of the contact hotspot at the trench mouth. It appears that by removing this contact pressure at the trench mouth, the maximum fatigue damage is mostly less than the peak damage in the non-trenched seabed, and it is independent of the magnitude of the sea states. In addition, the location of the critical node can be transferred to the anchor side significantly.

Considering the above points, further research work accompanied by real subsea observations is required for predicting the trench mouth shape, which governs the pressure hotspots remarkably created or not during the SCR operation.

### **Acknowledgments**

The authors gratefully acknowledge the financial support of this research by the “Natural Science and Engineering Research Council of Canada (NSERC)” through Discovery program, and the Memorial University of Newfoundland through school of graduate studies funding support.

### **Competing Interests Statement**

The authors declare there are no competing interests.

### **Data Availability Statement**

Data generated or analyzed during this study are provided in full within the published article.

### **Reference**

Aubeny, C., Biscontin, G. (2009). “Seafloor-Riser Interaction Model.” *International Journal of Geomechanics*, 9, 133-141.

Aubeny, C., White, T., Langford, T., Meyer, V. & Clukey, E. (2015). “Seabed stiffness model for steel catenary risers.” In *Frontiers in offshore geotechnics III* (ed. V. Meyer), pp. 351–356.

Bridge, C. (2005) 'Effects of seabed interaction on steel catenary risers', Ph.D. Thesis, University of Surrey.

Bridge, C., Howells, H. (2007) 'Observations and modeling of steel catenary riser trenches', In: The seventeenth international offshore and polar engineering conference, ISOPE 2007, Lisbon, Portugal.

Campbell, M. (1999) 'The Complexities of Fatigue Analysis for Deepwater Risers', New Orleans, USA. Proceedings of the Deepwater Pipeline Technology Conference.

Clukey, E. C., Aubeny, C. P., Randolph, M. F., Sharma, P. P., White, D. J., Sancio, R. & Cerkovnik, M. (2017) 'A Perspective on the state of knowledge regarding soil-pipe interaction for SCR fatigue assessments', Offshore Technology Conference 2017, OTC 27564, Houston, TX, USA.

Clukey, E.C., Ghosh, R., Mokalala, P., Dixon, M. (2007) 'Steel catenary riser (SCR) design issues at touchdown area', Proceedings of The 17<sup>th</sup> International Offshore and Polar Engineering Conference ISOPE-I-07-388, <https://doi.org/10.4043/22557-MS> July 1-6.

Clukey, E.C., Tognarelli, M.A., Li, G., Ghosh, R., Phillips, R., Zakeri, A., Elliot, B.J., Bhattacharyya, A., Sun, Q. (2011) 'Simulation of SCR behaviour at touchdown zone – part II: testing of a sectional SCR model in a geotechnical centrifuge', Offshore Technology Conference 2011, Brazil, 4-6 October.

Dong, X., Shiri, H. (2018) 'Performance of nonlinear seabed interaction models for steel catenary riser', Part I: nodal response. Ocean Eng. 154, 153–166.

Dong, X., Shiri, H. (2019) ‘Performance of nonlinear seabed interaction models for steel catenary riser’, Part II: global response. *Appl. Ocean. Res.* 82, 158-174.

DNV-RP-F204 (2017), Offshore Standard, Riser Fatigue, Det Norske Veritas.

Elliott, B.J., Zakeri, A., Barrett, J., Hawlader, B., Li. G., Clukey, E.C. (2013) ‘Centrifuge modeling of steel catenary risers at touchdown zone Part II: assessment of centrifuge test results using kaolin clay’, *Ocean. Eng.* 60 (March) 208–218.

Giertsen, E., Verley, R., Schröder, K. (2004) ‘CARISIMA: A Catenary Riser/Soil Interaction Model for Global Riser Analysis’, ASME 2004 23rd International Conference on Offshore Mechanics and Arctic Engineering 2004, pp. 633-640.

Hejazi, R., Kimiaei, M. (2016) ‘Equivalent linear soil stiffness in fatigue design of steel catenary risers’, *Ocean. Eng.* 111, 493–507.

Janbazi, H., Shiri, H., 2022. An alternative vessel excitation algorithm to incorporate the trench effect into the fatigue analysis of steel catenary risers in the touchdown zone, *Applied Ocean Research*, 126-103292, <https://doi.org/10.1016/j.apor.2022.103292>.

Kimiaei, M., Randolph, M., Ting, I. (2010) ‘A parametric study on effects of environmental loadings on fatigue life of steel catenary risers (using a nonlinear cyclic riser–soil interaction model)’, In: *Proceedings of the 29th International Conference on Ocean, Offshore and Arctic Engineering*, Shanghai, China, Paper OMAE2010-21153.

Langner, C. (2003) ‘Fatigue life improvement of steel catenary risers due to self-trenching at the touchdown point’, *Proceedings of the Offshore Technology Conference*, OTC 15104, May 5-8.



Leira, B.J., Passano, E., Karunakaran, D., Farnes, K.A., Giertsen, E. (2004) ‘Analysis guidelines and application of a riser–soil interaction model including trench effects’, Proceedings of the 23<sup>rd</sup> International Conference on Offshore Mechanics and Arctic Engineering OMAE 2004-51527, 955–962, June 20-25.

Li, F.Z., Low, Y.M. (2012) ‘Fatigue reliability analysis of a steel catenary riser at the touchdown point incorporating soil model uncertainties’. Appl. Ocean Res. 38, 100–110.

Nakhaee, A., Zhang, J. (2008) ‘Effects of the interaction with the seafloor on the fatigue life of a SCR’, Proceedings of the 18th International Society of Offshore and Polar Engineers Conference ISOPE-I-08-397 2008, July 6-11.

Orcina (2010), OrcaFlex User Manual 10.3. UK. <[www.orcina.com](http://www.orcina.com)>.

Randolph, M.F., Bhat, S., Mekha, B. (2013) ‘Modeling the touchdown zone trench and its impact on SCR fatigue life’, Proceedings of the Offshore Technology Conference 2013, OTC-23975-MS, <https://doi.org/10.4043/23975-MS> May 6-9.

Randolph, M.F., Quiggin, P. (2009) ‘Nonlinear hysteretic seabed model for catenary pipeline contact’, In: Proceedings of the 28th International Conference on Ocean, Offshore and Arctic Engineering. Honolulu, Hawaii, USA.

Randolph, M.F., White, D. (2008) ‘Pipeline embedment in deep water: processes and quantitative assessment’, Offshore Technology Conference 2008, Houston, Texas, USA, 5-8 May.

Rezazadeh, K., Shiri, H., Zhang, L., Bai, Y. (2012) 'Fatigue generation mechanism in touchdown area of steel catenary risers in nonlinear hysteretic seabed', Res. J. Appl. Sci. Eng. Technol. 4 (24), 5591–5601.

Sharma, P.P., Aubeny, C.P. (2011) 'Advances in pipe-soil interaction methodology and application for SCR fatigue design', Proceedings of the Offshore Technology Conference OTC-21179-MS.

Shiri, H. (2014a) 'Response of steel catenary risers on hysteretic nonlinear seabed', Appl. Ocean. Res. 44 (January), 20–28.

Shiri, H. (2014b) 'Influence of seabed trench formation on fatigue performance of steel catenary risers in touchdown zone', Marine Structure. 36 (April), 1–20.

Shiri, H., Randolph, M. (2010) 'The influence of seabed response on fatigue performance of steel catenary risers in touchdown zone', In: Proceedings of the 29<sup>th</sup> international conference on offshore mechanics and arctic engineering, OMAE 2010, Shanghai, China 2010, p. 20051.

Shoghi, R., Shiri, H. (2019) 'Modeling touchdown point oscillation and its relationship with fatigue response of steel catenary risers', Appl. Ocean. Res. 87, 142-154.

Shoghi, R., Shiri, H. (2020) 'Re-assessment of trench effect on fatigue performance of steel catenary risers in the touchdown zone', Appl. Ocean Res. 94, 1–16.

Shoghi, R., Pesce, C. P., Shiri, H. (2021) 'Influence of trench geometry on fatigue response of steel catenary risers by using a boundary layer solution on a sloped seabed', Ocean Eng. 221, 108447.

Thethi, R., Moros, T. (2001) 'Soil interaction effects on simple catenary riser response', Deepwater Pipeline and Riser Technology Conference, Houston, Texas, USA.

Wang, K., Low, Y.M. (2016). "Study of seabed trench induced by steel catenary riser and seabed interaction." Proceedings of the 35th International Conference on Ocean, Offshore and Arctic Engineering OMAE 2016-54236.

Zargar, E. (2017). "New hysteretic seabed model for riser-soil interaction." PhD Thesis, University of Western Australia.

Zargar, E., Kimiaei, M., Randolph, M.F. (2019) 'A new hysteretic seabed model for riser-soil interaction', Marine Structures, 64, 360-378.

## CHAPTER 7

# Investigation of trench effect on fatigue response of steel catenary risers using an effective stress analysis

Hossein Janbazi<sup>1</sup>, Hodjat Shiri<sup>2</sup>

1: Department of Civil Engineering  
Memorial University of Newfoundland  
e-mail: [hjanbaziokn@mun.ca](mailto:hjanbaziokn@mun.ca)

2: Department of Civil Engineering  
Memorial University of Newfoundland  
e-mail: [hshiri@mun.ca](mailto:hshiri@mun.ca)

This chapter was published in *Computer and Geotechnics* .

<https://doi.org/10.1016/j.compgeo.2023.105506>

## **Abstract**

The design of Steel Catenary Risers (SCR) heavily relies on the interaction between the riser and seabed in the touchdown zone (TDZ). To accurately estimate the SCR-seabed stiffness, the soil behaviour must be assessed in two main phases: (1) during cyclic SCR motions, which generate excess pore pressure, leading to soil softening and remoulding in the TDZ, and (2) during inactivity periods throughout the SCR's lifespan, causing dissipation of excess pore pressure associated with the consolidation state. The latter was neglected by the existing non-linear hysteretic soil models, which are based on the total stress approach. In the current study, a global riser analysis was conducted and the consolidation effect was incorporated using an effective stress framework. Long-term soil stiffness was determined by capturing both the remoulding and consolidation effects, which are respectively associated with the damage accumulation during the SCR cyclic motions and soil strength recovery during the intervening pause period. The constructed model was then combined with a new methodology named Hybrid Trench Model to investigate how the consolidation effect contributes to the fatigue performance in different trench depths. Stochastic fatigue analysis showed that the consolidation effect might increase the damage by around 10%-40% over the long-term assessment.

**Keywords:** Steel catenary riser, effective stress framework, consolidation, soil stiffness, trench effect, fatigue analysis

## 7.1. Introduction

Steel Catenary Risers (SCRs) have been extensively used in offshore fields to transport hydrocarbon products between the platform and the seabed. Throughout their operational lifespan, SCRs are subjected to some level of cyclic loading, which can originate from the sources in the environment, such as waves and currents or from the motion of the host vessel during its operation. This cyclic loading leads to fatigue damage accumulation and affects the overall design of SCRs, especially in the touchdown zone (TDZ) where the riser comes into contact with the seabed on a continuous basis (Bridge, 2005; Clukey et al., 2011; Sharma and Aubeny, 2011; Clukey et al., 2017a; Dong and Shiri, 2019). The cyclic motions of a catenary riser often induce undrained shearing of the surrounding soil, resulting in the progressive buildup of excess pore water pressure. This, in turn, reduces the effective stress of the seabed soil, leading to progressive degradation over time (Hodder et al., 2008; Hodder et al., 2010; Aubeny et al., 2015; Yuan et al., 2017; Clukey and Zakeri, 2017). Over the early years of riser operation, the embedment of the riser gradually increases, eventually resulting in the formation of a trench with a maximum depth of approximately  $2.5D$  to  $5D$  (where  $D$  is the pipe diameter) (Thethi and Moros, 2001; Bridge and Howells, 2007), which is believed to have a significant impact on the fatigue performance of SCR (Shoghi and Shiri, 2019, 2020). A number of published papers have extensively investigated the impact of the trench effect on fatigue using two main methods. Some researchers have opted for an artificial insertion of the trench profile with the use of mathematical expressions (Langner, 2003; Li and Low, 2012; Randolph et al., 2013; Shiri, 2014b; Wang et al., 2016). This approach generally leads to inconsistencies between the natural catenary shape of the

riser and seabed, in which can create contact hot spots and distort the fatigue results in the TDZ. Automatic development of the trench using non-linear soil models was another approach that was developed to overcome the geometrical inconsistencies. This approach results in a consistent penetration that is completely compatible with the catenary shape of the riser (Nakhaei and Zhang, 2008; Shiri and Randolph, 2010, Shiri 2014a), but it is prematurely stabilized within a few cycles (e.g., Hejazi and Kimiaei, 2016; Dong and Shiri, 2018), somewhere between 0.5D to 1D penetration, which is much less than the ranges of trenches observed by remote operating vehicles (ROVs) (Bridge and Howells, 2007). A new methodology called “Hybrid Trench Model” (HTM) was introduced in the current study by using an equivalent soil stiffness to generate the compatible trench formation in the TDZ (Janbazi and Shiri, 2023). The study showed that the proposed trench profile is consistent with the riser catenary shape to resolve pressure hot spots and the premature stabilization problems repeatedly reported in the literature.

It is worth noting that the riser-seabed interaction model that has been used so far is mainly based on the total stress approach, which accounts for soil strength degradation under undrained conditions (Randolph and Quiggin, 2009; Aubeny et al., 2015; Clukey and Zakeri, 2017; Zargar et al., 2019). However, over a long period of time, soil undergoes a drainage condition during periods of calm weather or inactivity of SCR, which allows the gradual dissipation of pore water pressure through the seabed (Hodder et al., 2009; Chatterjee et al., 2013; Clukey and Zakeri, 2017; Yuan et al., 2017; Hou et al., 2018; Zhou et al., 2020). This consolidation process results in a regain of soil stiffness or strength (Hodder et al., 2013; Zhou et al., 2019; Al-Janabi et al., 2019; Al-Janabi and Aubeny,

2019), which is not captured by the existing advanced non-linear soil models with hysteretic load-displacement behaviour. This overlooked consolidation effect on soil strength may result in underestimating fatigue damage in design practice. Therefore, developing a reliable methodology to incorporate the trench effect into the fatigue analysis while considering the consolidation effect is still a knowledge gap that requires further investigation.

Over the past fifteen years, several studies have focused on an analytical effective stress framework based on the critical state model within interpreting the void ratio – effective stress path for a one-dimensional soil horizon (White & Hodder, 2010; Hodder et al., 2013; Zhou et al., 2019 and 2020). The framework’s applicability for vertical T-bar penetrometer displacements was first highlighted by White and Hodder, in 2010, which included three episodes of cyclic undrained loading of a T-bar, during the intervening pause periods between the episodes to consider both remoulding and reconsolidation effects. Due to the continuous– rather than episodic– nature of actual loadings, more investigations were conducted later with the same concept of the critical state model (Zhou et al., 2020). Compared with the centrifuge tests, the effective stress framework showed good functionality in terms of both soil degradation and reconsolidation. However, the literature has some limitations, such as addressing the shortened section of a sample pipe/SCR and not generalizing this framework for the global numerical analysis. The current study integrates an effective stress framework into the numerical model of SCR-seabed interaction through a coded UEL subroutine of ABAQUS to calculate the long-term vertical effective stress and soil resistance during SCR cyclic motions. Performing stochastic



fatigue analysis showed that the damage results could be more than twice within incorporation of consolidation effect in the presence of trenched seabed. The current numerical simulation aims to establish a new riser-seabed interaction model, which can accurately capture the behaviour of a full-scale SCR throughout its entire life history.

It is worth mentioning that cyclic soil remoulding and consolidation are not the sole mechanisms responsible for riser embedment. Other mechanisms may also increase the riser embedment by scraping the seabed soil such as seabed erosion due to combined vortices generated by subsea currents and seawater entrapped between the oscillating riser and the trench. Despite the limited number of studies on these mechanisms in the literature, they still need deeper investigation for better understanding and modelling of the riser-seabed-seawater interaction.

## **7.2. Effective stress framework**

An effective stress framework relies on the critical state soil mechanics, which can represent the soil softening during undrained shearing associated with excess pore pressure generation and the regaining of soil strength associated with the excess pore pressure dissipation. Figure 7-1 illustrates the effective stress path of a soil element assumed to be intact on a normal compression line (NCL), represented by point A. The cyclic motion of a riser was idealized as episodic, including three episodes of undrained loading within no-motion events between two consecutive episodes representing the intervening pause periods. The equations of the effective stress framework have been developed for the normalized form of pipe diameter. Therefore, it can be used both for T-bar penetrometer

(White and Hodder, 2010), and a riser pipe (Zhou et al., 2020) independent of the diameter size.

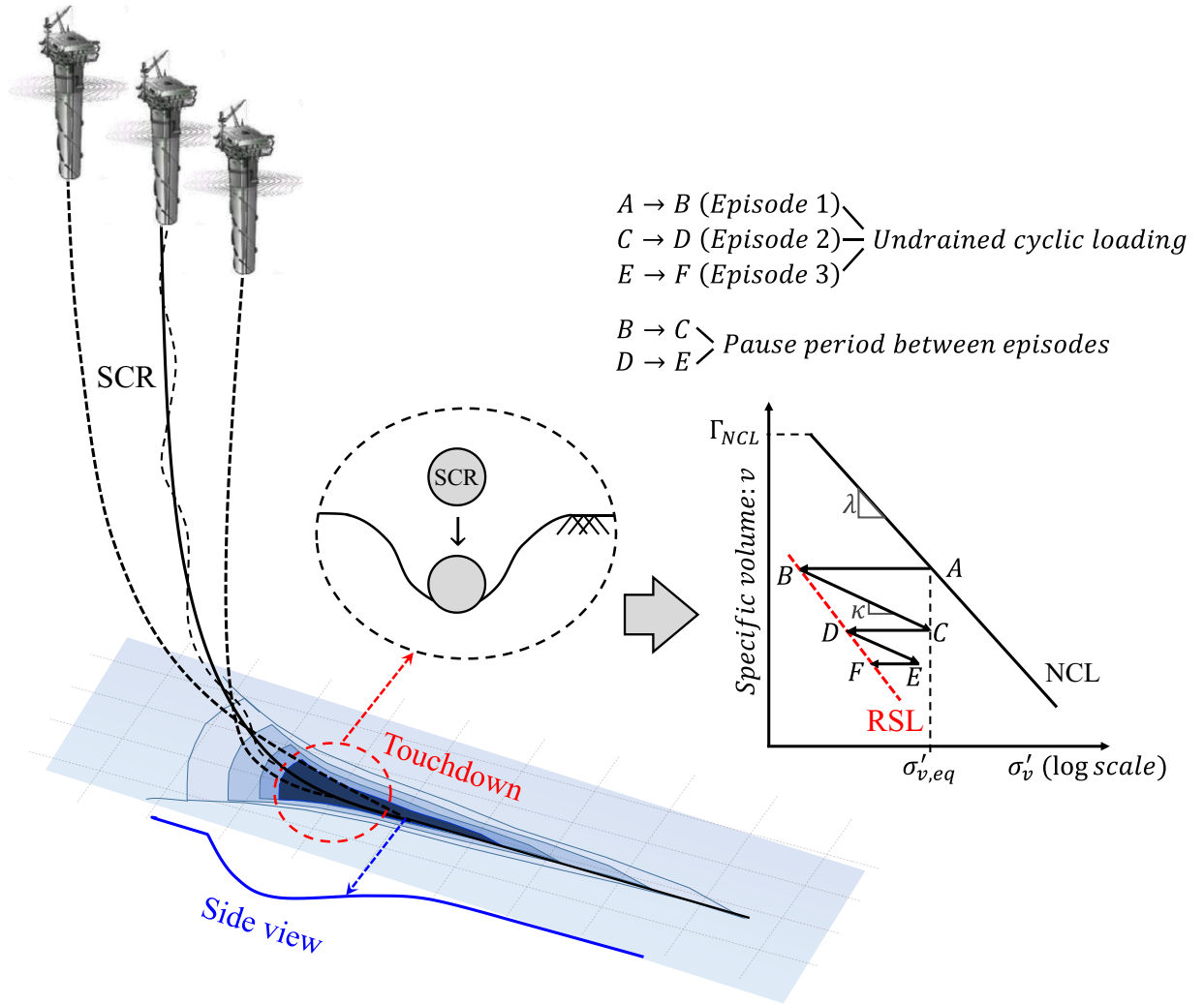


Figure 7-1. Definition of the effective stress framework associated with the remoulding and reconsolidation

The number of cycles,  $N(\hat{z})$ , is used to quantify the soil disturbance or remoulding process. It increases progressively as the pipe passes through the specific soil horizon, accumulated by  $N = 0.5$  during a one-half cycle (based on Einav & Randolph, 2005). The incremental cumulative damage is provided by equation (7-1).

$$\delta N(\hat{z}) = 0.5\mu(\hat{z})\delta\hat{z}_m \quad (7-1)$$

where  $\delta\hat{z}_m$  is the incremental embedment of the pipe.

The parameter  $\mu(\hat{z})$  represents an influence damage zone in which damage accumulates due to the passage of the pipe through the boundaries extending a normalized distance,  $\beta$ , above and below the mid-depth of the cylinder. Equation (7-2) provides a triangular expression for the influence damage zone. The parameter  $\beta$  is a non-dimensional value that defines the extent of the cycle number influence zone.

$$\mu(\hat{z}) = \frac{1}{\beta} \left( 1 - \frac{|\hat{\eta}|}{\beta} \right) \quad (7-2)$$

where  $\hat{\eta}$  is the current vertical location of the given soil horizon relative to the center of the pipe, normalized by the diameter as provided in equation (7-3).

$$\hat{\eta} = \hat{z} - \hat{z}_m \quad \text{where} \quad \hat{z} = \frac{z}{D} ; \hat{z}_m = \frac{z_m}{D} \quad (7-3)$$

where  $z$  is the given soil horizon, and  $z_m$  is the current embedment of the pipe.

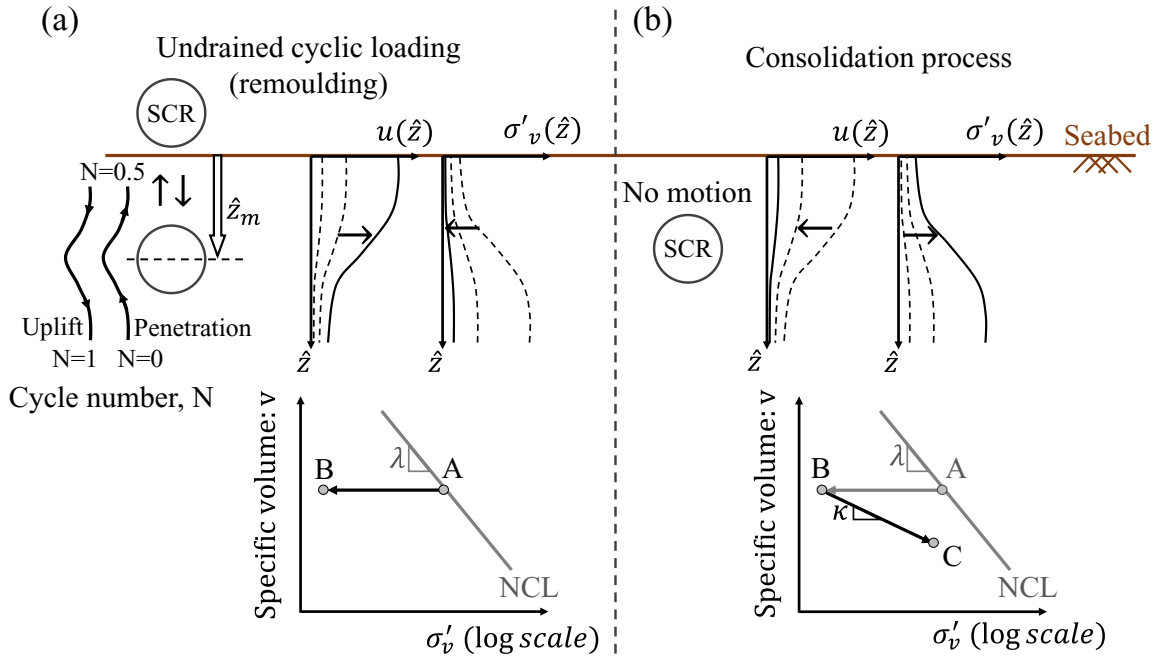


Figure 7-2: Cycle number definition with schematic variations of effective stress and excess pore pressure during (a) remoulding and (b) consolidation process

Cyclic undrained loading causes a reduction in effective stress associated with the accumulation of excess pore pressure generation, path  $A-B$  in Figure 7-2(a). The rate of excess pore pressure generation is represented by two components,  $u_1$  and  $u_2$  (where  $u = u_1 + u_2$ ), as provided in equation (7-4) (Hodder et al., 2013).

$$\frac{\Delta \hat{u}_1(\hat{z})}{\Delta N(\hat{z})} = \frac{3}{N_{95,u_1}} [a_u u_{max}(\hat{z}) - u_1(\hat{z})] \quad (7-4)$$

$$\frac{\Delta \hat{u}_2(\hat{z})}{\Delta N(\hat{z})} = \frac{3}{N_{95,u_2}} [(1 - a_u) u_{max}(\hat{z}) - u_2(\hat{z})]$$

where  $N_{95,u_1}$ , and  $N_{95,u_2}$  are the number of cycles to generate excess pore pressure within 95% of the maximum value, and  $a_u$  is a coefficient used to integrate the components of  $u_1$  and  $u_2$ .

Using the initial and remoulded states of the soil as the boundary conditions, equation (7-4) can be expressed in the form of equation (7-5).

$$u(\hat{z}) = u_{max}(\hat{z}) \left( 1 - a_u e^{-\frac{3N(\hat{z})}{N_{95,u1}}} - (1 - a_u) e^{-\frac{3N(\hat{z})}{N_{95,u2}}} \right) \quad (7-5)$$

where  $u_{max}(\hat{z})$  is the maximum excess pore pressure calculated by equation (7-6).

$$u_{max}(\hat{z}) = \sigma'_{v0}(\hat{z}) - \sigma'_{v,RSL}(\hat{z}) \quad (7-6)$$

Further soil disturbance causes the effective stress to move towards a fully remoulded value at a constant specific volume,  $\sigma'_{v,RSL}(\hat{z})$ , pointing  $D$  at the remoulded state line ( $RSL$ ), as shown earlier in Figure 3-2.

$$\sigma'_{v,RSL}(\hat{z}) = \left[ \frac{s_u}{\sigma'_{v0}} \right]_{NC} \frac{\sigma'_{v0}(\hat{z})}{\Phi S_{t,cycle}} \times \exp \left[ \frac{\Lambda \{ \Gamma_{NCL} - v_{initial}(\hat{z}) - \lambda \ln[\sigma'_{v0}(\hat{z})] \}}{\lambda - \kappa} \right] \quad (7-7)$$

where  $\Gamma_{NCL}$  is the specific volume at  $\sigma'_v = 1 \text{ kPa}$ , and  $\lambda$  and  $\kappa$  are the gradients of the compression and swelling lines, respectively.  $\left[ \frac{s_u}{\sigma'_{v0}} \right]_{NC}$  is the normally consolidated undrained strength ratio,  $S_{t,cycle}$  is the soil sensitivity, and  $\sigma'_{v0}(\hat{z})$  is the in-situ vertical effective stress. The parameter  $\Lambda$  is the plastic volumetric strain ratio, which is the ratio of the plastic component to the total component of the volumetric strain increment in normal consolidation (Schofield and Wroth, 1968).  $\Phi$  is the lumped strength parameter, which links the current vertical effective stress to the undrained shear strength. According to equation (7-7), the remoulded effective stress can be changed by adopting different values for  $\Phi$ , leading to an adjustment in  $RSL$  as highlighted in  $\log \sigma'_v - v$  space (see Figure 7-1). The following expression can be used for predicting  $\Phi$  which is decayed from peak value

$k_\phi \Phi_{steady}$  to  $\Phi_{steady}$  with a simple exponential expression, as provided in equation (7-8) (Hodder et al., 2013).

$$\Phi(\hat{z}) = k_\phi(\hat{z})\Phi_{steady} - [k_\phi(\hat{z}) - 1](1 - e^{-3N(\hat{z})/N_{95,\phi}})\Phi_{steady} \quad (7-8)$$

where  $N_{95,\phi}$  is the number of cycles required to cause a 95% drop from  $k_\phi \Phi_{steady}$  to  $\Phi_{steady}$  (since  $e^{-3} \approx 0.05$ ) (Einav & Randolph, 2005). The parameter  $k_\phi$  is related to the *OCR* and is calculated using equation (7-9).

$$k_\phi(\hat{z}) = OCR(\hat{z})^b \quad (7-9)$$

where “ $b$ ” is a peak strength parameter.

It is worth noting that the value of  $\Phi_{steady}$  can be selected using the measured data obtained from experimental tests. An appropriate value of  $\Phi_{steady} = 0.6$  was back-calculated by Hodder et al. (2013) through the fitting of three parameters, including soil sensitivity, swelling line slope, and remoulded undrained strength with the T-bar model tests.

As illustrated in Figure 7-2(b), the excess pore pressure dissipation at any soil horizon leads to the regaining of effective stress at a lower specific volume (path *B* to *C*). The specific volume reduction can be quantified by the effective stress variations equaling the pore pressure dissipation, denoted as  $\Delta\sigma'_v(\hat{z}) = -\Delta u_e(\hat{z})$ , as given in equation (7-10).

$$\Delta v(\hat{z}) = -\kappa \ln \left[ \frac{\sigma'_v(\hat{z}) + \Delta\sigma'_v(\hat{z})}{\sigma'_v(\hat{z})} \right] \quad (7-10)$$

where  $\sigma'_v$  is the vertical effective stress after each increment of undrained loading,  $\Delta\sigma'_v$  is the increase in effective stress from pore pressure dissipation, and  $\kappa$  is the gradient of the reconsolidation line.



Figure 7-3. Schematic concept of excess pore pressure dissipation with the given degree of consolidation

Subsequent undrained loading at a lower specific volume causes *RSL* to approach the effective stress at the higher value points *D* and *F* in the final two episodes.

### 7.2.1. Soil strength

As mentioned earlier, the current vertical effective stress of the soil can be related to the undrained shear strength using the lumped strength parameter.

$$s_u(\hat{z}) = \Phi(\hat{z})\sigma'_v(\hat{z}) \quad (7-12)$$

The shear strength of the soil at the current location of the pipe is controlled by the soil strength surrounding the pipe by a normalized distance,  $\alpha$ , below and above the pipe. The average strength is calculated by a weighted integration of the current soil strength with respect to a strength influence zone,  $v(\hat{z})$  as illustrated in Figure 7-4, defined by a triangular function similar to the cycle number influence function,  $\mu(\hat{z})$ .

$$v(\hat{z}) = \frac{1}{\alpha} \left( 1 - \frac{|\hat{\eta}|}{\alpha} \right) \quad (7-13)$$

$$s_{u,avg} = \int_{\hat{z}_m-\alpha}^{\hat{z}_m+\alpha} s_u(\hat{z}) v(\hat{z}) d\hat{z} \quad (7-14)$$



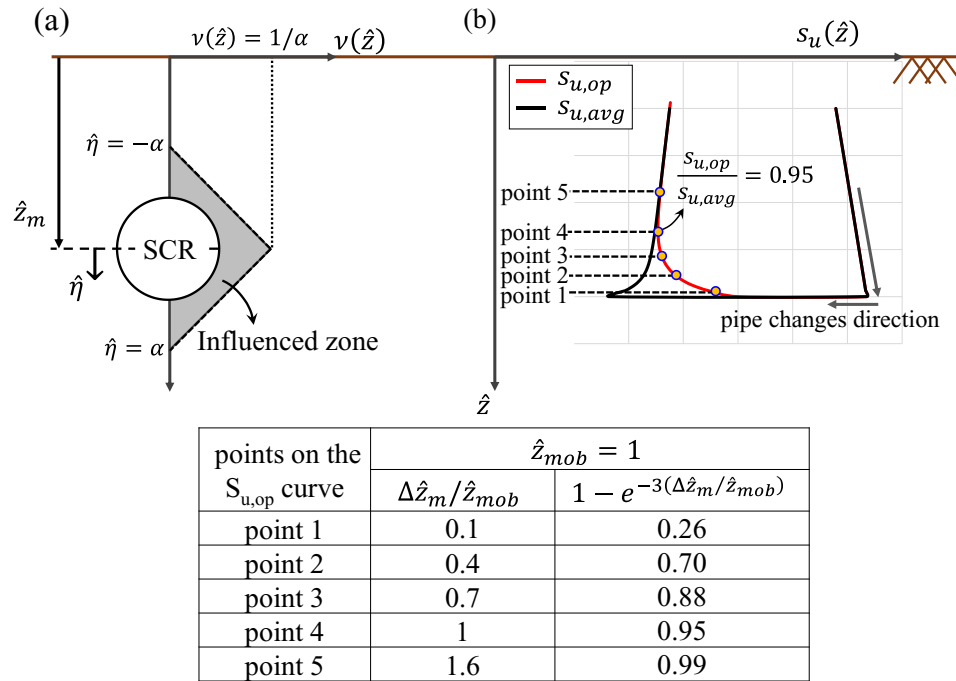


Figure 7-4. Definition of shear strength (a) Contribution of the surrounded soil for average strength (b) soil mobilization after the change in pipe direction

During a change in pipe direction, the gradual mobilization of soil strength can be modelled by an exponential function provided in equation (7-15). As shown in Figure 7-4(b), the secant stiffness of the soil model decays to such an extent that the operative strength,  $S_{u,op}$ , approaches 95% of the average soil strength,  $S_{u,avg}$ , within the strength mobilized distance,  $\hat{z}_{mob}$ .

$$\frac{S_{u,op}}{S_{u,avg}} = 1 - e^{-3(\Delta\hat{z}_m/\hat{z}_{mob})} \quad (7-15)$$

where  $\Delta\hat{z}_m$  is the change in pipe displacement due to a change of direction.

As shown in the superimposed table, the value of mobilized distance was considered as  $\hat{z}_{mob} = 1$ . Depending on the distance from the reversal point during the uplift mode of the

pipe ( $\Delta\hat{z}_m$ ), the  $s_{u,op}$  is obtained as a factor of  $s_{u,avg}$ , with this factor asymptotically approaching 1.

### 7.3. Validation of framework through an example T-bar model test

The analytical procedures of the framework used in this study were coded in the UEL subroutine of ABAQUS to validate the results against published works, such as the T-bar penetrometer model test that was conducted at Western Australia University with a diameter of 5 mm corresponding to 0.25 m at the prototype scale and an acceleration level of 50g in a geotechnical centrifuge test (Hodder et al., 2009). Three episodes of cyclic loading were simulated in the current study using predefined displacement ranges similar to those used in the model test. Each episode comprised 20 cycles, with an intervening pause period of 3.5 hours (equivalent to 1 year at the prototype scale). The values assumed for framework parameters are presented in Table 7-1, based on the work of Hodder et al. (2013).

Table 7-1. Main parameters for effective stress framework used in this study

Parameter	Sign	Value
Effective unit weight (kN/m <sup>3</sup> )	$\gamma'$	5.5
Specific volume at $\sigma'_v = 1 \text{ kPa}$	$\Gamma_{NCL}$	3.74
Slope of normal compression line	$\lambda$	0.311
Slope of swelling/reconsolidation line	$\kappa$	0.0667
Peak strength ductility	$N_{95,\phi}$	0.75
Cycle number influence zone extent	$\beta$	1
Plastic volumetric strain ratio	$\Lambda$	0.557
Steady strength parameter	$\Phi_{steady}$	0.6
Peak strength parameter	$b$	0.3
Pore pressure rate parameter	$N_{95,u1}$	0.25
Pore pressure rate parameter	$N_{95,u2}$	11
Pore pressure component parameter	$a_u$	0.77
Lateral extent of excess pore pressure column	$\chi$	1

Strength influence zone extent	$\alpha$	1
Strength mobilized distance	$\hat{z}_{mob}$	1
Soil sensitivity	$S_{t,cycle}$	2.48
Coefficient of consolidation (m <sup>2</sup> /year)	$c_v$	2

Figure 7-5 shows the results of operative undrained shear strength for a range of soil horizons affected by cyclic displacements. As shown in Figure 5, the operative undrained shear strength ( $s_{u,op}$ ) during the first unloading cycle of the second and third episodes is not completely matched with the experimental and analytical results published by Hodder et al., (2009) and Hodder et al., (2013), respectively. The discrepancy is attributed to the abrupt change in the reaction force of the user-defined element, which occurs after the consolidation process. The sudden change in soil resistance causes a significant difference in the initial unloading cycle after the consolidation period. However, the results of subsequent cycles are in good agreement with the published works where reasonable convergence is achieved through dynamic analysis.

A gradual reduction in soil strength due to excess pore pressure generation during the undrained loading can be observed in each cyclic episode. However, excess pore pressure dissipation during the intervening pause period resulted in a reduction of specific volume and regaining of vertical effective stress, leading to an increase in soil strength. This consolidation effect causes the fully remoulded strength to be achieved at higher values in later episodes. This concept is illustrated in Figure 7-6, which shows the degradation factor for a specific soil horizon,  $z = 1.75$  m.

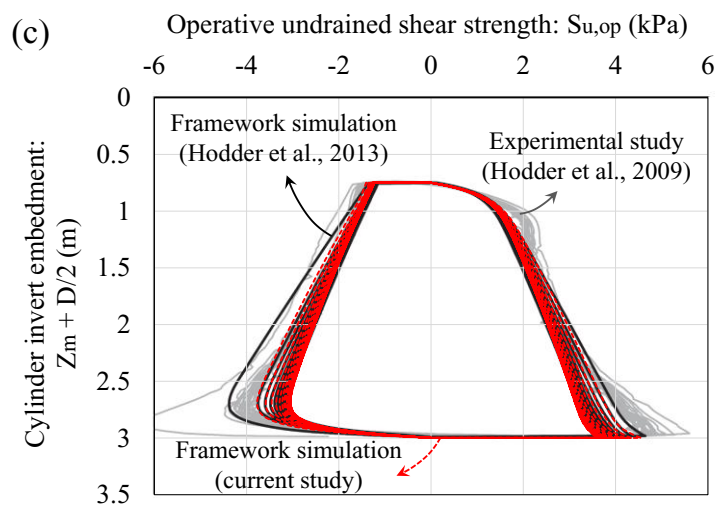
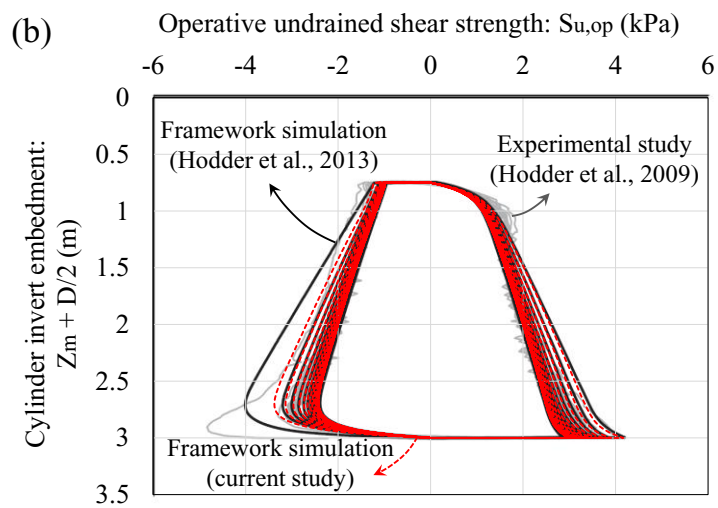
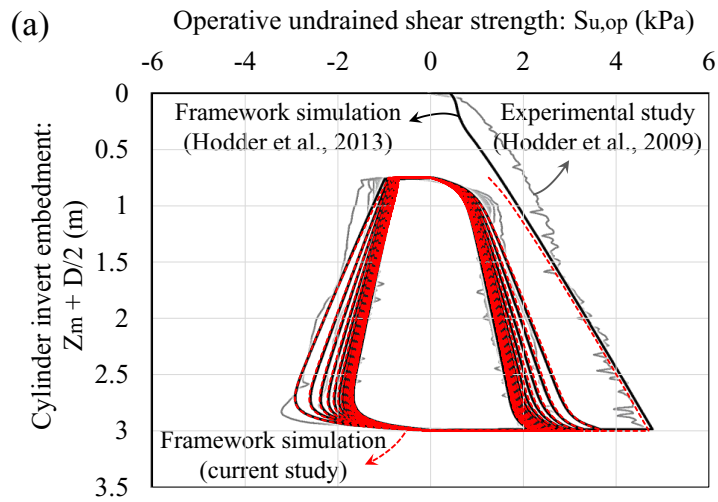


Figure 7-5. Operative shear strength for ranges of soil depth: (a) cyclic episode 1, (b) cyclic episode 2, (c) cyclic episode 3

The degradation factor (DF) is used to quantify the soil degradation caused by pipe motions by measuring the relative soil strength during cyclic penetration and extraction to the initial value,  $s_{u,cycle}/s_{u,initial}$ . As shown in Figure 7-6, DF gradually decreased to a steady value during each cyclic episode, indicating the remoulded state of the soil. Due to the regaining of soil strength after the consolidation process, the DF values increased by factors of 2 and 1.5 during the first cycles of episodes 2 and 3, respectively. Moreover, higher remoulded strengths were achieved in the later episodes, e.g.,  $DF_{Ep. 2}/DF_{Ep. 1} = 1.45$  and  $DF_{Ep. 3}/DF_{Ep. 1} = 1.86$ , associated with the reduction in specific volume resulting in lower soil sensitivity.

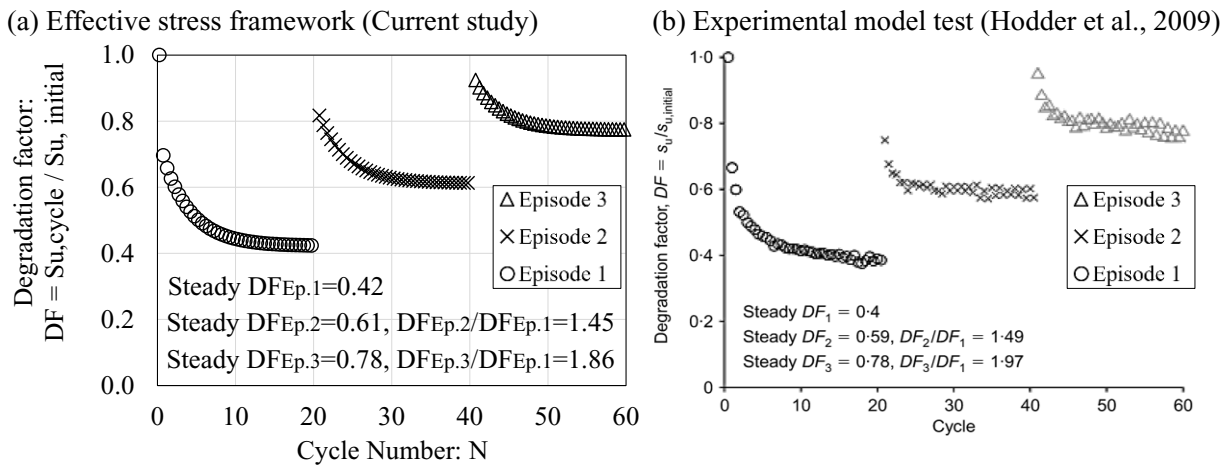


Figure 7-6. Results of degradation factor based on the (a) effective stress framework (current study) and (b) experimental model tests (Hodder et al., 2009)

For a better understanding of the remoulding and consolidation effects, the results of the current study were compared with the experimental study conducted by Al-Janabi et al., (2019). They subjected the short segment of the riser model to ten 100-cycle load parcels,

allowing the pipe to rest on the soil at the end of each sequence to measure the soil strength recovery due to the reconsolidation. Three distinct remoulded states were considered within two intervening pause periods in between. The pause period in each study was scaled to the same prototype, as provided in the superimposed table to have better insight into the consolidation process. Despite differences in the number of cycles and pause period between the current study and the model tests, the trend of the degradation factor was found to be similar in both. As shown in Figure 7-7, the degradation factor decreased through each remoulding episode and subsequently increased due to the consolidation process. The steady DF after two intervening pause periods was higher than the initial remoulded state by a factor of around ~1.8-1.9.

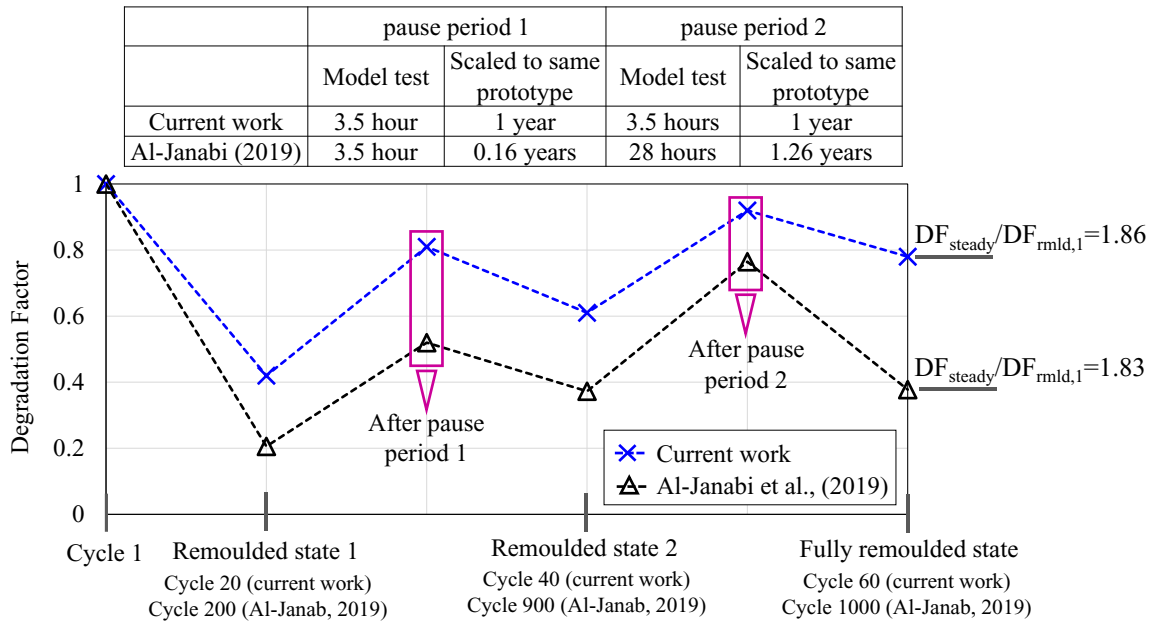


Figure 7-7. Degradation factor due to the remoulding and consolidation effects obtained from effective stress framework (current study) and experimental model tests (Al-Janabi et al., 2019)

The results of the framework used in this study demonstrate good agreement with the published works (Hodder et al., 2009 & 2013; Al-Janabi et al., 2019), as evidenced by Figure 7-5, Figure 7-6 and Figure 7-7. These results provide strong support for the validity of the framework implemented in the FORTRAN program.

#### 7.4. Numerical analysis of SCR

A global SCR model was developed in ABAQUS using an example SCR with a length of 2333 m and a water depth of 1800 m, located in the Gulf of Mexico. The key parameters of the SCR are summarized in Table 7-2.

Table 7-2. Main parameters of the SCR model developed in this study

Parameter	Sign	Value
pipe outer diameter (m)	D	0.324
pipe wall thickness (m)	t	0.0205
water depth (m)	$\Delta Z$	1600
cross-section area (m <sup>2</sup> )	A <sub>s</sub>	1.95E-02
moment of inertia (m <sup>4</sup> )	I	2.26E-04
submerged weight (kg/m)	m <sub>s</sub>	100
hang-off angle (deg)	$\theta_{HO}$	77.88

The PIPE21 elements available in the ABAQUS element library were employed to model the SCR, with the element length set to 1 m in the TDZ and 5 m in the catenary section. As boundary conditions, simple hinge supports were assumed at the anchored end and the hang-off point. For the displacement-controlled analyses, the vessel excitation resulting from cyclic motions was coded into a DISP user subroutine in ABAQUS.

The fatigue performance of an SCR is significantly affected by the soil stiffness in the TDZ, which is influenced by any soil resistance during pipe loading and unloading. A simple linear spring assumption cannot account for the variations in soil response during repeated

cycles, leading to inaccurate fatigue damage predictions (Randolph et al., 2013; Kimiaei et al., 2010; Kimiaei, 2017). Previous efforts to resolve uncertainties related to linear stiffness mostly rely on introducing non-linear hysteretic soil models that use a combination of hyperbolic and exponential functions of soil stiffness during the four main parts of the riser motions: a) initial penetration, b) uplift, c) suction, and d) re-penetration (e.g., Randolph and Quiggin, 2009; Aubeny and Bisconting, 2009). However, these models are based on the total stress approach and do not explicitly account for soil degradation and the aging effects. This study addresses this limitation by investigating the soil stiffness using the recently developed effective stress framework that captures both remoulding and consolidation effects. As explained earlier, the entire procedure of the effective stress framework was coded in FORTRAN coding program and integrated into the UEL subroutine to model the riser-seabed interaction using user-defined elements, called by ABAQUS at every increment of the dynamic analysis. Figure 7-8 provides a schematic of the 2D configuration of SCR and illustrates the UEL subroutine procedure in detail.



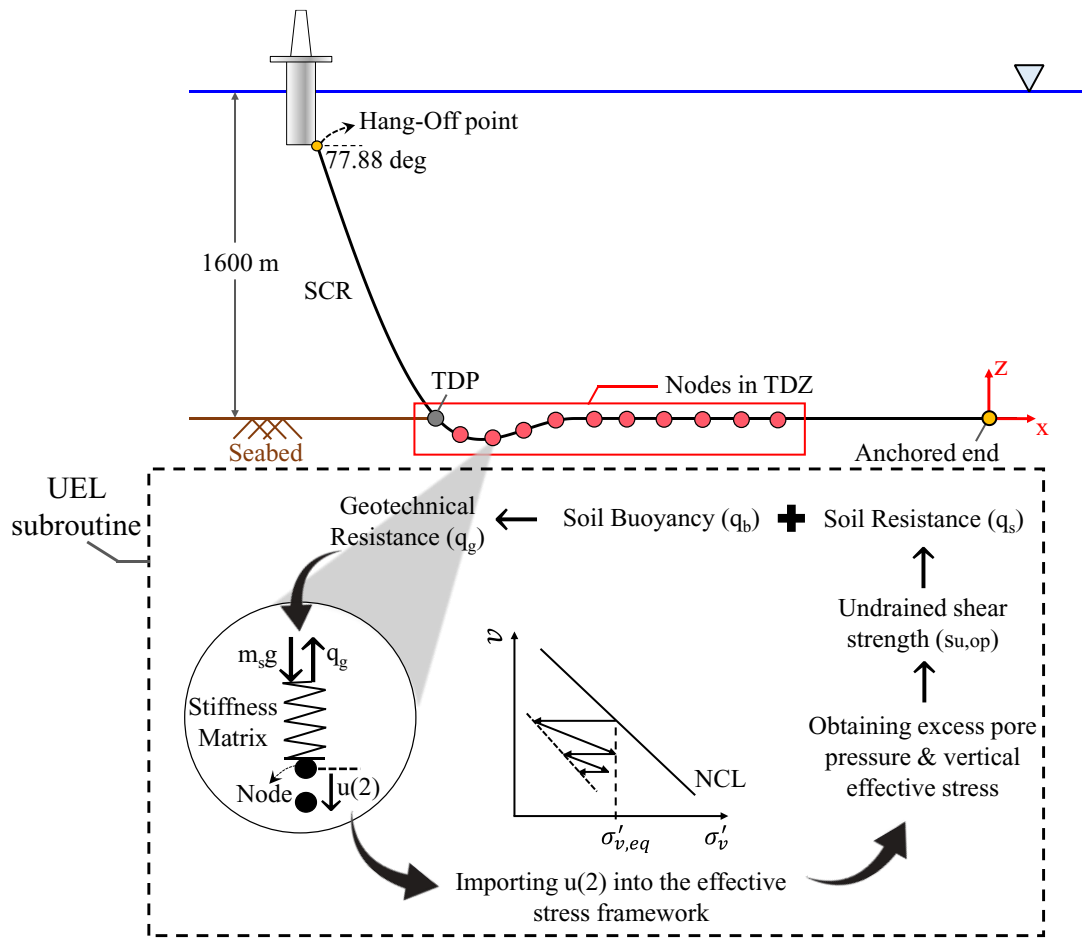


Figure 7-8. 2D configuration of SCR within user-defined elements implemented into the UEL subroutine

The stiffness matrix of each user-defined element distributed along the TDZ has been updated by getting the current pipe-soil resistance from the effective stress framework, which is in equilibrium with the submerged weight of the riser per unit length. The geotechnical bearing capacity is represented by Equation (7-16), which takes into account two components arising from soil resistance and soil buoyancy.

$$q_g = N_c s_{u,op} + f_b D (\rho_{soil} - \rho_{water}) \cdot g \quad (7-16)$$

where  $N_c$  is the soil bearing factor,  $s_{u,op}$  is the operative undrained shear strength,  $D$  is the outer pipe diameter,  $f_b$  is the soil buoyancy factor,  $\rho_{soil}$  is the saturated density of the soil,  $\rho_{water}$  is the density of water, and  $g$  is the acceleration due to gravity.

As expressed in equation (7-17), the concept of soil stiffness is defined by the normalized unloading secant stiffness.

$$K_{sec} = \frac{\frac{\Delta q}{\Delta z/D}}{q_0(z_0)} \quad (7-17)$$

where  $\Delta q = q_z - q_0$  is the resistance variation between the current depth of the soil and the last point of reversal load. A schematic illustration of the secant stiffness is provided in Figure 7-9.

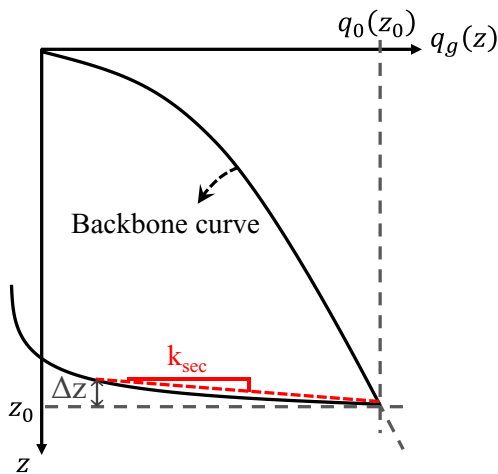


Figure 7-9. Definition of unloading secant stiffness

### 7.5. A SCR case study analysis

A series of dynamic analyses were conducted on a riser based on three episodes of undrained loading, each consisting of 200 cycles. The choice of 200 cycles in each episode was somewhat arbitrary, but was made to ensure that the riser embedment was sufficiently

stabilized with reasonable computational time. The direction of vessel oscillation was selected based on a study conducted by Kimiaei et al. (2010), which showed that the vessel oscillation in the tangential direction of the local coordinate system at the SCR hang-off point may contribute by over 95% to the overall fatigue damage accumulation in the TDZ. Therefore, in this study, to minimize the computational effort, the tangential direction at the hang-off point was selected for vessel oscillation by  $H = 2.00, 3.25, \text{ and } 4.5 \text{ m}$  with  $T = 15 \text{ s}$ . It should be noted that in reality, vessel oscillation may occur in a range of different directions, e.g., perpendicular to the tangential direction. However, later in this paper, for the SCR dynamic analysis under random waves, realistic oscillations were implemented instead of tangential oscillation. At the start of the dynamic step, the linear elastic springs at the seabed were replaced with user-defined non-linear elements to adjust the soil stiffness based on the submerged weight, soil buoyancy, and given soil strength calculated from the effective stress framework. Additionally, a higher value for the degree of dissipation was assumed between each two consecutive episodes,  $U \sim 90\%$ , to investigate the consolidation effect, equivalent to approximately 2 years of pause period. The parameters of the effective stress framework were assumed to be the same as those provided in Table 7-1 with some minor differences, e.g.,  $\gamma' = 6 \text{ kN/m}^3$ , and  $S_t = 3.5$ . Figure 7-10 illustrates the normalized SCR profiles in cycles 200, 400, and 600, which represent the remoulding states in each episode.

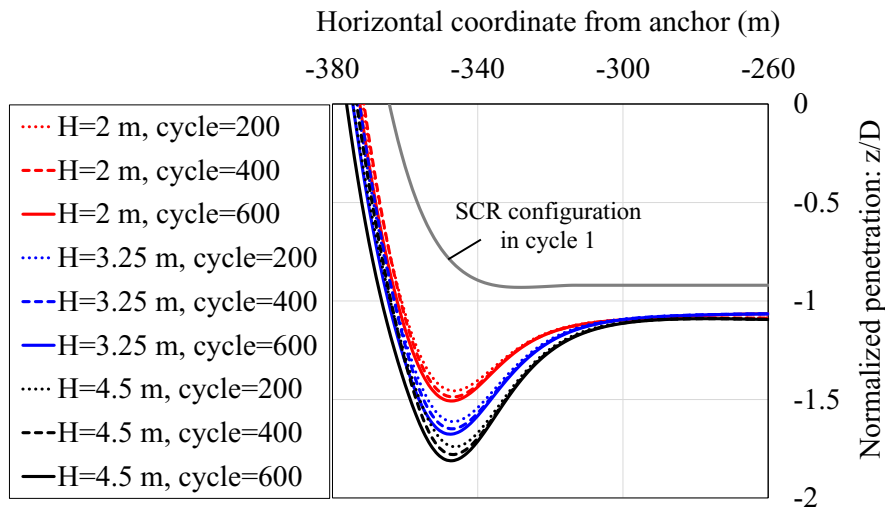


Figure 7-10. Numerical penetration of SCR at the remoulding states of each episode

It was observed that the major part of the riser penetration occurred during the first remoulding process, reaching a depth of around  $1.5D$  to  $1.8D$  for all three groups of dynamic motions. The penetration continued to increase progressively in the subsequent episodes, stabilizing by cycle 600. This suggests that the embedment for cycle 600 was not significantly different from 200.

### 7.5.1. SCR-Soil Stiffness based on remoulding and consolidation

Figure 7-11(a) depicts the normalized secant stiffness at  $\Delta z/D=0.0025$  based on the three groups of tangential motions, including  $H = 2, 3.25,$  and  $4.5$  m with  $T = 15$  s for node 356. The corresponding profiles of the riser were superimposed in the plot (b) to identify the mentioned node.

Throughout each cyclic episode, a gradual reduction in the normalized secant stiffness can be observed, indicating the degradation effect. Figure 7-11 shows an abrupt increase in  $K_{sec}$  between two consecutive episodes due to consolidation. By cycle 600, the secant stiffness stabilizes with a value greater than the initial stiffness for all three motion amplitudes.

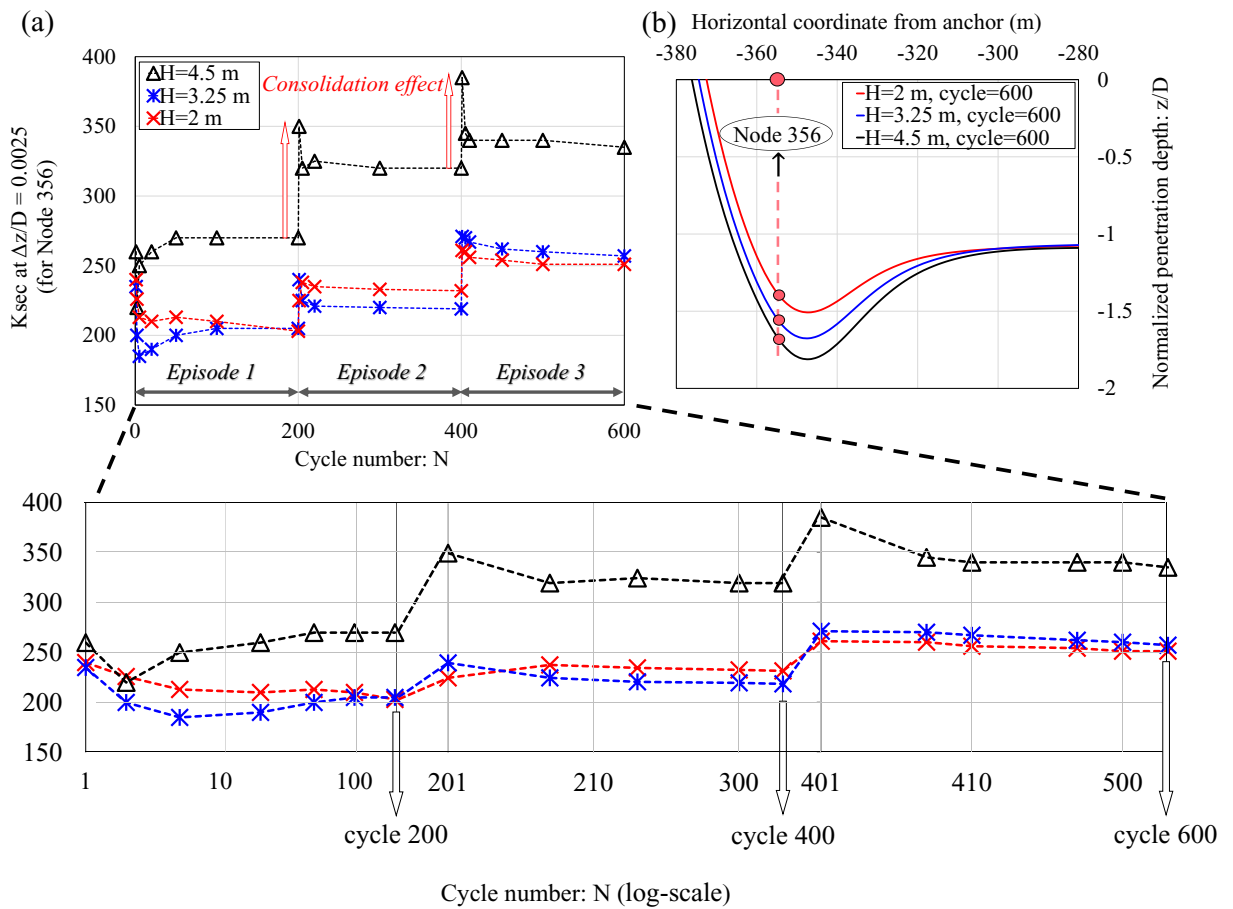


Figure 7-11. (a) Non-dimensional secant stiffness against cycle number at  $\Delta z/D = 0.0025$  for Node 356, (b) SCR profiles in the TDZ

To better understand the effect of the consolidation process, a series of numerical results were presented using a single tangential amplitude of  $H = 2$  m. The aim was to compare the results of an effective stress framework with those obtained from one of the widely accepted non-linear soil models proposed by Randolph and Quiggin (2009), which will be referred to as R-Q in this study.

Figure 7-12 illustrates the penetration-resistance response of the seabed based on the effective stress framework at node 356, a sample position along the TDZ. The results indicate a change in the slope of soil stiffness as the pipe undergoes its second and third

episodic loading (e.g., cycles 200-204 and cycles 400-404), because of the pause period, corresponding to  $U \sim 0.90$ . This value represents the dissipation of 90% of the maximum excess pore pressure during the assumed pause period.

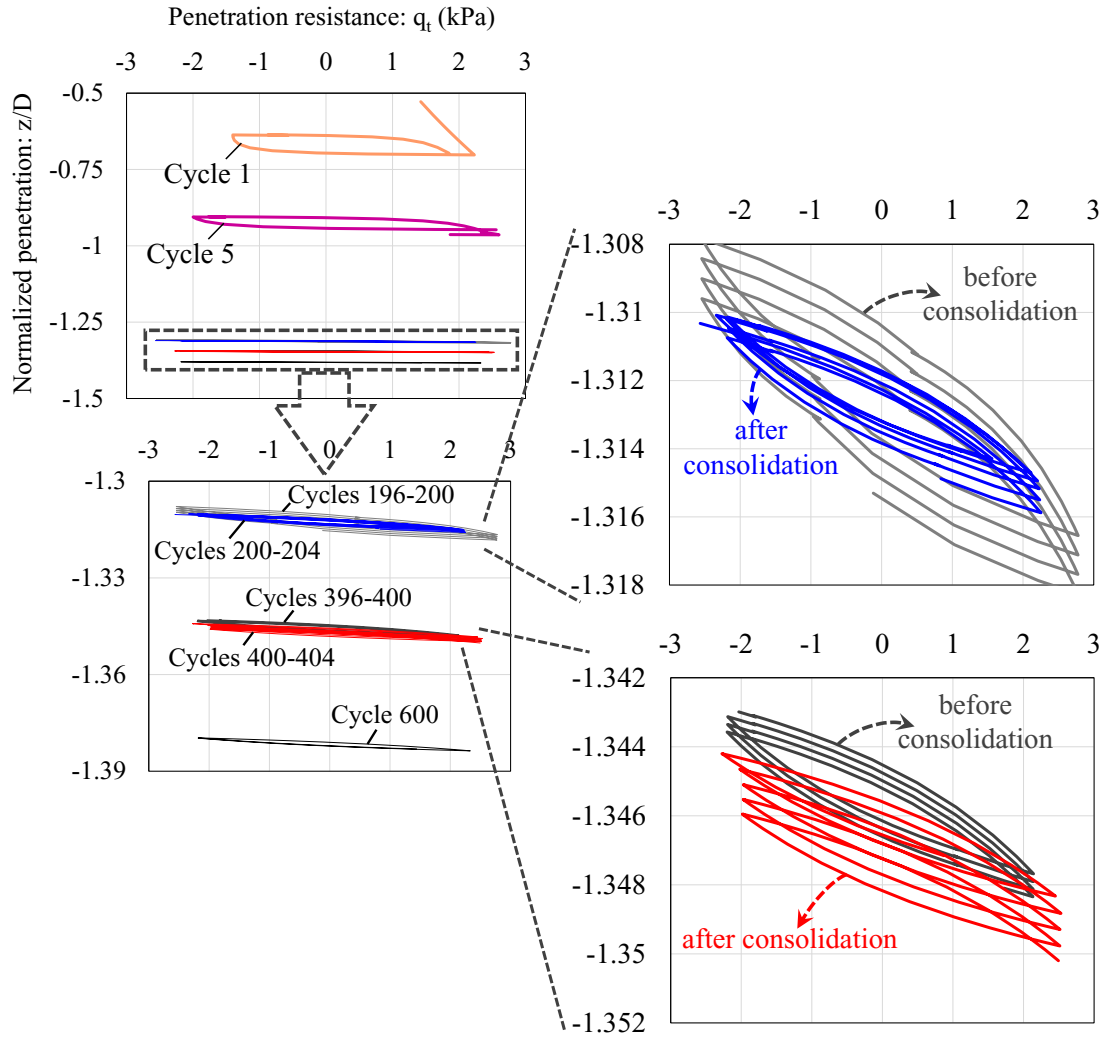


Figure 7-12. Numerical analysis of SCR over 600 cycles based on the effective stress framework:

SCR penetration-resistance for Node 356

Moreover, a numerical analysis with the same motion amplitude was conducted based on the R-Q model with the soil parameters provided in Table 7-3. The soil sediments in deep water are usually very soft clay with a low magnitude of undrained shear strength at the

mudline intercept. Although, assuming a zero undrained shear strength at the mudline may look purely theoretical, it has been reported in several studies in the literature (e.g. Hejazi and Kimiaei, 2016, Yuan et al., 2017) ( $0 \text{ kPa} \leq s_{u0} \leq 0.5 \text{ kPa}$ ). Two different set of mudline shear strength ( $s_{u0}$ ) and strength gradient ( $\rho$ ) have been reported in the current study with zero and non-zero mudline shear strength: ( $s_{u0}=0 \text{ kPa}$ ,  $\rho=1 \text{ kPa/m}$ ) and ( $s_{u0}=1 \text{ kPa}$ ,  $\rho=1.2 \text{ kPa/m}$ ).

Table 7-3. Input parameters for the R-Q model

Description	sign	value
Mudline shear strength (kPa)	$s_{u0}$	0, 1
Shear strength gradient (kPa/m)	$\rho$	1, 1.2
Saturated soil density ( $\text{kg/m}^3$ )	$\rho_{\text{soil}}$	1500
Power law parameter	a	6
Power law parameter	b	0.25
Normalized maximum stiffness	K	200
Suction ratio	$f_{\text{suc}}$	0.3
Suction decay parameter	$\lambda_{\text{suc}}$	0.5
Re-penetration parameter	$\lambda_{\text{rep}}$	0.5
Soil buoyancy factor	$f_b$	1.5

Although the R-Q model is not able to represent soil degradation explicitly, the remoulding effect is modelled by reaching the same soil strength in a greater depth until a sufficiently stabilized riser embedment is reached. This concept is observed in Figure 7-13 and Figure 7-14, which display the cyclic load displacement for sample nodes, Node 356 and Node 350. Due to the absence of consolidation effect in the R-Q model, the ratio of penetration-resistance first decreased but ultimately reached a constant value without any change. Figure 7-15 provides a visual comparison of the effective stress approach and R-Q model by demonstrating the ratio of the stabilized secant stiffness (at cycle 600) to its initial value for the TDZ node range.

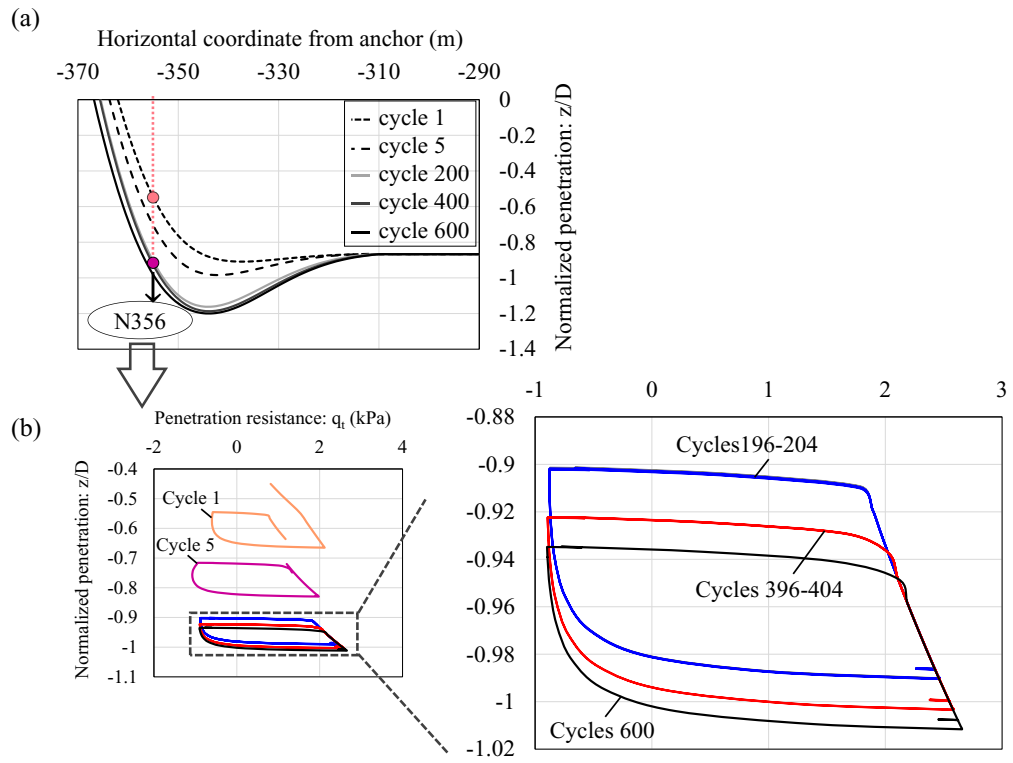


Figure 7-13. Numerical analysis of SCR over 600 cycles based on the non-linear soil model (R-Q),  $s_{u0}=0$  kPa,  $\rho=1$  kPa/m: (a) SCR profile, (b) SCR penetration resistance for node 356



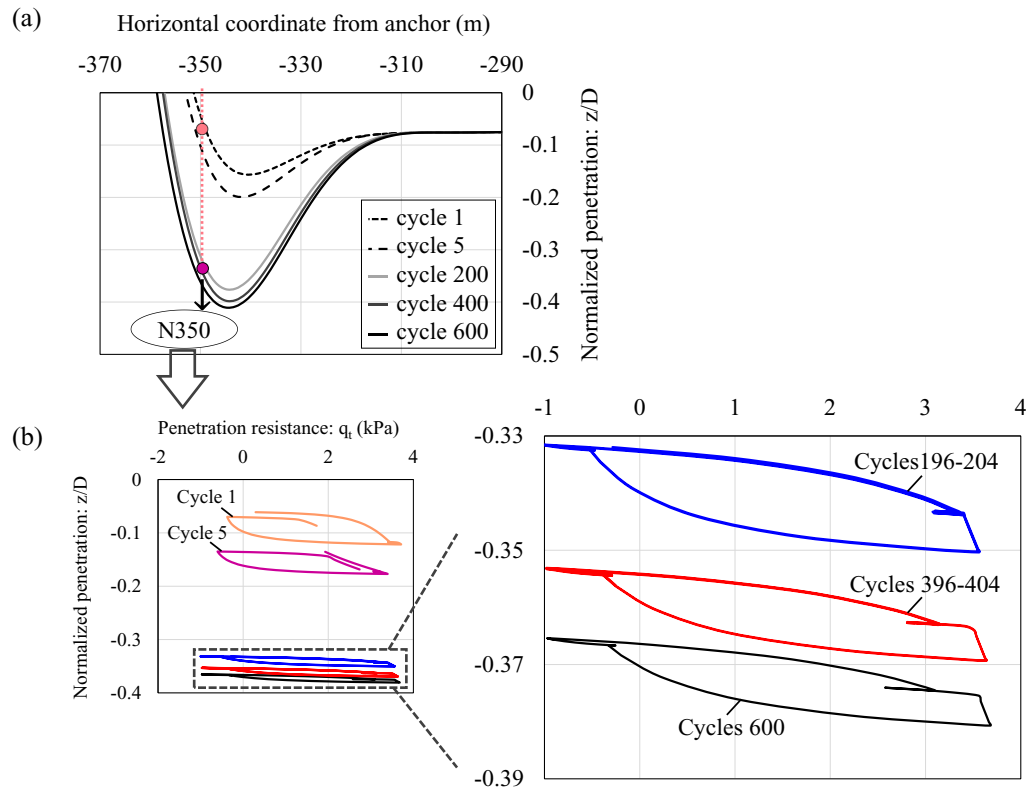


Figure 7-14. Numerical analysis of SCR over 600 cycles based on the non-linear soil model (R-Q),  $s_{u0}=1$  kPa,  $\rho=1.2$  kPa/m: (a) SCR profile, (b) SCR penetration resistance for node 350

The results presented in Figure 7-15 demonstrate that the effective stress approach shows a tendency for soil stiffness recovery due to the consolidation effect, with the highest ratio of stabilized stiffness to initial stiffness occurring at node 366. The results for this node have been superimposed based on the number of cycles. The normalized secant stiffness initially equals 280, but it falls during the first five cycles, reaching  $\sim 250$ . It then gradually rises as the cycles accumulate, achieving  $\sim 340$  at cycle 200. After two abrupt increases during the intervening pause periods, it ultimately stabilizes at cycle 600, exceeding the initial normalized stiffness by a factor of 1.9 (e.g., 2.2 times greater than remoulded value). These findings are consistent with other published works (Hodder et al., 2009, Clukey et

al., 2017b; Zhou et al., 2020). Furthermore, the same plot shows the gradual riser penetration over the initial 200 cycles, reflecting the soil softening. It is important to note that the  $z/D$  began to decrease slightly during each consolidation state, meaning that the riser settlement caused by a reduction in the volume of the soil due to the consolidation process was not considered in this analysis. However, no consolidation effect could be presented by the R-Q model, and the soil stiffness rapidly decreased during cyclic episodes, reaching around 0.7 – 0.9 of the initial value.

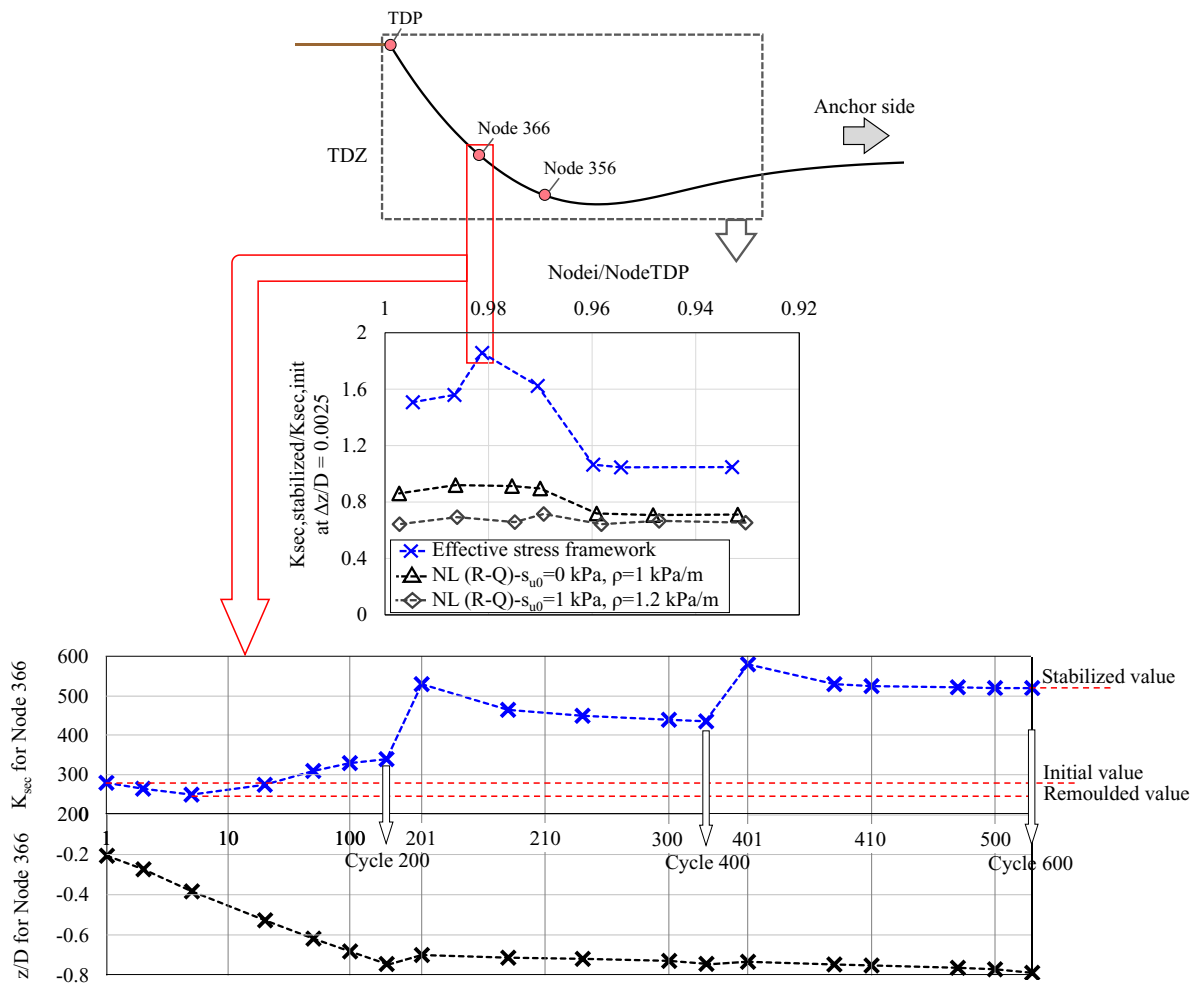


Figure 7-15. Normalized uplift secant stiffness based on the effective stress framework and non-linear soil model

The results obtained from the effective stress framework confirm that the episodes of remoulding were significantly eclipsed by a recovery due to the consolidation effect, which was not captured by the existing non-linear soil models, e.g., the R-Q model. It is worth noting that neglecting the possibility of consolidation and considering only the lower soil stiffness associated with the remoulding process could lead to unconservative fatigue life predictions, which will be discussed in the next section.

## **7.6. Incorporation of trench effect into fatigue analysis with the presence of consolidation**

### **7.6.1. Hybrid Trench Model for trench generation**

Underwater surveys have shown that the trench formation in the TDZ mostly stabilized during the first 2-3 years of riser production, resulting in a ladle-shaped profile with several diameters deep (Bridge and Howells, 2007). As discussed in the literature, non-linear soil models may cause premature trench stabilization through a few cycles, at a penetration depth of somewhere between 0.5D to 1D, which is much less than the ranges of 2.5D to 5D trenches observed in the field. Moreover, the artificial insertion of the trench through mathematical formulation leads to inconsistencies between the natural catenary shape of the riser and seabed, resulting in contact pressure hotspots and distortion of the stress distribution in the TDZ (Sharma and Aubeny, 2011; Randolph et al., 2013; Shiri, 2014b, Shoghi, 2020). Although some studies have used novel approaches to reliably incorporate the trench effect in the fatigue analysis of SCRs (Randolph et al., 2013; Hejazi and Kimiaei,



$$k_{eq} = \frac{k_0}{1 + [\alpha \cdot \exp(\alpha \cdot (\hat{x} - \eta))]} \quad (7-18)$$

where  $k_0$  is defined as the reference stiffness determined as the submerged weight ( $m_s g$ ) divided by the initial riser penetration ( $z_0$ ). The value of  $z_0$  can be calculated from the backbone curve comprising soil resistance and soil buoyancy (Randolph and Quiggin, 2009). The parameter  $\hat{x}$  is the absolute value of the horizontal coordinate of each node from the anchored end, which was normalized by 1 m. Two dimensionless parameters, depth correlation factor ( $\alpha$ ) and longitudinal adjustment factor ( $\eta$ ), are presented for creating the desired depth and adjusting the ladle-shaped longitudinal profile.

As part of the STRIDE JIP, Bridge and Howells (2007) published a set of subsea surveys from the trench formed beneath the SCR in the Allegheny field of the Gulf of Mexico (Figure 7-17a). Figure 7-17b shows a general comparison between the trench formed in the current study, the field measurements, and other artificially inserted trenches from the literature.

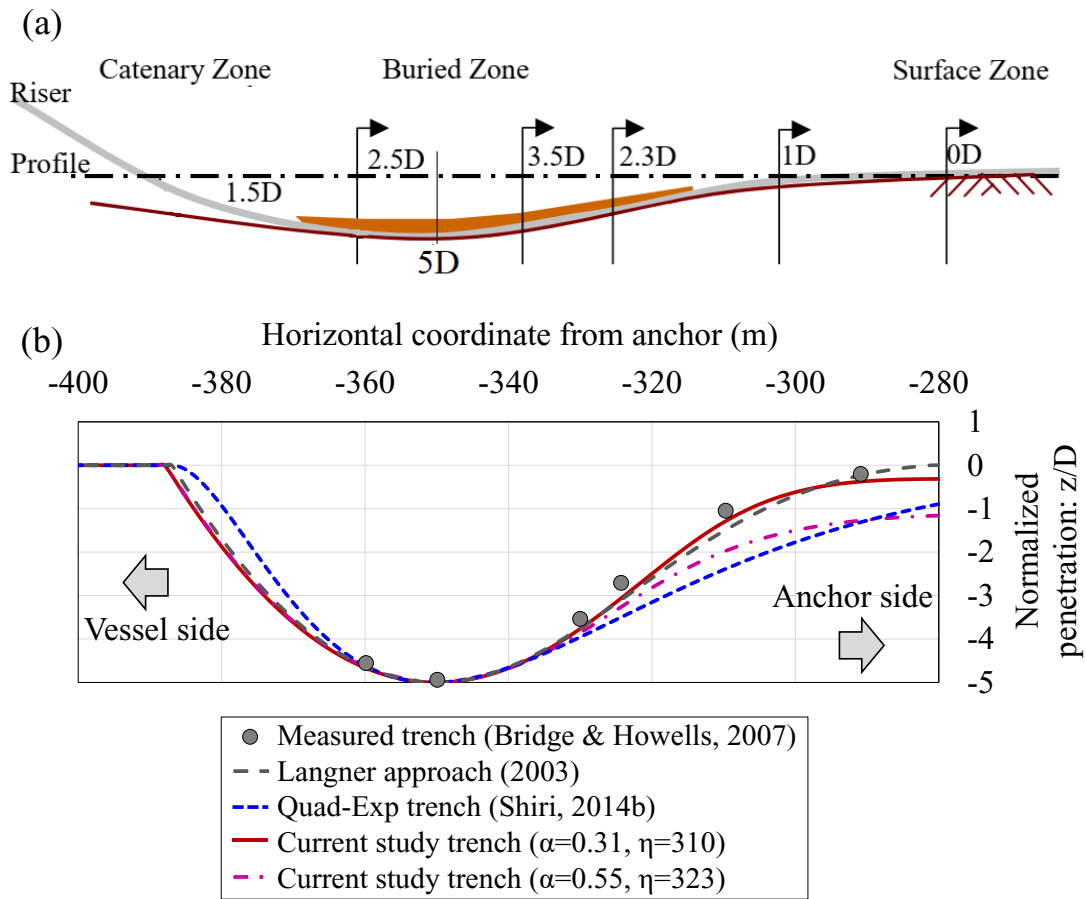


Figure 7-17. A general configuration of trench formation in profile view (a) Observations of Allegheny Trench Survey (Bridge and Howells, 2007) (b) comparison of different approaches for trench profile

It is worth mentioning that riser responses are not limited solely to vertical interaction and also include lateral and axial interaction with the surrounding soil. Depending on the vessel motion, different geometries of the trench wall can be formed in the transverse direction (Oliphant et al., 2009; Al-Janabi et al., 2020). Figure 7-18 provides an overview of trench definition from two different perspectives.

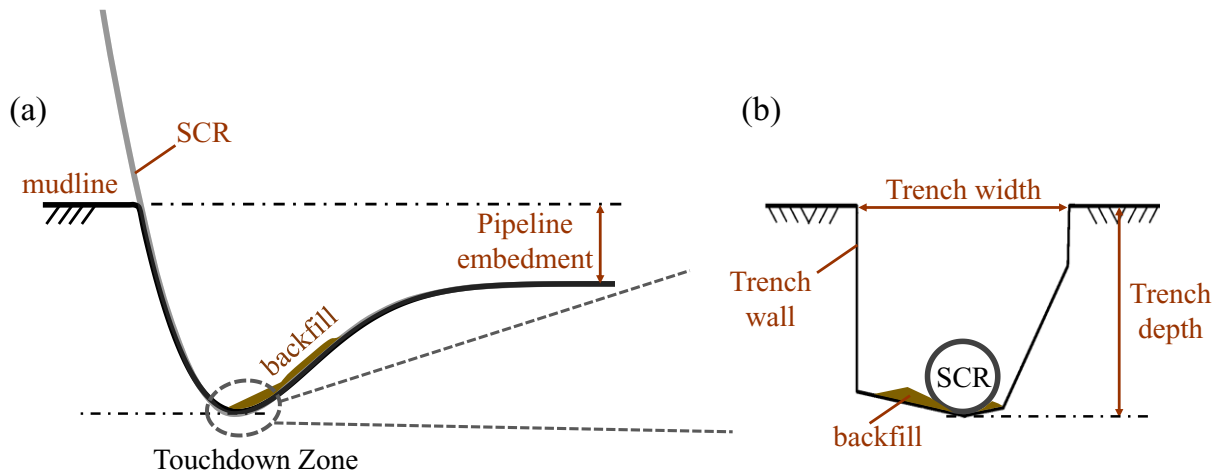


Figure 7-18. Overview of trench formation (a) profile view of the trench (b) transverse view of the trench

Lateral riser-soil interaction affects the overall design of the SCR by considering the ultimate limit state, which is related to the response of the riser to extreme environmental loads and out-of-plane motions (Dong et al., 2021). However, as this is not directly related to the focus of this study, only vertical riser-seabed interaction was taken into account for further fatigue assessment.

As shown in Figure 7-19(a), the trench profile generally includes three important points defined as (Shiri, 2014b): (1) touchdown point (TDP), representing the location where the SCR reaches the nominal seabed level, (2) trench bottom point (TBP), which refers to the maximum depth of trench profile, and (3) trench surface point (TSP), where the SCR reaches the zero gradient towards the anchored end of the riser. Figure 7-19 also shows the incremental penetration of the sample riser using an effective stress framework over 600 cycles of numerical simulation. Despite applying an extreme motion to the vessel, the ultimate trench stabilized at a depth less than  $2D$ . Therefore, the higher depth of the trench profile will be modelled through HTM by assuming appropriate values for  $\alpha$  and  $\eta$  to

achieve the target trench depths, such as the observed 5D depths in ROV surveys (Bridge and Howells, 2007).

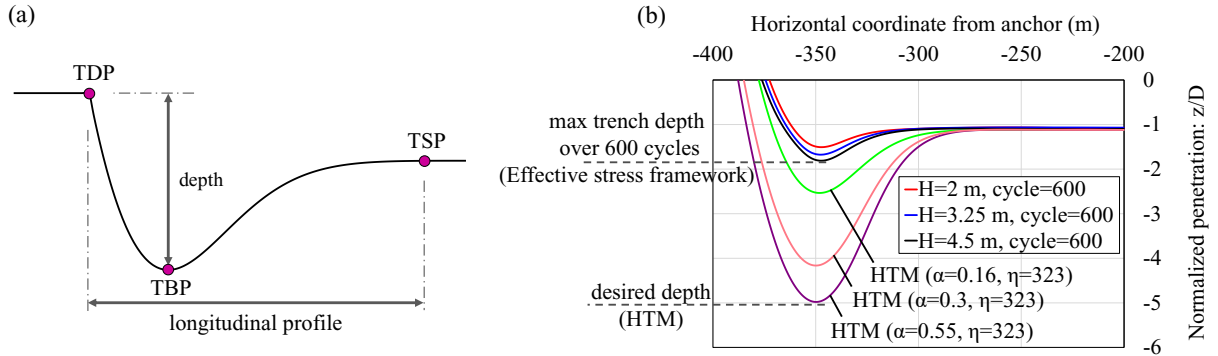


Figure 7-19. Configuration of the trenched seabed (a) trench profile with some key points, (b) incremental embedment of SCR by using effective stress framework and HTM

Comparisons of the SCR's contact force in its equilibrium condition were illustrated in Figure 7-20, based on the four groups of the trenched seabed. The trenched analyses were conducted using a linear soil stiffness ( $k = 300$  kPa) due to the real range of seabed sediments in the Gulf of Mexico (Randolph et al., 2013). These analyses were conducted only to demonstrate the capability of HTM in forming the trench profile compared to other methodologies.

Figure 7-20(a) and Figure 7-20(b) prove that a small gap exists after the riser is laid on Langner and Shiri's trench profiles, resulting in some contact pressure hotspots in the TDZ. Moreover, Shiri and Randolph (2010) used extreme values for the non-linear soil model parameters (assuming  $f_{suc} = 0.05$ ,  $\lambda_{rep} = 2$  in Figure 7-20(c)) to achieve the target depth without any premature stabilization and contact hotspot problems. However, this method leads to unreliable trench geometries, where the trench mouth shifts significantly to the vessel side, and the surface point moves slightly away from the vessel (Dong and Shiri,



2019). The recognized shortcomings of the previous methodologies can presumably imply the reason why different authors have reported contradictory results for the effect of the trench on fatigue damage; some have concluded that trench formation can improve the fatigue life in the TDZ (e.g., Langner, 2003; Nakhaei and Zhang, 2008; Elliot et al., 2013; Randolph et al., 2013; Sharma and Aubeny, 2011; Wang et al., 2016), while others have observed otherwise (e.g., Leira, 2004; Giertsen, 2004; Shiri and Randolph 2010; Rezazadeh et al., 2012; Shiri, 2014a, b).

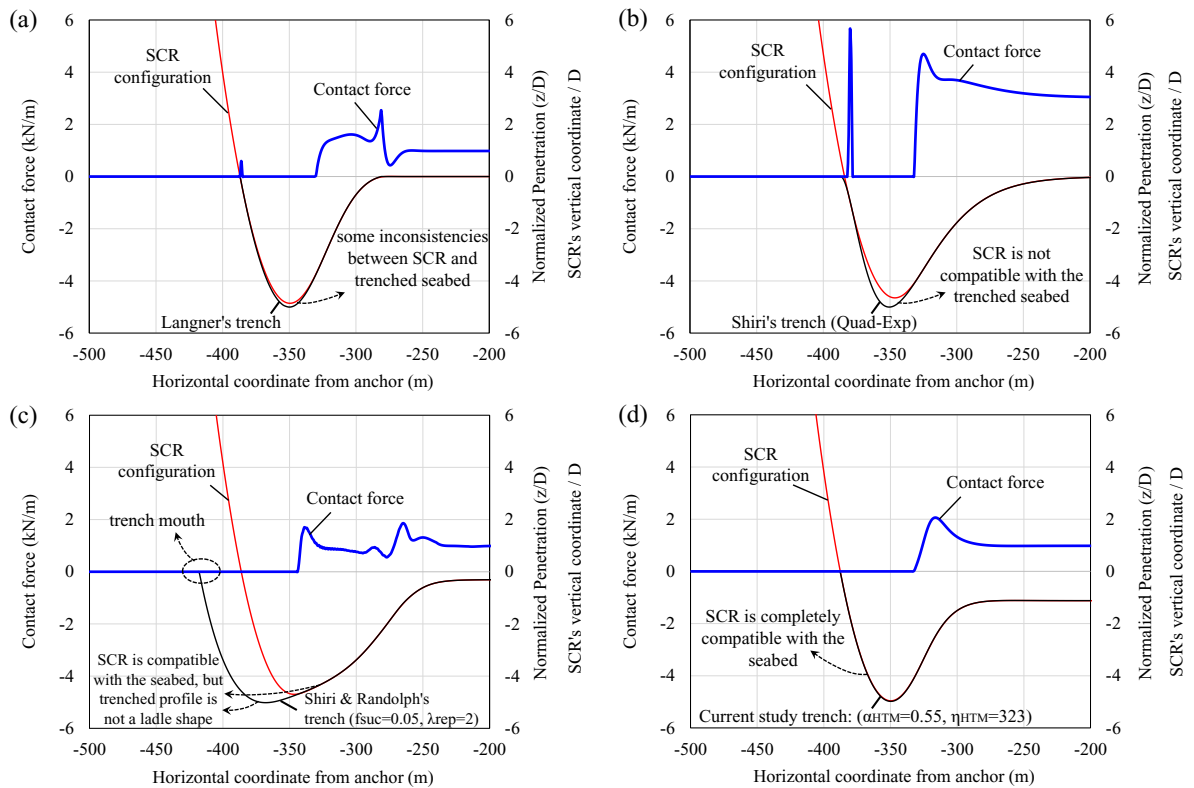


Figure 7-20. Contact force of riser in equilibrium condition, 5D trenched seabed with  $k = 300$  kPa  
 In Figure 7-20(d), the trench profile generated by the HTM ( $\alpha = 0.55$ ,  $\eta = 323$ ) is shown to be perfectly consistent with the natural curvature of the SCR in the TDZ. As explained earlier, the HTM creates the trench profile by adopting individual soil stiffness for each

node that comes into contact with the seabed, thereby eliminating gaps between the riser and the trenched seabed, as well as preventing the creation of local contact pressure along the shape of the trench. The analyses demonstrate that the results of the HTM have been very promising thus far and this method can be considered a reliable approach for incorporating the trench effect into fatigue analysis. In the next section, the HTM is combined with the effective stress approach to investigate the trench effect on fatigue results in the presence of consolidation.

### 7.6.2. Stochastic analysis of fatigue damage

The fatigue damage assessment was conducted using the S-N curve method that relates the number of stress cycles to failure ( $N$ ) with a total stress range ( $\Delta\sigma$ ) (DNV-RP-F204, 2017).

$$N = \bar{a}(\Delta\sigma^{-m}) \quad (7-19)$$

where  $\bar{a}$  and  $m$  are empirical factors determined by fatigue tests.

The Palmgren–Miner’s (DNV-RP-F204, 2017) rule is used to superpose the damage caused by the different stress ranges:

$$D = \sum_i \frac{n(\Delta\sigma_i)}{N(\Delta\sigma_i)} \quad (7-20)$$

where  $n(\Delta\sigma_i)$  is the number of stress cycles with a cyclic range of  $\Delta\sigma_i$ , and  $N(\Delta\sigma_i)$  is the number of stress cycles to failure as expressed by equation (7-19). The stress ranges are obtained through a series of dynamic analyses of the SCR under environmental loads. However, given the random nature of sea states, a stochastic approach was used in this study to produce more accurate and less conservative fatigue damage results (Kimiaei,

2017). Sea states are defined by different significant wave heights ( $H_s$ ) and wave periods ( $T_p$ ) and can be generated through the wave spectra, such as JONSWAP spectrum provided in equation (7-21) used in this study (DNV-RP-C205, 2019).

$$S(\omega) = A_\gamma \left[ \frac{5}{16} H_s^2 \omega_p^4 \omega^{-5} \exp\left(-\frac{5}{4} \left(\frac{\omega}{\omega_p}\right)^{-4}\right) \right] \gamma \exp\left[-0.5 \left(\frac{\omega - \omega_p}{\sigma \omega_p}\right)^2\right] \quad (7-21)$$

where  $H_s$  is the significant wave height,  $T_p$  is the spectral peak period  $= \frac{2\pi}{\omega_p}$ ,  $\gamma$  is the non-dimensional shape parameter, and  $\sigma$  is the spectral width parameter.

The parameters  $\sigma$  and  $A_\gamma$  are calculated by equations (7-22) and (7-23), respectively (DNV-RP-C205, 2019), as follows:

$$\sigma = \begin{cases} 0.07 & \text{if } \omega \leq \omega_p \\ 0.09 & \text{if } \omega > \omega_p \end{cases} \quad (7-22)$$

$$A_\gamma = 1 - 0.287 \ln(\gamma) \quad (7-23)$$

In this study, two distinct sea states were assumed, e.g., *SS3*:  $H_s = 2.3$  m,  $T_p = 6.7$  s and *SS4*:  $H_s = 3.2$  m,  $T_p = 7.8$  s, representing moderate wave heights in the Gulf of Mexico (Muraleedharan and Kimiaei, 2018). The spectral density,  $S(\omega)$ , was divided into  $N$  parts by the frequency bandwidth of  $\Delta\omega$  to reach the time history of the wave amplitudes based on the linear theory that represents the random wave as a composition of  $N$  linear waves (Faltinsen, 1990). The velocity and acceleration of wave particles and the dynamic pressure were then obtained through different wave elevations. Subsequently, the Response Amplitude Operator (RAO) was used to relate the wave amplitudes to the response amplitudes of the floating vessel at the centre of gravity (CoG), which was then transferred to the hang-off point having a horizontal and vertical offset from the CoG. This entire

procedure was coded into the UWAVE subroutine of ABAQUS, as demonstrated in Figure 7-21, where  $a_i$  is the wave component amplitude  $= \sqrt{2\Delta\omega_i S(\omega_i)}$ ,  $\omega_i$ ,  $k_i$ , and  $\delta_i$  are the wave frequency, wave number, and initial phase (between 0 and  $2\pi$ ), respectively, and  $\eta(t)$  is the wave surface elevation at time  $t$ . The AQUA module of ABAQUS was used to automatically apply the buoyancy forces and hydrostatic pressure to the SCR.

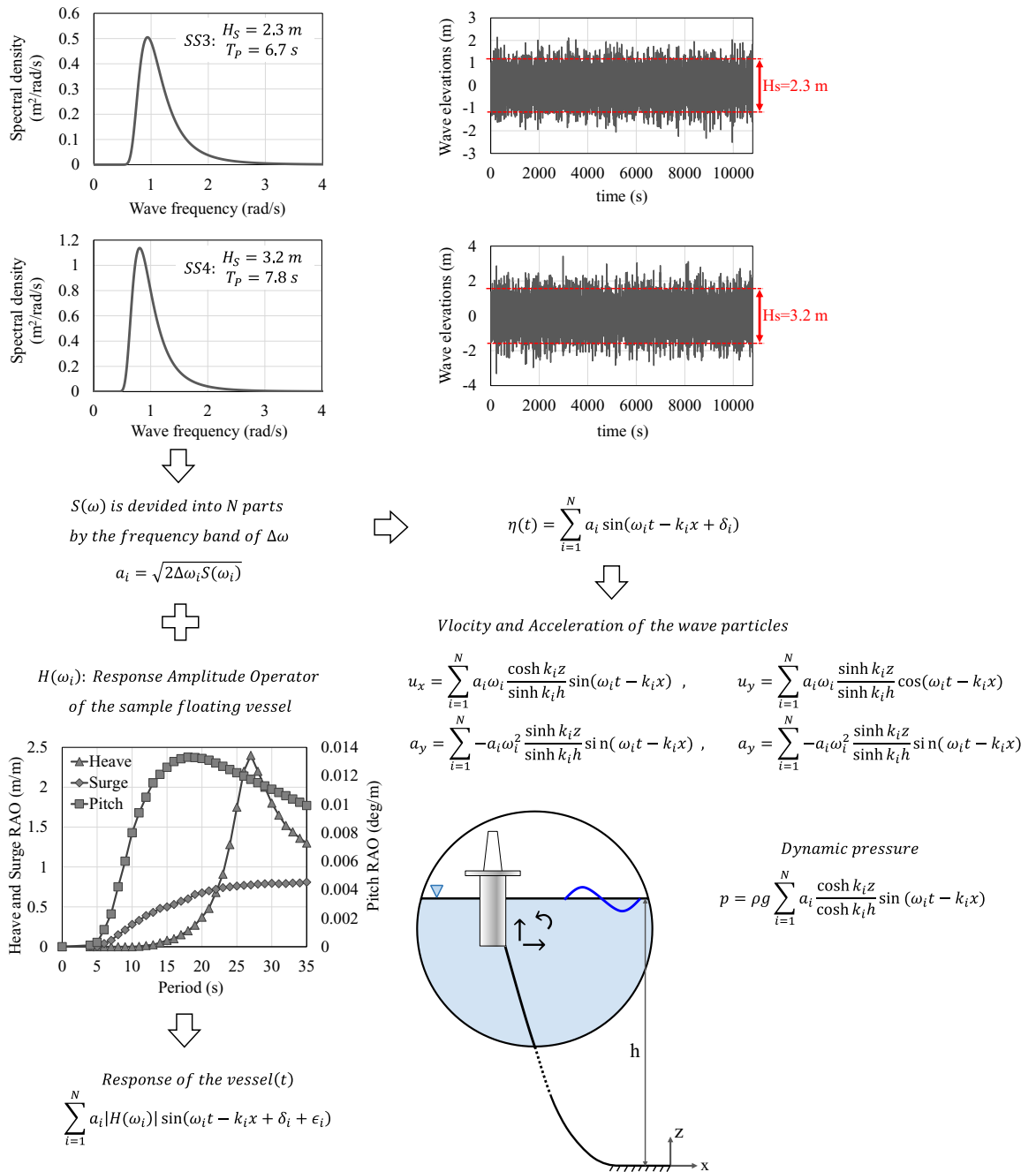


Figure 7-21: The procedure of wave analysis implemented in the UWAVE subroutine of ABAQUS

As explained earlier, the trench that evolved during the remoulding states mostly stabilized at around 1-2D. As shown in Figure 7-22(a), it is possible to progressively lower the

mudline to generate the desired trench depth using HTM. For this purpose, two different values of depth correlation factor ( $\alpha$ ) were initially considered, and then a dynamic analysis of the riser was conducted based on the effective stress approach, which comprised three cyclic episodes with an intervening pause period. Each cyclic episode lasted for 3600 s, resulting in a total 3-hour simulation period to generate the stable loading of irregular waves (see Figure 7-22(b)). Three different trench depths were obtained, namely 1D, 3.8D and 5D, which are good samples of the trench depth ranges reported from the ROV surveys (Bridge et al., 2005).

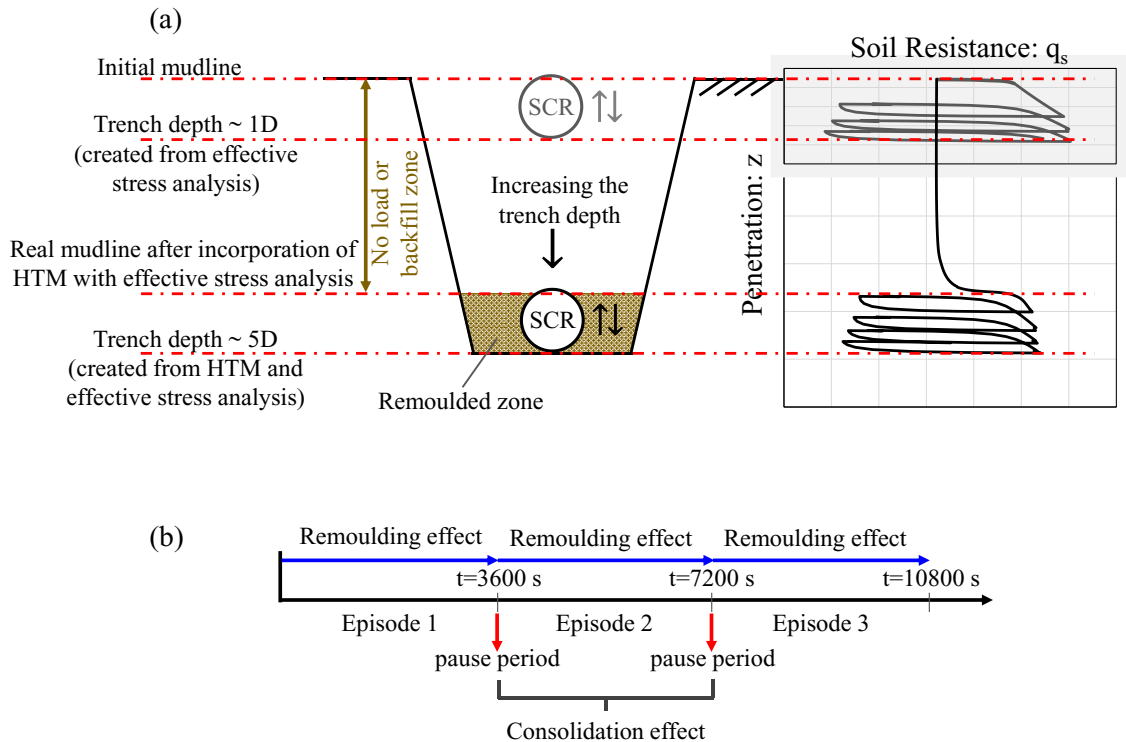


Figure 7-22. Combination of HTM and effective stress framework for stochastic fatigue analysis:

(a) schematic view of deep trench generation, (b) 3-hour simulation time with considering remoulding and reconsolidation processes

The annual fatigue damage for the length of the riser in the TDZ is provided in Figure 7-23 and Figure 7-24 for two different sea states, *SS3* and *SS4*. A trench profile is also superimposed on each plot. In each trench scenario, the results indicate a significant increase in fatigue damage in later episodes of motion as episode 1 gradually changed to episode 3, which was well captured by the effective stress simulation, reflecting the consolidation process. It is interesting to note that the fatigue life deterioration is affected by the trench depth, increasing the damage by around 36% and 34% under the sea states *SS3* and *SS4* for the lower trench depth (1D), and this percentage slightly decreased to 16% and 9.5% as the trench becomes deeper, reaching around 5D.

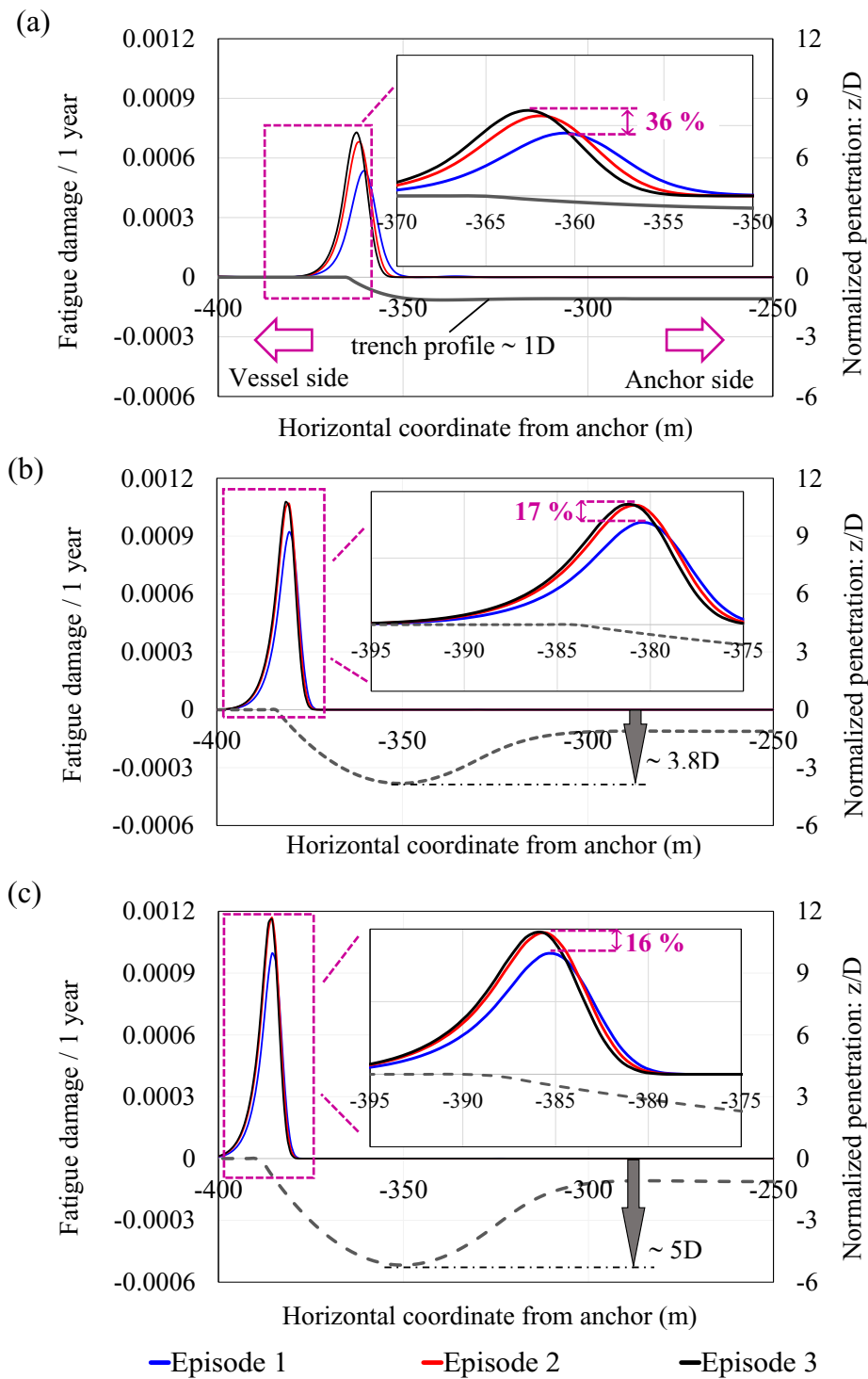


Figure 7-23: Consolidation effect on fatigue performance under 3-hour simulation of SS3 based on the effective stress framework in different trench depths: (a) 1D, (b) 3.8D, (c) 5D



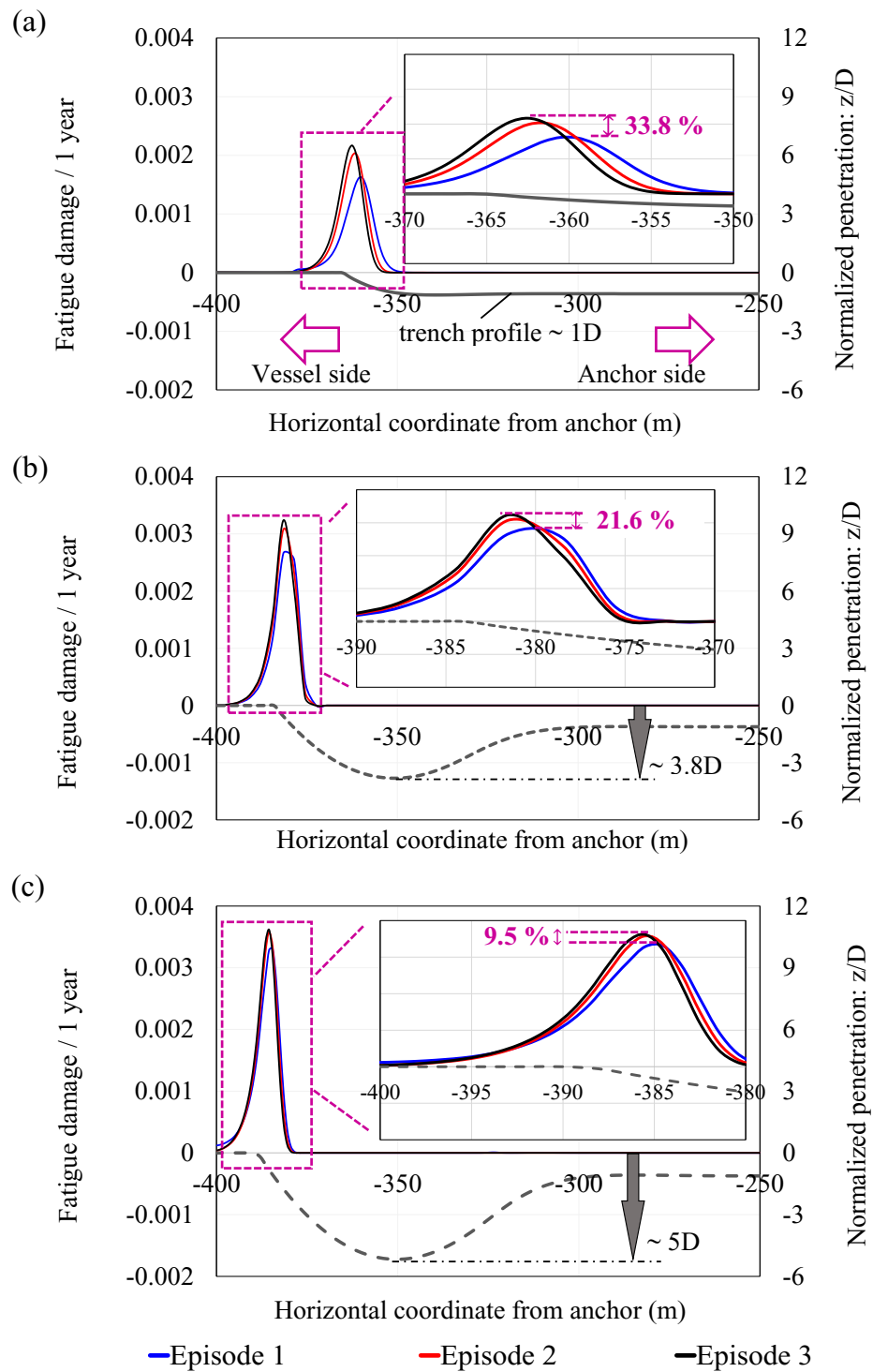


Figure 7-24: Consolidation effect on fatigue performance under 3-hour simulation of SS4 based on the effective stress framework in different trench depths: (a) 1D, (b) 3.8D, (c) 5D

In view of the critical damage results, we have a better understanding of the trench effect with and without consolidation, as shown in Figure 7-25. The maximum fatigue damage in TDZ was normalized by the corresponding peak damage in the first episode of the lowest trench depth ( $\sim 1D$ ).

It can be seen that the trenched seabed has a detrimental effect on fatigue performance, with an increase in damage by a factor of 1.86 and 2.04 under *SS3* and *SS4*, respectively, as the trench depth was changed from 1D to 5D in the absence of consolidation. It is worth noting that the critical damage occurred around the TDP, indicating the likelihood of contact between the SCR and the trench mouth due to its cyclic fluctuations. This distorted fatigue damage at the leading edge of the trench profile towards the vessel side may be considered a potential reason behind the contradictory results on the effect of the trench on fatigue damage (Shoghi and Shiri, 2020).

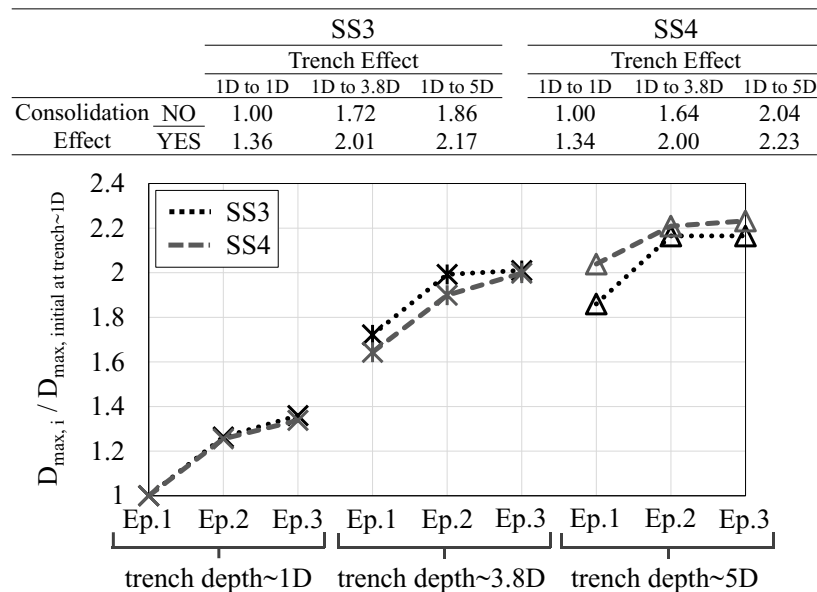


Figure 7-25: Normalized peak fatigue damage for different trench depths with and without consolidation effect under two sea states *SS3* & *SS4*

It can be concluded that the deterioration of the fatigue lifetime was influenced not only by the gradual deepening of the trench beneath the riser, but also by the consolidation effect during the pause period, leading to an increase in fatigue damage by a factor of  $\sim 2.2$  for each sea state.

## **7.7. Conclusion**

As highlighted in the literature, the existing non-linear hysteretic soil models can only account for undrained soil behaviour using a total stress approach, disregarding the excess pore water pressure variations that occur during the lifetime operation of SCRs. This could lead to some inaccuracies in predicting the long-term fatigue damage of SCRs, which is impacted by the excess pore pressure dissipation or consolidation effect.

The methodology used in this study represents a significant improvement in accurately modelling the riser-seabed interaction proposing the correct by employing a recently developed effective stress framework. To accomplish this, a series of user-defined elements were established through UEL subroutine of ABAQUS to model the soil behaviour in the TDZ by getting the historical displacements and calculating the stiffness matrix of each element through an effective stress approach that was coded into the same subroutine. Three cyclic episodes of loading were considered in which the undrained soil strength was quantified by the accumulation of damage surrounding the pipe during the cyclic motions of the riser, resulting in excess pore pressure generation and a corresponding reduction in soil strength. The consolidation effect was also modelled by considering two pause periods between each two consecutive episodes. According to the given degree of dissipation,  $U \sim 90\%$ , the changes in the effective stress were captured by linking the dissipation model to

the current excess pore pressure, resulting in a lower specific volume and an increase in the new effective stress to higher values. The results indicate that the consolidation effect can recover the soil stiffness by a factor of approximately 2, which is a significant phenomenon in accurately predicting the fatigue performance in the TDZ.

This methodology was further considered for the incorporation of the trench effect into the fatigue analysis. However, the riser embedment obtained through an effective stress approach prematurely stabilized somewhere around 1D-2D, which was less than the trench depth ranges reported by ROVs, e.g., 5D. To address this limitation, the authors introduced a simplified alternative solution named HTM by defining an equivalent vertical stiffness along the riser in the TDZ. The analyses showed that the catenary shape of the riser was completely compatible with the trenched seabed, suggesting that this consistent trench creation can be an appropriate approach to guarantee the prevention of contact hotspots along the trench profile, particularly inside the ladle shape. The damage analysis was conducted under the random waves based on the three-hour dynamic simulation of two distinct sea states, and the results showed that the consolidation effect could generally increase the fatigue damage, but the rate of fatigue life deterioration varied depending on the magnitude of the trench depth.

In summary, the numerical analysis of the riser in combination with the effective stress framework allows an accurate assessment of the riser-seabed interaction taking into account the remoulding and reconsolidation effects. Additionally, a stochastic analysis of the fatigue results that considers the real depth of the trench could potentially yield less conservative and more precise fatigue damage estimates, as discussed in the paper.

## **Acknowledgments**

The authors gratefully acknowledge the financial support of this research by the “Natural Science and Engineering Research Council of Canada (NSERC)” through Discovery program, and the Memorial University of Newfoundland through school of graduate studies funding support.

## **Reference**

Al-Janabi, H.A., and Aubeny, C.P. 2019. Experimental Measurement of Thixotropy and Sensitivity in Gulf of Mexico Clay. In the International Society of Offshore and Polar Engineers Conference, 2019-TPC-0593. Honolulu, HI, USA.

Al-Janabi, H.A., Aubeny, C.P., Chen, J., and Luo, M. 2019. Experimental measurement of touchdown zone stiffness for SCR in Gulf of Mexico clay. In Offshore Technology Conference, 6–9 May, OTC-29504-MS, Houston, Texas, USA.

Al-Janabi, H.A., Aubeny, C.P., Chen, J., and Luo, M. 2020. Experimental measurement of monotonic and cyclic lateral resistance of risers and pipelines in Gulf of Mexico clays, *Can. Geotech. J.* 57, 1534–1549.

Aubeny, C. & Biscontin, G. 2009. Seafloor–riser interaction model. *Int. J. Geomech.* 9, No. 3, 133–144.

Aubeny, C., White, T., Langford, T., Meyer, V. & Clukey, E. 2015. Seabed stiffness model for steel catenary risers. In *Frontiers in offshore geotechnics III* (ed. V. Meyer), Boca Raton, FL, USA: CRC Press, 351–356.

Bolton, M. D., 1979. *A guide to soil mechanics*. London, UK: Macmillan.

Bridge, C., 2005. Effects of seabed interaction on steel catenary risers, (Ph.D. thesis). University of Surrey.

Bridge, C., Howells, H., 2007. Observations and modeling of steel catenary riser trenches. In: The seventeenth international offshore and polar engineering conference, ISOPE 2007, Lisbon, Portugal, 803–13.

Chatterjee, S., White, D. J. & Randolph, M. F., 2013. Coupled consolidation analysis of pipe–soil interactions. *Can. Geotech. J.* 50, No. 6, 609–619.

Clukey, E.C., Tognarelli, M.A., Li, G., Ghosh, R., Phillips, R., Zakeri, A., Elliot, B.J., Bhattacharyya, A., Sun, Q., 2011. Simulation of SCR behaviour at touchdown zone – part II: testing of a sectional SCR model in a geotechnical centrifuge. Offshore Technology Conference, 4-6 October, Brazil.

Clukey, E. C., Aubeny, C. P., Randolph, M. F., Sharma, P. P., White, D. J., Sancio, R. & Cerkovnik, M., 2017. A Perspective on the state of knowledge regarding soil-pipe interaction for SCR fatigue assessments. Offshore Technology Conference, OTC 27564, Houston, TX, USA.

Clukey E.C., Zakeri, A., 2017. Recent advances in non-linear soil models for fatigue evaluation of steel catenary risers (SCRs). Proc. Offshore Technology Conference, OTC-27627-MS, Houston.

Dong, X., Shiri, H., 2018. Performance of non-linear seabed interaction models for steel catenary riser, Part I: nodal response. *Ocean Eng.* 154, 153–166.

Dong, X., Shiri, H., 2019. Performance of non-linear seabed interaction models for steel catenary riser, Part II: global response. *Appl. Ocean. Res.* 82, 158-174.

The influence of pipeline-backfill-trench interaction on the lateral soil resistance: A numerical investigation

Dong, X., Shiri, H., Zhang, W., and Randolph, M.F., 2021. The influence of pipeline-backfill-trench interaction on the lateral soil resistance: A numerical investigation, *Computers and Geotechnics*, 137 104307, <https://doi.org/10.1016/j.compgeo.2021.104307>.

DNV-RP-C205, 2019. Environmental conditions and environmental loads. Recommended practice, Det Norske Veritas.

DNV-RP-F204, 2017. Offshore Standard, Riser Fatigue. Recommended practice, Det Norske Veritas.

Einav, I. & Randolph, M. F., 2005. Combining upper bound and strain path methods for evaluating penetration resistance. *Int. J. Numer. Methods Engng* 63, No. 14, 1991–2016.

Elliott, B.J., Zakeri, A., Barrett, J., Hawlader, B., Li. G., Clukey, E.C., 2013. Centrifuge modeling of steel catenary risers at touchdown zone Part II: assessment of centrifuge test results using kaolin clay. *Ocean. Eng.* 60 (March) 208–218.

Faltinsen, O.M., 1990. Sea loads on ships and offshore structures. University of Cambridge.

Giertsen, E., Verley, R., Schroder, K., 2004. CARISIMA: A Catenary Riser/Soil Interaction Model for Global Riser Analysis. ASME 2004 23rd International Conference on Offshore Mechanics and Arctic Engineering, 633-640.

Hejazi, R., Kimiaei, M., 2016. Equivalent linear soil stiffness in fatigue design of steel catenary risers. *Ocean. Eng.* 111, 493–507.

Hodder, M. S., White, D. J., and Cassidy, M. J. 2008. Centrifuge modelling of riser-soil stiffness degradation in the touchdown zone of a steel catenary riser. *Proc., Int. Conf. on Offshore Mechanics and Arctic Engineering, OMAE2008, American Society of Mechanical Engineering, Estoril, Portugal.*

Hodder, M. S., White, D. J. & Cassidy, M. J. 2010. An analysis of soil strength degradation during episodes of cyclic loading, illustrated by the T-bar penetration test. *Int. J. Geomech.* 10, No. 3, 117–123.

Hodder, M. White, D. J. & Cassidy, M. J. 2009. Effect of remolding and reconsolidation on the touchdown stiffness of a steel catenary riser: Observations from centrifuge modelling. *Proceedings of the offshore technology conference, Houston, TX, USA, paper no. OTC 19871.*

Hodder, M. S., White, D. J. & Cassidy, M. J. 2013. An effective stress framework for the variation in penetration resistance due to episodes of remoulding and reconsolidation. *Géotechnique* 63, No. 1, 30–43, <https://doi.org/10.1680/geot.9.P.145>.

Hou, Z., Sahdi, F., Gaudi, C. & Randolph, M. F., 2018. Evolution of riser–soil stiffness in a soil crust layer. In *Proceedings of the 1st Vietnam symposium on advances in offshore engineering:*

*energy and geotechnics* (eds M. F. Randolph, D. H. Doan, A. M. Tang, M. Bui and V. N. Dinh), 130–136. Singapore: Springer Nature Singapore.



Janbazi, H., Shiri, H., 2022. An alternative vessel excitation algorithm to incorporate the trench effect into the fatigue analysis of steel catenary risers in the touchdown zone. *Applied Ocean Research*, <https://doi.org/10.1016/j.apor.2022.103292>.

Janbazi, H., Shiri, H., 2023. A hybrid model to simulate the trench effect on the fatigue analysis of steel catenary risers in the touchdown zone. *Can. Geotech. J.* Published online, <https://doi.org/10.1139/cgj-2022-0103>.

Kimiaei, M., Randolph, M., Ting, I. (2010) ‘A parametric study on effects of environmental loadings on fatigue life of steel catenary risers (using a nonlinear cyclic riser–soil interaction model)’, In: *Proceedings of the 29th International Conference on Ocean, Offshore and Arctic Engineering*, Shanghai, China, Paper OMAE2010-21153.

Kimiaei, M., 2017. Effects of non-linear riser-soil interaction model on fatigue design of steel catenary riser under random waves. *37th International Conference on Ocean, Offshore and Arctic Engineering*, Trondheim, Norway, OMAE2017-62295.

Langner, C., 2003. Fatigue life improvement of steel catenary risers due to self-trenching at the touchdown point. *Proceedings of the Offshore Technology Conference OTC 15104*, May 5-8.

Leira, B.J., Passano, E., Karunakaran, D., Farnes, K.A., Giertsen, E., 2004. Analysis guidelines and application of a riser–soil interaction model including trench effects. *Proceedings of the 23rd International Conference on Offshore Mechanics and Arctic Engineering OMAE 2004-51527*, , June 20-25, 955–962.

Li, F.Z., Low, Y.M., 2012. Fatigue reliability analysis of a steel catenary riser at the touchdown point incorporating soil model uncertainties. *Appl. Ocean Res.* 38, 100–110.

Muraleedharan, A., Kimiaei, M., 2018. Comparing results of time domain fatigue design of steel catenary risers using linear and non-linear riser soil interaction models under random waves. *Proceedings of the Offshore Technology Conference OTC 28571*, March 20-23.

Nakhaee, A., Zhang, J., 2008. Effects of the interaction with the seafloor on the fatigue life of a SCR, *Proceedings of the 18th International Society of Offshore and Polar Engineers Conference ISOPE-I-08-397*, July 6-11, 87–93.

Oliphant, J., Maconochie, A., White, D., and Bolton, M. 2009. Trench interaction forces during lateral SCR movement in deepwater clays. In *Proceedings of the Offshore Technology Conference, OTC-19944*, Houston, Texas, USA.

Randolph, M.F., Quiggin, P., 2009. Non-linear hysteretic seabed model for catenary pipeline contact. In: *Proceedings of the 28th International Conference on Ocean, Offshore and Arctic Engineering*. Honolulu, Hawaii, USA.

Randolph, M.F., Bhat, S., Mekha, B., 2013. Modeling the touchdown zone trench and its impact on SCR fatigue life. *Proceedings of the Offshore Technology Conference OTC-23975-MS*, <https://doi.org/10.4043/23975-MS> May 6-9.

Rezazadeh, K., Shiri, H., Zhang, L., Bai, Y., 2012. Fatigue generation mechanism in touchdown area of steel catenary risers in non-linear hysteretic seabed. *Res. J. Appl. Sci. Eng. Technol.* 4 (24), 5591–5601.

Schofield, A. N. & Wroth, C. P., 1968. Critical state soil mechanics. London, UK: McGraw-Hill.

Sharma, P.P., Aubeny, C.P., 2011. Advances in pipe-soil interaction methodology and application for SCR fatigue design, Proceedings of the Offshore Technology Conference OTC-21179-MS.

Shiri, H., Randolph, M., 2010. The influence of seabed response on fatigue performance of steel catenary risers in touchdown zone. In: Proceedings of the 29th international conference on offshore mechanics and arctic engineering, OMAE 2010, Shanghai, China, p. 20051.

Shiri, H., 2014a. Response of steel catenary risers on hysteretic non-linear seabed. Appl. Ocean. Res. 44 (January), 20–28.

Shiri, H., 2014b. Influence of seabed trench formation on fatigue performance of steel catenary risers in touchdown zone. Marine Structure. 36 (April), 1–20.

Shoghi, R., Shiri, H., 2019. Modeling touchdown point oscillation and its relationship with fatigue response of steel catenary risers. Appl. Ocean. Res. 87, 142-154.

Shoghi, R., Shiri, H., 2020. Re-assessment of trench effect on fatigue performance of steel catenary risers in the touchdown zone. Appl. Ocean Res. 94, 1–16.

Shoghi, R., Pesce, C. P., Shiri, H., 2021. Influence of trench geometry on fatigue response of steel catenary risers by using a boundary layer solution on a sloped seabed. Ocean Eng. 221, 108447.

Thethi, R., Moros, T., 2001. Soil interaction effects on simple catenary riser response. Deepwater Pipeline and Riser Technology Conference, Houston, Texas, USA.

Wang, K., Low, Y.M., 2016. Study of seabed trench induced by steel catenary riser and seabed interaction. Proceedings of the 35th International Conference on Ocean, Offshore and Arctic Engineering OMAE2016-54236.

White, D. J. & Hodder, M. 2010. A simple model for the effect on soil strength of episodes of remoulding and reconsolidation. *Can. Geotech. J.* 47, No. 7, 821–826.

Yuan, F., White, D. J. & O’Loughlin, C. D. 2017. The evolution of seabed stiffness during cyclic movement in a riser touchdown zone on soft clay. *Géotechnique* 67, No. 2, 127–137, <https://doi.org/10.1680/jgeot.15.P.161>.

Zargar, E., Kimiaei, M., Randolph, M.F., 2019. A new hysteretic seabed model for riser-soil interaction. *Marine Structures.* 64, 360-378.

Zhou, Z., White, D. J. & O’Loughlin, C. D. 2019. An effective stress framework for estimating penetration resistance accounting for changes in soil strength from maintained load, remoulding and reconsolidation. *Géotechnique* 69, No. 1, 57–71, <https://doi.org/10.1680/jgeot.17.P.217>.

Zhou, Z., O’Loughlin, C. D., White, D. J. 2020. An effective stress analysis for predicting the evolution of SCR-seabed stiffness accounting for consolidation. *Géotechnique* 70, No. 5, 448–467 <https://doi.org/10.1680/jgeot.18.P.313>.

## CHAPTER 8

### Conclusions, Limitations and Recommendations

#### 8.1. Conclusion

The current study has produced a range of crucial observations and conclusions that are recognized as significant contributions to the field of riser-seabed interaction, with a specific focus on SCRs as a case study. This study has undertaken comprehensive research to address various aspects, including the incorporation of remoulding and reconsolidation effects, water entrainment into the soil, and the formation of trenches beneath the risers. These efforts have effectively filled the existing gaps in the literature, resulting in significant advancements that have not been achieved before. The key findings of the study are summarized as follows:

- A time-dependent seabed model has been developed in this study by integrating effective stress analysis into the numerical analysis of SCR. This is achieved through a user-defined element coded in FORTRAN as a subroutine within the ABAQUS, allowing for a realistic simulation of a full-scale SCR during its life history.
- While the effective stress framework has been extensively studied in the literature, these investigations have been confined to a truncated section of sample pipes or SCRs, making it challenging to extrapolate their findings to the fatigue performance of the entire SCR due to the non-uniform nature of the consolidation effect along the TDZ.

- The proposed model takes into consideration the SCR-soil stiffness at each increment of dynamic analysis, accounting for the accumulation of damage around the pipe during cyclic motions, as well as the reconsolidation process resulting from the dissipation of excess pore pressure during intervening pause periods.
- The results of the consolidation assessment indicate a significant trend in stabilized soil stiffness, which is observed to increase by a factor of 1.9 when compared to the initial stiffness. Moreover, this recovered stiffness is found to be 2.2 times greater than the remoulded value typically employed in long-term fatigue analysis using non-linear soil models such as the R-Q model.
- The findings indicate a noteworthy 24% increase in peak fatigue damage, attributed to the full consolidation process with a 90% degree of dissipation. It is important to highlight that current non-linear hysteretic soil models utilized for global analysis of SCRs solely account for cyclic soil strength degradation, neglecting the consolidation effect. This overlooked consolidation effect could lead to an underestimation of fatigue damage in design practice, highlighting the significance of the present study.
- The simulation of a large deformation problem was carried out using the Coupled Eulerian-Lagrangian (CEL) technique within the Abaqus finite element (FE) software, in order to incorporate the water fluid as a third key influential parameter in the TDZ which has been neglected in the non-linear hysteretic SCR-soil models.

- A numerical analysis was conducted to evaluate the erosion of the seabed resulting from the combined effect of vortices generated by subsea fluid and the entrapment of water between the oscillating riser and the trenched seabed.
- A certain modification was proposed for the bearing capacity factors in order to account for the effects of water entrainment. This adjustment was achieved by fitting the bearing capacity force as well as the heave effect of the surrounding soil, with the corresponding numerical outcomes.
- The results indicate that water flow has the ability to infiltrate into gaps, creating additional pressure on the soil, leading to erosion or displacement. This phenomenon not only deepens the trench beneath the pipeline over time but also extends erosion to the surrounding berms as soil particles are carried away in a lateral direction. The influence of water entrainment, when combined with lateral oscillations, has the potential to exacerbate this situation and result in an estimated 60% increase in the depth of the trench.
- The impact of water entrainment has the potential to worsen when combined with lateral oscillations, leading to an estimated 60% increase in the depth of the trench, which has been neglected in the existing non-linear SCR-soil models.
- Despite previous research examining the impact of a trench on the fatigue behavior of SCRs in the TDZ, there remains an unresolved issue regarding whether the trench has a beneficial or detrimental effect. The potential source of this contradiction may be attributed to the methodologies employed for incorporating the trench in numerical simulations. The artificial insertion of pre-defined or mathematical

trench profiles create non-realistic contact pressure hot spots in the seabed, resulting in inaccurate results by distorting the damage distribution in the TDZ. Certain studies have attempted to address this issue by employing nonlinear hysteretic seabed interaction models to produce trench profiles that are consistent with the catenary shape of the riser. However, the cyclic trench formation is stabilized prematurely through a few oscillations achieving an embedment of 0.5D to 1D, which is much less than the ranges of 3.5D to 5D trenches observed in the field.

- The equivalent motion method (EMM) was developed as a methodology that introduces an alternative vessel excitation algorithm on a rigid seabed to achieve a target peak damage, which is derived from the same riser on a linear elastic seabed.
- The proposed solution, EMM, provides a reliable prediction of the damage in stiff seabed. However, as the seabed soil becomes softer, the EMM tends to slightly underestimate the stress range when compared to the linear elastic soil results.
- The EMM exhibits the capability to simulate accumulative fatigue damage with an average difference of less than 12%, highlighting its potential as a promising methodology for predicting the stress range of the riser with a reasonable level of accuracy. While the EMM showed relative accuracy in estimating peak damage, it is not a suitable approach for predicting the damage across the entire length of the riser.
- Another methodology known as the Hybrid Trench Model (HTM) was developed to reliably incorporate the trench effect into fatigue performance of SCR by



combining a linear soil stiffness and a nonlinear hysteretic seabed interaction model. This hybrid model enables the simulation of a trench profile that is entirely compatible with the natural catenary shape of the SCR by providing an equivalent stiffness distribution in the TDZ.

- The HTM was introduced as a solution to address issues commonly found in previous literature, such as inconsistencies between the natural catenary shape of the riser and the trench profile, as well as premature stabilization.
- It was possible to estimate the gradual cyclic embedment produced by the nonlinear soil model, e.g., R-Q, by using appropriate values for two dimensionless parameters,  $\alpha$  and  $\eta$ , within the HTM. The stress range results obtained from HTM showed good agreement with the R-Q model, exhibiting a maximum relative difference of 5.75% in the maximum stress range.
- Despite the HTM uses intelligent approach in generating a trench profile that is completely compatible with the natural catenary shape of the riser, the trench mouth still leads to a sudden increase in contact force, albeit less severe than the mathematical trench insertions.
- The findings indicate that a trenched seabed offers beneficial effects on fatigue performance during lower amplitudes of vessel motions, primarily due to reduced TDP oscillations and a consequent decrease in the impact of contact pressure hotspots at the trench mouth. However, this effect could potentially become detrimental when motion amplitudes reach extreme levels, leading to the formation

of abrupt contact hotspots at the trench mouth. These findings presumably imply why different authors have reported contradictory results for the effect of the trench on fatigue damage.

## **8.2. Limitations**

While specific limitations were discussed individually in each chapter, here is a summary of the overall limitations. The effective stress analysis in the current research consists of two components: remolding conditions under episodic loading and consolidation effects during the pause period. It is worth noting that this methodology could be implemented as continuous loading instead of episodic loading to more accurately capture dissipation. However, this continuous loading approach would require significant computational resources and time to accurately represent the real dissipation process. Chapter 4 focused on SCR-soil-seawater interaction using the CEL technique. However, it has limitations in simulating water flow with varying velocities, which is particularly relevant in shallow water areas where waves and currents are more significant. To address this, the use of Computational Fluid Dynamics (CFD) techniques can provide a more precise representation, especially for capturing scouring effects around soils. The EMM was employed in chapter 5 demonstrates high accuracy in predicting peak fatigue damage. However, it has certain constraints when it comes to predicting damage across the entire length of TDZ.

### **8.3. Recommendations for Future Study**

The riser-seabed interaction is a complex phenomenon encompassing various aspects that require in-depth investigation. The following research works are recommended for future studies:

- To enhance the numerical model incorporated within the effective stress framework, it is suggested to consider continuous cyclic loading instead of episodic loading, as this better reflects the actual loading conditions and enables the incorporation of the real dissipation rate during the consolidation process. This investigation will be applicable to both Steel Catenary Risers and Steel Lazy Wave Risers, providing valuable insights into their behavior and performance in various operational conditions.
- In the current study, a comprehensive analysis was performed on Fluid-Pipe-Soil interaction, with specific attention given to the water entrainment effect. To further advance the research, it would be intriguing to incorporate the current flow as well into cohesive soil. These findings could be integrated into existing non-linear soil models, which primarily consider the interaction between the pipe and soil while disregarding the fluid as a third influential parameter.
- An important aspect to investigate is whether the actual fully developed trench profile effectively accommodates all riser configurations throughout their operational lifespan without giving rise to pressure hot spots, particularly at the trench mouth.

- While the trench mouth may introduce certain challenges, it offers some benefits in improving fatigue lifetime, particularly in lower TDP oscillations. Subsea surveys play a vital role in obtaining essential data to conduct a reliable assessment of the trench effect on fatigue in the TDZ. With the gathered information, appropriate mitigation procedures can be implemented to effectively reduce fatigue damage and enhance the long-term performance of SCRs.

## Bibliography

Al-Janabi, H.A., and Aubeny, C.P. 2019. Experimental Measurement of Thixotropy and Sensitivity in Gulf of Mexico Clay. In the International Society of Offshore and Polar Engineers Conference, 2019-TPC-0593. Honolulu, HI, USA.

Al-Janabi, H.A., Aubeny, C.P., Chen, J., and Luo, M. (2019). “Experimental measurement of touchdown zone stiffness for SCR in Gulf of Mexico clay.” In Offshore Technology Conference, 6–9 May, OTC-29504-MS, Houston, Texas, USA.

Al-Janabi, H.A., Aubeny, C.P., Chen, J., and Luo, M. (2020). “Experimental measurement of monotonic and cyclic lateral resistance of risers and pipelines in Gulf of Mexico clays.” *Can. Geotech. J.* 57, 1534–1549.

API-STD-2RD. (2013). “Standard for riser systems that are part of a floating production system (FPS).” American Petroleum Institute, Washington, DC, USA.

Aubeny, C. P., Shi, H., and Myrff, J. D. (2005). “Collapse loads for a cylinder embedded in trench in cohesive soil.” *International Journal of Geomechanics*, ASCE, 5(4), 320-325.

Aubeny, C., and Biscontin, G., (2008). “Interaction model for Steel Compliant Riser on Soft Seabed.” OTC194193, Houston, TX.

Aubeny, C., and Biscontin, G., (2009). “Seafloor-Riser Interaction Model.” *International Journal of Geomechanics* 9(3), 133–141.

Aubeny, C., White, T., Langford, T., Meyer, V. & Clukey, E. (2015). "Seabed stiffness model for steel catenary risers." In *Frontiers in offshore geotechnics III* (ed. V. Meyer), pp. 351–356.

Barbosa-Cruz, E.R., and Randolph, M.F. (2005). "Bearing capacity and large penetration of a cylindrical object at shallow embedment." In *Proceedings of the 1<sup>st</sup> International Symposium on Frontiers in Offshore Geotechnics (ISFOG)*. pp. 615–621. doi:10.1201/NOE0415390637.ch67.

Bolton, M. D., 1979. *A guide to soil mechanics*. London, UK: Macmillan.

Bridge, C. (2005). "Effects of seabed interaction on steel catenary risers." (Ph.D. thesis). University of Surrey.

Bridge, C., Laver, K., Clukey, E., and Evans, T. (2004), "Steel Catenary Riser Touchdown Point Vertical Interaction Models." *Offshore Technology Conference*, Houston, Texas, USA, OTC16628.

Bridge, C., and Willis, N. (2002), "Steel Catenary Risers—Results and Conclusions from Large Scale Simulations of Seabed Interaction." *14<sup>th</sup> Annual Conference Deep Offshore Technology*, Cape Town, South Africa, 40-60.

Bridge, C., Howells, H. (2007). "Observations and modeling of steel catenary riser trenches." In: *The seventeenth international offshore and polar engineering conference, ISOPE 2007*, Lisbon, Portugal.

Brørs, B., 1999. "Numerical modeling of flow and scour at pipelines." *J. Hydraul. Eng.* 125, 511–523.

Campbell, M. (1999). “The Complexities of Fatigue Analysis for Deepwater Risers.” Deepwater Pipeline Conference, New Orleans, USA.

Cathie, D. N., Jaeck, C., Ballard, J. C., and Wintgens, J. F. (2005). “Pipeline geotechnics—State of the Art.” Proceedings of the international symposium on frontiers in offshore geotechnics, Perth, Australia, 95–114.

Chatterjee, S., White, D. J. & Randolph, M. F. (2013). “Coupled consolidation analysis of pipe–soil interactions.” *Can. Geotech. J.* 50, No. 6, 609–619.

Chatterjee, S., Randolph, M.F., White, D., 2012a. The effects of penetration rate and strain softening on the vertical penetration resistance of seabed pipelines. *Géotechnique*, vol. 62, no. 7, p. 573.

Chatterjee, S., White, D., Randolph, M.F., (2012b). “Numerical simulations of pipe-soil interaction during large lateral movements on clay.” *Géotechnique*, vol. 62, no. 8, p. 693.

Chen, J., Newlin, J.A., Luo, M., Zhang, H., Hadley, C.J., Hu, S. (2019). “Practice of Riser-Soil Interactions at Touch Down Zones for Steel Catenary Risers.” Offshore Technology Conference, 6-9 May, Houston, Texas.

Clukey, E. C., Hausermans, L. & Dyvik, R. (2005). “Model tests to simulate riser–soil interaction in touchdown point region.” In *Frontiers in offshore geotechnics* (eds S. Gourvenec and M. Cassidy), pp. 651-658. Boca Raton, FL, USA: CRC Press/ Balkema.

Clukey, E.C., Ghosh, R., Mokalala, P., Dixon, M. (2007). “Steel catenary riser (SCR) design issues at touchdown area.” Proceedings of the 17<sup>th</sup> International Offshore and Polar Engineering Conference ISOPE-I-07-388, <https://doi.org/10.4043/22557-MS> July 1-6.

Clukey, E. C., Young, A. G., Dobias, J. R. & Garmon, G. R. (2008). “Soil response and stiffness laboratory measurements of SCR pipe/soil interaction.” Proceedings of the offshore technology conference, Houston, TX, USA, paper no. OTC 19303.

Clukey, E., Jacobs, P., and Sharma, P.P. (2008) “Investigation of riser seafloor interaction using explicit finite element methods.” Offshore Technology Conference, Houston, Texas, OTC19432-MS.

Clukey, E.C., Tognarelli, M.A., Li, G., Ghosh, R., Phillips, R., Zakeri, A., Elliot, B.J., Bhattacharyya, A., Sun, Q. (2011). “Simulation of SCR behaviour at touchdown zone – part II: testing of a sectional SCR model in a geotechnical centrifuge.” Offshore Technology Conference 2011, Brazil, 4-6 October.

Clukey, E. C., Aubeny, C. P., Randolph, M. F., Sharma, P. P., White, D. J., Sancio, R. & Cerkovnik, M. (2017). “A Perspective on the state of knowledge regarding soil-pipe interaction for SCR fatigue assessments.” Proceedings of the offshore technology conference, Houston, TX, USA, paper no. OTC 27564.

Clukey, E.C., Zakeri, A., (2017). “Recent Advances in Nonlinear Soil Models for Fatigue Evaluation of Steel Catenary Risers SCRs.” Offshore Technology Conference, 1-4 May, Houston, Texas, USA.

Cheng, L., Yeow, K., Zang, Z., and Li, F. (2014). “3D scour below pipelines under waves and combined waves and currents.” Coastal Eng., 83, 137–149.

DNV-RP-C205, (2019). “Environmental conditions and environmental loads.” Recommended practice, Det Norske Veritas.



DNV-RP-F204, (2017). “Offshore Standard, Riser Fatigue.” Recommended practice, Det Norske Veritas.

Dong, X., Shiri, H. (2018). “Performance of nonlinear seabed interaction models for steel catenary riser, Part I: nodal response.” *Ocean Eng.* 154, 153–166.

Dong, X., Shiri, H. (2019). “Performance of nonlinear seabed interaction models for steel catenary riser, Part II: global response.” *Appl. Ocean. Res.* 82, 158-174.

Dong, X., Zhang, W., Shiri, H., Randolph, M.R., (2021). “Large deformation coupled analysis of embedded pipeline – Soil lateral interaction.” *Marine Structures* 78, 102971.

Draper, S., An, H., Cheng, L., White, D. J., Griffiths, T. (2015). “Stability of subsea pipelines during large storms.” *Phil. Trans. R. Soc. A* 373: 20140106. <http://dx.doi.org/10.1098/rsta.2014.0106>.

Dutta, S., Hawlader, B., Phillips, R., (2014). “Finite element modeling of partially embedded pipelines in clay seabed using Coupled Eulerian–Lagrangian method.” *Can. Geotech. J.* 52: 58–72, <https://doi.org/10.1139/cgj-2014-004>.

Einav, I. & Randolph, M. F. (2005). “Combining upper bound and strain path methods for evaluating penetration resistance.” *Int. J. Numer. Methods Engng* 63, No. 14, 1991–2016.

Elliott, B. J., Zakeri, A., Barrett, J., Macneill, A., Phillips, R., Clukey, E. C., and Li, G. (2013). “Centrifuge modeling of steel catenary risers at touchdown zone Part I: Development of novel centrifuge experimental apparatus.” *Ocean Engineering*, March 1; 60, 200-207. <https://doi.org/10.1016/j.oceaneng.2012.11.012>.

Elliott, B.J., Zakeri, A., Barrett, J., Hawlader, B., Li, G., Clukey, E.C. (2013). “Centrifuge modeling of steel catenary risers at touchdown zone Part II: assessment of centrifuge test results using kaolin clay.” *Ocean. Eng.* 60 (March) 208–218.

Faltinsen, O.M., (1990.) “Sea loads on ships and offshore structures.” University of Cambridge.

Fuhrman, D. R., Baykal, C., Sumer, B. M., Jacobsen, N. G., and Fredsøe, J. (2014). “Numerical simulation of wave-induced scour and backfilling processes beneath submarine pipelines.” *Coastal Eng.*, 94, 10–22.

Fouzder, A., Zakeri, A., and Hawlader, B. (2012). “Steel catenary risers at touchdown zone - A fluid dynamics approach to the water-riser-soil interaction”, 9<sup>th</sup> Int. Pipeline Conf., Calgary, V4, 31-36.

Giertsen, E., Verley, R., Schroder, K. (2004). “CARISIMA: A Catenary Riser/Soil Interaction Model for Global Riser Analysis.” ASME 2004 23<sup>rd</sup> International Conference on Offshore Mechanics and Arctic Engineering 2004, pp. 633-640.

Gourvenec, S. M. & White, D. J. (2010). “Elastic solutions for consolidation around seabed pipelines.” Proceedings of the offshore technology conference, Houston, TX, USA, paper no. OTC 20554.

Hejazi, R., Kimiaei, M. (2016). “Equivalent linear soil stiffness in fatigue design of steel catenary risers.” *Ocean. Eng.* 111, 493–507.

Hodder, M. S., White, D. J., and Cassidy, M. J. (2008). “Centrifuge modelling of riser-soil stiffness degradation in the touchdown zone of a steel catenary riser.” *Proc., Int. Conf. on*

Offshore Mechanics and Arctic Engineering, OMAE2008, American Society of Mechanical Engineering, Estoril, Portugal.

Hodder, M. White, D. J. & Cassidy, M. J. (2009). “Effect of remolding and reconsolidation on the touchdown stiffness of a steel catenary riser: Observations from centrifuge modelling.” Proceedings of the offshore technology conference, Houston, TX, USA, paper no. OTC 19871.

Hodder, M. S., White, D. J. & Cassidy, M. J. (2010). “An analysis of soil strength degradation during episodes of cyclic loading, illustrated by the T-bar penetration test.” *Int. J. Geomech.* 10, No. 3, 117–123.

Hodder, M. S., White, D. J. & Cassidy, M. J. (2013). “An effective stress framework for the variation in penetration resistance due to episodes of remoulding and reconsolidation.” *Géotechnique* 63, No. 1, 30-43, <https://doi.org/10.1680/geot.9.P.145>.

Hou, Z., Sahdi, F., Gaudi, C. & Randolph, M. F. (2018). “Evolution of riser–soil stiffness in a soil crust layer.” In Proceedings of the 1st Vietnam symposium on advances in offshore engineering: energy and geotechnics (eds M. F. Randolph, D. H. Doan, A. M. Tang, M. Bui and V. N. Dinh), pp. 130–136. Singapore: Springer Nature Singapore.

House, A., Olivera, J. R. M. S. & Randolph, M. F. (2001). “Evaluating the coefficient of consolidation using penetration tests.” *Int. J. Phys. Modelling Geotech.* 1, No. 3, 17–26.

Howells H. (1995). “Advances in Steel Catenary Riser Design.” 2H Offshore Engineering Ltd, Surrey.

Hu, Y., and Randolph, M.F. (1998). “Deep penetration of shallow foundations on non-homogeneous soil.” *Soils and Foundations*, 38(1): 241–246. doi:10.3208/sandf.38.241.

Janbazi, H., Shiri, H. (2022). “An alternative vessel excitation algorithm to incorporate the trench effect into the fatigue analysis of steel catenary risers in the touchdown zone.” *Applied Ocean Research*, 126-103292.

Janbazi, H., Shiri, H. (2023a). “A hybrid model to simulate the trench effect on the fatigue analysis of steel catenary risers in the touchdown zone.” *Can. Geotech. J.* Published online, <https://doi.org/10.1139/cgj-2022-0103>.

Janbazi, H., Shiri, H. (2023b). “Investigation of trench effect on fatigue response of steel catenary risers using an effective stress analysis.” *Computers and Geotechnics*, 160, 105506, <https://doi.org/10.1016/j.compgeo.2023.105506>.

Kimiaei, M., Randolph, M., Ting, I. (2010). “A parametric study on effects of environmental loadings on fatigue life of steel catenary risers (using a non-linear cyclic riser–soil interaction model).” In: *Proceedings of the 29th International Conference on Ocean, Offshore and Arctic Engineering*, Shanghai, China, Paper OMAE2010-21153.

Kimiaei, M. (2017). “Effects of non-linear riser-soil interaction model on fatigue design of steel catenary riser under random waves.” *37<sup>th</sup> International Conference on Ocean, Offshore and Arctic Engineering*, Trondheim, Norway, OMAE2017-62295.

Langford, T. and Aubeny, C. (2008). “Model tests for steel catenary riser in marine clay.” *Proceedings of the Offshore Technology Conference*, Paper 19495, Houston, USA.

Langner, C. (2003). “Fatigue life improvement of steel catenary risers due to self- trenching at the touchdown point.” Proceedings of the Offshore Technology Conference, OTC 15104, May 5-8.

Larsen C. M., Halse K. H., (1997). “Comparison of models for vortex-induced vibrations of slender marine structures.” *Marine Structures* 1997 July; 10(6):413-441. [https://doi.org/10.1016/S0951-8339\(97\) 00011-7](https://doi.org/10.1016/S0951-8339(97) 00011-7).

Larsen, B.E., Fuhrman, D.R., Sumer, B.M., (2016). “Simulation of wave-plus-current scour beneath submarine pipelines.” *J. Waterw. Port, Coast. Ocean Eng.* 142, 04016003.

Leeuwestein, W., Bijker, E. W., Peerbolte, E. B., Wind, H. G., (1985). “The Natural Self Burial of Submarine Pipelines.” *Behaviour of Offshore Structures*, Elsevier Publishers, pp717-728.

Lehane, B., O’Loughlin, C., Gaudin, C., and Randolph, M. (2009). “Rate effects on penetrometer resistance in kaolin.” *Géotechnique*, 59(1): 41–52 [doi:10.1680/geot.2007.00072](https://doi.org/10.1680/geot.2007.00072).

Leira, B.J., Passano, E., Karunakaran, D., Farnes, K.A., Giertsen, E. (2004). “Analysis guidelines and application of a riser–soil interaction model including trench effects.” Proceedings of the 23<sup>rd</sup> International Conference on Offshore Mechanics and Arctic Engineering OMAE 2004-51527, 955–962, June 20-25.

Li, F., Cheng, L., (2000). “Numerical simulation of pipeline local scour with lee-wake effects.” *Int. J. Offshore Polar Eng.* 10.

Li, F., Cheng, L., (2001). "Prediction of lee-wake scouring of pipelines in currents." *J. Waterw. Port, Coast. Ocean Eng.* 127, 106–112.

Li, F.Z., Dwivedi, A., Low, Y., and Hong, J. (2013). "Experimental investigation on scour under a vibrating catenary riser." *Journal of Engineering Mechanics*, vol. 139, No. 7.

Li, Y., Ong, M.C., Fuhrman, D.R., Larsen, B.E., (2020). "Numerical investigation of waveplus-current induced scour beneath two submarine pipelines in tandem." *Coast. Eng.* 156, 103619.

Li, F., Cheng, L., (2000). "Numerical simulation of pipeline local scour with lee-wake effects." *Int. J. Offshore Polar Eng.* 10.

Li, F., Cheng, L., (2001). "Prediction of lee-wake scouring of pipelines in currents." *J. Waterw. Port, Coast. Ocean Eng.* 127, 106–112.

Li, F.Z., Low, Y.M. (2012). "Fatigue reliability analysis of a steel catenary riser at the touchdown point incorporating soil model uncertainties." *Appl. Ocean Res.* 38, 100–110.

Liang D., Cheng, L., Li, F., (2005a). "Numerical modeling of flow and scour below a pipeline in currents Part I. Flow simulation." *Coastal Engineering* 52 25-42.

Liang D., Cheng, L., Li, F., (2005b). "Numerical modeling of flow and scour below a pipeline in currents Part II." *Coastal Engineering* 52 43-62.

Liu, J. (2018). "Numerical modelling of seabed trench and its effect on the structural response of steel catenary riser." PhD Thesis University of Western Australia.

Lu, Y., Chiew, Y.M., Cheng, N.S., (2008). "Review of seepage effects on turbulent open channel flow and sediment entrainment." *J. Hydraul. Res.* 46, 476–488.

Lucassen, R. J., (1984). "Scour underneath submarine pipelines." Rep. No. PL-4 2A, Netherlands Marine Technical Research, Netherlands Industrial Council for Oceanology, Delft Univ. of Technology, Delft, The Netherlands.

Lu, Y., Chiew, Y.-M., (2007). "Seepage effects on dune dimensions." *J. Hydraul. Eng.* 133, 560–563.

Lu, Y., Chiew, Y.-M., Cheng, N.-S., (2008). "Review of seepage effects on turbulent open channel flow and sediment entrainment." *J. Hydraul. Res.* 46, 476–488.

Mao, Y., (1986). "The interaction between a pipeline and an erodible bed. Series Paper No. 39, Institute of Hydrodynamic and Hydraulic Engineering." Technical Univ. of Denmark, Copenhagen, Denmark.

Martin, C.M., White, D.J. (2012). "Limit analysis of the undrained capacity of offshore pipelines." *Géotechnique* 62 (9) 847–863.

Merifield, R. S., White, D. J. & Randolph, M. F. (2008). "The ultimate undrained resistance of partially embedded pipelines." *Geotechnique* 58, No. 6, 461–470, <http://dx.doi.org/10.1680/geot.2007.00097>.

Merifield, R.S., White, D.J., and Randolph, M.F. (2009). "Effect of surface heave on response of partially embedded pipelines on clay." *Journal of Geotechnical and Geoenvironmental Engineering*, 135(6): 819–829. doi:10.1061/(ASCE)GT. 1943-5606.0000070.

Muraleedharan, A., Kimiaei, M. (2018). "Comparing results of time domain fatigue design of steel catenary risers using linear and non-linear riser soil interaction models under

random waves.” Proceedings of the Offshore Technology Conference OTC 28571, March 20-23.

Myrhaug, D., Ong, M. C., Føien, H., Gjengedal, C., and Leira, B. J. (2009). “Scour below pipelines and around vertical piles due to second-order random waves plus current.” *Ocean Eng.*, 36(8), 605–616.

Nakhaee, A., Zhang, J., (2008). “Effects of the interaction with the seafloor on the fatigue life of a SCR.” Proceedings of the 18<sup>th</sup> International Society of Offshore and Polar Engineers Conference ISOPE-I-08-397; 2008 July 6-11; Vancouver, Canada. pp 87-93.

Ogbeifun, A. M., Oterkus, S., Race, J., Naik, H., Moorthy, D., Bhowmik, S., Ingram, J. (2021). “Vessel relocation solution for steel catenary riser touch down fatigue management.” *Ocean Eng.* 237, 109632.

Ogbeifun, A. M., Oterkus, S., Race, J., Naik, H., Moorthy, D., Bhowmik, S., Ingram, J. (2022). “Vessel relocation strategy for multiple steel catenary riser fatigue damage mitigation.” *Ocean Eng.* 248, 110493.

Oliphant, J., Maconochie, A., White, D., and Bolton, M. (2009). “Trench interaction forces during lateral SCR movement in deepwater clays.” In Proceedings of the Offshore Technology Conference, OTC-19944, Houston, Texas, USA.

Orcina Ltd. (1986). “Orcaflex User Manual.” Cumbria, UK.

Palmer, A. (1997). “Geotechnical evidence of ice scour as a guide to pipeline burial depth.” *Can. Geotech. J.* 34, No. 6, 1002–1003.



Pesce, C. P., Aranha, J. A. P., and Martins, C. A. (1998). "The Soil Rigidity Effect in the Touchdown Boundary-Layer of a Catenary Riser: Static Problem." Eighth International Offshore and Polar Engineering Conference, Montreal, Canada, 207-213.

Phifer, E. H., Frans, K., Swanson, R. C., Allen, D. W., and Langner, C. G. (1994), "Design And Installation Of Auger Steel Catenary Risers." Offshore Technology Conference, Houston, Texas, USA, OTC7620.

Pike, K., Duan, G., Sun, J., and Jukes, P. (2010). "Comprehensive FEA of thermal mitigation buoyancy module (TMBM)-soil interaction using the coupled Eulerian-Lagrangian (CEL) method." In Proceedings of the 28<sup>th</sup> International Conference on Ocean, Offshore and Arctic Engineering, OMAE 2009, Honolulu, Hawaii, 31 May – 5 June 2009. pp. 865–870. doi: 10.1115/OMAE2010-20885.

Quéau, L.M., Kimiaei, M., Randolph, M.F. (2013). "Dimensionless groups governing response of steel catenary risers." *Ocean Eng.* 74, 247–259.

Quéau, L.M., Kimiaei, M., Randolph, M.F. (2014a). "Analytical estimation of static stress range in steel catenary risers at touchdown area and its application with dynamic amplification factors." *Ocean. Eng.* 88, 63–80.

Quéau, L.M. (2015). "Estimating the fatigue damage of steel catenary risers in the touchdown zone." (Ph.D. thesis), The University of Western Australia.

Quintin, H., Legras, J. L., Huang, K., and Wu, M. (2007). "Steel Catenary Riser Challenges and Solutions for Deepwater Applications." Offshore Technology Conference, Houston, Texas, USA, OTC19118.

- Randolph, M. F. (2004). "Characterization of soft sediments for offshore applications." Keynote lecture. Proc. 2nd Int. Conf. on Site Characterization, Porto, Portugal 1, 209–231. Rotterdam, The Netherlands: Millpress Science Publishers.
- Randolph, M. F., and White, D. J. (2008) "Pipeline embedment in deep water: processes and quantitative assessment." Offshore Technology Conf., Houston, USA, OTC 19128.
- Randolph, M.F., Quiggin, P. (2009). "Non-linear hysteretic seabed model for catenary pipeline contact." In: Proceedings of the 28<sup>th</sup> International Conference on Ocean, Offshore and Arctic Engineering. Honolulu, Hawaii, USA.
- Randolph, M.F., Bhat, S., Mekha, B. (2013). "Modeling the touchdown zone trench and its impact on SCR fatigue life." Proceedings of the Offshore Technology Conference 2013, OTC-23975-MS, <https://doi.org/10.4043/23975-MS> May 6-9.
- Rezazadeh, K., Shiri, H., Zhang, L., Bai, Y. (2012). "Fatigue generation mechanism in touchdown area of steel catenary risers in nonlinear hysteretic seabed." Res. J. Appl. Sci. Eng. Technol. 4 (24), 5591–5601.
- Schofield, A. N. & Wroth, C. P. (1968). "Critical state soil mechanics." London, UK: McGraw-Hill.
- Sharma, P.P., Aubeny, C.P. (2011). "Advances in pipe-soil interaction methodology and application for SCR fatigue design." Proceedings of the Offshore Technology Conference OTC-21179-MS.
- Shiri H., (2010). "Influence of seabed response on fatigue performance of steel catenary risers in touchdown zone." PhD Thesis, University of Western Australia.

Shiri, H., Randolph, M. (2010). "The influence of seabed response on fatigue performance of steel catenary risers in touchdown zone." In: Proceedings of the 29<sup>th</sup> international conference on offshore mechanics and arctic engineering, OMAE 2010, Shanghai, China, p. 20051.

Shiri, H. (2014a). "Response of steel catenary risers on hysteretic non-linear seabed." Appl. Ocean. Res. 44 (January), 20–28.

Shiri, H. (2014b). "Influence of seabed trench formation on fatigue performance of steel catenary risers in touchdown zone." Marine Structure. 36 (April), 1–20.

Shoghi, R., Shiri, H. (2019). "Modeling touchdown point oscillation and its relationship with fatigue response of steel catenary risers." Appl. Ocean. Res. 87, 142-154.

Shoghi, R., Shiri, H. (2020). "Re-assessment of trench effect on fatigue performance of steel catenary risers in the touchdown zone." Appl. Ocean Res. 94, 1-16.

Shoghi, R., Pesce, C. P., Shiri, H. (2021). "Influence of trench geometry on fatigue response of steel catenary risers by using a boundary layer solution on a sloped seabed." Ocean Eng. 221, 108447.

Smith, H.D., Foster, D.L., (2005). "Modeling of flow around a cylinder over a scoured bed." J. Waterw. Port, Coast. Ocean Eng. 131, 14-24

Staub, C., Bijker, R., (1990). "Dynamic Numerical Models for Sandwaves and Pipeline Self-Burial." Journal of Coastal Engineering.

Sumer, B.M., Fredsbe, J., (2002). "The Mechanics of Scour in the Marine Environment." World Scientific, Singapore.

Sumer, B.M., Baykal, C., Fuhrman, D.R., Jacobsen, N.G. & Fredsøe, J., (2014). “Numerical calculation of backfilling of scour holes.” Proceedings of the 7<sup>th</sup> International Conference on Scour and Erosion, ICSE-7 Perth.

Sumer, B. M., Fredsøe, J., (1993). “Self Burial of Pipelines at Span Shoulders.” Proceedings of the International Symposium in Offshore and Polar Engineering, I-93-111.

Sumer, B.M., Fredsøe, J., (1996). “Scour Around Pipelines in Combined Waves and Current.” Technical Report American Society of Mechanical Engineers, New York, NY (United States).

Thethi, R., Moros, T. (2001). “Soil interaction effects on simple catenary riser response.” Deepwater Pipeline and Riser Technology Conference, Houston, Texas, USA.

Tom, J.G., Draper, S., White, D.J., (2018). “Sediment transport and trench development beneath a cylinder oscillating normal to a sandy seabed.” Coastal Engineering 140, 395-410.

Wang, D., White, D. J., and Randolph, M. F., (2010). “Large-Deformation Finite Element Analysis of Pipe Penetration and Large-Amplitude Lateral Displacement.” Can. Geotech. J., 47(8), pp. 842–856.

Wang, K., Low, Y.M. (2016). “Study of seabed trench induced by steel catenary riser and seabed interaction.” Proceedings of the 35th International Conference on Ocean, Offshore and Arctic Engineering OMAE2016-54236, June 19-24.

Wang, K., Xue, H., Tang, W., Guo, J. (2013). “Fatigue analysis of steel catenary riser at touch-down point based on linear hysteretic riser-soil interaction model.” *Ocean. Eng.* 68, 102–111.

White, D. J. & Hodder, M. (2010). “A simple model for the effect on soil strength of episodes of remoulding and reconsolidation.” *Can. Geotech. J.* 47, No. 7, 821–826.

Yuan, F., White, D. J. & O’Loughlin, C. D. (2017). “The evolution of seabed stiffness during cyclic movement in a riser touchdown zone on soft clay.” *Géotechnique* 67, No. 2, 127–137, <https://doi.org/10.1680/jgeot.15.P.161>.

Zargar, E., Kimiaei, M., Randolph, M.F. (2019). “A new hysteretic seabed model for riser-soil interaction.” *Marine Structures*, 64, 360-378, <https://doi.org/10.1016/j.marstruc.2018.08.002>.

Zargar, E. (2017). “New hysteretic seabed model for riser-soil interaction.” PhD Thesis, University of Western Australia.

Zhao, Y., Haveman, C. E., Cribbs, A. R., Miller, J. D. (2015). “Global benefits and operational challenges of vessel relocation, Proceedings of the 34<sup>th</sup> International Conference on Ocean, Offshore and Arctic Engineering OMAE2015 May 31-June 5, St. John's, Newfoundland, Canada.

Zhao, F., Griffiths, T., Shen, W., Draper, S., An, H., Leggoe, J., Carneiro, D., (2015) “Sediment Attractors: Seabed Shear Stress Shadows Around Subsea Pipelines Cause Net Sediment Accretion.” OMAE2015-41651.

Zhou, H. & Randolph, M. F. (2007). “Computational techniques and shear band development for cylindrical and spherical penetrometers in strain-softening clay.” *Int. J. Geomech.* 7, No. 4, 287–295.

Zhou, H. & Randolph, M. F. (2009). “Resistance of full-flow penetrometers in rate-dependent and strain-softening clay.” *Géotechnique* 59, No. 2, 79–86, <http://dx.doi.org/10.1680/geot.2007.00164>.

Zhou, Z., White, D. J. & O’Loughlin, C. D. (2019). “An effective stress framework for estimating penetration resistance accounting for changes in soil strength from maintained load, remoulding and reconsolidation.” *Géotechnique* 69, No. 1, 57–71, <https://doi.org/10.1680/jgeot.17.P.217>.

Zhou, Z., O’Loughlin, C. D., White, D. J. (2020). “An effective stress analysis for predicting the evolution of SCR-seabed stiffness accounting for consolidation.” *Géotechnique* 70, No. 5, 448–467. <https://doi.org/10.1680/jgeot.18.P.313>.

## **APPENDIX**

## **Appendix A**

# **Incorporation of the Compatible Trench into the SCR Fatigue Performance by Using an Equivalent Soil Stiffness Methodology**

Hossein Janbazi<sup>1</sup>, Hodjat Shiri<sup>2</sup>

1: Department of Civil Engineering  
Memorial University of Newfoundland  
e-mail: [hjanbaziokn@mun.ca](mailto:hjanbaziokn@mun.ca)

2: Department of Civil Engineering  
Memorial University of Newfoundland  
e-mail: [hshiri@mun.ca](mailto:hshiri@mun.ca)

This paper was presented in the 33<sup>rd</sup> International Ocean and Polar Engineering Conference (ISOPE 2023), Ottawa, Canada, June 19-23.



## **Abstract**

Several studies have incorporated the trench effect into the SCR's fatigue analysis based on the two main approaches: artificial insertion of a trench profile in the TDZ, and automated trench formation using non-linear hysteretic riser-seabed interaction models. There have been contradictory results with no coherent agreement on the beneficial or detrimental effect of the trench on fatigue life. The current study has been conducted to resolve existing challenges by proposing a reliable methodology by defining an equivalent stiffness to generate a consistent trench profile entirely compatible with the natural curvature of the SCR in the TDZ.

**Keywords:** Steel Catenary Riser; equivalent linear stiffness; nonlinear soil model; trench formation; fatigue analysis; hotspot contact

## **A.1. Introduction**

Steel Catenary Risers (SCRs) are widely used in deep-water offshore facilities to convey hydrocarbon products from the seabed to the floating structures. Due to the cyclic motion of the floating vessel, the riser repeatedly makes contact with the seabed resulting in progressive soil degradation in touchdown zone (TDZ), leading to the gradual penetration of the riser into the seabed. Subsea surveys showed that this riser embedment further develops over the early years of riser operation (first 2-3 years of operation), reaching the ultimate profile with a maximum depth of around  $3.5D$  to  $5D$ , where  $D$  is the pipe diameter (Thethi and Moros, 2001; Bridge and Howells, 2007). Previous studies have widely investigated the influence of the trench effect on the fatigue analysis of catenary risers, particularly SCRs. Some of the studies have shown the fatigue life improvement in the TDZ due to trench formation (e.g., Langner, 2003; Nakhaei and Zhang, 2008; Elliot et al., 2013; Randolph et al., 2013; Sharma and Aubeny, 2011; Wang et al., 2016), while other studies have shown a reduced fatigue life (e.g., Leira, 2004; Giertsen, 2004; Shiri and Randolph 2010; Rezazadeh et al., 2012; Shiri, 2014a, b; Zargar 2017). Also, some studies have obtained scattered results showing improved or reduced fatigue life because of trench formation (Randolph et al., 2013; Dong and Shiri, 2019; Shoghi and Shiri, 2019; 2020). It can be seen that there is not a coherent answer among the researchers, and the beneficial or detrimental effect of the trench is still a point of the question. Shoghi and Shiri (2020) conducted a qualitative assessment of the trench effect based on the results reported in the literature and showed that some of these contradictory results are related to the methodology used to implement the trench profile underneath the riser.

There are two main methodologies in the literature to incorporate the trench effect: i) artificial insertion of trench profile using mathematical formulation (e.g., Langner, 2003; Clukey et al., 2007; Sharma and Aubeny, 2011; Li and Low, 2012; Randolph et al., 2013; Shiri, 2014b; Wang et al., 2016) ii) automatic development of trench with non-linear soil models (e.g., Nakhaei and Zhang, 2008; Shiri and Randolph, 2010; Shiri 2014a, b; Zargar, 2017). However, the first approach led to some contact pressure hotspots and distortion of fatigue damage in TDZ due to inconsistencies between the natural catenary shape of the riser and the trenches created by mathematical expressions (Sharma and Aubeny, 2011; Randolph et al., 2013; Shiri, 2014b). The second methodology was proposed as an alternative solution to prevent any mismatch between the SCR catenary shape and the seabed in the TDZ, but it has some limitations in creating deep trenches (e.g., 5D as observed by ROVs) due to the premature stabilization of riser through a few cycles, somewhere in between 0.5D to 1D penetration.

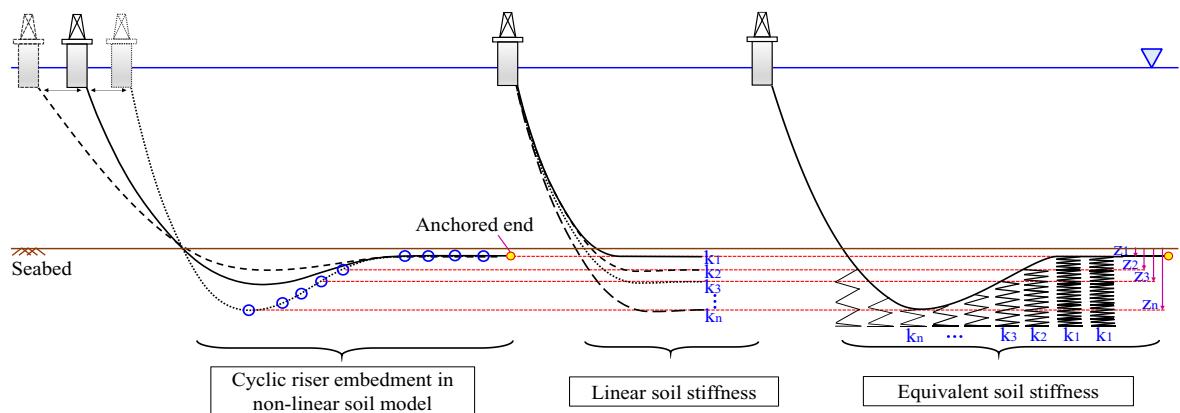


Figure A-1. Schematic concept of the non-linear, linear and equivalent stiffness along the SCR. Efforts were made to resolve some of the aforementioned issues (e.g., Randolph et al., 2013; Shoghi and Shiri, 2021; Janbazi and Shiri, 2022). However, there is still a need for

developing simple but robust methodologies to reliably incorporate the trench effect into the fatigue analysis of the SCRs.

The current study developed a new model by proposing an equivalent linear stiffness distributed along the length of SCR contacting with the seabed. As shown in Figure A-1, the idea of the equivalent soil stiffness was taken from the concept of linear and non-linear soil stiffness to generate the target trench profile that can be obtained from the non-linear hysteretic riser-seabed interaction models. Also, this model was further explored to reach the ultimate depth of the trench as observed in real operations, e.g., 5D, which non-linear seabed models have limitation to create it.

## **A.2. Concept of the Proposed Methodology**

Figure A-2(a) shows the incremental penetration of the sample riser with a non-linear soil model, such as one proposed by Randolph and Quiggin (2009), called R-Q hereafter. As the embedment gradually increases, touchdown point (TDP) moves toward the vessel, and trench bottom point (TBP) moves down with a different depth, but the trench surface point (TSP) is less affected. These three points specify the trench's depth and longitudinal profile. The idea used in the current study is defining individual equivalent stiffness in every single node contact with the seabed to achieve the same trench profile that non-linear soil model created during the cyclic embedment of the riser. As can be seen from Figure A-2(b), this equivalent stiffness should be equal in the pipeline zone due to the same riser embedment of the nodes located beyond the TSP to the anchored end. However, the equivalent stiffness is not the same for nodes in the touchdown zone.

Accordingly, two patterns of linear soil stiffness along the riser were introduced, leading to the target riser embedment that is usually obtained from the non-linear hysteretic riser-seabed interaction models. As demonstrated in Figure A-3, the reduction in soil stiffness was defined by pattern 1 to simulate the depth of the ladle shape. Moreover, pattern 2 is used for a horizontal translation of the soil stiffness in TDZ to adjust the surface point of the trench.

To satisfy both stiffness patterns mentioned above, a nonlinear equation, as provided in equation (A-1), was proposed to factorize the linear seabed stiffness in every single node in contact with the seabed.

$$k_{eq} = \frac{k_0}{1 + [\alpha \cdot \exp(\alpha \cdot (\hat{x} - \eta))]} \quad (A-1)$$

where  $k_0$  is defined as reference stiffness. As shown in equation (A-2), it represents the riser embedment in the pipeline zone that is in equilibrium with the submerged weight of the riser.

$$k_0 = \frac{m_s g}{z_0} \quad (A-2)$$

where  $z_0$  is the riser embedment under the submerged weight ( $m_s g$ ).

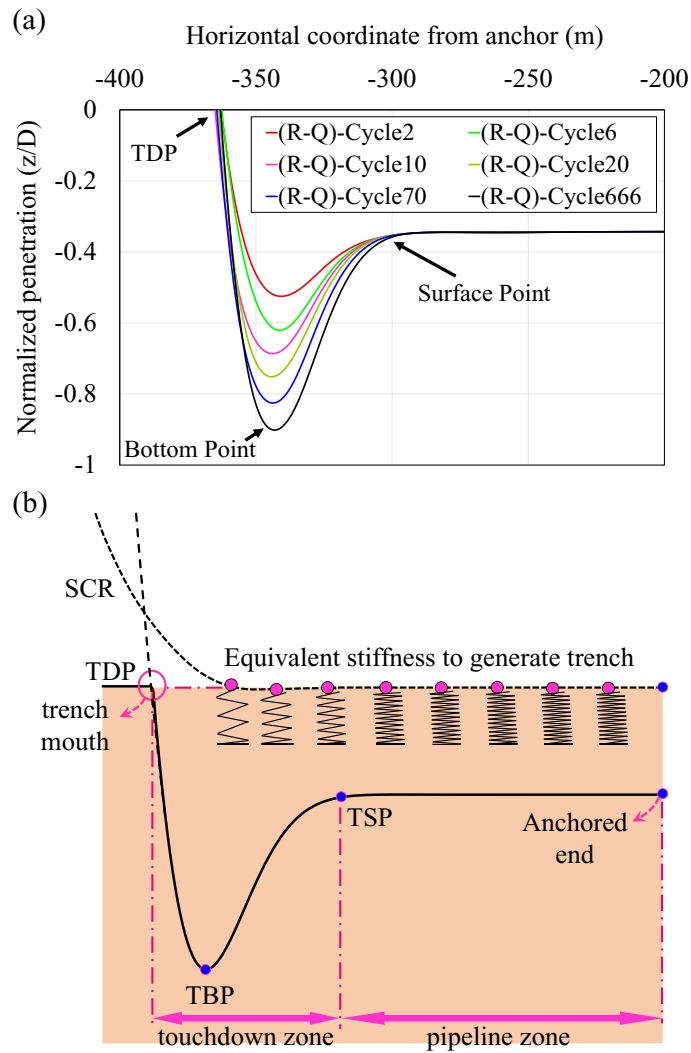


Figure A-2. Definition of trench formation created by (a) non-linear soil model (R-Q), (b) equivalent soil stiffness

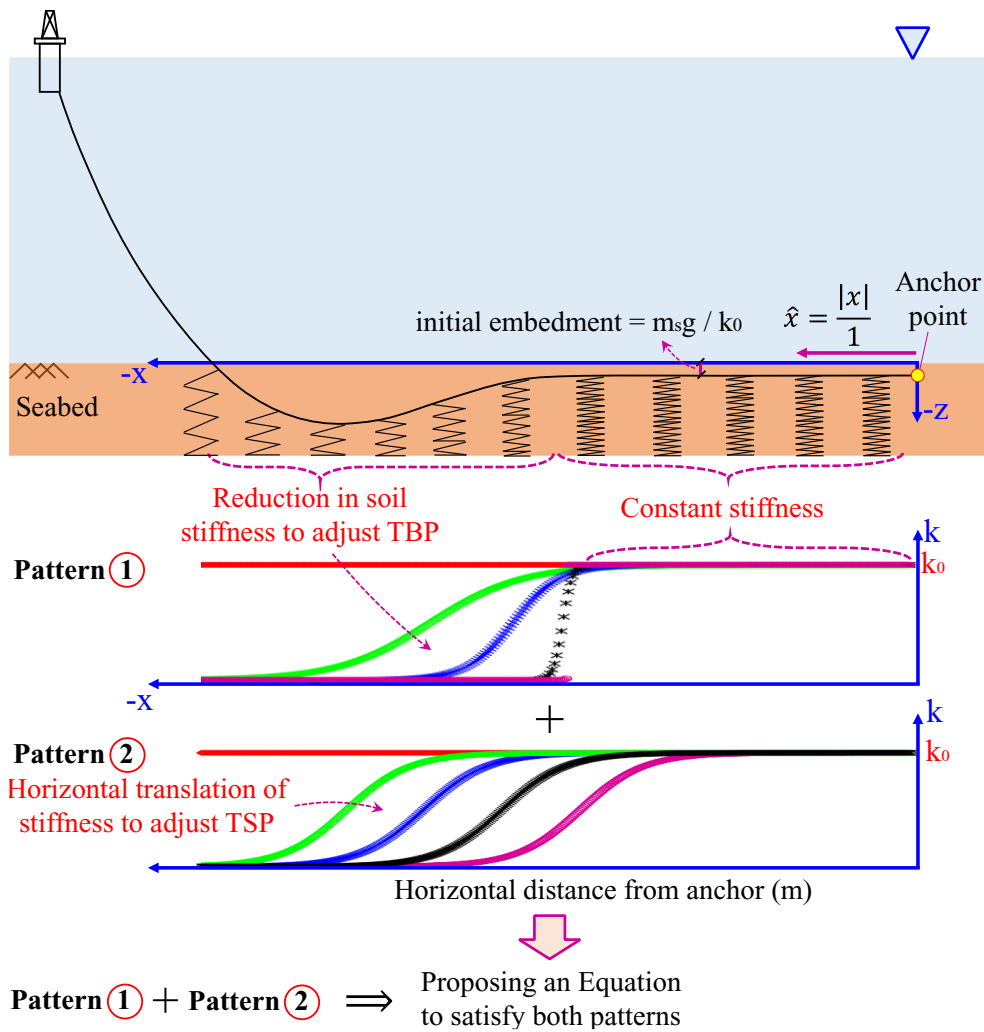


Figure A-3. Patterns of equivalent stiffness used in the current study

The value of  $z_0$  can be calculated from the backbone curve comprising the soil resistance and the soil buoyancy force, as shown in equation (A-3) (Randolph and Quiggin, 2009).

$$P_u = N_c S_u D + f_b A_{disp} \cdot (\rho_{soil} - \rho_{water}) \cdot g \quad (A-3)$$

where  $P_u(z)$  is the ultimate geotechnical penetration resistance,  $N_c(z/D)$  is the soil bearing factor,  $s_u$  is the undrained shear strength,  $D$  is the outer pipe diameter,  $f_b$  is the soil buoyancy factor,  $A_{disp}$  is the nominal area of the pipe that is below the seabed tangent plane,  $\rho_{soil}$  is the saturated density of the soil,  $\rho_{water}$  is the density of water, and  $g$  is the acceleration due

to gravity. Regarding equation (A-1), the parameter  $\hat{x}$  is the absolute value of the horizontal coordinate of each node from the anchored end normalized by 1 m (see Figure A-3). Moreover, the depth correlation factor ( $\alpha$ ) and longitudinal adjustment factor ( $\eta$ ) are dimensionless parameters related to the bottom and surface points of the trench, respectively.

### **A.3. Case Study : A Sample SCR**

A global SCR model was constructed in ABAQUS using an example SCR with a length of 2333 m and a water depth of 1800 m located in the Gulf of Mexico. The riser-seabed interaction can be modeled by a user-defined element, which is coded in FORTRAN as a subroutine within the ABAQUS user element library (UEL). The model boundary conditions were defined by assuming simple hinge supports at both the anchored end and the hang-off point. These boundary conditions are acceptable enough to focus on the TDZ behaviour (Quéau et al., 2013). Figure A-4 schematically illustrates the modelled SCR within the main structural characteristics of the riser.



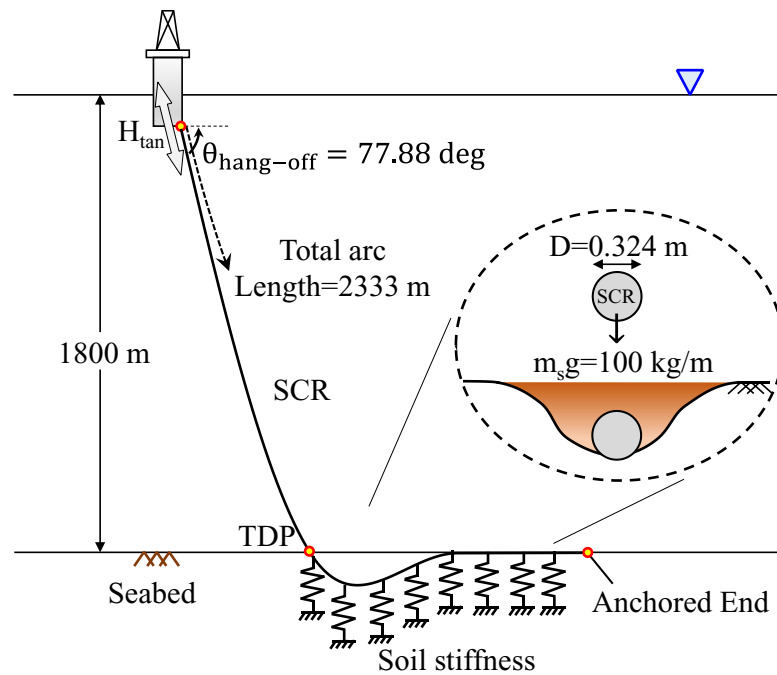


Figure A-4. The global geometry of case study modelled by ABAQUS

The vessel excitation is considered as the heave motions applied in the tangential direction of the local coordinate system located at the SCR attachment point, which is known to be the major contributor to fatigue damage accumulation (Kimiaei, 2010). This was coded into a DISP user subroutine in ABAQUS for dynamic analysis.

#### A.4. Creation of Trench

##### Comparing the Equivalent Stiffness Method with the R-Q Soil Model

The performance of the proposed equivalent stiffness methodology was verified against the non-linear hysteretic riser-seabed interaction model, R-Q, developed by Randolph and Quiggin (2009). Table A-1 shows the soil parameters used for R-Q model. The mudline shear strength is equal to 0.5 kPa with a gradient of 1 kPa/m, representing soft clay usually found in deep water regions (Randolph, 2004; Hejazi and Kimiaei, 2016). As shown in

Figure A-5(a), the gradual penetration of the riser was shown under the individual harmonic motion with an amplitude of  $H_{tan} = 3.3$  m and a period of  $T = 15$  s.

Table A-1. Input parameters for R-Q soil model

Description	sign	value
Mud-line shear strength (kPa)	$s_{u0}$	0.5
Shear strength gradient (kPa/m)	$\rho$	1
Saturated soil density (kg/m <sup>3</sup> )	$\rho_{soil}$	1500
Power law parameter	$a$	6
Power law parameter	$b$	0.25
Normalized maximum stiffness	$K$	200
Suction ratio	$f_{suc}$	0.3
Suction decay parameter	$\lambda_{suc}$	0.5
Re-penetration parameter	$\lambda_{rep}$	0.5
Soil buoyancy factor	$f_b$	1.5

It can be seen that the appropriate values of  $\alpha$  and  $\eta$  were adopted for the equivalent stiffness proposed in equation (A-1) to validate the functionality of the current model in simulating the similar trench profiles created by the R-Q model. The choice of 666 cycles shown in Figure A-5 was somewhat arbitrary but adopted to ensure that the trench of the R-Q soil model had stabilized and that the depth of penetration no more increased with a higher number of cycles.

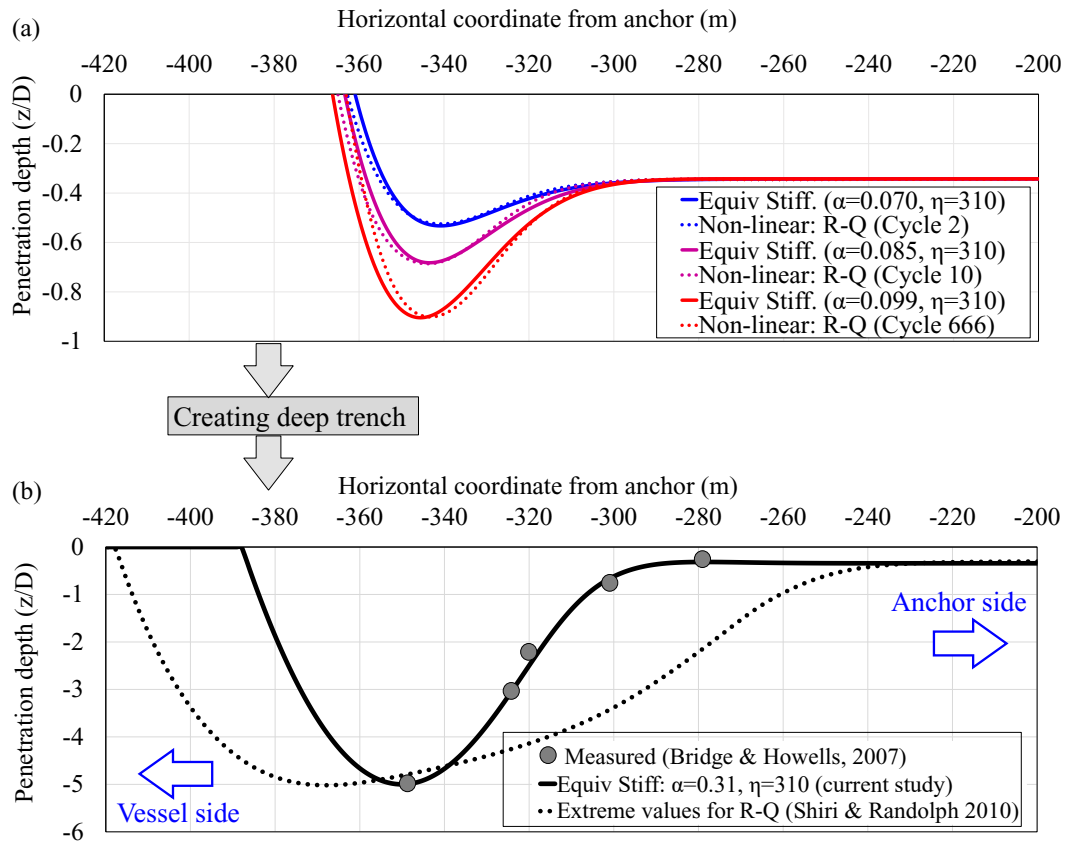


Figure A-5. Comparison of the trench profiles (a) gradual penetration based on the R-Q model and equivalent stiffness, (b) creation of deep trench

As explained in the literature, the penetration profiles created by the non-linear soil models (e.g., R-Q model) rapidly deepen and stabilize somewhere between  $0.5D$  and  $1D$  within a few cycles. This stabilization depth is lower than the trench depth ranges reported from the ROV surveys, e.g.  $3.5D$  to  $5D$ , which is mostly stabilized during the first 2-3 years of riser production (Bridge and Howells, 2007).

It is worth noting that Shiri and Randolph (2010) applied severe sea states to the vessel by adopting extreme and unreal values for non-linear soil model parameters to artificially push the SCR down the seabed. However, these unusual values, assuming  $f_{suc} = 0.05$ ,  $\lambda_{rep} = 2$  as

shown in Figure A-5(b), have a significant influence on the trench longitudinal geometry where the trench mouth shifted remarkably to the vessel side, and the surface point moved away from the vessel, violating the ratio of the trench's length to depth.

Conversely, deep trench formation was perfectly simulated within the equivalent soil stiffness by adopting a higher value for depth correlation factor,  $\alpha$ . It means that by selecting different values for  $\alpha$ , from small to large, the gradual deepening of the trench can be simulated by moving TDP towards the vessel, moving TBP downward, and keeping TSP almost in the same position. Detailed comparisons of the current equivalent stiffness approach with the R-Q model in generating certain riser embeddings were provided in Janbazi and Shiri, 2023.

### **Comparing the Equivalent Stiffness Method with the Artificial Trench Methodologies**

In this section, the created trench of the current study was compared with the artificial trench expressions proposed by Langner (2003), who proposed a trench profile based on the circular arc on the SCR side of the trench and a seventh-order polynomial fit to the anchor side of the trench; and Shiri (2014b) who examined linear and quadratic exponential functions to generate the trench profiles with the desired depth.

According to Figure A-6, the result of contact force in the riser equilibrium condition was examined based on the different methodologies. It can be seen that the artificial insertion of the trench led to some inconsistencies between the seabed and natural shape of the riser, distorting the contact force distribution along the TDZ. As illustrated in Figure A-6(a) and Figure A-6(b), the SCR ends up suspended over the deepest part of the trenched seabed, with a significant contact hotspot towards the vessel end of the trench.

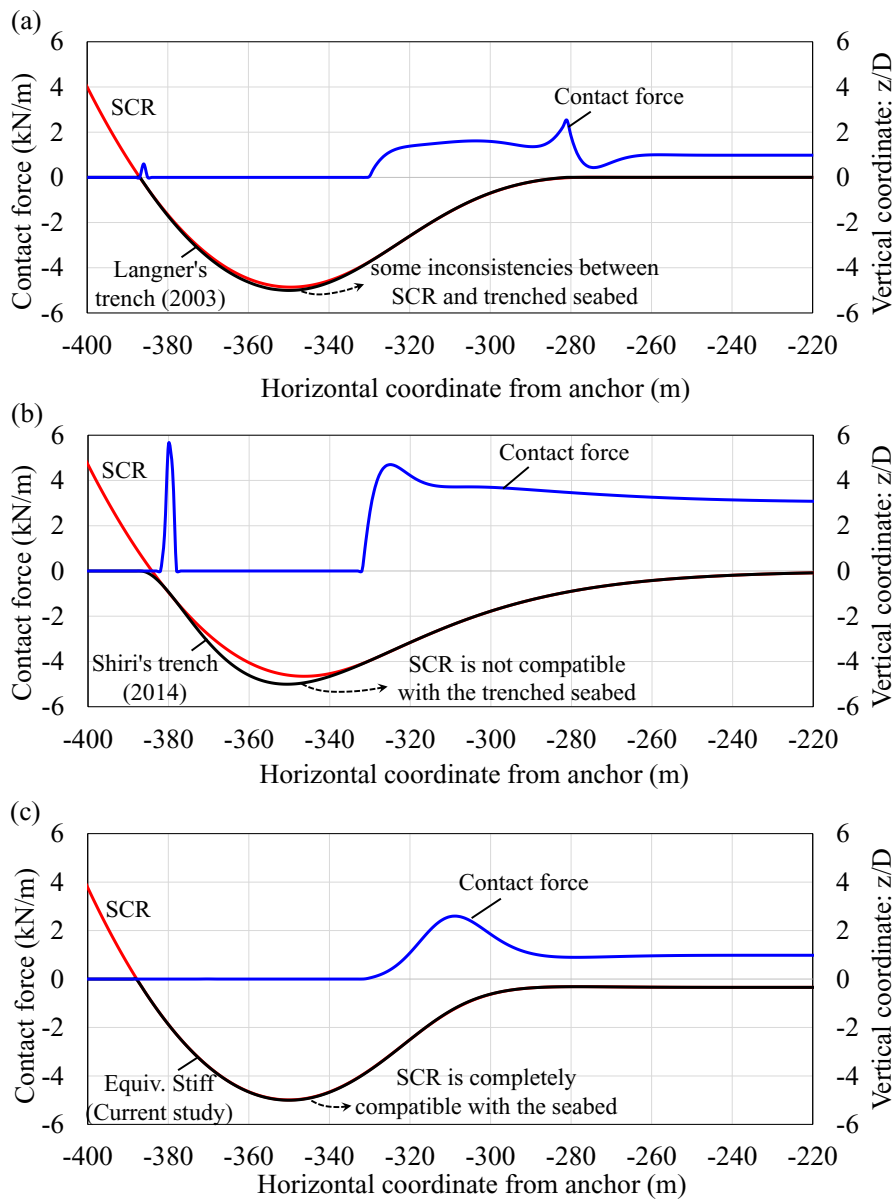


Figure A-6. Contact forces in SCR equilibrium condition based on: (a) Langner's trench, (b) Shiri's trench, (c) Equivalent stiffness method

Alternatively, the current model developed by the equivalent soil stiffness is entirely compatible with the riser catenary shape, removing any noise of contact pressure hotspots through the trench ladle shape. From the point of fatigue performance's view, it is important

to find the response of the riser in dynamic simulations, which will be further assessed in the next section.

#### **A.5. Fatigue Analysis of SCR with Incorporation of Trench Effect**

A series of riser dynamic analyses were conducted on the trenched and non-trenched (flat) seabed based on the linear ( $k = 300$  kPa) and non-linear soil model, R-Q (see Table A-1). This range of soil properties was assumed based on the real range of seabed sediments in the Gulf of Mexico (Randolph et al., 2013). The vessel fluctuations are in tangential heave motion within four different amplitudes in a range of 0.3 m, 1 m, 2 m and 3.3 m. The trench profile was created by the equivalent stiffness methodology with the 5D depth, five times the pipe diameter, as much as the trench depth observed in the field. Fatigue damage results were normalized by the corresponding maximum damage in the linear flat seabed and provided in Figure A-7~10. Moreover, a summary of the maximum damage is superimposed in each plot.

The trenched seabed analyses have shown that a similar damage distribution is observed in all ranges of motion amplitudes, including two peaks of damage in both trench edges, the leading edge towards the vessel side and the trailing edge towards the anchor side.

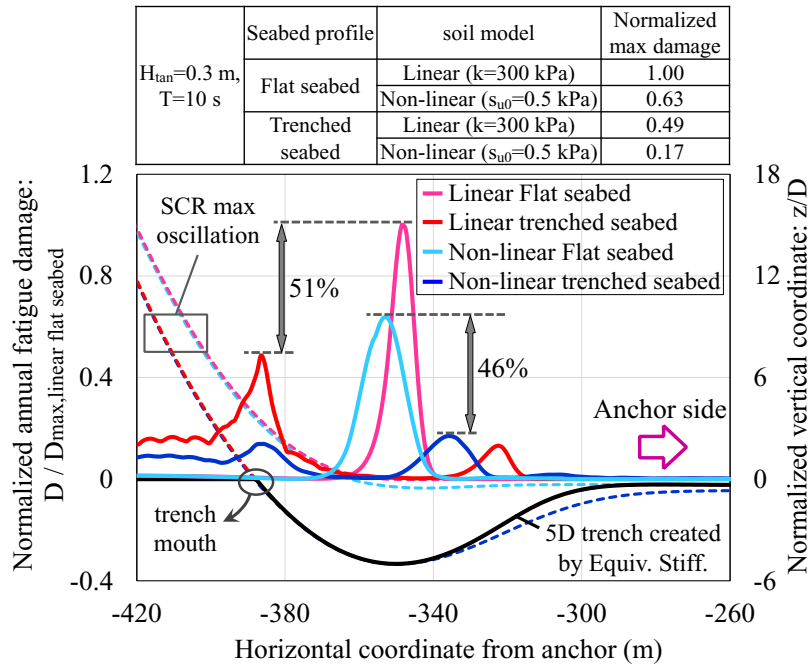


Figure A-7. Normalized fatigue damage and SCR oscillations based on the trenched and flat seabed,  $H_{tan} = 0.3\text{ m}$  and  $T = 10\text{ s}$

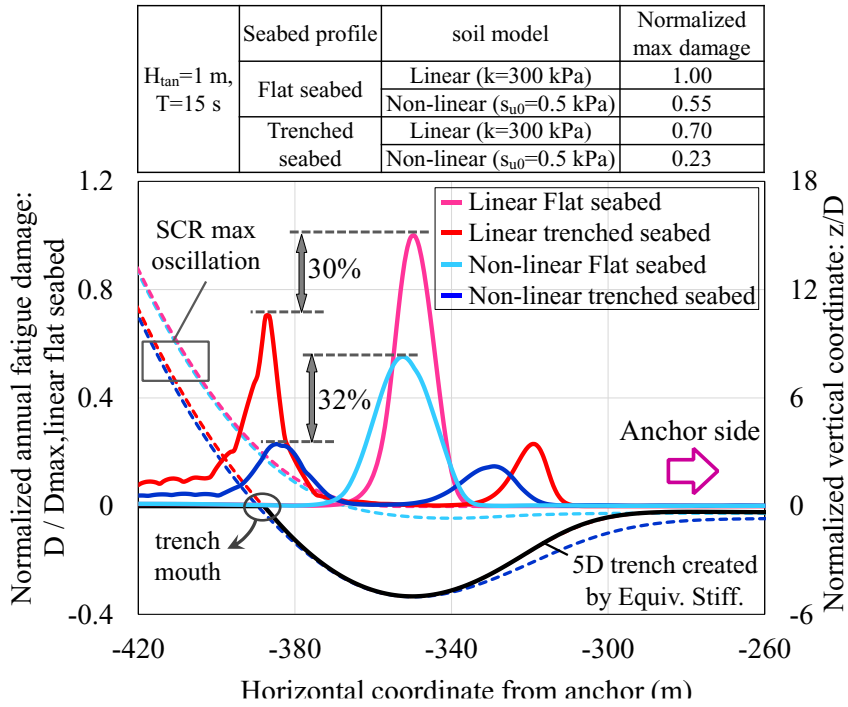


Figure A-8. Normalized fatigue damage and SCR oscillations based on the trenched and flat seabed,  $H_{tan} = 1$  m and  $T = 15$  s

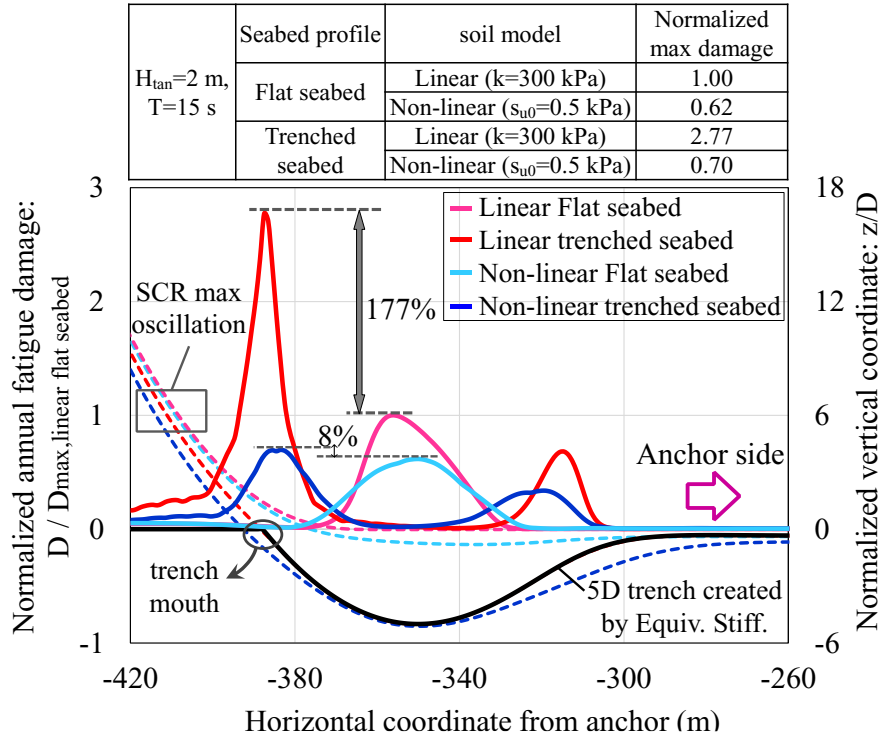


Figure A-9. Normalized fatigue damage and SCR oscillations based on the trenched and flat seabed,  $H_{tan} = 2$  m and  $T = 15$  s

As can be seen from Figure A-7 and Figure A-8, trenched case decreased the peak fatigue damage by around 50% compared to the flat seabed for  $H_{tan} = 0.3$  m, in both linear and non-linear soil models, and this damage reduction was around 30% for  $H_{tan} = 1$  m. This positive influence of trench could possibly be detrimental when motion amplitude becomes higher. As demonstrated in Figure A-9 and Figure A-10, the maximum damage of the trenched seabed was remarkably increased for  $H_{tan} = 2$  m and 3.3 m, due to the abrupt damage distortion arising from contact pressure hotspots at the trench mouth.



It is worth noting that the equivalent stiffness method uses a smart approach in generating a trench profile that is completely compatible with the natural catenary shape of the riser, but any local contact of the riser with the trench mouth due to the riser oscillations induced by floating vessel could distribute the fatigue damage response in TDZ.

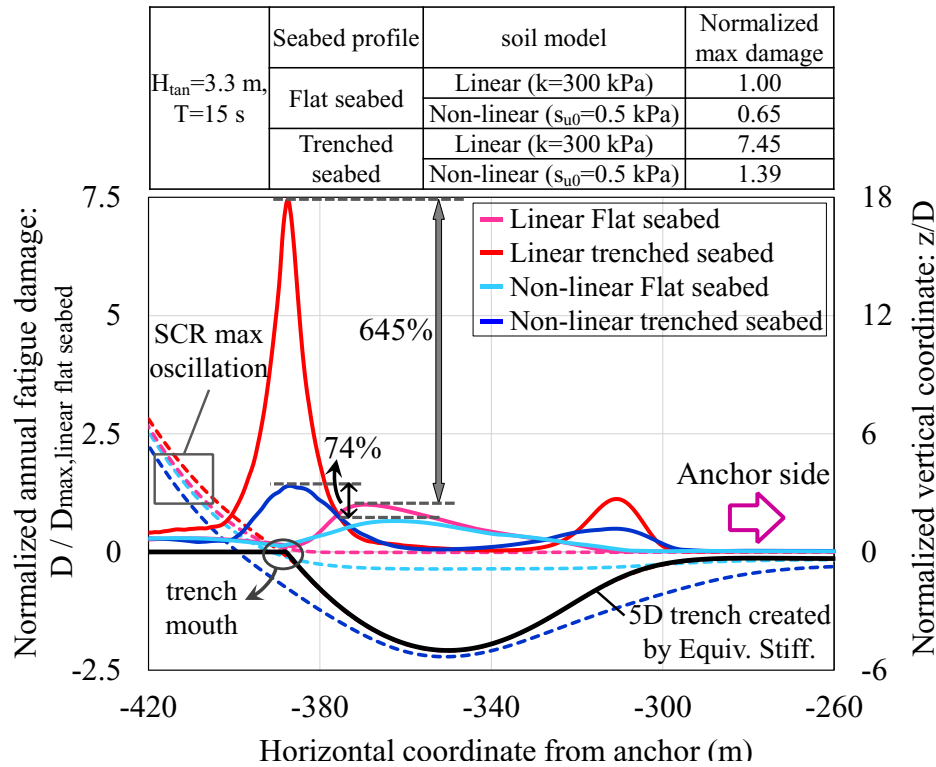


Figure A-10. Normalized fatigue damage and SCR oscillations based on the trenched and flat seabed,  $H_{tan} = 3.3\text{ m}$  and  $T = 15\text{ s}$

The analyses confirm that the left peak of damage in trenched conditions is mostly the governing factor in finding the influence of the trench on fatigue performance due to its dominant magnitude. Depending on the motion amplitude of the vessel, the trench effect could be beneficial or detrimental. These findings presumably imply why different authors have reported contradictory results for the effect of the trench on fatigue damage.

## Modified Trench Profile

Detailed assessment has been conducted around the trench mouth, where the trench profile makes a relatively sharp edge with the original flat seabed towards the vessel. Subsea surveys have shown that tension cracks occur for steep edges of the young trench due to the riser oscillations in TDZ (Bridge, 2005). This can lead to trench walls collapsing and covering the riser with backfill. Hence, the sharp trench mouth created in the current study has been modified with using an exponential arc, as shown in Figure A-11.

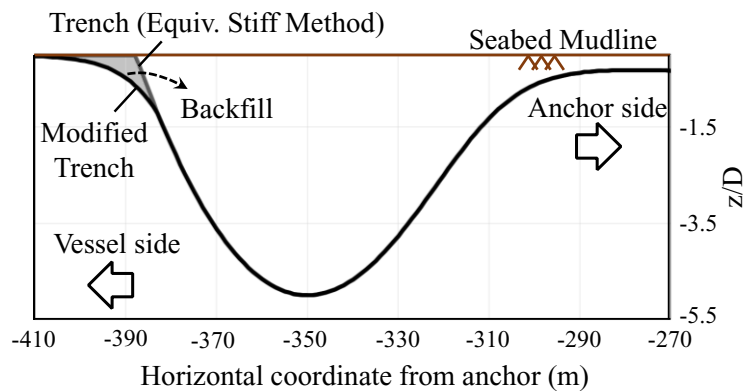


Figure A-11. Elimination of the sharp edge at the trench mouth

The response of the riser was performed based on the modified trench profile within motion amplitude of  $H_{tan} = 3.3$  m due to its worst case in creating contact hotspots at the trench mouth.

As shown in Figure A-12, both linear and non-linear soil models were considered to examine the fatigue analysis. It is noted that the results of fatigue damage were normalized by the corresponding maximum damage in the linear flat seabed. Results show that the modified trench profile could not eliminate the left peak damage, resulting in a further shift of peak fatigue damage toward the anchor side. It is observed that the riser inevitably came

into contact with the leading edge toward the vessel side due to its large fluctuations in TDZ and consequently leading to the local pressure hotspot, even though the steep edge of the trench profile was corrected to be smooth at the trench mouth.

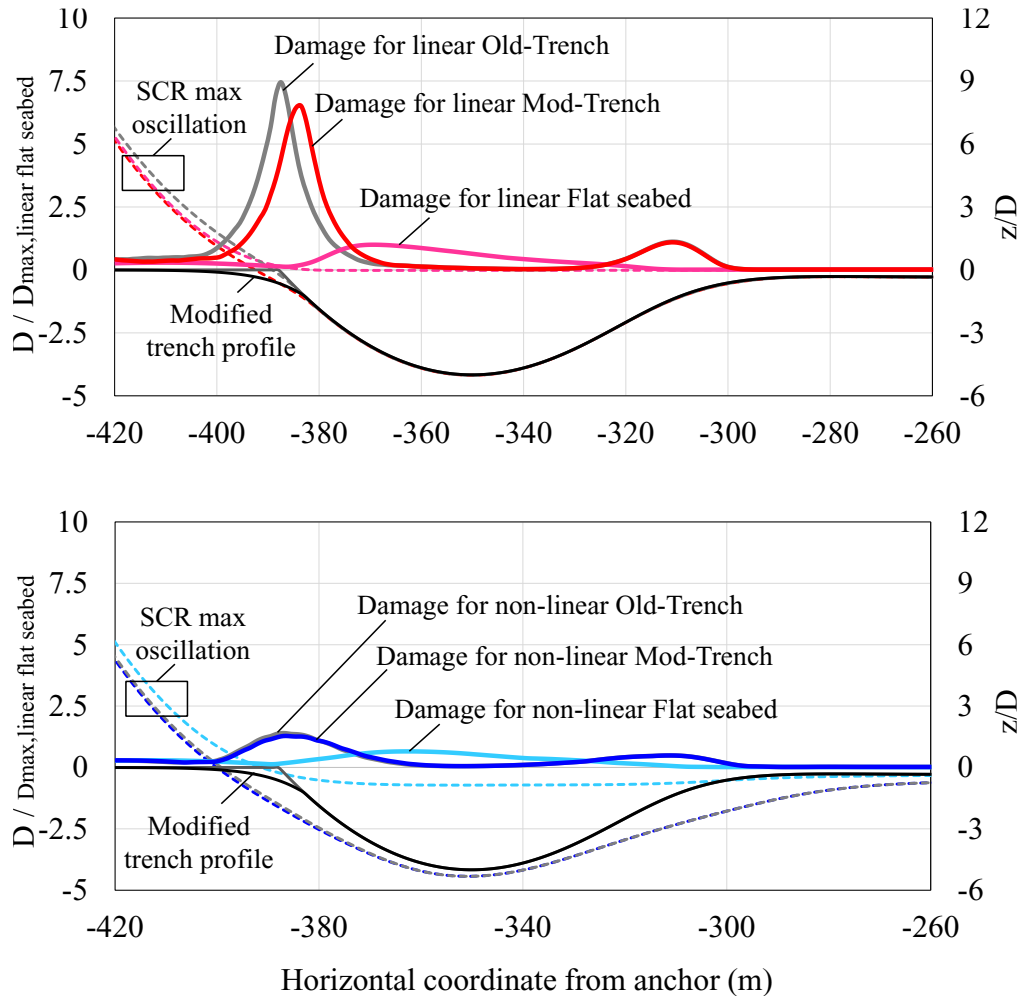


Figure A-12. Normalized fatigue damage and SCR oscillations based on the modified trench, old trench and flat seabed,  $H_{tan} = 3.3$  m and  $T = 15$  s

## A.6. Conclusion

The main contribution of this study is developing an alternative methodology to incorporate the trench effect into the fatigue analysis of steel catenary risers for resolving any pressure

hot spots along the seabed and premature stabilization problems that were repeatedly reported in the literature. Accordingly, an equivalent stiffness was used in each node of the riser contacting with the seabed to achieve the target trench depth. This automatic trench creation can be an appropriate approach to generate consistent trench formation that is perfectly compatible with the natural catenary shape of the riser, guaranteeing the prevention of contact hotspots inside the ladle shape. However, cyclic oscillations of the riser in trenched seabed resulted in two peaks in fatigue damage. The left peak, occurring around the touchdown point, is the governing factor in finding the influence of the trench. Numerical analyses confirmed that the 5D trench depth could be beneficial or detrimental for fatigue performance, depending on the magnitude of the contact hotspot at the trench mouth.

Furthermore, a modified trench profile was developed based on the detailed assessment of the real trench shapes accompanied by supporting field observations in order to eliminate the sharp edge at the trench mouth. Dynamic analyses have shown that the fatigue response in modified trenched seabed appears to remain unchanged with some minor differences as the left peak was decreased by around 10% and slightly moved to the anchor side in both linear and non-linear soil models.

It can be concluded that the trenched seabed could possibly distribute the fatigue results in two critical zones, the leading edge towards the vessel side and the trailing edge towards the anchor side. Depending on the nominal vessel position and its fluctuations, the trenched seabed can be beneficial or detrimental to fatigue performance. These findings may reveal the source of contradictions in the studies published to date.

## **Acknowledgements**

The authors gratefully acknowledge the financial support of this research by the “Natural Science and Engineering Research Council of Canada (NSERC)” through Discovery program, and the Memorial University of Newfoundland through school of graduate studies funding support.

## **References**

Bridge, C, Howells, H (2007). “Observations and modeling of steel catenary riser trenches.” In: The seventeenth international offshore and polar engineering conference, ISOPE 2007, Lisbon, Portugal.

Bridge, C (2005). “Effects of seabed interaction on steel catenary risers.” Ph.D. Thesis, University of Surrey.

Dong, X, Shiri, H (2019). “Performance of nonlinear seabed interaction models for steel catenary riser, Part II: global response.” *Appl. Ocean. Res.*, 82, 158-174.

Giertsen, E, Verley, R, Schröder, K (2004). “CARISIMA: A Catenary Riser/Soil Interaction Model for Global Riser Analysis.” 23<sup>rd</sup> International Conference on Offshore Mechanics and Arctic Engineering 2004, ASME 2004, 633-640.

Janbazi, H, Shiri, H (2022). “An alternative vessel excitation algorithm to incorporate the trench effect into the fatigue analysis of steel catenary risers in the touchdown zone.” *Applied Ocean Research*, 126-103292.

Janbazi, H., Shiri, H (2023). “A hybrid model to simulate the trench effect on the fatigue analysis of steel catenary risers in the touchdown zone.” *Canadian Geotechnical Journal*, <https://doi.org/10.1139/cgj-2022-0103>.

Langner, C (2003). “Fatigue life improvement of steel catenary risers due to self-trenching at the touchdown point.” *Proceedings of the Offshore Technology Conference, OTC 15104*, May 5-8.

Leira, BJ, Passano, E, Karunakaran, D, Farnes, KA, Giertsen, E (2004). “Analysis guidelines and application of a riser–soil interaction model including trench effects.” *Proceedings of the 23<sup>rd</sup> International Conference on Offshore Mechanics and Arctic Engineering, OMAE 2004-51527*, June 20-25, 955–962.

Li, FZ., Low, YM (2012), “Fatigue reliability analysis of a steel catenary riser at the touchdown point incorporating soil model uncertainties.” *Appl. Ocean Res.* 38, 100–110.

Nakhaee, A, Zhang, J (2008). “Effects of the interaction with the seafloor on the fatigue life of a SCR.” *Proceedings of the 18th International Society of Offshore and Polar Engineers Conference, ISOPE-I-08-397 2008*, July 6-11.

Queau, L.M., Kimiaei, M., Randolph, M.F (2013). “Dimensionless groups governing response of steel catenary risers,” *Ocean Engineering*, 74, 247–259.

Randolph, MF, Quiggin, P (2009). “Nonlinear hysteretic seabed model for catenary pipeline contact.” In: *Proceedings of the 28th International Conference on Ocean, Offshore and Arctic Engineering*. Honolulu, Hawaii, USA.

Randolph, MF., Bhat, S, Mekha, B (2013), “Modeling the touchdown zone trench and its impact on SCR fatigue life.” Proceedings of the Offshore Technology Conference 2013, OTC-23975-MS.

Rezazadeh, K, Shiri, H, Zhang, L, Bai, Y (2012). “Fatigue generation mechanism in touchdown area of steel catenary risers in nonlinear hysteretic seabed.” Res. J. Appl. Sci. Eng. Technol., 4 (24), 5591–5601.

Sharma, PP, Aubeny, CP (2011). “Advances in pipe-soil interaction methodology and application for SCR fatigue design,” Proceedings of the Offshore Technology Conference, OTC-21179-MS.

Shiri, H, Randolph, M (2010) “The influence of seabed response on fatigue performance of steel catenary risers in touchdown zone.” In: Proceedings of the 29th international conference on offshore mechanics and arctic engineering, OMAE 2010, Shanghai, China 2010, p. 20051.

Shiri, H (2014a). “Response of steel catenary risers on hysteretic nonlinear seabed.” Appl. Ocean. Res. 44 (January), 20–28.

Shiri, H (2014b). “Influence of seabed trench formation on fatigue performance of steel catenary risers in touchdown zone.” Marine Structure. 36 (April), 1–20.

Shoghi, R, Shiri, H (2019). “Modeling touchdown point oscillation and its relationship with fatigue response of steel catenary risers.” Appl. Ocean. Res. 87, 142-154.

Shoghi, R, Shiri, H (2020). “Re-assessment of trench effect on fatigue performance of steel catenary risers in the touchdown zone.” Appl. Ocean Res. 94, 1–16.

Shoghi, R, Pesce, C.P, Shiri, H (2021). “Influence of trench geometry on fatigue response of steel catenary risers by using a boundary layer solution on a sloped seabed.” *Ocean Eng.* 221, 108447.

Thethi, R, Moros, T (2001). “Soil interaction effects on simple catenary riser response.” *Deepwater Pipeline and Riser Technology Conference, Houston, Texas, USA.*

Wang, K, Low, YM (2016). “Study of seabed trench induced by steel catenary riser and seabed interaction.” *Proceedings of the 35th International Conference on Ocean, Offshore and Arctic Engineering, OMAE 2016-54236.*

Zargar, E (2017). “New hysteretic seabed model for riser-soil interaction.” *PhD Thesis, University of Western Australia.*